“There may be people that have more talent than you, but there’s no excuse for anyone to work harder than you do”
- Derek Jeter

“He who is not courageous enough to take risks will accomplish nothing in life”
- Muhammad Ali

“See, in my line of work you got to keep repeating things over and over and over again for the truth to sink in, to kind of catapult the propaganda”
- George W. Bush

University of Alberta

CHARACTERIZATION OF RESERVOIR QUALITY USING ICHNOLOGICAL, SEDIMENTOLOGICAL, AND GEOCHEMICAL METHODS

by

GREGORY MARK BANIAK

A thesis submitted to the Faculty of Graduate Studies and Research
in partial fulfillment of the requirements for the degree of

DOCTOR OF PHILOSOPHY

DEPARTMENT OF EARTH AND ATMOSPHERIC SCIENCES

Fall 2013
Edmonton, Alberta

DEDICATION

To my parents, Morris and Marilyn, and two Uncles, Leon and Matt, I dedicate my thesis to you as your never-ending love, support, and encouragement of my university endeavors during the past nine of university has been nothing short of amazing! Mom and Dad, your selfless demeanor, patience, and generosity will never go forgotten. I am forever indebted to you for everything you have done for me. You provided me with the encouragement, strength, and support to work through some of the most challenging stages of my university studies and have helped me in ways unimaginable. I am very lucky to call you my parents and I love you both dearly. To Leon and Matt, your support and encouragement instilled me with the confidence that no challenge is insurmountable without hard work and dedication. I consider both you of amazing role models and I feel very fortunate to have you in my life!

ABSTRACT

A detailed analysis of subsurface reservoirs from offshore Norway and Alberta, Canada is undertaken in this thesis to better categorize the influence trace fossils have on reservoir quality. Specifically, the data collected focuses on understanding burrow fabrics in two- and three-dimensions (2D and 3D), assessing the influence trace fossils have on fluid flow, and understanding burrow-associated diagenesis.

Using imaging techniques such as microtomography (micro-CT) and computed tomography (helical-CT), a better understanding of burrow fabrics and their associated properties is completed. Particularly, each sample is found to have a distinctive X-ray attenuation due to factors such as grain size and sorting. This is particularly true for samples that contain moderate to extreme contrasts in lithology and permeability between the burrows and matrix. As such, the 3D generated volumes of the burrows help show that the distribution of X-ray attenuations within a sample can be linked to measured permeabilities.

The influence of bioturbation on reservoir quality within carbonates (Upper Devonian Wabamun Group, central Alberta) and siliciclastics (Upper Jurassic Ula Formation, offshore Norway) is investigated using spot-permeametry measurements, thin sections, analytical models, and numerical models. In both case studies, analytical and numerical models show that the arithmetic mean best characterizes intervals dominated by moderate to high bioturbation intensities or horizontal to sub-vertical burrows. The harmonic mean best represents intervals with vertical burrows or low bioturbation intensities. The geometric mean best characterizes intervals where horizontal and vertical permeabilities within the sample are roughly equal. A new term, Ichnofossil Hosted Tight Gas (IHG), is also introduced in this thesis to demarcate tight gas reservoirs, such as the Wabamun Group, wherein natural gas is produced primarily from the burrows relative to the low-permeability matrix.

Using core data, thin sections, and isotopes (carbon and oxygen), the influence burrows have on mediating dolomitization is examined in the Mississippian Debolt Formation (Dunvegan gas field, northwestern Alberta). Compositional differences observed in the isotopic distributions reflect the different biogeochemical processes occurring within and adjacent to the burrows. Organic matter, an essential component for bacterial sulfate reduction and subsequent near-surface dolomitization, is likely derived in part from the organisms and their by-products.

ACKNOWLEDGEMENTS

A little more than six years ago, I had the opportunity to take a petroleum geology class offered by Stephen Halabura at the University of Saskatchewan. I can truly say that taking Stephen's class was one of the best decisions I have ever made! Stephen's passion for geology, and life in general, is incredible and I feel humbled for having had the opportunity to learn from him. Graciously, Stephen also took me under his guidance during the summers of 2007 and 2008 and provided me with opportunities and real-world experiences that are priceless to a young geologist. I feel truly fortunate to have had the chance to work with Stephen and I have no doubt that I would not be where I am today without his guidance and friendship!

During my last fall semester as an undergraduate, I also had the opportunity to take an ichnology class offered by Luis Buatois and Gabriela Mángano. Luis and Gabriela's passion for ichnology was amazing and I feel fortunate for having had the opportunity to learn from them. It was also during this ichnology class that my desire to begin graduate school occurred. While studying for the final exam from a textbook titled '*Ichnology and Sedimentology of Shallow to Marginal Marine Systems*' by George Pemberton *et al*., I stumbled upon the concept of biogenic permeability. At this moment, I became completely fascinated by ichnology and its different applications. I knew then that I wanted to pursue a graduate degree.

Having never met George, in combination with not having the highest undergraduate grades, I was pretty realistic about my chances of getting into graduate school or even soliciting a positive response from George. Despite my fears, George replied to my initial emails with great enthusiasm and was genuinely interested in my desire to become one of his students. I sincerely thank George from the bottom of my heart for the opportunity he has given me! During my time as a graduate student, I have had to extreme privilege of learning from George in so many different ways. His wisdom and knowledge is unparalleled and I feel fortunate for every moment he took time out of his busy schedule to talk with me about science, sports, and life in general. I will forever be indebted towards George for the endless support, wisdom, and opportunities he has bestowed upon me. Thank-you for everything George, past and present!

Outside of George, Murray Gingras has truly been the biggest influence on my academic graduate career. Without a doubt, Murray is one of the most genuine, down-to-earth individuals you will ever meet. From giving me the wonderful opportunity to attend international conferences, to continuously supporting my ideas and providing valuable feedback/edits, to always pushing to me and never

settling for nothing but the best, Murray has given me the foundation to blossom as a geologist. More importantly, I have become a better person under Murray's guidance and would not be where I am today without Murray's support. I am truly honored to have had the opportunity to work alongside Murray these past five years and consider him a great friend. Thank-you Murray!

At this point, I would be foolish not to recognize the amazing support and help I have received from the Ichnology Research Group (IRG). I am very thankful to Curtis Lettley for all the edits and supervision he offered me during the early years in the lab. Ryan Lemiski, Andrew La Croix, Jesse Schoengut, Luke McHugh, Ryan King, and Dave Herbers helped separate many long days with endless shenanigans and never-ending discussions on sports related topics (many of which continue to be debated after five years!). I also wish to thank Andrew La Croix for all his help and support regarding various parts of the thesis. Chelsea Fefchak and Jenna Phillips delivered a constant source of celebrity gossip and fashion advice and I am very thankful for all their help and friendship. Tiffany Playter is one of the most courageous individuals I have ever come across and is truly a special person. Cheryl Hodgson provided a constant source of energy to the lab and I truly appreciate all her edits and support these past couple years. Thank you to Camilo Polo for helping me log core in Norway and complete mundane tasks on the micro-CT. Robynn Dicks, Tomonori Hyodo, Carolyn Currie, Reed Myers, Eric Timmer, Joel Gagnon, Scott Botterill, Alina Shchepetkina, Carolyn Furlong, Gordon Campbell, and Rares Bistran are some of the nicest people you will ever meet and certainly helped make the IRG lab a fun place to gather. And last, but not least, J.P. Zonneveld, who provided endless stories, numerous jokes, and offered continuous support of my thesis and academic endeavors from the beginning. Although J.P. was not one of my supervisors, I graciously thank him for all the opportunities he has bestowed upon me during the past five years.

I was also fortunate to have many people provide logistical support and most certainly deserve recognition. Mark Labbe was timely in his preparation of thin sections and always provided help when asked questions regarding the spot-permeameter and cutting core samples. Aleisha Rosse was very helpful in collecting isotope samples. Graduate secretaries Marsha Boyd and Colleen Hanrahan were always around to provide help regarding scholarships, teaching assistant positions, and were nothing short of amazing. Computer guru Chris Lough provided helpful service and advice regarding my computer on numerous occasions and Igor Jakab was always there to provide help for printing posters.

A sincere thank you to the following companies and organizations for financial assistance: Canadian Association of Petroleum Producers, Canadian Society of Unconventional Resources, Government of Alberta (Advanced Education & Technology Division), American Association of Petroleum Geologists (Research Grant), and University of Alberta. Additionally, I would also like to acknowledge the generous funding to Murray Gingras and George Pemberton from Natural Sciences and Engineering Research Council (NSERC), Statoil, ConocoPhillips Norway, BP Canada, and Devon Energy. Without these research monies, I certainly would never have been able to accomplish any of my research endeavors.

I would also like to thank the members of my thesis committee, Ben Rostron, Nicholas Harris, and Grant Wach, for their valuable advice and edits. Also, a big thank you goes to journal reviewers David Morrow, Gene Rankey, Kevin Cunningham, Tracy Frank, Rodmar Ravnås, Mariano Marzo, Stephen Laubach, Charles Savrda, Jack Horkowitz, Terrilynn Oslen, Luis Buatois, Hilary Corlett, Adrian Immenhauser, James MacEachern, and Richard Callow for all their helpful comments, edits, and suggestions on different portions of this thesis submitted/ accepted for publication into peer-reviewed journals.

I would also be remiss not to acknowledge Drs. Courvoisier, Gibson, Hennessy, Pilsner, and Wiser for their help and support during the weaker moments of this thesis! Furthermore, I would also like to thank the Toronto Maple Leafs and Edmonton Oilers for being so embarrassingly dreadful at hockey these past five years so that I could focus my efforts on graduate school and not watching hockey.

And finally, I wish to thank those who have had a significant impact on my life outside of university. To my two brothers, Nick and Matt Baniak, you have always provided words of encouragement and support. You have each done remarkable things in your own two lives and I consider both of you role models. To my amazing parents, Morris and Marilyn, you are my biggest supporters and I am truly blessed to have you two in my life. To my Alberta family, Uncles Matt and Leon, Aunty Linda, and cousins Tyler (Jess), Scotty, and Jackline (Jack), I wish to say thank you so very much. You have been absolutely amazing and I feel truly fortunate for everything you have done for me. Indeed, I am a really lucky guy to have such as great family! To my amazing girlfriend Michelle Mudryk, thank you for everything. I am truly thankful for your emotional support during the numerous highs and lows of the past couple years. You are a remarkable person with a big heart and I am very lucky to have you in my life!

TABLE OF CONTENTS

CHAPTER 3:
AN EXAMPLE OF A HIGHLY BIOTURBATED, STORM INFLUENCED SHOREFACE DEPOSIT: UPPER JURASSIC ULA FORMATION, NORWEGIAN NORTH SEA, EUROPE

CHAPTER 4:
PETROPHYSICAL CHARACTERIZATION OF BIOTURBATED SANDSTONE RESERVOIRS: UPPER JURASSIC ULA FORMATION, NORTH SEA, EUROPE

CHAPTER 5:
RESERVOIR CHARACTERIZATION OF BURROW-MOTTLED DOLOMITES: UPPER DEVONIAN WABAMUN GROUP, PINE CREEK GAS FIELD, CENTRAL ALBERTA, CANADA

CHAPTER 6:
SABKHA AND BURROW-MEDIATED DOLOMITIZATION: MISSISSIPPIAN DEBOLT FORMATION, NORTHWESTERN ALBERTA, CANADA

CHAPTER 7:
SUMMARY AND CONCLUSIONS

LIST OF TABLES

CHAPTER 1

CHAPTER 4

CHAPTER 6

LIST OF FIGURES

CHAPTER 1

CHAPTER 2

CHAPTER 3

CHAPTER 4

CHAPTER 5:

CHAPTER 6:

LIST OF SYMBOLS AND ABBREVIATIONS

MISCELLANEOUS

2D	Two-dimensional	3D	Three-dimensional
CT	Computed Tomography	^{o}	Degree of Rotation
kV	Kilovolts	µA	Microampere
%	Percentage	mD	Millidarcy
m^3	Cubic Metres	BI	Bioturbation Intensity
µm	Micrometre	mm	Millimetre
cm	Centimetre	m	Metre
δ	Delta	Σ	Sigma
EPS	Microbial Exopolymer Secretions	‰	Parts per Thousand (per mil)

SYMBOLS USED IN EQUATIONS

Chapter 2

I_o	Initial X-ray Energy	I	Attenuated Intensity
M	Linear Attenuation Coefficient	x	Length of the X-ray path
p_e	Electron Density	Z	Atomic Number
A	Atomic Weight	E	Photon Energy
A	Klein–Nishina Coefficient	b	9.8×10^{-24}
p	Object Density	N_{AV}	Avogadro's Number
f_i	Fraction of Electrons, *i*th element	Z_i	Atomic Number, *i*th element

Chapters 4 and 5

k_i	Permeability of Each Layer	d_i	Individual Layer Thickness
d	Total Thickness of Layer	d_i/d	Volume Filled by Burrows

ICHNOFOSSILS

As	*Asterosoma*	Di	*Diplocraterion habichi*
Ch	*Chondrites*	Fu	Fugichnia
Oi	*Ophiomorpha irregulaire*	On	*Ophiomorpha nodosa*
Pa	*Palaeophycus*	Ph	*Phycosiphon*
Pl	*Planolites*	Ro	*Rosselia*
Sch	*Schaubcylindrichnus freyi*	Sk	*Skolithos*
Te	*Teichichnus*	Th	*Thalassinoides*
Zo	*Zoophycos*		

LIST OF SYMBOLS AND ABBREVIATIONS (CONTINUED)

CHAPTER 2

CCD	Charge-Coupled Device

CHAPTER 3

FA1	Facies Association 1	FA2	Facies Association 1
F1	Facies 1	F2	Facies 2
F3	Facies 3	F4	Facies 4
F5	Facies 5	F6	Facies 6
TSE	Transgressive Surfaces of Erosion	MFS	Marine Flooding Surfaces
HCS	Hummocky Cross-Stratification	SCS	Swaley Cross-Stratification
CB	Cryptic Bioturbation	XB	Cross-Bedding
Py	Pyrite	S	Siderite

CHAPTER 5

N_2	Nitrogen Gas	IHG	Ichnofossil Hosted Gas

CHAPTER 6

MSR	Microbial Sulfate Reduction	Mg^{2+}	Magnesium Ion
CO_3^{2-}	Carbonate Ion	CH_2O	Organic Carbon
O_2	Oxygen	CO_2	Carbon Dioxide
H_2O	Water	H^+	Hydrogen Ion
NO_3^-	Nitrate Ion	NH_4^+	Ammonium Ion
MnO_2	Manganese Dioxide	Mn^{2+}	Manganese Ion
FeOOH	Iron Oxide	Fe^{2+}	Iron Ion
SO_4^{2-}	Sulfate Ion	HS^-	Hydrogen Sulfide Ion
CH_4	Methane	HCO_3^-	Bicarbonate Ion
H_3PO_4	Phosphoric Acid	Pe	Peloidal Grainstone
Os	Ostracode	Me	Micrite Envelopes
R^2	Coefficient of Determination	F1	Facies 1
F2	Facies 2	F3	Facies 3
F4	Facies 4	F5	Facies 5
F6	Facies 6		

CHAPTER 1: INTRODUCTION

Following the discovery of oil by James Williams in 1858 (Oil Springs, Ontario, Canada) and Colonel Edwin Drake in 1859 (Titusville, Pennsylvania, United States), hydrocarbons have become the catalyst for economic growth, prosperity, and globalization of world markets. A common by-product of this economic expansion, however, has been the steady increase in the global consumption of coal, oil, and natural gas (Fig. 1.1). For example, the global consumption of oil has increased from roughly 65 million barrels of oil per day in 1986 to over 88 million barrels of oil per day in 2011 (Fig. 1.2) (BP World Energy Review, 2012). Due to the continued economic expansion and population growth in Eastern Asia, India, and South America, the global consumption of oil and natural gas is expected to increase significantly in the coming years. By 2035, the global consumption of oil is projected to reach a staggering 112 million barrels of oil per day (DOE/EIA, 2011). Similarly, consumption of natural gas is anticipated to rise from 111 trillion cubic feet per year in 2008 to 169 trillion cubic feet per year in 2035 (DOE/EIA, 2011). Given these massive increases, future exploration geologists and reservoir engineers will be challenged with the task of locating and producing higher volumes of hydrocarbons. Perhaps more importantly, academics and politicians will hopefully finally begin asking serious questions as to whether current and future reserves of oil and natural gas have the capacity to meet growing global demand.

In this context, peak oil has been introduced as a theory to evaluate the unavoidable decline in oil production around the world. Marion King Hubbert, a former geophysicist with Shell Oil, initially proposed this theory in his paper '*Nuclear Energy and the Fossil Fuels*' (Hubbert, 1956). Hubbert's model, accurately predicting the United States oil production would peak between 1965 and 1970, has become known as the Hubbert Peak Theory. The theory states that any oil field will follow a bell-shaped curve with the top of the curve representing the peak (i.e., maximum production). Following this peak, the oil field will enter into a state of decline wherein production will become more difficult and costly. In recent years, scientists and economists have been applying the Hubbert Peak Theory with varying degrees of success to estimate the peak production in oil producing counties around the world (Bardi, 2009; Newman et al., 2009; Friedrichs, 2010).

At present, reserves of oil and natural gas are distributed among all regions of the world. Within many of these areas, new reserves of hydrocarbons are continually being identified due to advanced exploration techniques and new technologies. However, despite the overall abundance of identified oil fields, only 1% of the

world's oil reservoirs are believed to have the capacity to produce greater than 500 million barrels of oil (Robelius, 2007). More importantly, a large majority of these 'giant' oil fields are located either in politically instable regions such as the Middle East (i.e., Iran, Iraq, Kuwait) or is in current production decline. In areas with abundant reserves of conventional natural gas, such as the Middle East and Russia, discovery of more than 50% of the total resource is believed to have already occurred (Odedra et al., 2005). Production of oil and natural gas from conventional reservoirs is therefore believed to have a limited capacity to meet growing global demand and undoubtedly follows Hubbert's peak oil theory. As a result, a more thorough understanding of reservoir properties, such as bioturbation and its textural attributes, is required in order to maximize current production from conventional oil and natural gas reservoirs. More importantly, additional demand for hydrocarbons in future years will also have to be supplemented by unconventional resources such as oil sands, oil shales, and shale gas. Many of these unconventional resources, unsurprisingly, are also bioturbated and therefore require proper understanding for optimal recovery.

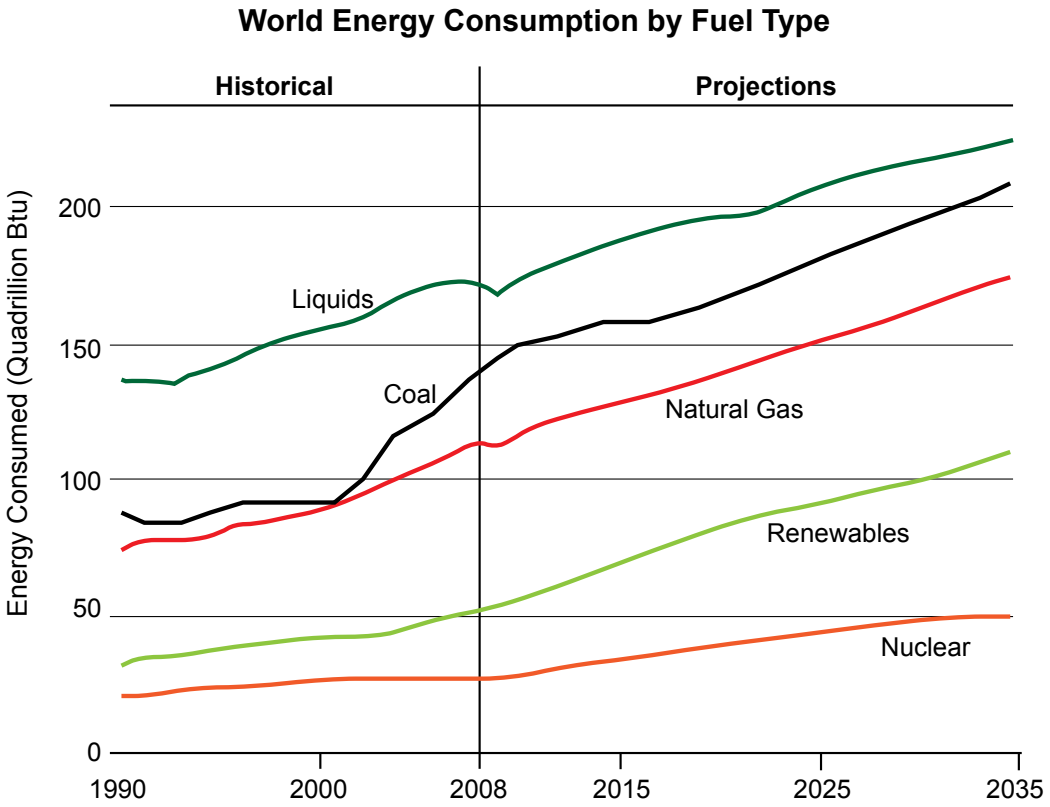

Figure 1.1: Line graph showing the historical and predicted consumption of different energy sources around the world. Unsurprisingly, consumption of all energy types are expected to increase considerably over the next 20 years due to factors such as increased global trading and population growth. Modified from United States Department of Energy (DOE/EIA, 2011).

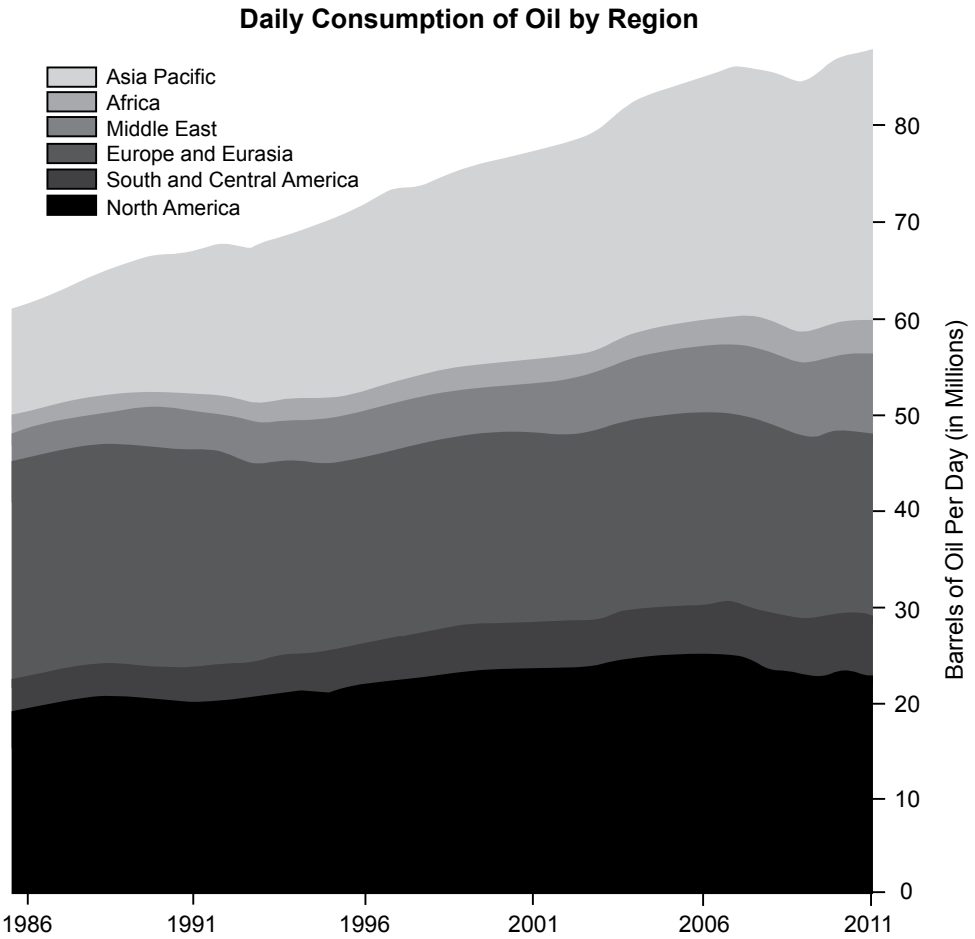

Figure 1.2: A graph showing the daily consumption of oil by different regions. Within the past 25 years, the emerging economies of South and Central America and Asia Pacific (e.g., China, India) have resulted in massive increases in the global consumption of oil per day. More importantly, these markets will most likely continue increasing their daily consumption and help offset slow declines from Europe and North America. Figure modified from BP World Energy Review (2012).

1.1 BIOTURBATION AND ITS IMPACT ON RESERVOIR QUALITY

Massive volumes of hydrocarbons occur within bioturbated carbonate and siliciclastic strata worldwide. Examples of conventional bioturbated reservoirs include the Cretaceous Avalon and Ben Nevis formations in offshore Newfoundland, Canada (Pemberton et al., 2001; Spila et al., 2007; Tonkin et al., 2010), Lower Cretaceous Viking Formation in western Canada (Raychaudhuri et al., 1992; MacEachern et al., 1999; Dafoe et al., 2010), and the world famous Ghawar oil field in Saudi Arabia (Pemberton and Gingras, 2005; Swart et al., 2005; Lindsay et al., 2006). Examples of unconventional bioturbated reservoirs include the Cretaceous McMurray Formation in Alberta, Canada (Pemberton et al., 1982; Ranger and Pemberton, 1992; Ranger and Gingras, 2005), and most shale/siltstone gas reservoirs (Lemiski et al., 2011; Angulo and Buatois, 2012; Bednarz and McIlroy, 2012; Zonneveld and Gingras, 2012; La Croix et al., 2013; Gingras et al., 2013).

Despite these obvious trace fossil heterogeneities within reservoir strata, an understanding of their origin and significance, both sedimentologically and petrophysically, has eluded many engineers and geologists. Instead, evaluations of permeability and porosity distribution within reservoirs has historically focused on parameters such as cementation, diagenesis, fracturing, and lithology (Weber, 1982; McKinley et al., 2004). More importantly, many geologists and engineers commonly disregarded the influences of bioturbation on fluid movement within reservoirs. It has been shown, however, in many recent examples that trace fossils contain textural heterogeneities that positively influence the distribution and magnitude of permeability and porosity within reservoirs and aquifers (e.g., Gingras et al., 1999; Keswani, 1999; Pemberton et al., 2001; Gingras et al., 2002a; Gingras et al., 2002b; Gingras et al., 2004a; Pemberton and Gingras, 2005; Gingras et al., 2007; Spila et al., 2007; Pemberton et al., 2008; Knaust, 2009; Cunningham et al., 2009; Gordon et al., 2010; Lemiski et al., 2011; Tonkin et al., 2010; Cunningham et al., 2012; Gingras et al., 2012; La Croix et al., 2012, Polo, 2013; La Croix et al., 2013; Baniak et al., in press).

Most notable among these aforementioned references is the body of work directed by Drs. Murray Gingras and George Pemberton, along with their associates and graduate students, at the University of Alberta. Focusing on reservoir examples from around the world, they have evolved a classification scheme detailing the characteristics of biogenic permeability. This classification scheme, first presented by Pemberton and Gingras (2005), outlines five interrelated classifications of biogenic permeability and includes: (1) surface-constrained textural-heterogeneities; (2) nonconstrained textural heterogeneities; (3) weakly defined textural heterogeneities; (4) cryptic textural heterogeneities; and (5) diagenetic textural heterogeneities (Table 1.1). Proper recognition and understanding of this classification sheme during core logging is critical, as it can help serve as the foundation for reservoir modeling and subsequent economic calculations.

Within this framework of reservoir characterization through the analysis of trace fossils, it is generally accepted that two mechanisms account for biogenically enhanced permeability. These mechanisms include biogenic reworking of the original sedimentary fabric and diagenetic modification through recrystallization or dissolution of the sedimentary media (Meadows and Tait, 1989; Green et al., 1992; Bromley, 1996; Bastardie et al., 2003; Katrak and Bird, 2003). Because bioturbated fabrics are typically three-dimensional in nature and have a wide range of orientations (Gingras et al., 1999; McIlroy, 2007; La Croix et al., 2012),

Biogenic Enhancement	Occurance	Impact on Reservoir	Reservoir Examples
1) Surface-Constrained Textural Heterogeneities	Dominantly clastics, occasionally in carbonates. Restricted to *Glossifungities*-demarcated surfaces.	Abundant cutoffs, high tortuosity, flow only through burrow conduits.	Jurassic Ghawar oil field Saudi Arabia) Triassic Baldonnel Formation (British Columbia, Canada)
2) Nonconstrained Textural Heterogeneities	Distal offshore transition surfaces, offshore deposits, and carbonate shelf deposits.	Abundant cutoffs, high tortuosity, flow only through burrow conduits.	Cretaceous Lysing Formation (offshore Norway) Miocene Paciran Member (East Java Sea)
3) Weekly Defined Textural Heterogeneities	Distal lower offshore, upper shoreface, and sandy bay sediments.	Interbedded zones of higher permeability within lower permeable zones.	Jurassic Ula Formation (offshore Norway) Cretaceous Medicine Hat Member (Alberta, Canada)
4) Cryptic Textural Heterogeneities	Estuarine to distributary channels and upper shoreface sandstones.	Microscale zones of higher permeability within lower permeable zones.	Jurassic Ula Formation (offshore Norway) Cretaceous Bluesky Formation (Alberta, Canada)
5) Diagenetic Textural Heterogeneities	Carbonate platform and offshore deposits.	Abundant cutoffs, high tortuosity, flow only through burrow conduits.	Devonian Wabamun Group (Alberta, Canada) Ordovician Yeoman Formation (Saskatchewan, Canada)

Table 1.1: Classification of biogenic permeability. The examples highlighted in grey (i.e., weakly, cryptic and diagenetic) form the foundation for this thesis and are evaluated in detail in Chapters 2, 4, 5, and 6. Table modified after Gingras and Pemberton (2005) and Gingras et al. (2012).

they are spatially complex and very difficult to image and model (Gingras et al., 1999; Gingras et al., 2002a; Gingras et al., 2002b; Bednarz and McIlroy, 2012; Knaust, 2012; Chapters 2 and 5 in this thesis). As a result, important parameters such as bioturbation intensity, burrow connectivity, burrow surface area, burrow architecture, and burrow-associated diagenesis are studied in this thesis to better understand their influence on reservoir quality.

1.2 ORGANIZATION OF THESIS

In this thesis, an expansion of the weakly defined, cryptic, and diagenetic textural hetergenity concepts presented by Pemberton and Gingras (2005) are completed using subsurface examples from western Canada and offshore Norway. This thesis is divided into seven chapters (including introduction and conclusion) that examines the value of using ichnology, sedimentology, and geochemistry to evaluate reservoir quality. A paper-based format was chosen to simplify publication of each chapter into peer-reviewed journals. As a result, some replication of data occurs in this thesis in order to provide the necessary context for each chapter. The subject of each chapter is outlined below.

Chapter 2 examines the advantage of using X-ray microtomography (micro-CT) to evaluate porosity and permeability contrasts in bioturbated reservoir strata in two- and three-dimensions (2D and 3D). Case studies from subsurface reservoirs in offshore Norway (i.e., Ula Formation, Lysing Formation, and Nise Formation)

and Western Canada (i.e., Debolt Formation, Wabamun Group, and Medicine Hat Member) are used as examples. Core analysis, spot-permeametry measurements, and petrographic thin-sections of the six different case studies show that the trace fossils modify the permeability and porosity of the reservoir through sediment reworking and diagenesis of the sediment. As such, micro-CT images are integrated in this chapter with sedimentological and petrographic data to identify the trace fossils and matrix in 2D cross-sections. When processed into 3D volumes, the micro-CT images help show the complexity in burrow connectivity and burrow orientations within a core sample. More importantly, the 3D volumes help show the distribution of porosity that can be linked to measured permeability values within a bioturbated core sample. It is from these 3D volumes that a more thorough quantification of reservoir and resource quality can be made.

Chapter 3 examines core samples recovered from the Upper Jurassic Ula Formation in the Norwegian North Sea. Two reoccurring facies associations- offshore and shoreface- are recognized within the cored intervals. The facies observed within the offshore setting were characterized by massive to finely laminated silts and silty shale. Bioturbation intensity was moderate to high and dominated by deposit-feeding structures (e.g., *Planolites*, *Phycosiphon*, *Thalassinoides*). It is believed that heightened wave currents generated through storm events precluded the development of grazing behaviors. Trace fossil suites found within the shoreface display low- to moderate-diversity and dominance of dwelling-structures. The occurrence of higher-energy events, such as hurricanes, is believed to have precluded the development of diverse communities within these shoreface environments. Based on these results, it is concluded that the Ula Formation represents a storm-influenced shoreface succession. As such, the potential to better characterize the paleogeography of complex successions, such as the Ula Formation, is greatly improved through the addition of ichnofossil data.

Chapter 4 examines the influence of bioturbation on porosity and permeability distribution within the Upper Jurassic Ula Formation of the Norwegian North Sea. Core analysis, spot-permeametry measurements, and petrographic thin-sections show that the burrows enhance the porosity and permeability within the shoreface facies association outlined in Chapter 3. The resulting enhancement in permeability resulted in the formation of a dual-porosity fabric. Using this data, the first detailed analysis of a dual-porosity biogenic flow media is completed using numerical models. Moreover, a new conceptual framework for assigning bulk permeability to bioturbated reservoir media is presented. Evaluation of the bioturbated units

is completed using arithmetic, harmonic, and geometric numerical models. The arithmetic mean characterized intervals dominated by high bioturbation intensities or horizontal to sub-vertical burrows. The harmonic mean characterized intervals with low bioturbation intensities or vertical burrows. Because the arithmetic and harmonic mean represent end-member numerical calculations, the geometric mean best characterized intervals where vertical and horizontal permeabilities were roughly equal (e.g., cryptic bioturbation). At extreme bioturbation intensities (greater than roughly 80% bioturbation), isotropic flow units begin developing irrespective of the burrow orientation. The arithmetic and harmonic means therefore become roughly equivalent to the geometric mean at extreme bioturbation intensities.

Chapter 5 examines the influence of bioturbation on permeability distribution within the Upper Devonian Wabamun Group of western Canada. Core analysis, spot-permeametry measurements, and petrographic thin-sections show that the dolomitized burrows enhance the bulk permeability of the reservoir. Because the adjacent lime mudstone-wackestone matrix is of low permeability (i.e., less than 1 mD), the higher permeable burrows (1 to 350 mD) form the primary fluid flow pathways. As such, Ichnofossil Hosted Tight Gas (IHG) is a new term introduced in Chapter 5 to demarcate tight gas reservoirs wherein natural gas is produced primarily from the burrows. Moreover, a new conceptual framework for assessing fluid flow within IHG reservoirs is presented in Chapter 5. 2D and 3D images generated by the micro-CT and helical-CT show that the burrows within the Wabamun Group are commonly horizontal and contain a highly variable range of dimensions and volumes. Numerical models show that the bulk reservoir permeability is influenced by the volume of bioturbation and magnitude of permeability difference between the burrows and matrix. Within dual-porosity models, bulk permeability is best estimated using the geometric mean at low to moderate volumes of burrow dolomite (25 to 65%) and arithmetic mean at high volumes of burrow dolomite (65 to 80%). Within dual-permeability models, bulk permeability is best estimated using the geometric mean at low to moderate volumes of burrow dolomite (10 to 50%) and arithmetic mean at moderate to high volumes of burrow dolomite (50 to 80%).

Chapter 6 examines the role burrows have in mediating dolomitization within the Mississippian Debolt Formation of western Canada. Core analysis and petrographic thin-sections show that the depositional setting is a carbonate ramp that includes sub-environments such as sabkhas, hypersaline lagoons, restricted subtidal lagoons, intertidal mud flats, and peloidal shoals. Bioturbation within the lagoonal settings is typically suppressed and expressed dominantly as monospecific

assemblages of either *Planolites* or *Chondrites*. Physico-chemical stresses, such as reduced oxygen and fluctuating salinities, are therefore prevalent within these settings. Isotopically, the Debolt Formation provides an ideal example of early dolomitization occurring within a sabkha setting. However, burrow-mediated dolomitization is being asserted in Chapter 6 as an *additional* dolomite-promoting mechanism. This is because the compositional differences observed in the stable isotopic distributions reflect the different biogeochemical processes occurring within and adjacent to the burrows. The isotopic values for calcite values within and adjacent to dolomitized burrows follow a linear trend on a $\delta^{13}C$ versus $\delta^{18}O$ plot. Dolomite values within the burrows plot into two distinct zones either above or below the calcite linear trend. Dolomite that is $\delta^{13}C$ enriched relative to calcite is interpreted to be formed in a zone of methanogenesis. The vast majority of dolomite values measured, however, are depleted in $\delta^{13}C$ relative to average calcite values. This amount of isotopic depletion is similar to samples that are measured in laboratory and field-based studies where dolomite has been found in association with bacterial sulfate reduction coupled to the oxidation of organic carbon (Vasconcelos et al., 1995; Mazzullo, 2000). High organic content, an essential component for bacterial sulfate reduction and subsequent near-surface dolomitization, was likely derived in part from the organisms and their by-products (e.g., burrow wall linings).

In summary, the data presented in this thesis is intended to provide a more thorough examination of the biogenic permeability domains outlined by Pemberton and Gingras (2005). Within this thesis, conventional techniques such as core analysis and thin sections were used as an underpinning to developing a stronger understanding of the sedimentary environments and depositional setting associated with each case study. This was critical as it helped form the foundation for subsequent reservoir modeling (e.g., Dreyer, 1990; Castle et al., 2004; La Croix et al., 2013). At the facies level, distinguishing between different bedding layers within each case study was essential to properly understanding the interlocking flow units contained within the reservoir. It was from these core evaluations that a more accurate assessment of biogenic permeability domains could be obtained using techniques such as micro-CT, helical-CT, spot-permeametry, and numerical modeling. The petrophysical evaluation of biogenic permeability modification is evaluated in both carbonates and siliciclastics using conceptual models and tangible examples from producing oil and natural gas fields. Key diagenetic models are also introduced and discussed for the Debolt Formation in order to help better explain burrow-dolomite successions within the geological rock record.

1.3 REFERENCES CITED

Angulo, S., and Buatois, L.A., 2012, Integrating depositional models, ichnology, and sequence stratigraphy in reservoir characterization: The middle member of the Devonian-Carboniferous Bakken Formation of subsurface southeastern Saskatchewan revisited: American Association of Petroleum Geologists Bulletin, v. 96, p. 1017-1043.

Baniak, G.M., and Gingras, M.K., and Pemberton, S.G., in press, Reservoir characterization of burrow-associated dolomites in the Upper Devonian Wabamun Group, Pine Creek Gas Field, central Alberta, Canada: Marine and Petroleum Geology.

Bardi, U., 2009, Peak oil: The four stages of a new idea: Energy, v. 34, p. 323-326.

Bastardie, F., Capowiez, Y., de Dreuzy, J.R., and Cluzeau, D., 2003, X-ray tomographic and hydraulic characterization of burrowing by three earthworm species in repacked soil cores: Applied Soil Ecology, v. 24, p. 3-16.

Bednarz, M., and McIlroy, D., 2012, Effect of phycosiphoniform burrows on shale hydrocarbon reservoir quality: American Association of Petroleum Geologists Bulletin, v. 96, p. 1957-1980.

British Petroleum (BP) Energy., 2012, BP Statistical Review of World Energy June 2012: Available at http://bp.com/statisticalreview (Accessed on March 26, 2013).

Bromley, R.G., 1996, Trace Fossils: Biology, Taphonomy and Applications, Second Edition. Chapman and Hall, London, United Kingdom, 361 p.

Castle, J.W., Molz, F.J., Lu, S., and Dinwiddie, C.L., 2004, Sedimentology and fractal-based analysis of permeability data, John Henry Member, straight Cliffs Formation (Upper Cretaceous), Utah, U.S.A.: Journal of Sedimentary Research, v. 74, p. 270-284.

Cunningham, K.J., Sukop, M.C., Huang, H., Alvarez, P.F., Curran, H.A., Renken, R.A., and Dixon, J.F., 2009, Prominence of ichnologically influenced macroporosity in the karst Biscayne aquifer: Stratiform "super-K" zones: Geological Society of America Bulletin, v. 121, p. 164-180.

Cunningham, K.J., Sukop, M.C., and Curran, H.A., 2012, Carbonate aquifers: *in* Knaust, D., and Bromley, R.G., eds., Trace Fossils as Indicators of Sedimentary Environments. Developments in Sedimentology 64, Amsterdam, Elsevier, p. 869-896.

Dafoe, L.T., Gingras, M.K., and Pemberton, S.G., 2010, Wave-influenced deltaic sandstone bodies and offshore deposits in the Viking Formation, Hamilton Lake area, south-central Alberta, Canada: Bulletin of Canadian Petroleum Geology, v. 58, p. 173-201.

Dreyer, T., Scheie, A., and Walderhaug., O., 1990, Minipermeameter-based study of permeability trends in channel sand bodies: American Association of Petroleum Geologists Bulletin v. 74, p. 359-374.

Friedrichs, J., 2010, Global energy crunch: How different parts of the world would react to a peak oil scenario: Energy Policy, v. 38, p. 4562-4569.

Gingras, M.K., Pemberton, S.G., Mendoza, C.A., and Henk, F., 1999, Assessing the anisotropic permeability of *Glossifungites* surfaces: Petroleum Geoscience, v. 5, p. 349-357.

Gingras, M.K., MacMillan, B., Balcom, B.J., Saunders, T., and Pemberton, S.G., 2002a, Using magnetic imaging and petrographic techniques to understand the textural attributes and porosity distribution in *Macaronichnus*-burrowed sandstone: Journal of Sedimentary Research, v. 72, p. 552-558

Gingras, M.K., MacMillan, B., and Balcom, B.J., 2002b, Visualizing the internal physical characteristics of carbonate sediments with magnetic resonance imaging and petrography: Bulletin of Canadian Petroleum Geology, v. 50, p. 363-369.

Gingras, M.K., Mendoza, C., and Pemberton, S.G., 2004, Fossilized worm-burrows influence the resource quality of porous media: American Association of Petroleum Geologists Bulletin, v. 88, p. 875-883.

Gingras, M.K., Bann, K.L., MacEachern, J.A., Waldron, J., and Pemberton, S.G., 2007, A conceptual framework for the application of trace fossils: *in* MacEachern, J.A., Bann, K.L., Gingras, M.K., and Pemberton, S.G., eds., Applied Ichnology. Society of Economic Paleontologists and Mineralogists (SEPM), Short Course Notes, no. 52, p. 1-26.

Gingras, M.K., Baniak, G., Gordon, J., Hovikoski, J., Konhauser, K.O., La Croix, A., Lemiski, R., Mendoza, C., Pemberton, S.G., Polo, C., and Zonneveld, J.-P., 2012, Porosity and permeability in bioturbated sediments: *in* Knaust, D., and Bromley, R.G., eds., Trace Fossils as Indicators of Sedimentary Environments. Developments in Sedimentology 64, Amsterdam, Elsevier, p. 837-868.

Gingras, M., Angulo, S., and and Buatois, L., 2013, Biogenic permeability in the Bakken Formation: American Association of Petroleum Geologists Annual Convention (Pittsburgh, Pennsylvania), Search and Discovery Article # 90163.

Gordon, J.B., Pemberton, S.G., Gingras, M.K., and Konhauser, K.O., 2010, Biogenically enhanced permeability: A petrographic analysis of *Macaronichnus segregatus* in the Lower Cretaceous Bluesky Formation, Alberta, Canada: American Association of Petroleum Geologists Bulletin, v. 94, p. 1779-1795.

Green, M.A., Aller, R.C., and Aller, J.Y., 1992, Experimental evaluation of the influences of biogenic reworking on carbonate preservation in nearshore sediments: Marine Geology, v. 107, p. 175-181.

Hubbert, M.K., 1956, Nuclear Energy and the Fossil Fuels (Shell Development Company, Exploration and Production Research Division): *in* American Petroleum Institute, Drilling and Production Practice. Proceedings of Spring Meeting, San Antonio, Texas, no. 95, 40 p.

Katrak, G., and Bird, F.L., 2003, Comparative effects of the large bioturbators, *Trypaea australiensis* and *Heloecius cordiformis*, on intertidal sediments of Western Port, Victoria, Australia: Marine and Freshwater Research, v. 54, p. 701-708.

Keswani, A.D., 1999, An integrated ichnological perspective for carbonate diagenesis: University of Alberta M.Sc. Thesis, Unpublished, 124 p.

Knaust, D., 2009, Ichnology as a tool in carbonate reservoir characterization: A case study from the Permian-Triassic Khuff Formation in the Middle East: GeoArabia, v. 14, p. 17-38.

Knaust, D., 2012, Methodology and techniques: *in* Knaust, D., and Bromley, R.G., eds., Trace Fossils as Indicators of Sedimentary Environments. Developments in Sedimentology 64, Amsterdam, Elsevier, p. 245-271.

La Croix, A.D., Gingras, M.K., Dashtgard, S.E., and Pemberton, S.G., 2012, Computer modeling bioturbation: the creation of porous and permeable fluid-flow pathways: American Association of Petroleum Geologists Bulletin, v. 96, p. 545-556.

La Croix, A.D., Gingras, M.K., Pemberton, S.G., Mendoza, C.A., MacEachern, J.A., and Lemiski, R.T., 2013, Biogenically enhanced reservoir properties in the Medicine Hat Gas Field, Alberta, Canada: Marine and Petroleum Geology, v. 43, p. 464-477.

Lemiski, R.T., Hovikoski, J., Pemberton, S.G., and Gingras, M., 2011, Sedimentological, ichnological and reservoir characteristics of the low-permeability, gas-charged Alderson Member (Hatton gas field, southwest Saskatchewan): Implications for resource development: Bulletin of Canadian Petroleum Geology, v. 59, p. 27-53.

Lindsay, R.F., Cantrell, D.L., Hughes, G.W., Keith, T.H., Mueller III, H.W., and Russell, S.D., 2006, Ghawar Arab-D reservoir: Widespread porosity in shoaling-upward carbonate cycles, Saudi Arabia: *in* Harris, P.M., and Weber, L.J., eds., Giant Hydrocarbon Reservoirs of the World: From Rocks to Reservoir Characterization and Modeling. American Association of Petroleum Geologists, Memoir no. 88, Society of Economic Paleontologists and Mineralogists (SEPM) Special Publication, p. 97-147.

MacEachern, J.A., Zaitlin, B.A., and Pemberton, S.G., 1999, A sharp-based sandstone of the Viking Formation, Joffre Field, Alberta, Canada: Criteria for recognition of transgressively incised shoreface complexes: Journal of Sedimentary Research, v. 69, p. 876-892.

Mazzullo, S.J., 2000, Organogenic dolomitization in peritidal to deep-sea sediments: Journal of Sedimentary Research, v. 70, p. 10-23.

McKinley, J.M., Lloyd, C.D., and Ruffell, A.H., 2004, Use of variography in permeability characterization of visually homogeneous sandstone reservoirs with examples from outcrop studies: Mathematical Geology, v. 36, p. 761-779.

Meadows, P.S., and Tait, J., 1989, Modification of sediment permeability and shear strength by two burrowing invertebrates: Marine Biology, v. 101, p. 75-82.

Newman, P., Beatley, T., and Boyer, H., 2009, Resilient Cities: Responding to Peak Oil and Climate Change. Island Press, Washington D.C., United States, 184 p.

Odedra, A., Burley, S.D., Lewis, A., Hardman, M., and P. Haynes, 2005, The world according to gas: *in* Doré, A. G., and Vining, B.A., eds., Petroleum Geology: North-West Europe and Global Perspectives: Proceedings of the 6th Petroleum Geology Conference. Geological Society, London, p. 571-586.

Pemberton, S.G., and Gingras, M.K., 2005, Classification and characterizations of biogenically enhanced permeability: American Association of Petroleum Geologists Bulletin, v. 89, p. 1493-1517.

Pemberton, S.G., Flach, P.D., and Mossop, G.D., 1982, Trace fossils from the Athabasca Oil Sands, Alberta, Canada: Science, v. 217, p. 825-827.

Pemberton, S.G., Spila, M., Pulham, A.J., Saunders, T., MacEachern, J.A., Robbins, D., and Sinclair, I.K., 2001, Ichnology and Sedimentology of Shallow to Marginal Marine Systems: Ben Nevis and Avalon Reservoirs, Jeanne D'Arc Basin. Geological Association of Canada, St. John's, Newfoundland, 343 p.

Pemberton, S.G., MacEachern, J.A., Gingras, M.K., and Saunders, T.D.A., 2008, Biogenic chaos: Cryptobioturbation and the work of sedimentologically friendly organisms: Palaeogeography, Palaeoclimatology, Palaeoecology, v. 270, p. 273-279.

Polo, C., 2013, Bioturbation and resource quality: A case study of the Upper Cretaceous Lysing and Nise Formations, Ellida and Midnatsoll fields area, Norwegian Sea: University of Alberta M.Sc. Thesis, Unpublished, 155 p.

Ranger, M.J., and Pemberton, S.G., 1992, The sedimentology and ichnology of estuarine point bars in the McMurray Formation of the Athabasca oil sands deposit, north-eastern Alberta, Canada: *in* Pemberton, S.G., ed., Applications of Ichnology to Petroleum Exploration. Society of Economic Paleontologists and Mineralogists (SEPM), Core Workshop, no. 17, Calgary, Alberta, p. 401-421.

Ranger, M.J., and Gingras, M.K., 2005, Geology of the Athabasca Oil Sands: Field Guide and Overview, Fifth Edition. Canadian Society of Petroleum Geologists, 123 p.

Raychaudhuri, I., Brekke, H.G., Pemberton, S.G., and MacEachern, J.A., 1992, Depositional facies and trace fossils of a low wave energy shoreface succession, Albian Viking Formation, Chigwell Field, Alberta, Canada: *in* Pemberton, S.G., ed., Applications of Ichnology to Petroleum Exploration. Society of Economic Paleontologists and Mineralogists (SEPM), Core Workshop, no. 17, Calgary, Alberta, p. 319-337.

Robelius, F., 2007, Giant oil fields- The highway to oil: Giant oil fields and their importance for future oil production: Uppsala University PhD Thesis, Unpublished, 168 p.

Spila, M.V., Pemberton, S.G., Rostron, B., and Gingras, M.K., 2007, Biogenic textural heterogeneity, fluid flow and hydrocarbon production: Bioturbated facies Ben Nevis Formation, Hibernia field, offshore Newfoundland: *in* MacEachern, J.A., Bann, K.L., Gingras, M.K., and Pemberton, S.G., eds., Applied Ichnology. Society of Economic Paleontologists and Mineralogists (SEPM), Short Course Notes, no. 52, p. 363-380.

Swart, P.K., Cantrell, D.L., Westphal, H., Handford, C.R., and Kendall, C.G., 2005, Origin of Dolomite in the Arab-D Reservoir from the Ghawar Field, Saudi Arabia: Evidence from petrographic and geochemical constraints: Journal of Sedimentary Research, v. 75, p. 476-491.

Tonkin, N.S., McIlroy, D., Meyer, R., and Moore-Turpin, A., 2010, Bioturbation influence on reservoir quality: A case study from the Cretaceous Ben Nevis Formation, Jeanne d'Arc Basin, offshore Newfoundland, Canada. American Association of Petroleum Geologists Bulletin, v. 94, p. 1059-1078.

United States Department of Energy/Energy Information Agency (DOE/EIA)., 2010, International Energy Outlook 2010. Report DOE/EIA-0484 (2010), 328 p.

Vasconcelos, C., McKenzie, J.A., Bernasconi, S., Grujic, D., and Tien, A.J., 1995, Microbial mediation as a possible mechanism for natural dolomite formation at low temperatures: Nature, v. 377, p. 220-222.

Weber, K.J., 1982, Influence of common sedimentary structures on fluid flow in reservoir models: Journal of Petroleum Technology, v. 34, p. 665-672.

Zonneveld, J.-P., and Gingras, M., 2012, The role of bioturbation in permeability distribution in the Upper Montney Formation, Northeastern British Columbia: American Association of Petroleum Geologists Annual Convention (Long Beach, California), Search and Discovery Article # 90142.

CHAPTER 2: ASSOCIATING X-RAY COMPUTED MICROTOMOGRAPHY (MICRO-CT) WITH POROSITY AND PERMEABILITY CONTRASTS IN BIOTURBATED MEDIA*

2.1 INTRODUCTION

The study of trace fossils has a long and rich history, dating back to first drawings of *Paleodictyon* by Leonardo di Vinci in the early 16th century (Baucon, 2010). Using the pioneering work of ichnologists such as Rudolf Richter, Adolf Seilacher, Walter Häntzschel, and Robert Frey as a foundation, ichnologists have strived to understand and visualize the character of trace fossils in two- and three-dimensions (2D and 3D). Several approaches have successfully addressed this problem, including: (1) resin-casting of modern burrow networks (Shinn, 1968; Pemberton et al., 1976; Gingras et al., 2002a), (2) radiographs of bioturbation in soft sediments (Howard, 1968; Howard and Frey, 1973; Migeon et al., 1999), and (3) serial slabbing rock or sediment (Genise and Laza, 1998; Garton and McIlroy, 2006; Naruse and Nifuku, 2008; Bednarz and McIlroy, 2009).

More recently, issues such as the spatial distribution of burrow porosity (Gingras et al., 2002b; Gingras et al., 2002c; Bednarz and McIlroy, 2012) and burrow permeability (Spila et al., 2007; Tonkin et al., 2010; Lemiski et al., 2011; La Croix et al., 2013) in 2D and 3D have been studied. These properties are important emerging topics because bioturbation has been shown to have the ability to impact the values and distribution of porosity and permeability within aquifers and reservoirs (Pemberton and Gingras, 2005; Gingras et al., 2007a; Knaust, 2009a; Cunningham et al., 2012; Gingras et al., 2012; and references therein). Biogenic modifications of the substrate can result in the development of dual-porosity or dual-permeability flow networks or both (Gingras et al., 2004; Pemberton and Gingras, 2005; Gingras et al., 2007a). Dual-porosity and dual-permeability systems are defined herein by permeability values that differ by less than, or greater than two orders of magnitude between the burrow and the rock or sediment matrix, respectively.

X-ray computed microtomography (micro-CT) is introduced as a useful technique to study bioturbation and its impact on reservoir and resource quality. First used in the early 1980's to study gastropods (Elliott and Dover, 1982), micro-CT has emerged as valuable geologic tool for the imaging and analysis of

* A version of this chapter has been submitted for publication in *Geosphere* as "Associating X-ray Microtomography with Porosity and Permeability Contrasts in Bioturbated Media" by Greg M. Baniak, Andrew D. La Croix, Camilo A. Polo, Tiffany L. Playter, S. George Pemberton, and Murray K. Gingras.

micro-features. Examples include high-resolution 3D scanning of paleontological specimens (Dierick et al., 2007; Garwood and Sutton, 2010; Pakhnevich, 2010), analysis of bioerosion by sponges (Beuck et al., 2007; Schönberg and Shields, 2008), examination of reservoir pore structure (Arns et al., 2005; Appoloni et al., 2007; Sarker and Siddiqui, 2009; Cnudde et al., 2011), and measurement of fracture apertures (Ketcham et al., 2010). Non-destructive imaging via micro-CT is unique in that it allows for comparisons of X-ray attenuation within a sample. Accordingly, the density and composition of the sample can be acquired, thereby permitting detailed analysis of micron- through mm-scale density heterogeneities within a sample. Through the combination of X-ray transmission with tomographical reconstruction, high-resolution 2D and 3D data of the internal microstructure of samples can be obtained. From these images, detailed reconstructions of the burrow connectivity and burrow orientations can be established. More importantly, identification of the contrasts in porosity and permeability that exist between the matrix and burrows within a sample can be accomplished.

Within this chapter, datasets from subsurface reservoir cores in western Canada (Debolt Formation, Wabamun Group, and Medicine Hat Member, Fig. 2.1A) and offshore Norway (Ula Formation, Lysing Formation, and Nise Formation, Fig. 2.1B) are used to show the utility of micro-CT in trace fossil research. Using conventional core analysis, thin sections, and spot-permeability measurements as an underpinning, the core samples are scanned using the micro-CT to highlight the variability of burrow connectivity and burrow orientations in 2D and 3D. From these processed micro-CT images, quantification of the bioturbated fabric on permeability contrasts and overall reservoir quality can be completed.

2.2 APPLICABILITY TOWARDS TRACE FOSSIL RESEARCH

Micro-CT scanners have evolved as a useful tool for study of heterogeneities within geological media. Examples include detailed visualization of small borings, burrows, pore networks, fractures, and mineral distribution within sediments and sedimentary rocks. Micro-CT permits the visualization of samples without the need for vacuums or specimen coating. With special stages, objects can be observed under external influence (i.e., loading, chemical reactions, interaction with other solids, liquids, gases). While a complete description of micro-CT scanning is beyond the scope of this paper, it is important to understand how micro-CT works and how it applies to the visualization of permeability contrasts in bioturbated media. A more comprehensive description and discussion of the theory and methodology of X-ray

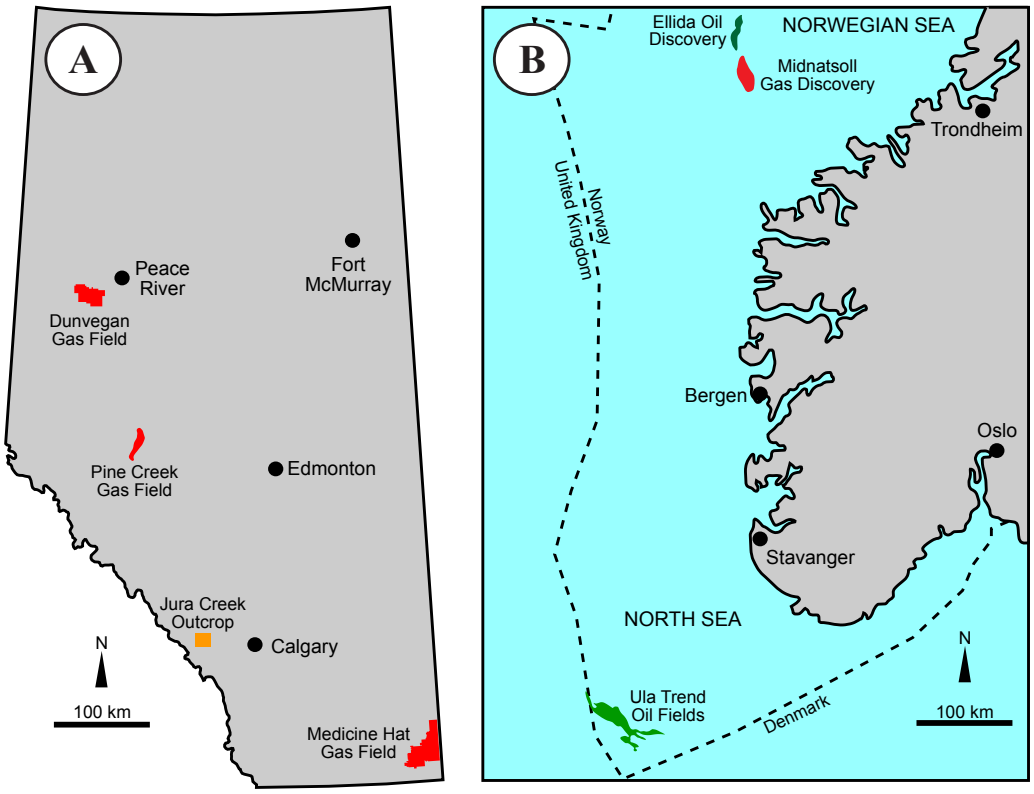

Figure 2.1: Location maps of Alberta, Canada and offshore Norway. **(A)** Location of the Pine Creek gas field (Wabamun Group), Jura Creek Outcrop (Palliser Formation), Dunvegan gas field (Debolt Formation), and Medicine Hat gas field (Medicine Hat Member) in the Canadian province of Alberta. **(B)** Location of the Ula Trend oil fields (Ula Formation), Elida oil field discovery (Lysing and Nise formations), and Midnatsoll gas field discovery (Nise Formation) in offshore Norway.

CT and its geological applications is provided by Ketcham and Carlson (2001), Akin and Kovscek (2003), and Mees et al. (2003).

2.2.1 Basic Computed Tomography (CT) Theory

Tomographic imaging consists of directing X-rays at an object at a series of angles, and using computer software to reconstruct the images into a 3D volume. To better understand the theory behind CT imaging, consider a uniform and homogenous sample. As X-rays pass through the sample, they become absorbed and turned into secondary X-rays. These secondary X-rays, commonly lower in energy, exit the sample and are measured to determine the absorption potential (i.e., attenuation) of the material. The absorptivity of a sample can be calculated from Beer-Lambert's Law:

$$\frac{I}{I_o} = \exp\,(-ux) \qquad (1)$$

where I_o is the initial X-ray intensity, μ is the linear attenuation coefficient for the

material being scanned, and x is the length of the X-ray path through the material to yield an attenuated intensity I. Equation 1, however, does not apply to porous aggregates, and thus, samples that are bioturbated. Burrowing organisms modify the chemical and physical conditions of the sedimentary environment through burrow formation, locomotion, feeding, and defecation (Gingras et al., 2007b). As a result, textural heterogeneities commonly develop within the substrate and pass into the geological record.

Due to the rearrangement of textures within bioturbated samples, care must be taken to account for how incident X-rays are attenuated along the matrix and burrow. The absorption of X-rays is a function of several physical parameters, including local density and atomic number of the material(s) (Bernard, 2005). With the advent of CT, Equation 1 was modified to allow for the estimation of the spatial variation of attenuation values along the X-ray path within a heterogeneous sample (Wildenschild et al., 2002). Accordingly, Beer-Lambert's Law becomes:

$$\frac{I}{I_o} = \exp\left[\sum_i -u_i x_i\right] \tag{2}$$

where, each increment i reflects a single material with attenuation coefficient μ_i over a linear extent x_i. The ability to discriminate between two materials with similar linear attenuation values depends on the accuracy with which differences in attenuation can be detected (Denison et al., 1997).

The X-ray linear attenuation coefficient, μ, as defined by Wellington and Vinegar (1987) and Homem et al. (2000), is a measure of the transmissivity or absorptivity of a sample to the incident X-rays. The attenuation coefficient is primarily a function of electron density, p_e, effective atomic number, Z, and photon energy of the X-ray beam, E. It can be approximated as the sum of Compton scatter and photoelectric contributions:

$$u = p_e\left(a + \frac{bZ^{3.8}}{E^{3.2}}\right) \tag{3}$$

where a (Klein–Nishina coefficient) is only weakly dependent on energy level, and b (9.8×10^{-24}) is a constant (Vinegar and Wellington, 1987). The electron density, p_e, as given by McCullough (1975), is:

$$p_e = p\left(\frac{Z}{A}\right)N_{AV} \tag{4}$$

where p is the object density, Z and A the atomic number and atomic weight, respectively, and N_{AV} is the Avogadro's number (6.022 x 10^{23}) (Wildenschild et al., 2002). For low X-ray energies of 50-100 keV used within sample imaging, X-rays interact with matter predominantly by photoelectric absorption, which is strongly dependent on the atomic number (i.e., $Z^{3.8}$) (Wellington and Vinegar, 1987; Wildenschild et al., 2002). For a mixture of atomic species, the effective atomic number, Z_e, is given by:

$$Z_e = \left(\sum f_i Z_i^{3.8}\right)^{\frac{1}{3.8}} \quad (5)$$

where f_i is the fraction of electrons on the ith atomic species and Z_i is the atomic number of the ith element (Wellington and Vingear, 1987).

Whereas these equations are accurate strictly for low Z, they emphasize the sediment characteristics that a CT scanner can detect. With regards to micro-CT, X-ray attenuation allows for improved differentiation of trace fossils and surrounding matrix within siliciclastics and carbonates as sensitivity to bulk density (i.e., mass/volume) and sediment composition (i.e., porosity) allows for thorough examination. More so, sensitivity to Z makes it possible to detect shell fragments, iron deposits, or other heavy elements within samples even if the bulk density of these features is similar to that of the surrounding sediment.

2.3 METHODS

The core samples presented in this chapter were scanned on a SkyScan 1172 desktop X-ray microtomograph (Fig. 2.2). Micro-CT equipment comprises an X-ray point source, a rotary stage with X-Y translation, a 2D planar detector, an X-ray charge-coupled device (CCD) camera, and an external computer (data recorder). For all specimens, the X-ray point source was operated at 110 kV and 250 μA, resulting in a 5 μm focal spot. Aluminum-copper and aluminum filters were applied, when necessary, to reduce beam hardening and allow for clearer images. The rotary stage and detector were moved either closer or further away from the X-ray point source, as needed, to allow image resolutions of between 8 and 34 μm.

Transmission X-ray images were acquired as the bioturbated rock sample on the stage rotated through 180° at 0.5° increments. All the rays from one projection were recorded simultaneously with the X-ray CCD camera. In most cases, over 360 projections were recorded for each sample. Once the images were generated, the 2D cross-sectional projections were opened using NRecon software (SkyScan, 2005).

The NRecon software was used to reconstruct the images and correct for beam hardening, ring artifacts, and provide alignment optimization. The application of CT-Analyser software was then used to open the reconstructed dataset of the 2D image projections (SkyScan, 2005). Within the opened dataset, histograms of the attenuation coefficients were analyzed for each sample. From these histograms, a range of coefficients was selected to build 3D reconstructions of the sample. CT-Volume software (SkyScan, 2005) was used for the manipulation and viewing of the 3D reconstructions. CT-Volume is capable of stereo-visualization, 3D visualization, and rotating and sectioning the 3D renderings.

In many of the case studies, permeability values were obtained to correlate to the micro-CT images. The surfaces of slabbed core were divided into a grid (Dreyer et al., 1990) and permeability values were measured using a Core Laboratories PDPK 400 Pressure-Decay Profile Permeameter. Using nitrogen gas, the permeameter measures permeabilities ranging from 0.001 millidarcy (mD) to greater than 30 darcy through a probe tip (Jones, 1994; Core Laboratories Instruments, 1996; Lemiski et al., 2011; La Croix et al., 2013). Nitrogen gas injected through the probe tip is recorded as a function of time on a slabbed and cleaned core surface and the maximum pressure-decay time allowed was 30 seconds. Contour maps of the permeability measurements were generated using Surfer 9 gridding and contouring software (Rockware ®, Inc., 2009). Once generated, the permeability contours maps were edited to highlight the nature of the permeability domains within the

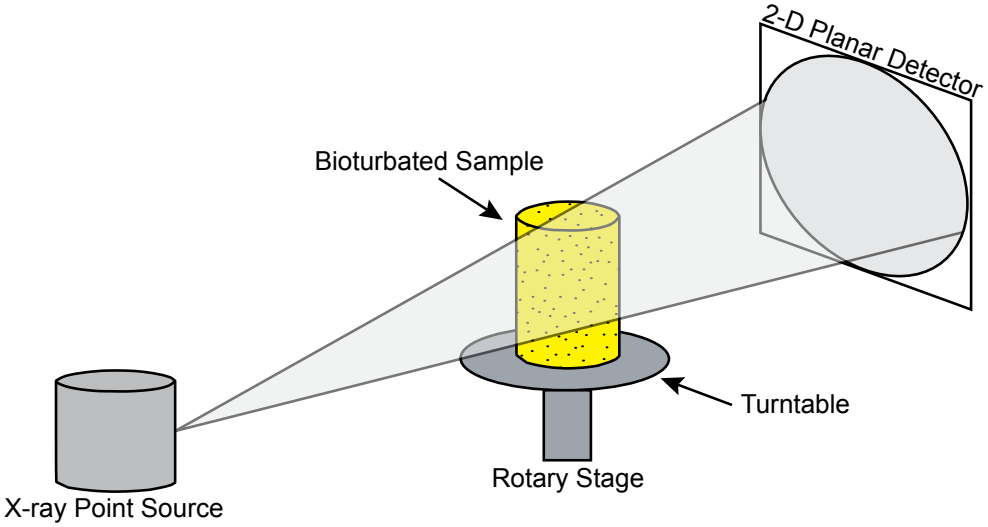

Figure 2.2: Experimental arrangement of a SkyScan 1172 desktop X-ray microtomograph. The bioturbated sample rotates on a stage between a static X-ray source and a detector. The images of the sample are acquired as a series of 2D projections. After image acquisition, NRecon software reconstructs the 2D images and corrects for issues such as beam hardening and ring artifacts. CT-Analyzer software then processes the reconstructed 2D images. CT-Volume software can then reconstruct the processed 2D images into a 3D visualization of the sample.

bioturbated intervals. Visual observation of permeability distribution within the core samples was done to identify the three highest (i.e., 100% bioturbation) and three lowest (i.e., 0% bioturbation or 100% matrix) values.

In scenarios where the slabbed cores were too large to be imaged using micro-CT, core plugs were used instead. The core plugs were drilled from the slabbed core in areas that represented the greatest permeability contrast between the burrow and matrix. The slabbed cores were also analyzed from a sedimentological and ichnological perspective, with evaluation including assessment of bioturbation intensities (BI) (Reineck, 1963; Taylor and Goldring, 1993; Bann et al., 2004), sedimentary structures, grain-size, and lithological accessories.

2.4 RESULTS

Six intervals of reservoir rock that include siliciclastics and carbonates from Alberta, Canada, and offshore Norway provide case studies that illustrate the utility of micro-CT imaging for the study of porosity and permeability contrasts in bioturbated rocks. The case studies include rock specimens from the Devonian Wabamun Group, Mississippian Debolt Formation, Jurassic Ula Formation, Cretaceous Lysing Formation, Cretaceous Nise Formation, and Cretaceous Medicine Hat Member of the Niobrara Formation.

2.4.1 Devonian Wabamun Group, West-Central Alberta, Canada

The Upper Devonian (Fammenian) Wabamun Group in the Pine Creek gas field of west-central Alberta represents a series of shallow-water carbonate platform deposits. Two reservoir facies (peloidal packstone-grainstone and bioturbated mudstone-wackestone) occur within the platform succession (see Chapter 5). The bioturbated mudstone-wackestone is composed of *Chondrites*, *Palaeophycus*, and *Thalassinoides* trace fossils. Notably, the bioturbated reservoir intervals are chaotically mottled and commonly dolomitized (Fig. 2.3A), thereby containing characteristics similar to those described by Beales (1953) and Gingras et al. (2002c) for the outcropping equivalent Upper Devonian Palliser Formation.

Spot-permeametry measurements on a slabbed core from the Wabamun Group showed that the overall permeability of the three lowest values in the matrix is 0.01 mD, and that overall permeability of the three highest values in the burrows is 297 mD (Fig. 2.3B). Within this context, the majority of the permeability within dolomitized burrows ranges from 10 and 300 mD, whereas permeability values are from 0.01 to 1.0 mD for the limestone matrix. The highly permeable burrows

thereby constitute a dual-permeability zone while the matrix represents a dual-porosity zone. These highly permeable burrows likely permitted dolomitizing fluids to move preferentially through them as opposed to the less permeable lime mud matrix during diagenesis. As a result, early dolomitization likely occurred within the burrows following sedimentation and resulted in a distinct textural heterogeneity.

Micro-CT scans of a core sample at 34 μm resolution show intricate 3D burrow fabrics where the dolomite filled burrows are distinguishable from the lime mud matrix (Fig. 2.3C). An aluminum-copper filter setting is applied during the scanning stage to better differentiate the dolomitic burrows from the calcite matrix. When viewed in 2D cross-sectional slices at various levels throughout the sample, the overall volumes of dolomite and calcite vary considerably. Corresponding 3D volumes revealed an interconnected network of burrows, with the burrow density and burrow interconnectivity varying considerably throughout the sample. These results are consistent with outcrop sections of the Palliser Formation in the mountains of western Canada (Fig. 2.3D-E). In outcrop, the Palliser Formation contains variability in burrow interconnectivity and burrow density on a decimeter to meter vertical scale over a large lateral area (10 m to kilometer scale). The contrast in permeabilities within the Wabamun Group is therefore highly variable and higher permeabilities are commonly constrained in intervals wither higher bioturbation intensities.

2.4.2 Mississippian Debolt Formation, North-Western Alberta, Canada

The Mississippian (Visean) Debolt Formation is host to between 1.2 and 1.6 trillion cubic feet (3.4×10^{10} to 4.5×10^{10} m^3) of natural gas in place within the Dunvegan gas field (Al-Aasm and Packard, 2000; Packard et al., 2004). Dolomitized trace fossils such as *Planolites*, *Chondrites*, *Quebecichnus* (Fig. 2.4A), and *Thalassinoides* are common within the lime mudstone and wackestone. Natural gas production within the Dunvegan Field occurs primarily from porous microsucrosic dolomite located within the interior of the trace fossils (Packard et al., 2004) and provides an example of a diagenetic textural heterogeneity (*sensu* Pemberton and Gingras, 2005).

Spot-permeametry measurements reveal that the dolomitized burrows have permeabilities that range from 0.05 to 0.5 mD, and the surrounding lime mud matrix has permeabilities ranging from 0.01 to 0.05 mD (Fig. 2.4B). The majority of permeability within the dolomitized burrows is between one and two orders of magnitude greater than the matrix, resulting in a dual-porosity system. When an

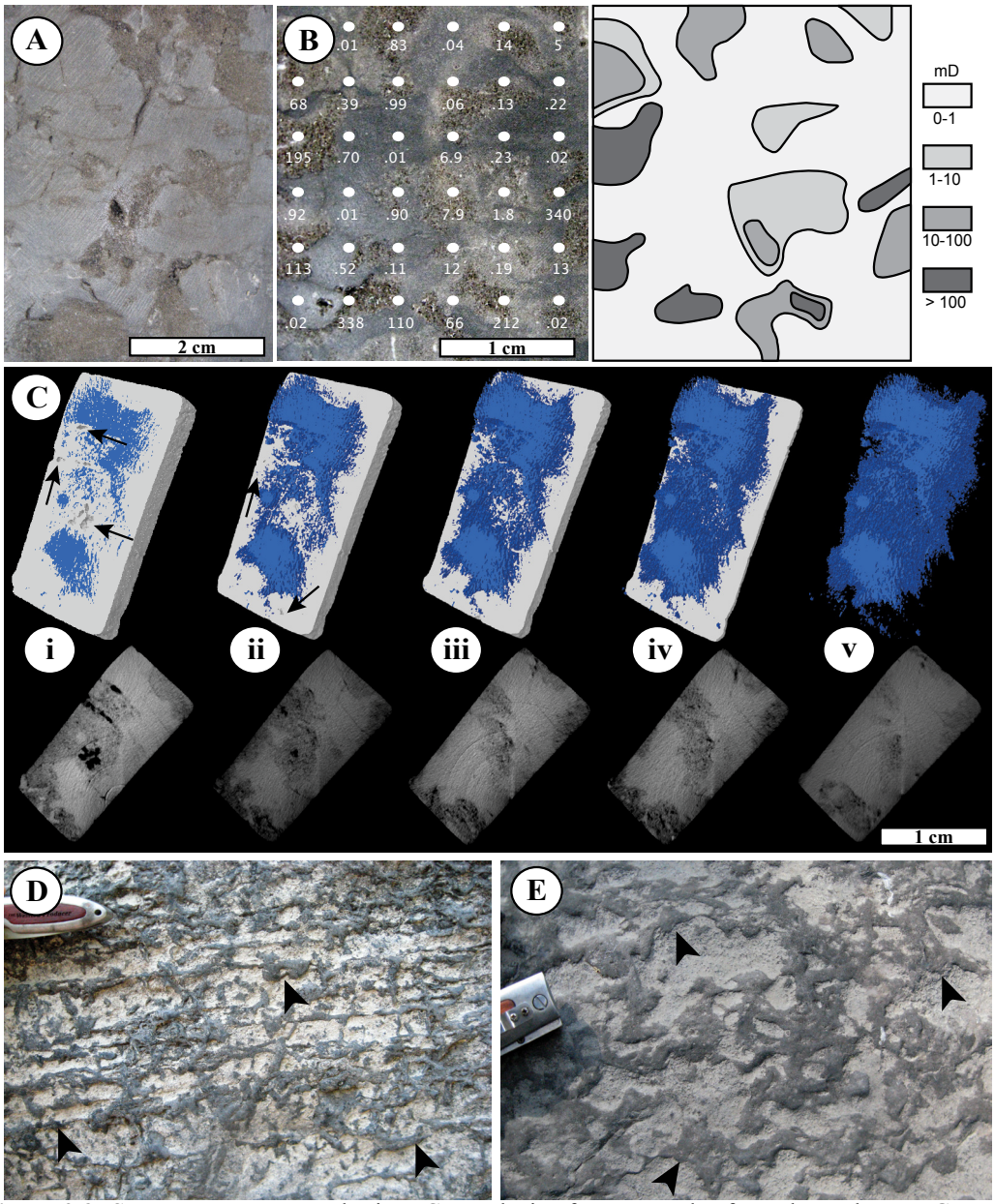

Figure 2.3: Spot-permeametry and micro-CT analysis of core samples from the Wabamun Group. **(A)** Core sample with dolomite-filled trace fossils (light brown) and non-dolomitized lime mudstone matrix (light grey). **(B)** Spot-permeametry of a core sample (left) and associated contour map (right). Note that the highest permeability values, up to 340 mD, correspond to the dolomitized trace fossils. **(C)** Example of five micro-CT scans (i to v) in 2D and corresponding 3D images at 34 µm resolution. The images at the top represent 3D visualization of mineral phases throughout the different depths of the scanned core sample. Starting from the left (i) and moving right (v), the matrix (light grey) is removed from the 3D image. As the matrix is removed, the 3D sample shows a progressive increase in burrow (blue) density and burrow interconnectivity throughout the sample. Porous vugs are represented as unfilled holes (demarcated by black arrows). The 2D cross-section images at the bottom (i to v), which correspond with the 3D images above, represent the different attenuation phases. The sample was scanned using an aluminum-copper filter, resulting in clearer definition of the dolomitic burrows (light grey), limestone matrix (dark grey), and porous vugs (black) in the 2D sections. **(D-E)** Examples of outcropping sections of the Palliser Formation from Jura Creek outcrop located in south-western Alberta, Canada (see Fig. 2.1a). Black arrows indicate the location of dolomitized burrows. The burrows generally display high density and high interconnectivity in both vertical and horizontal directions within the Palliser Formation.

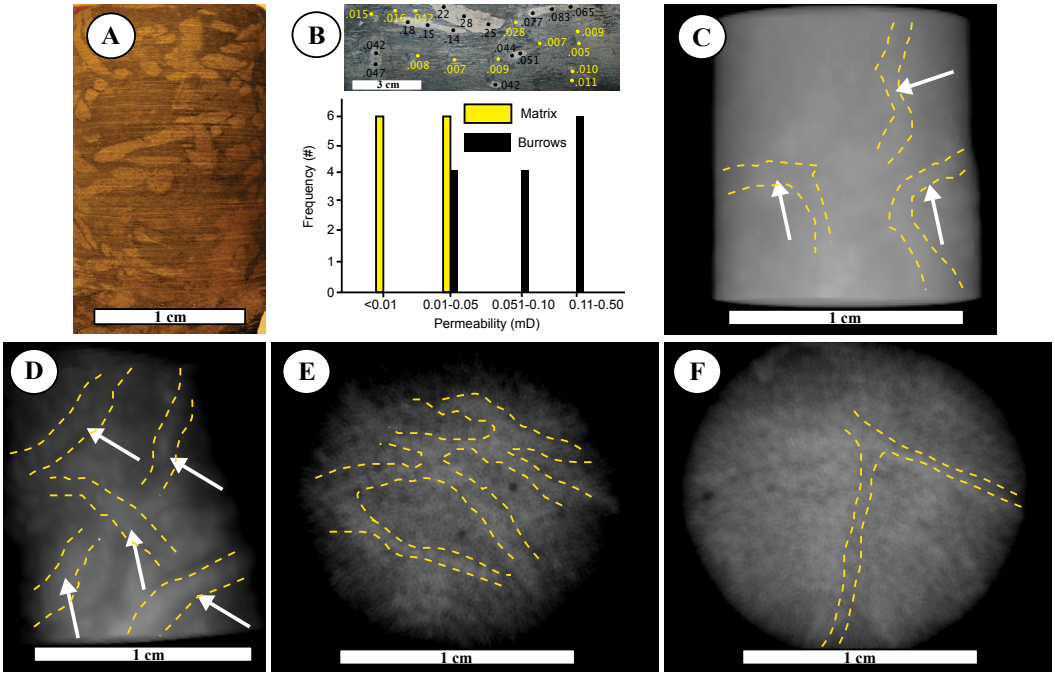

Figure 2.4: Spot-permeametry and micro-CT analysis of a core plug from the Debolt Formation. **(A)** A *Quebecichnus* bioturbated core plug with a diameter of 1.5 cm. **(B)** Spot-permeametry analysis of the dolomitized burrows (yellow) and surrounding lime mud matrix (black). As shown by the bar graph, the burrows have higher permeability values than the matrix. **(C-D)** Computer rendered 3D visualization of the entire core plug reconstructed from 2D scan data at 34 µm resolution. The *Quebecichnus* burrows appear as the faint, lighter color (white arrows and yellow hashed lines). In Fig. 2.4C, a nearly homogeneous rendering of the sample was obtained as no filters were applied during scanning. In Fig. 2.4D, Aluminum-copper filters were applied during the scanning phase, resulting in clearer delineation of the trace fossils. **(E-F)** 2D cross-sectional slices of micro-CT scans through the core plug using aluminum-copper filters. The *Quebecichnus* trace fossils (yellow hash lines) show high levels of branching and interconnectivity.

example of *Quebecichnus* trace fossils is viewed in 3D (Fig. 2.4C-D), the interaction between the trace fossils and lime mud matrix is extensive. In 2D, the *Quebecichnus* burrows are branching and highly interconnected (Fig. 2.4E-F). Due to the burrows and matrix having similar permeabilities and being interconnected throughout large sections of the sample, it is probable that both the natural gas-bearing matrix and *Quebecichnus* burrows contribute to overall natural gas deliverability within the Debolt Formation.

2.4.3 Upper Jurassic Ula Formation, North Sea, Norway

The Upper Jurassic (Kimmeridgian-Oxfordian) Ula Formation is located in the northeastern corner of the Norwegian Central Graben and is host to a number of hydrocarbon fields within the oil-rich Ula Trend (Spencer et al., 1986; Home, 1987). Representing a storm-influenced shoreface deposit (see Chapter 3), most Ula Formation oil production occurs primarily from bioturbated units that include examples of weakly defined textural heterogeneities and cryptic bioturbation (*sensu*

Pemberton and Gingras, 2005). *Ophiomorpha* and *Siphonichnus* trace fossils that are more permeable than the matrix constitute examples of weakly defined reservoir units. Cryptically bioturbated textures dominate the remaining parts of the bioturbated reservoir intervals.

Spot-permeametry measurements demonstrate that the permeability enhancement within *Ophiomorpha*-dominated sandstone intervals represents a dual-porosity network (Fig. 2.5A). Mean permeability of the three lowest values in the matrix is 20 mD, and that mean burrow permeability of the three highest values is 111 mD. Sedimentologically, the *Ophiomorpha* contains a sandstone burrow infill that occurred after deposition of the sandstone matrix. Due to the different sediment sorting and rounding characteristics between the sandstones in the burrows and matrix, a dual-porosity system formed.

Micro-CT on *Ophiomorpha* datasets at 17 μm resolution (Fig. 2.5B) using an aluminum filter revealed that greater X-ray attenuation occurred within the *Ophiomorpha* burrow wall linings and sediment infill than in the surrounding sandstone matrix (Fig. 2.5C). Petrographic analysis (Fig. 2.5D) of the core plug revealed that the burrow wall is relatively sharp lined and therefore reflective of the compaction process, wherein the pellets are amalgamated together by the organism during sedimentation (Frey et al., 1978). In 3D, the *Ophiomorpha*, and accompanying peloidal sediment, encompass a large volume within the scanned core plug (Fig. 2.5E-F). When coupled with the high level of bioturbation intensity in the Ula Formation, and overall similar lithology and permeability between the *Ophiomorpha* burrow infill and surrounding matrix, it is probable that both the *Ophiomorpha* and surrounding matrix contribute to oil production in the Ula Formation.

Analysis of cryptically bioturbated intervals within the Ula Formation showed that cryptic bioturbation did not result in the enhancement of permeabilities. Instead, cryptic bioturbation resulted in the reduction of internal heterogeneities and led to more uniform permeability distribution (Pemberton et al., 2008). To this point, micro-CT scans at 8 μm resolution using an aluminum-copper filter revealed no identifiable distinctive trace fossils in rock samples with cryptic textural heterogeneities (Fig. 2.6A). Despite no visible trace fossils, widespread, but subtle, disruptions of grain textures are visible in 2D cross-sections. When the 2D cross-sections were compared with thin sections, activity by burrowing micro-organisms appears to have improved reservoir quality by mechanically sorting the minerals by mineralogy (i.e., quartz grains preferentially) (Pemberton et al., 2008). In short,

micro-organisms commonly feed on bacteria and diatoms that preferentially adhere to sand and feldspar minerals (Mills and Maubrey, 1981; Krejci and Lowe, 1986). As a result, cryptically bioturbated intervals appear to be reworked completely without actual obliteration of the preexisting sedimentary texture when viewed in 2D (e.g.,

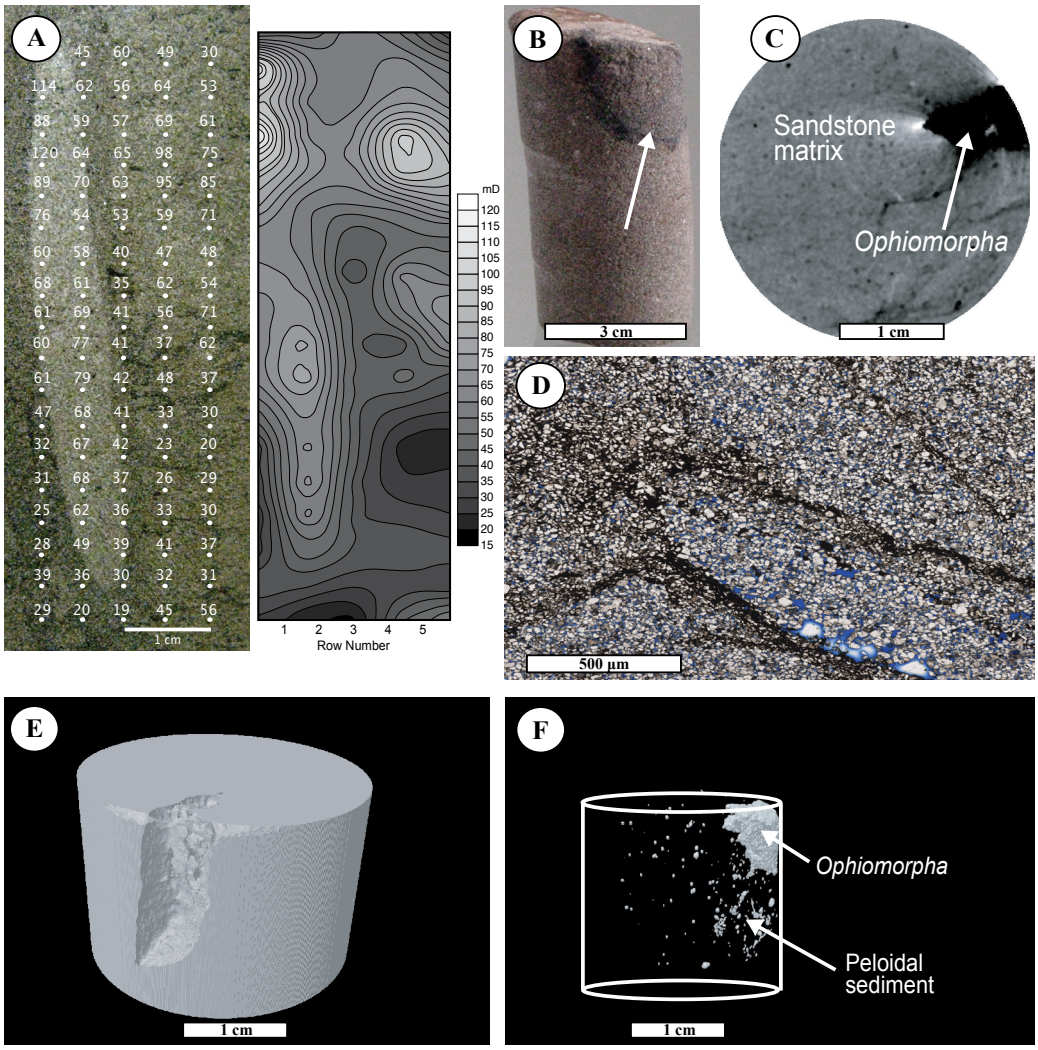

Figure 2.5: Spot-permeametry, micro-CT, and thin-section analysis of the Ula Formation. **(A)** Spot-permeametry measurements of an *Ophiomorpha nodosa* bioturbated core sample (left) and associated contour map (right). Although the burrow has higher overall permeabilities, the matrix also contributes to fluid movement within the reservoir due to high permeable conduits adjacent to the burrow. **(B)** Core plug with *Ophiomorpha* (demarcated by a white arrow). **(C)** A 2D cross-sectional slice of the core plug at 17 µm resolution using an aluminum filter. Within the cross-section, there is a clear distinction between the *Ophiomorpha* and sandstone matrix. **(D)** Photomicrograph of the *Ophiomorpha* from the core plug. Generally higher porosities occur within the *Ophiomorpha* burrow than in the surrounding matrix, as shown by a number of areas with larger pore space filled with blue epoxy. **(E)** 2D scan data reconstructed to produce a 3D visualization of the sandstone matrix. The *Ophiomorpha* was removed from the sandstone matrix to highlight the overall volume the burrow occupies within the core plug. **(F)** A 3D reconstruction of the *Ophiomorpha*, and associated peloidal sediment, without the sandstone matrix present.

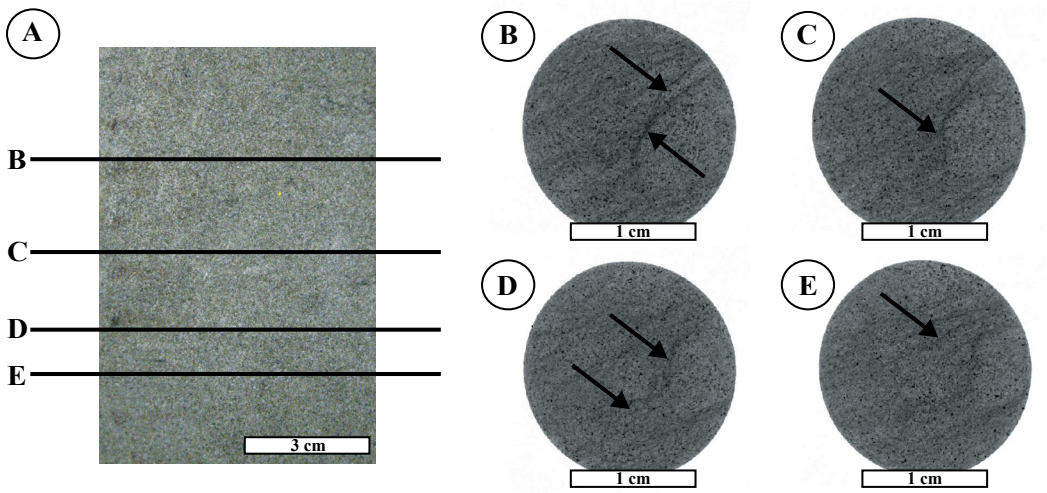

Figure 2.6: Cryptobioturbation in a core sample from the Ula Formation, including micro-CT scans at 8 µm resolution. **(A)** Photograph of slabbed core sample and the associated four areas (B-E) where cross-sectional slices were taken for 2D micro-CT analysis. From the slabbed core sample, a 1.5 cm core plug was obtained for micro-CT imaging. **(B-E)** Four 2D cross-section slices that demonstrate the overall homogenous nature of the cryptically bioturbated sample. No distinctive trace fossils are identifiable in the 2D slices. The core sample was scanned using an aluminum-copper filter, which allowed for the clarification of a few structures (black arrows) that could be attributed to possible whispy concentrations of clay.

whispy concentrations of clay) (Fig. 2.6B-D). Cryptic bioturbation therefore acts as an agent producing more homogeneous textures and uniform distribution of porosity and permeability within the Ula Formation.

2.4.4 Upper Cretaceous Lysing Formation, Norwegian Sea, Norway

The Lysing Formation is part of a thick Upper Cretaceous (Turonian-Coniacian) succession of siliciclastic sediment distributed across the Norwegian continental shelf. Within the Ellida oil field discovery area, the Lysing Formation is composed of interbedded very-fine sandstones and mudstones that contain a diverse trace fossil assemblage. The trace fossil assemblage consists of *Thalassinoides, Planolites, Scolicia, Chondrites, Ophiomorpha, Palaeophycus, Zoophycos, Helminthopsis*, and *Phycosiphon*. Less common ichnogenera include *Arenicolites*, *Skolithos*, and *Schaubcylindrichnus*. Collectively, the Lysing Formation represents deposition in a mesopelagic to bathypelagic, tectonically active setting with a steep depositional gradient (Polo, 2013).

Reservoir analysis by Polo (2013) demonstrated that coarser-grained sediment occurred preferentially within the trace fossils (*Thalassinoides*, *Planolites*) relative to the fine-grained matrix. Polo (2013) used an aluminum-copper filter setting during the micro-CT scanning phase to help differentiate the coarser-

grained sediment within the burrows from the fine-grained sand matrix. At 30 μm resolution, a dense, highly connected, horizontal to inclined burrow fabric of *Palaeophycus* and *Planolites* is rendered in 3D (Fig. 2.7A-B). The nature of the bioturbated fabric led Polo (2013) to suggest the burrow systems within the Lysing Formation are highly connected and typically parallel to the bedding plane. Vertical connectivity between the bioturbated horizons, where present, occurs through thin storm-deposited sand bodies that contain isolated vertical ichnogenera (*Skolithos*). As a result, permeability contrast between bioturbated horizons will be limited, except in the areas containing trace fossils present in storm-deposited sand bodies.

2.4.5 Upper Cretaceous Nise Formation, Norwegian Sea, Norway

The Upper Cretaceous (Campanian) Nise Formation of the offshore Norwegian continental shelf is found within the Ellida oil field discovery area and Midnatsoll natural gas discovery area. Comprised of unburrowed to completely bioturbated fine- to very-fine sandstones and mudstones, the bioturbated intervals within the Nise Formation constitute an important reservoir unit in the Møre basin (Polo, 2013) and Vøring basin (Knaust, 2009b). The bioturbated assemblages have a high diversity of ichnofauna that includes *Thalassinoides, Planolites, Nereites, Teichichnus, Asterosoma, Palaeophycus, Rhizocorallium, Phycosiphon, Zoophycos, Arenicolites, Scolicia, Rosselia, Schaubcylindrichnus, Skolithos, Helminthopsis,* and *Chondrites*. Sediment accumulation is the result of alternating fine- and coarse-grained sedimentation within an epipelagic to bathypelagic, tectonically active setting with a steep depositional gradient (Polo, 2013).

The bioturbated intervals were scanned by Polo (2013) in the micro-CT at 30 μm resolution using an aluminum-copper filter setting. Combining petrographic assessments and micro-CT scanning, Polo (2013) showed that higher permeability within the Nise Formation is influenced strongly by the location and nature of bioturbation that modified the original sediment by sediment sorting and churning. Subsequent packing of fine-grained sand as burrow infill within a low-permeability matrix resulted in a dual-porosity network. An aluminum-copper filter setting allowed Polo (2013) to identify an interconnected, horizontal burrow network within the Nise Formation that contained subordinate inclined burrows (Fig. 2.7C-D). These modifications constitute selective fluid flow pathways within the Nise Formation and are responsible for the permeability zonation within the bioturbated intervals.

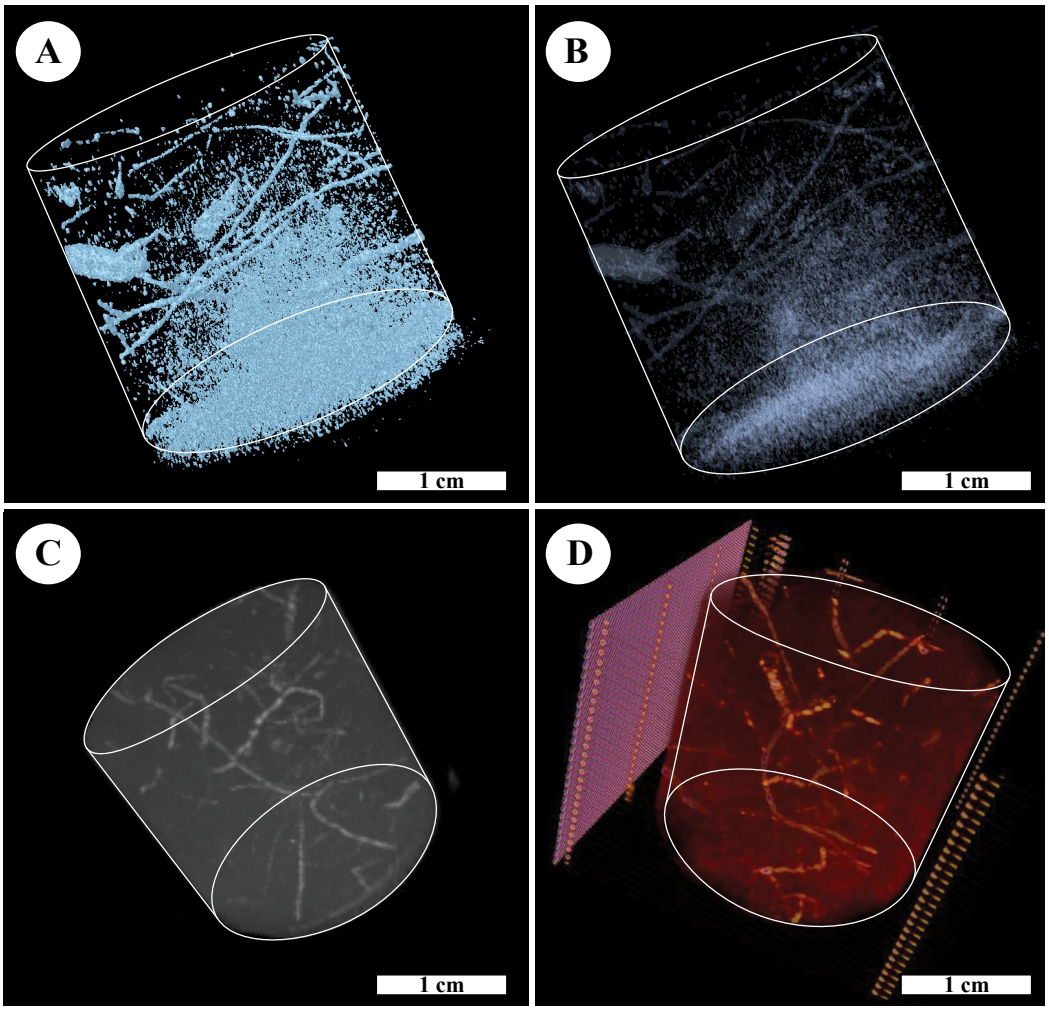

Figure 2.7: Micro-CT rendered 3D volumes for samples from the Lysing and Nise formations. **(A-B)** Micro-CT scans at 30 µm resolution for the Lysing Formation. An aluminum-copper filter setting was applied during the scanning stage that permitted the identification of the coarser-grained sediment (i.e., burrows) from the fine-grained matrix. Highlighted in blue is an intricate 3D burrow network of horizontal to inclined *Palaeophycus* and *Planolites*. **(C-D)** Micro-CT scans at 30 µm resolution using an aluminum-copper filter setting for a sample from the Nise Formation. The trace fossils within these samples are expressed in 3D as interconnected, highly irregular series of burrow networks. The trace fossils are shown as light grey and the matrix as dark grey in Fig. 2.7C. The trace fossils are shown as bright orange and the matrix as red in Fig. 2.7D.

2.4.6 Upper Cretaceous Medicine Hat Member, Alberta, Canada

The Medicine Hat Member of the Upper Cretaceous (Santonian) Niobrara Formation lies above the Verger Member and is overlain by the First White Specks Member. In the Medicine Hat gas field, the Medicine Hat Member is estimated to contain between four and six trillion cubic feet (1.13×10^{11} to 1.70×10^{11} m^3) of natural gas in place (O'Connell, 2003). La Croix et al. (2013) identified four recurring facies in the Medicine Hat Member, arranged into a progradational parasequence set consisting of five parasequences. They interpreted the four facies to represent the distal prodelta, proximal prodelta, distal delta-front, and

subaqeous interdistributary bay environments, respectively, in a wave-dominated delta complex. Within the proximal prodelta, trace fossils are commonly obscure, but where identifiable include *Planolites, Thalassinoides, Palaeophycus, Schaubcylindrichnus freyi, Phycosiphon, Skolithos, Cylindrichnus, Siphonichnus, Teichichnus, Rhizocorallium, Scolicia,* and fugichnia. Five core slabs from the proximal prodelta unit were selected for spot-permeametry and micro-CT analysis. Variability in bioturbation intensity within the sample set ranged from BI 0 to 5, thus a spectrum of non-burrow associated permeability and burrow-associated permeability was analyzed.

The spot-permeametry measurements indicate that moderately burrowed (BI 2 to 4) to burrow-homogenized (BI 5 to 6) fabrics are associated with the highest permeability values. Alternatively, non-burrowed (BI 0) layers and layers displaying low bioturbation intensity (BI 1-2) show some of the lowest permeability values. Original depositional texture is ruled out as the primary control on permeability because of the clear presence of bioturbated textures. Sedimentary structures (laminations, current or oscillation ripples) were commonly overprinted or homogenized depending upon the bioturbation intensity. The spot-permeametry analysis, combined with micro-CT imaging of the fabric, indicates that biogenic admixing of sand-sized grains into a silt- and clay-rich matrix locally increases the bulk permeability (La Croix et al., 2013). In clay-rich intervals near the base of the proximal prodelta, permeability measurements range between 0.01 to 10 mD. Within the middle of proximal prodelta, bioturbated beds that comprise sub-equal proportions of siltstone and sandstone exhibit permeability ranging between 0.2 and 68 mD. Near the top of the succession, sandy portions of the heterolithic facies exhibit permeabilities between 0.2 and 160 mD (Fig. 2.8A). These data suggest an overall upwards increase in biogenic permeability enhancement.

Micro-CT scans at 33 μm resolution demonstrated that burrowed strata were dominated by planiform zones of disrupted grain fabrics, with rare connections between these zones by vertical to inclined trace fossils (e.g., *Skolithos, Thalassinoides*). La Croix et al. (2013) concluded that biogenic heterogeneity is discontinuous, but with a planiform distribution (Fig. 2.8B-D). These results are consistent with burrows that are relatively well connected in the bedding-parallel direction. Vertical burrow interpenetrations, however, are limited and permeability fields are most likely to be strongly anisotropic with a dominant bedding-parallel flow, except in the most pervasively bioturbated horizons (Fig. 2.8E).

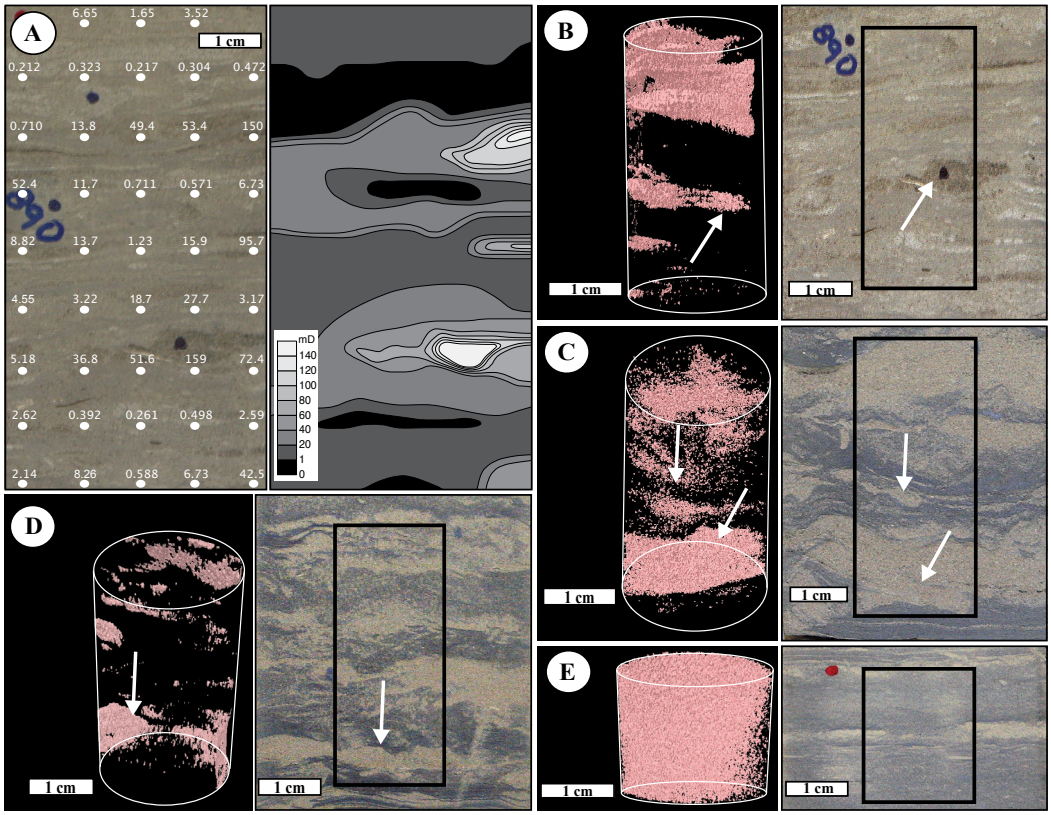

Figure 2.8: Spot-permeametry and 3D surface volumes generated images from micro-CT at 33 µm resolution for core samples (outlined in black for each core photograph in Fig. 2.8B-E) from the Medicine Hat Member. **(A)** Characterization of permeability within the sandy heterolithic facies of the proximal prodelta. On the left is a core photograph and the respective permeability values (in mD) for each measurement. On the right is a contour plot of permeability measurements throughout the core sample. The highest permeabilities, ranging up to 160 mD, correspond to the position of greatest burrow homogenization within the core sample**. (B-D)** 3D micro-CT images on the left and corresponding core photos on the right. The positions of white arrows shown in the core photos correspond to the white arrows in the 3D reconstructions. Using an aluminum-copper filter, the bioturbated horizons (shown in pink) can be seen as dominantly planiform in nature. **(E)** Example of burrow homogenization that results in isotropic porosity. Modified from La Croix et al. (2013).

2.5 DISCUSSION

Burrowing organisms modify the sediment in several ways. Among others, these include altering the original sedimentary fabric and influencing diagenetic processes (Meadows and Tait, 1989; Green et al., 1992; Bastardie et al., 2003; Katrak and Bird, 2003). Due to our lack of information regarding burrow geometry, bioturbated intervals are difficult to assess for reservoir models and fluid flow studies. These challenges underscore the importance of using micro-CT to evaluate bioturbated intervals. Using micro-CT allows for the high-resolution identification of microscale heterogeneities within small hand samples. As a result, the micro-spatial distribution of burrow infills, burrow orientation, burrow permeability, and bioturbation intensity become tractable. Consequently, these heterogeneities can be analyzed to allow for a more robust evaluation of flow-media behavior.

2.5.1 Using Micro-CT to Assess Reservoir Quality in Burrowed Media

Historically, the influence of trace fossils on reservoir quality has been overlooked in favor of more commonly understood parameters such as cementation, diagenesis, fracturing, and lithology (Weber, 1982; McKinley et al., 2004). Yet, reservoirs with trace fossils contain biogenically induced textural heterogeneities that influence the distribution and magnitude of permeability and porosity. Parameters such as bioturbation intensity, burrow connectivity, burrow surface area, burrow associated diagenesis, and burrow architecture have been identified as important features contributing to the distribution of porosity and permeability (Gingras et al., 1999; Pemberton and Gingras 2005; La Croix et al., 2012). Because burrowed fabrics are typically 3D in nature and contain a wide range of orientations (Gingras et al., 1999; McIlroy, 2007; La Croix et al., 2012), they are more spatially complex than bedded sediment and thus very difficult to image and model (Gingras et al., 1999; Gingras et al., 2002b; Gingras et al., 2002c; Knaust, 2012). These characteristics emphasize the need to visually image bioturbated fabrics in high-resolution to model the impact of trace fossils on reservoir quality.

Herein, six case studies are used to illustrate how micro-CT aids in the spatial characterization of burrow systems within subsurface reservoirs. The micro-CT sections effectively illustrate some of the morphologic characteristics of the trace fossils. For example, *Quebecichnus* exhibits branching and high interconnectivity (Fig. 2.4C-F) whereas *Planolites* are not branching and dominantly horizontally situated, and interpenetrations are comparably rare (Fig. 2.7A-B). Although discrete burrows are definable within the CT-images, individual grains or pores are not apparent. It is notable, however, that the greatest X-ray attenuations correlate to parts of the samples that have the highest measured porosities and permeabilities (i.e., burrows). Because the images represent reconstructions of the distribution of X-ray attenuations, absolute porosity is not assigned to the image signals. However, assessment of the X-ray attenuation within the samples enables evaluation of the volumes occupied by burrows and matrix, and the burrow connectivity and burrow orientations. In reservoirs where the burrows and matrix possess different petrophysical characteristics, micro-CT imaging of density and lithological contrasts between the burrow and matrix permits characterization of the permeability contrasts in 3D. As a result, an assessment of potential fluid flow and effective permeability conduits is possible.

2.5.2 Perspectives on Fluid Flow Behavior Using Integrated Micro-CT, Petrographic, and Permeability Data

Most reservoir engineers and geologists model fluid flow at the outcrop or basin scale, and therefore overlook micron- through mm-scale scale heterogeneities present within a reservoir (Pickup et al., 1995). Consequently, small-scale features such as bioturbation are commonly overlooked despite their importance to fluid flow at the mm- to meter-scale (Gingras et al., 1999; Gingras et al., 2004; Spila et al., 2007; Chapters 4 and 5). If the processes of fluid flow, reserve estimates, and field development are to be accurately modeled and understood, it is imperative that features such as bioturbation become better understood.

Within the Wabamun Group and Debolt Formation, development of permeability and porosity within the bioturbated facies is recognized as a function of primary sedimentation, chemical and physical alteration of the substrate by burrowing organisms, and facies-selective dolomitization of the burrow fabric. Physical alteration of the substrate includes modification of grain size, compaction and sorting. Chemical modification includes the concentration of organic material in the form of mucous or fecal material within the burrows (Gingras et al., 2004; Konhauser and Gingras, 2011; Petrash et al., 2011; Corlett and Jones, 2012). Together, the physical and chemical factors result in a net contribution of porosity and may contribute to the dolomitization process within the burrows. The burrows therefore comprise discrete, complex juxtaposed zones of porosity and permeability relative to the non-dolomitized matrix.

Spot-permeametry revealed the presence of a dual-permeability flow media in the Wabamun Group (Fig. 2.3B). Micro-CT renderings showed that high levels of interconnectivity occur between the burrows in 2D and 3D (Fig. 2.3C). Together, the physical, biological and chemical factors control the distribution of porosity and permeability within dolomitized burrows and can only be spatially understood using 3D imaging techniques. Due to the large contrasts in permeabilities between the burrows and matrix, fluid flow is anticipated to preferentially occur within the tortuous burrow fabrics. As a result, the burrows within the Wabamun Group might behave as potential biogenic fracture systems (Gingras et al., 1999; Pemberton and Gingras, 2005; Gingras et al., 2007a; Gingras et al., 2012). Unlike natural fracture systems, however, interconnected burrow networks have considerably larger surface areas and are therefore strongly influenced by the lower permeability matrix. In practice, resources may be produced from the matrix within the Wabamun Group through the spatially complex permeability streaks provided by the burrows.

For the Debolt Formation, spot-permeametry confirms the presence of a dual-porosity flow media. As with the Wabamun Group, the matrix permeabilities within the Debolt Formation are less than 1 mD. However, unlike the dolomitized burrows the Wabamun Group, the *Quebecichnus* burrows within the Debolt Formation have permeabilities that are similar to the surrounding matrix. Due to similar burrow and matrix permeabilities and high burrow interconnectivity within the Debolt Formation (Fig. 2.4C-F), both the natural gas-bearing matrix and *Quebecichnus* burrows likely contribute to fluid flow equally.

In the siliciclastic case studies (Ula Formation, Lysing Formation, Nise Formation, Medicine Hat Member), development of permeability and porosity within the bioturbated facies is largely a function of sediment grain-size distributions. The permeability and porosity fabrics are most dependent on trace fossil morphology, nature of burrow infill, burrow size, and overall bioturbation intensity (also see Gingras et al., 1999; Tonkin et al., 2010; La Croix et al., 2012). In the Ula Formation, clean sandstones, the permeability of which exceeds the sandstone matrix, occur with the *Ophiomorpha* burrow fills (Fig. 2.5A). Micro-CT renderings revealed that *Ophiomorpha* occupied large volumes within the scanned samples (Fig. 2.5E-F). Due to high bioturbation intensities within the Ula Formation reservoir intervals (BI 4-6), it is probable that fluid flow will occur from the matrix and burrows due to the dual-porosity nature of the reservoir.

Within the Lysing and Nise formations, sand-filled burrows (*Thalassinoides*, *Planolites*) occur within a fine- to very-fine sandstone and mudstones matrix. In 3D reconstructions for both datasets, horizontal parts of the burrow networks are interconnected (Fig. 2.7A-D). Notably, the local presence of sub-vertical to vertical burrows (e.g., *Skolithos*) suggests that permeability fields may be comparably isotropic (e.g., Weaver and Schultheiss, 1983; Gingras et al., 1999). In the Medicine Hat Member, biogenic admixing of sand-sized grains into a silt- and clay-rich matrix resulted in the localized increase in bulk permeability (Fig. 2.8A). As with the Lysing and Nise formations, the Medicine Hat Member exhibits a predominantly planiform zonation of burrow fabrics (Fig. 2.8B-D), with rare connections between the zones by vertical to inclined trace fossil forms (*Skolithos, Thalassinoides*).

These six case studies help emphasize the importance of micro-CT in understanding contrasts in porosity and permeability in bioturbated reservoirs and assessing reservoir quality. As a result, a more accurate assessment of fluid flow can be achieved through integrating permeability measurements from the spot-permeameter and ichnological data from the micro-CT.

2.5.3 Common Challenges and Solutions

One of the limitations encountered in the imaging process is the small sample size required. In order to achieve high-resolution images, optimal sample size is roughly 4 cm in height and 2 cm in diameter. Sample sizes any larger commonly result in reduced image resolution, and in most cases, are unable to fit onto the rotating stage. Unfortunately, many trace fossils, such as *Thalassinoides*, are larger than the size dimensions required for imaging. For these trace fossils, utilization of larger CT scanners, such as those used in medical research, exist as an alternative to micro-CT (see Chapter 5). Likewise, small-diameter core plugs drilled from large-diameter core or outcrop could provide data for comparative analysis of permeability and porosity distribution between the burrow and matrix. Accordingly, samples that contain small trace fossils, such as *Chondrites*, *Planolites,* and *Quebecichnus*, provide the most ideal specimens for micro-CT research.

In evaluating trace fossils, differences in attenuation coefficients between the matrix and burrow are critical towards proper identification. In scenarios where the matrix and burrow contain similar densities and compositions (e.g., arenite sandstone within the *Skolithos* trace fossil and surrounding matrix; calcified *Planolites* burrows in a limestone matrix), the X-ray attenuation for the burrow and matrix is comparable and difficult to distinguish. Therefore, the application of X-ray filters is critical to avoid issues such as beam hardening and ring artifacts that may prevent the proper identification of the trace fossils and matrix within the 2D image cross-sections.

In short, beam hardening is the preferential absorption of lower energy X-rays over higher energy X-rays at the surface of the sample (Bonse and Busch, 1996). As a result, lower-energy X-rays are preferentially absorbed in the surface layer and the rest of the higher-energy X-rays are passed through. Consequently, the surface of the sample appears more dense and interior of the sample less dense (SkyScan, 2005). Correction of beam hardening by mathematical means has proven to be difficult due to the dependency on material composition and sample thickness (Bonse and Busch, 1996). To mitigate this problem, metal filters are placed in front of the camera (Aluminum and Aluminum-Copper) during imaging. The filters absorb lower-energy X-rays and only the high-energy X-rays reach the sample (SkyScan, 2005). NRecon software is applied during the reconstruction phase of the 2D image projections to help further correct beam hardening. In case studies such as the Debolt Formation, delineation of the burrows in 2D and 3D is very difficult without the use of filters (Fig. 2.9A-B).

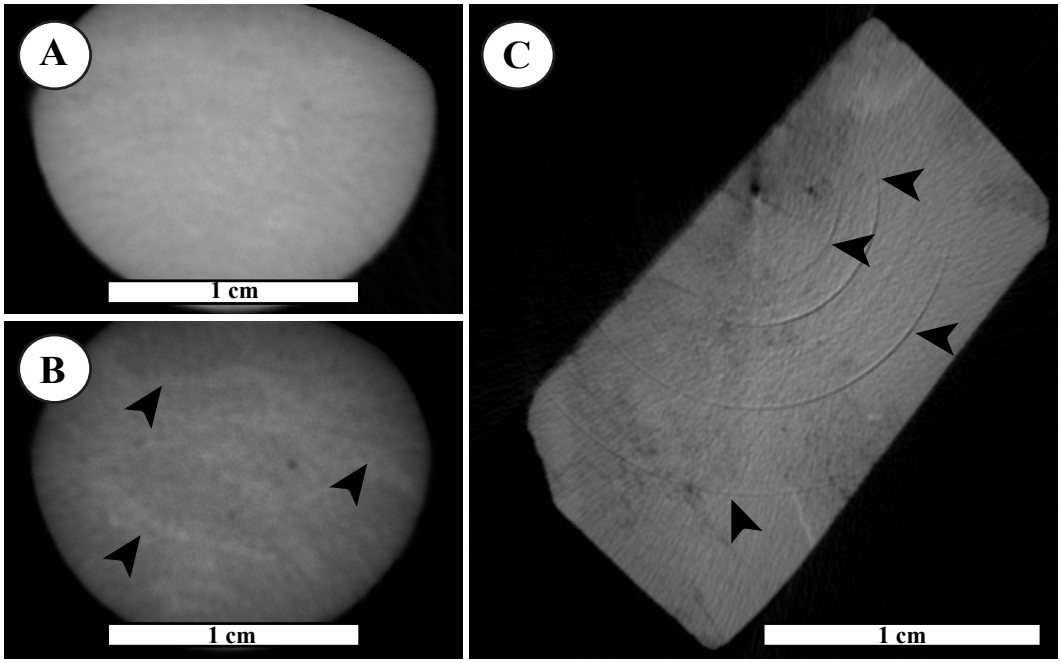

Figure 2.9: Examples of imaging artifacts. **(A)** Beam hardening in a 2D image from the Debolt Formation when no filter is applied during acquisition, resulting in a fuzzy image. **(B)** Aluminum-copper filter applied to the same sample as above, resulting in clearer sample resolution and delineation of trace fossils (black arrows). **(C)** Ring artifacts in a 2D image (black arrows).

In addition to beam hardening, additional image artifacts, such as rings, can also appear on 2D and 3D images. In short, ring artifacts are caused by imperfections within the detector absorbing the X-rays. They commonly appear on 2D images as concentric rings superimposed on the structures being sampled (Fig. 2.9C). Although many scenarios exist for the generation of ring artifacts within micro-CT imaging (Sijbers and Postnov, 2004), irregular sample shape (i.e., non-spherical) and surface roughness (i.e., sharp corners) were commonly found as external generators of ring artifacts during imaging in this study. Samples that have small thickness to width ratios (e.g., less than 0.1) are also susceptible to generating ring artifacts during imaging. Flat-field corrections applied prior to imaging of the samples help mitigate potential ring artifacts. NRecon software applied during the reconstruction phase helps alleviate the effects of ring artifacts within the samples. Special care is therefore advised during the sampling, imaging, and reconstruction process to help eliminate imaging artifacts and reduced image quality.

2.6 CONCLUSIONS

Bioturbation is a common texture in siliciclastics and carbonates and can alter the distribution and magnitude of porosity and permeability. The data presented herein show the potential of micro-CT as a tool to evaluate bioturbated reservoirs.

Samples included bioturbated carbonates and siliciclastics from western Canada and bioturbated siliciclastics from offshore Norway.

The results of the six case studies are notable because micro-CT reveals that distinct X-ray attenuations exist between the burrows and matrix. The rendered 2D and 3D visualizations show the complexity of burrow connectivity and bioturbation intensity within a sample. Perhaps more importantly, the technique is useful for identifying the contrasts in permeability between the matrix and burrows within a sample. It must be emphasized that micro-CT images represent differences in porosity associated with the burrows and matrix. In this application, higher X-ray attenuation values are calibrated to known porous zones (i.e., burrows) by integrating core data, thin sections, and spot-permeametry. By combining these data, it is possible to gain a more thorough understanding of the tortuous, heterogeneous fabrics associated with bioturbation in 2D and 3D. Furthermore, the potential impact of the bioturbated fabric on reservoir quality and fluid flow can be considered in a more robust fashion. As such, future research should focus on upscaling the burrow and matrix relationships observed at the micro-CT level to the core, well bore, and reservoir level.

2.7 REFERENCES CITED

Akin, S., and Kovscek, A.R., 2003, Computed tomography in petroleum engineering research: *in* Mees, F., Swennen, R., Van Geet, M., and Jacobs, P., eds., Applications of X-ray Computed Tomography in the Geosciences. Geological Society, London, Special Publication v. 215, p. 23-38.

Al-Aasm, I.S., and Packard, J.J., 2000, Stabilization of early-formed dolomite: A tale of divergence from two Mississippian dolomites: Sedimentary Geology, v. 131, p. 97-108.

Appoloni, C.R., Fernandes, C.P., and Rodrigues, C.R.O., 2007, X-ray microtomography study of a sandstone reservoir rock: Nuclear Instruments and Methods in Physics Research, Section A, v. 580, p. 629-632.

Arns, C., Bauget, F., Limaye, A., Sakellariou, A., Senden, T.J., Sheppard, A.P., Sok, R.M., Pinczewski, W.V., Bakke, S., Berge, L.I., Øren, P.-E., and Knackstedt, M.A., 2005, Pore-scale characterization of carbonates using X-ray microtomography: Society of Petroleum Engineers Journal, v. 10, p. 475-484.

Bann, K.L., Fielding, C.R., MacEachern, J.A., and Tye, S.C., 2004, Differentiation of estuarine and offshore marine deposits using integrated ichnology and sedimentology: Permian Pebbly Beach Formation, Sydney Basin, Australia: *in* McIlroy, D., ed., The Application of Ichnology to Palaeoenvironmental and Stratigraphic Analysis. Geological Society, London, Special Publication, v. 228, p. 179-211.

Bastardie, F., Capowiez, Y., de Dreuzy, J.R., and Cluzeau, D., 2003, X-ray tomographic and hydraulic characterization of burrowing by three earthworm species in repacked soil cores: Applied Soil Ecology, v. 24, p. 3-16.

Baucon, A., 2010, Leonardo da Vinci, the founding father of ichnology: Palaios, v. 25, p. 361-367.

Beales, F.W., 1953, Dolomitic mottling in Palliser (Devonian) Limestone, Banff and Jasper National Parks, Alberta: American Association of Petroleum Geologists Bulletin, v. 37, p. 2281-2293.

Bednarz, M., and McIlroy, D., 2009, Three-dimensional reconstruction of "Phycosiphoniform" burrows: Implications for identification of trace fossils in core: Palaeontologia Electronica, v. 12, p. 1-15.

Bednarz, M., and McIlroy, D., 2012, Effect of phycosiphoniform burrows on shale hydrocarbon reservoir quality: American Association of Petroleum Geologists Bulletin, v. 96, p. 1957-1980.

Bernard, D., 2005, 3D quantification of pore scale geometrical changes using synchrotron computed microtomography: Oil & Gas Science and Technology, v. 60, p. 747-762.

Beuck, L., Vertino, A., Stepina, E., Karolczak, M., and Pfannkuche, O., 2007, Skeletal response of *Lophelia pertusa* (Scleractinia) to bioeroding sponge infestation visualised with micro-computed tomography: Facies, v. 53, p. 157-176.

Bonse, U., and Busch, F., 1996, X-ray computed microtomography (mCT) using synchrotron radiation (SR): Progress in Biophysics and Molecular Biology, v. 65, p. 133-169.

Cnudde, V., Boone, M., Dewanckele, J., Dierick, M., Van Hoorebeke, L., and Jacobs, P., 2011, 3D characterization of sandstone by means of X-ray computed tomography: Geosphere, v. 7, p. 54-61.

Core Laboratories Instruments., 1996, Profile Permeameter PDPK-400 Operations Manual, 40 p.

Corlett, H.J., and Jones, B., 2012, Petrographic and geochemical contrasts between calcite- and dolomite-filled burrows in the Middle Devonian Lonely Bay Formation, Northwest Territories, Canada: Implications for dolomite formation in Paleozoic burrows: Journal of Sedimentary Research, v. 82, p. 648-663.

Cunningham, K.J., Sukop, M.C., and Curran, H.A., 2012, Carbonate aquifers: *in* Knaust, D., and Bromley, R.G., eds., Trace Fossils as Indicators of Sedimentary Environments. Developments in Sedimentology 64, Amsterdam, Elsevier, p. 869-896.

Denison, C., Carlson, W.D., and Ketcham, R.A., 1997, Three-dimensional quantitative textural analysis of metamorphic rocks using high-resolution computed x-ray tomography: Part I. Methods and techniques: Journal of Metamorphic Geology, v. 15, p. 29-44.

Dierick, M., Cnudde, V., Masschaele, B., Vlassenbroek, J., Van Hoorebeke, L., and Jacobs, P., 2007, Micro-CT of fossils preserved in amber: Nuclear Instruments and Methods in Physics Research, Section A, v. 580, p. 641-643.

Elliot, J.C., and Dover, S.D., 1982, X-ray microtomography: Journal of Microscopy, v. 126, p. 211-213.

Frey, R.W., Howard, J.D., and Pryor, W.A., 1978, *Ophiomorpha*: Its morphologic, taxonomic, and environmental significance: Palaeogeography, Palaeoclimatology, Palaeoecology, v. 23, p. 199-229.

Fürsich, F.T., 1975, Trace fossils as environmental indicators in the Corallian of England and Normandy: Lethaia, v. 8, p. 151-172.

Garton, M., and McIlroy, D., 2006, Large thin slicing: A new method for the study of fabrics in lithified sediments: Journal of Sedimentary Research, v. 76, p. 1252-1256.

Garwood, R., and Sutton, M., 2010, X-ray micro-tomography of Carboniferous stem-Dictyoptera: New insights into early insects: Biology Letters, v. 6, p. 699-702.

Genise, J.F., and Laza, J.H., 1998, *Monesichnus ameghinoi* Roselli: A complex insect trace fossil produced by two distinct trace makers: Ichnos, v. 5, p. 213-223.

Gingras, M.K., Pemberton, S.G., Mendoza, C.A., and Henk, F., 1999, Assessing the anisotropic permeability of *Glossifungites* surfaces: Petroleum Geoscience, v. 5, p. 349-357.

Gingras, M.K., Pickerill, R., and Pemberton, S.G., 2002a, Resin cast of modern burrows provides analogues for composite trace fossils: Palaios, v. 17, p. 206-211.

Gingras, M.K., MacMillan, B., Balcom, B.J., Saunders, T., and Pemberton, S.G., 2002b, Using magnetic imaging and petrographic techniques to understand the textural attributes and porosity distribution in *Macaronichnus*-burrowed sandstone: Journal of Sedimentary Research, v. 72, p. 552-558

Gingras, M.K., MacMillan, B., and Balcom, B.J., 2002c, Visualizing the internal physical characteristics of carbonate sediments with magnetic resonance imaging and petrography: Bulletin of Canadian Petroleum Geology, v. 50, p. 363-369.

Gingras, M.K., Mendoza, C., and Pemberton, S.G., 2004, Fossilized worm-burrows influence the resource quality of porous media: American Association of Petroleum Geologists Bulletin, v. 88, p. 875-883.

Gingras, M.K., Pemberton, S.G., Henk, F., MacEachern, J.A., Mendoza, C.A., Rostron, B., O'Hare, R., and Spila, M.V., 2007a, Applications of ichnology to fluid and gas production in hydrocarbon reservoirs: *in* MacEachern, J.A., Bann, K.L., Gingras, M.K., and Pemberton, S.G., eds., Applied Ichnology. Society of Economic Paleontologists and Mineralogists (SEPM), Short Course Notes, no. 52, p. 129-143.

Gingras, M.K., Bann, K.L., MacEachern, J.A., Waldron, J., and Pemberton, S.G., 2007b, A conceptual framework for the application of trace fossils: *in* MacEachern, J.A., Bann, K.L., Gingras, M.K., and Pemberton, S.G., eds., Applied Ichnology. Society of Economic Paleontologists and Mineralogists (SEPM), Short Course Notes, no. 52, p. 1-26.

Gingras, M.K., Baniak, G., Gordon, J., Hovikoski, J., Konhauser, K.O., La Croix, A., Lemiski, R., Mendoza, C., Pemberton, S.G., Polo, C., and Zonneveld, J.-P., 2012, Porosity and permeability in bioturbated sediments: *in* Knaust, D., and Bromley, R.G., eds., Trace Fossils as Indicators of Sedimentary Environments. Developments in Sedimentology 64, Amsterdam, Elsevier, p. 837-868.

Green, M.A., Aller, R.C., and Aller, J.Y., 1992, Experimental evaluation of the influences of biogenic reworking on carbonate preservation in nearshore sediments: Marine Geology, v. 107, p. 175-181.

Home, P.C., 1987, Ula: *in* Spencer, A.M., Campbell, C.J., Hanslien, S.H., Nelson, P.H., Nysaether, E., and Ormaasen, E.G., eds., Geology of the Norwegian Oil and Gas Fields. Graham and Trotman, London, United Kingdom, p. 143-152.

Homem, M.R.P., Mascarenhas, N.D.A., and Cruvinel, P.E., 2000, The linear attenuation coefficients as features of multiple energy CT image classification: Nuclear Instruments and Methods in Physics Research, Section A, v. 452, p. 351-360.

Howard, J.D., 1968, X-ray radiography for examination of burrowing by marine invertebrate organisms: Sedimentology, v. 11, p. 249-258.

Howard, J.D., and Frey, R.W., 1973, Characteristic physical and biogenic sedimentary structures in Georgia estuaries: American Association of Petroleum Geologists Bulletin, v. 57, p. 1169-1184.

Jones, S.C., 1994, A new, fast, accurate pressure-decay probe permeameter: Society of Petroleum Engineers Journal, v. 9, p. 193-199.

Katrak, G., and Bird, F.L., 2003, Comparative effects of the large bioturbators, *Trypaea australiensis* and *Heloecius cordiformis*, on intertidal sediments of Western Port, Victoria, Australia: Marine and Freshwater Research, v. 54, p. 701-708.

Ketcham, R.A., and Carlson, W.D., 2001, Acquisition, optimization and interpretation of X-ray computed tomographic imagery: Applications to the geosciences: Computers and Geosciences, v. 27, p. 381-400.

Ketcham, R.A., Slottke, D.A., and Sharp, J.M. Jr., 2010, Three-dimensional measurement of fractures in heterogeneous materials using high-resolution X-ray computed tomography: Geosphere, v. 6, p. 499-514.

Knaust, D., 2009a, Ichnology as a tool in carbonate reservoir characterization: A case study from the Permian-Triassic Khuff Formation in the Middle East: GeoArabia, v. 14, p. 17-38.

Knaust, D., 2009b, Characterisation of a Campanian deep-sea fan system in the Norwegian Sea by means of ichnofabrics: Marine and Petroleum Geology, v. 26, p. 1199-1211.

Knaust, D., 2012, Methodology and techniques: *in* Knaust, D., and Bromley, R.G., eds., Trace Fossils as Indicators of Sedimentary Environments. Developments in Sedimentology 64, Amsterdam, Elsevier, p. 245-271.

Konhauser, K.O., and Gingras, M.K., 2011, Are animal burrows a major sedimentary sink for metals?: Ichnos, v. 18, p. 1-3.

Krejci, M.E., and Lowe, R.L., 1986, Importance of sand grain mineralogy and topography in determining micro-spatial distribution of epipsammic diatoms: Journal of the North American Benthological Society, v. 5, p. 211-220.

La Croix, A.D., Gingras, M.K., Dashtgard, S.E., and Pemberton, S.G., 2012, Computer modeling bioturbation: The creation of porous and permeable fluid-flow pathways: American Association of Petroleum Geologists Bulletin, v. 96, p. 545-556.

La Croix, A.D., Gingras, M.K., Pemberton, S.G., Mendoza, C.A., MacEachern, J.A., and Lemiski, R.T., 2013, Biogenically enhanced reservoir properties in the Medicine Hat Gas Field, Alberta, Canada: Marine and Petroleum Geology, v. 43, p. 464-477.

Lemiski, R.T., Hovikoski, J., Pemberton, S.G., and Gingras, M.K., 2011, Sedimentological, ichnological and reservoir characteristics of the low-permeability, gas-charged Alderson Member (Hatton gas field, southwest Saskatchewan): Implications for resource development: Bulletin of Canadian Petroleum Geology, v. 59, p. 1-28.

McCullough, E.C., 1975, Photon attenuation in computed tomography: Medical Physics, v. 2, p. 307-320.

McIlroy, D., 2007, Lateral variability in shallow marine ichnofabrics: Implications for the ichnofabric analysis method: Journal of the Geological Society, London, v. 164, p. 359-369.

McKinley, J.M., Lloyd, C.D., and Ruffell, A.H., 2004, Use of variography in permeability characterization of visually homogeneous sandstone reservoirs with examples from outcrop studies: Mathematical Geology, v. 36, p. 761-779.

Meadows, P.S., and Tait, J., 1989, Modification of sediment permeability and shear strength by two burrowing invertebrates: Marine Biology, v. 101, p. 75-82.

Mees, F., Swennen, F., Van Geet, M., and Jacobs, P., 2003, Applications of X-ray computed tomography in the geosciences: *in* Mees, F., Swennen, R., Van Geet, M., and Jacobs, P., eds., Applications of X-ray Computed Tomography in the Geosciences: Geological Society, London, Special Publication, v. 215, p. 1-6.

Migeon, S., Weber, O., Faugeres, J.-C., and Saint-Paul, J., 1999, SCOPIX: A new X-ray imaging system for core analysis: Geo-Marine Letters, v. 18, p. 251-255.

Mills, A.L., and Maubrey, R., 1981, Effect of mineral composition on bacterial attachment to submerged rock surfaces: Microbial Ecology, v. 7, p. 315-322.

Naruse, H., and Nifuku, K., 2008, Three-dimensional morphology of the ichnofossil *Phycosiphon incertum* and its implication for paleoslope inclination: Palaios, v. 23, p. 270-279.

O'Connell, S.C., 2003, The unknown giants-low-permeability shallow gas reservoirs of southern Alberta and Saskatchewan, Canada: Canadian Society of Exploration Geophysicists, Conference Abstracts. Available at http://www.cspg.org/documents/Conventions/Archives/Annual/2003/105S0127.pdf (Accessed on December 17, 2012).

Packard, J.J., Al-Aasm, I.S., and Devon Canada Exploration Team., 2004, Reflux dolomitization of Mississippian-age sabkha and restricted subtidal sediments resulting in a 1.6 Tcf giant gas field: The Upper Debolt Formation of west-central Alberta: Canadian Society of Petroleum Geologists, Seminar and Core Conference Abstracts, CD-ROM.

Pakhnevich, A.V., 2010, Study of fossil and recent brachiopods, using a skyscan 1172 X-ray microtomograph: Paleontological Journal, v. 44, p. 1217-1230.

Pemberton, S.G., and Gingras, M.K., 2005, Classification and characterizations of biogenically enhanced permeability: American Association of Petroleum Geologists Bulletin, v. 89, p. 1493-1517.

Pemberton, S.G., Risk, M.J., and Buckley, D.E., 1976, Supershrimp: Deep bioturbation in the Strait of Canso, Nova Scotia: Science, v. 192, p. 790-791.

Pemberton, S.G., MacEachern, J.A., Gingras, M.K., and Saunders, T.D.A., 2008, Biogenic chaos: Cryptobioturbation and the work of sedimentologically friendly organisms: Palaeogeography, Palaeoclimatology, Palaeoecology, v. 270, p. 273-279.

Petrash, D.A., Lalonde, S.V., Gingras, M.K., and Konhauser, K.O., 2011, A surrogate approach to studying the chemical reactivity of burrow mucous linings in marine sediments: Palaios, v. 26, p. 594-600.

Pickup, G.E., Ringrose, P.S., Corbett, P.W.M., Jensen, J.L., and Sorbie, K.S., 1995, Geology, geometry and effective flow: Petroleum Geoscience, v. 1, p. 37-42.

Polo, C., 2013, Bioturbation and resource quality: A case study of the Upper Cretaceous Lysing and Nise Formations, Ellida and Midnatsoll fields area, Norwegian Sea: University of Alberta Master's Thesis, Unpublished, 182 p.

Reineck, H.E., 1963, Sedimentgefüge im Bereich der südlichen Nordsee: Abhandlungen der Senckenbergischen Naturforschenden Gesellschaft, v. 505, p. 1-138.

Rockware ®, Inc., 2009, Surfer 9.0 Gridding and Contouring Software.

Sarker, M.R.H., and Siddiqui, S., 2009, Advances in micro-CT based evaluation of reservoir rocks: Technical Symposium Saudi Arabia Section, Al Khobar, Saudi Arabia, May 9-11, Society of Petroleum Engineers, paper SPE 126039.

Schönberg, C.H.L., and Shields, G., 2008, Micro-computed tomography for studies on *Entobia*: Transparent substrate versus modern technology: *in* Wisshak, M., and Tapanila, L., eds., Current Developments in Bioerosion. Springer-Verlag, Berlin, p. 147-164.

Shinn, E.A., 1968, Burrowing in recent lime sediments of Florida and the Bahamas: Journal of Paleontology, v. 42, p. 879-894.

Sijbers, J., and Postnov, A., 2004, Reduction of ring artifacts in high resolution micro-CT reconstructions: Physics in Medicine and Biology, v. 49, p. 247-253.

SkyScan., 2005, SkyScan 1172 desktop x-ray microtomograph instruction manual, 53 p.

Spencer, A.M., Home, P.C., and Wiik, V., 1986, Habitat of hydrocarbons in the Jurassic Ula Trend, Central Graben, Norway: *in* Spencer, A.M., ed., The Habitat of Hydrocarbons on the Norwegian Continental Shelf. Graham and Trotman, London, United Kingdom, p. 111-127.

Spila, M.V., Pemberton, S.G., Rostron, B., and Gingras, M.K., 2007, Biogenic textural heterogeneity, fluid flow and hydrocarbon production: Bioturbated facies Ben Nevis Formation, Hibernia field, offshore Newfoundland: *in* MacEachern, J.A., Bann, K.L., Gingras, M.K., and Pemberton, S.G., eds., Applied Ichnology. Society of Economic Paleontologists and Mineralogists (SEPM), Short Course Notes, no. 52, p. 363-380.

Taylor, A.M., and Goldring, R., 1993, Description and analysis of bioturbation and ichnofabric: Journal of the Geological Society, London, v. 150, p. 141-148.

Tonkin, N.S., McIlroy, D., Meyer, R., and Moore-Turpin, A., 2010, Bioturbation influence on reservoir quality: A case study from the Cretaceous Ben Nevis Formation, Jeanne d'Arc Basin, offshore Newfoundland, Canada. American Association of Petroleum Geologists Bulletin, v. 94, p. 1059-1078.

Weaver, P.P.E., and Schultheiss, P.J., 1983, Vertical open burrows in deep-sea sediments 2 m in length: Nature, v. 329, p. 329-331.

Weber, K.J., 1982, Influence of common sedimentary structures on fluid flow in reservoir models: Journal of Petroleum Technology, v. 34, p. 665-672.

Wellington, S.L., and Vinegar, H.J., 1987, X-ray computerized tomography: Journal of Petroleum Technology, v. 39, p. 885-898.

Wildenschild, D., Hopmans, J.W., Vaz, C.M.P., Rivers, M.L., Rikard, D., and Christensen, B.S.B., 2002, Using X-ray computed tomography in hydrology: Systems, resolutions, and limitations: Journal of Hydrogeology, v. 267, p. 285-297.

CHAPTER 3: AN EXAMPLE OF A HIGHLY BIOTURBATED, STORM-INFLUENCED SHOREFACE DEPOSIT: UPPER JURASSIC ULA FORMATION, NORWEGIAN NORTH SEA*

3.1 INTRODUCTION

Ichnology, a discipline of geology that blends together sedimentology, paleontology, and geochemistry, provides geoscientists with many useful applications. Among many others, applications of ichnology include reservoir characterization (e.g., Pemberton and Gingras, 2005; Tonkin et al., 2010; Lemiski et al., 2011) and reconstruction of continental and marine depositional successions (e.g., Frey and Pemberton, 1985; Pemberton et al., 2001; MacEachern et al., 2007a, MacEachern et al., 2007b). The underpinning of ichnology as a valuable tool for the study of ancient and modern sedimentary successions (e.g., Howard and Reineck, 1972; Howard and Frey, 1975; Gingras et al., 1998; Dashtgard et al., 2009) can be credited towards the valuable work done by Alfred Nathorst, Rudolf Richter, and Adolf Seilacher, among others, over the last 130 years. As a result of these studies, the distribution of trace fossils produced under different environmental conditions can be predicted using the ichnofacies paradigm (Seilacher, 1964, Pemberton et al., 2001; MacEachern et al., 2007a). One of the many strengths of the ichnofacies concept is being able to distinguish different groups of ichnofossils based on specific combinations of organism behavior that record a response to different environmental conditions (Frey and Seilacher, 1980; MacEachern et al., 2007a). Developed by Adolf Seilacher in the 1950s and 1960s, ichnofacies analysis was originally regarded as an exclusive indicator of paleobathymetry (Seilacher, 1967). Subsequent research has shown, however, that ichnofacies analysis more accurately depicts depositional subtleties such as substrate consistency, water turbidity, water salinity, oxygenation, and temperature within the geological rock record (Frey and Pemberton, 1985; Gingras et al., 2007; MacEachern et al., 2007b).

The processes that control sedimentation and neoichnological processes in modern, wave-dominated shorelines are generally well understood. The term shoreface was first applied by Barrell (1912) to represent the interface between the subaerial and subaqueous regions in a deltaic topset system. Johnson (1919) later redefined the shoreface to represent the setting between the low-tide shoreline

---

* A version of this chapter has been accepted for publication in *Sedimentology* as "An Example of a Highly Bioturbated, Storm-Influenced Shoreface Succession: Upper Jurrasic Ula Formation, Norwegian North Sea" by Greg M. Baniak, Murray K. Gingras, Beverly A. Burns, and S. George Pemberton.

and horizontal surface of the offshore. Subsequent research into shoreline morphodynamics, generation of sedimentary structures, and distribution of neoichnological assemblages have led to the development of a number of facies and ichnofacies models in the past couple decades (e.g., Walker and Plint 1992; Reading, 1996; Pemberton et al., 2001; Plint, 2011).

Well-preserved trace fossils characterize shallow-marine successions of the Upper Jurassic Ula Formation in the Norwegian Central Graben. Earlier studies have documented the high abundance and diversity of biogenic structures in Upper Jurassic successions across the Central North Sea, particularly within the UK Central Graben (e.g., Taylor and Gawthorpe, 1993; Gowland, 1996; Martin and Pollard, 1996). Initial observations of the Ula Formation suggested depositional settings such as bioturbated shelf, offshore bar, and tidal sand wave deposits (Bailey et al., 1981). These interpretations require further clarification, however, as questions regarding sediment transport mechanisms, abnormally large packages of bioturbated strata, and general scarcity of sedimentary structures remain unanswered. The aim of this this chapter is to therefore describe and interpret the Ula Formation from an ichnological and sedimentological perspective. From this, an evaluation of how the trace fossil assemblages reflect paleoenvironmental stresses typical of a storm-dominated shoreface will be discussed.

3.2 ECONOMIC SIGNIFICANCE OF THE ULA FORMATION

The Upper Jurassic Ula Formation is the primary reservoir in the Ula Trend, which is located in the northeastern corner of the Norwegian Central Graben (Spencer et al., 1986) (Fig. 3.1). Since its discovery in the late 1970s and early 1980s, the Ula Trend has been a major hydrocarbon producing province in Norwegian Central Graben (Bjørnseth and Gluyas, 1995). Historical hydrocarbon production has occurred primarily from Ula Field (435 to 562 million barrels of reserves; Home, 1987; Brown et al., 1992; Bjørnseth and Gluyas, 1995; British Petroleum Energy, 2011), Gyda Field (200 million barrels of reserves; Gluyas et al., 1992), and Tambar Field (295 million barrels reserves; British Petroleum Energy, 2011). Several smaller un-developed reservoirs, with reserves typically less than 100 million barrels, remain to be exploited (Bjørnseth and Gluyas, 1995; Gluyas, 1997). The economic potential that remains in these aforementioned oil and gas fields is highly sensitive to reservoir quality. For example, the porosity and permeability of the Ula Formation sandstones are strongly controlled by centimeter to decimeter scale features such as bioturbation (see Chapter 4), quartz cementation, and detrital clay

content. To this end, a stronger understanding of the sedimentology and ichnology is required to better exploit remaining hydrocarbons within the Ula Trend.

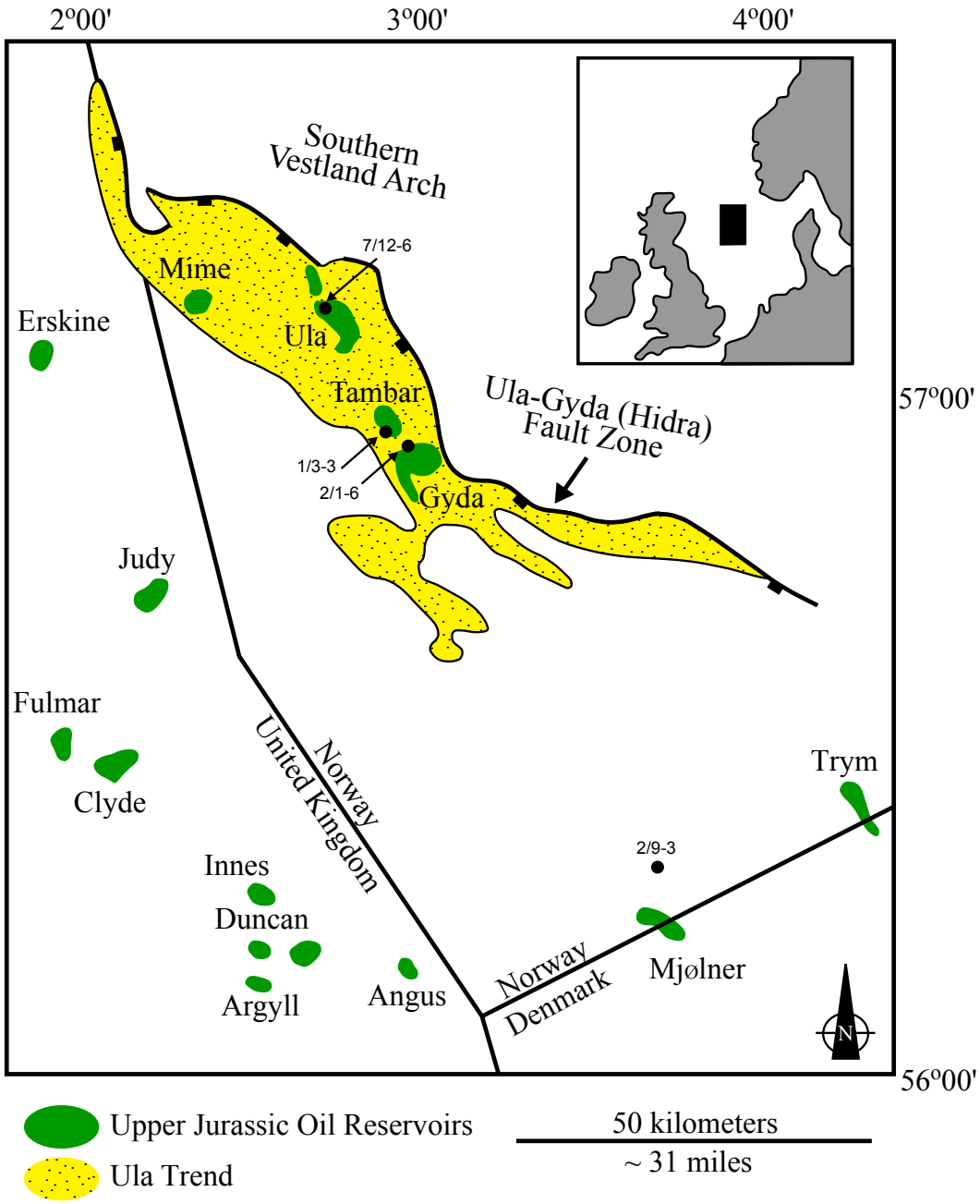

Figure 3.1: Regional location map of the Ula Trend and principal Upper Jurassic oil fields in the southern Central Graben. Demarcated onto the location map is the location of the four subsurface wells (7/12-6, 2/9-3, 2/1-6, and 1/3-3) analyzed in this study. Modified after Stewart (1993), Bjørnseth and Gluyas (1995), and Gluyas (1997).

3.3 REGIONAL GEOLOGY

The present day North Sea is a marginal epeiric sea located on the European continental shelf, and is underlain by a series of extensional fault-bounded basins. Episodic basin extension led to the development of the Viking Graben, Central Graben, and Moray Forth Basins, with the most active rifting taking place during the Late Jurassic (Ziegler, 1982). These three basins have been interpreted as failed arms of a triple junction (Whiteman et al., 1975; Brown et al., 1992). Other interpretations have also explored the probability that a thin continental crust underlies most of the grabens (Christie and Sclater, 1980; Donato and Tully, 1981), indicating that the structures formed during a period of regional lithospheric stretching (McKenzie, 1978).

Extensional faulting in the Central Graben resulted in the development of sub-basins that are commonly oriented in a NNW-SSE direction (Roberts et al., 1990; Fraser et al., 2003; Fig. 3.2). The structural history of the Central Graben has been summarized by numerous authors (e.g., Ziegler, 1982; Roberts et al., 1990; Gowers et al., 1993). In short, western and central Europe became episodically subjected to regional extension during Late Permian and Triassic. During the Late Permian, glacio-eustatic rise in sea level resulted from the melting of ice during the break up of Gondwana (Coward et al., 2003). Marine transgression led to the establishment of a Zechstein Sea across much of northern and central Europe. Due to the development of a hyper arid desert environment during Late Permian, flooding and evaporation occurred repeatedly within the Zechstein Sea (Glennie et al, 2003). As a result of salt sedimentation during the Late Permian, the Triassic and Jurassic evolution of the Central Graben became strongly influenced by halokinesis (i.e., salt tectonics) (Hodgson et al., 1992; Zanella and Coward, 2003). Halokinesis also influenced Late Jurassic rifting and provided accommodation space within secondary rim synclines (Johnson et al., 1986; Brown et al., 1992).

At the Jurassic stage, the Norwegian Central Graben was separated from the Southern Vestland Arch (part of a stable Jurassic Platform) by a NW-SE trending zone of SW dipping faults referred to as the Hidra Fault Zone (Home, 1987; Fig. 3.1). Sediments were deposited around the eastern flanking highs of the Central Graben, in particular on the SW flank of the Southern Vestland Arch (Home, 1987). The Hidra Fault Zone defines the northeastern limits of the Ula Field and the reservoir intervals occur within the hanging wall of the fault zone (Brown et al., 1992). Extensional activity is believed to have peaked between the Callovian and Kimmeridgian (Gowers et al., 1993; Zanella and Coward, 2003). Just prior to the

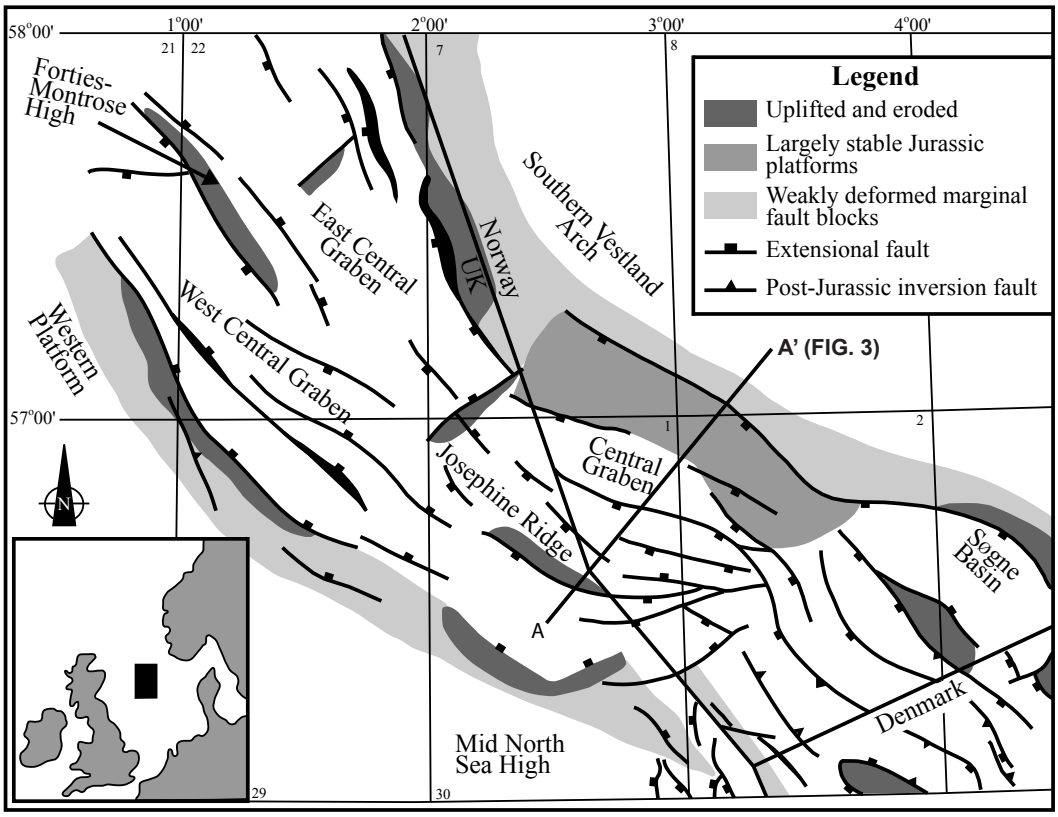

Figure 3.2: Structural elements present within the North Sea Central Graben during the Upper Jurassic. Modified after Gowland (1996).

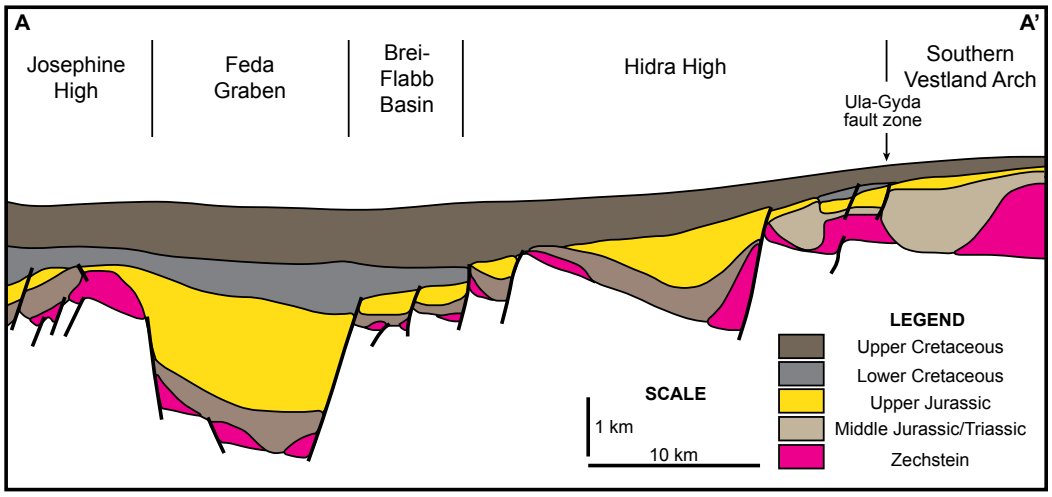

Figure 3.3: Schematic sketch illustrating the complexity in structural styles across the Norwegian Central Graben (see Fig. 3.2 for location). Modified after Gowers et al. (1993).

Lower Cretaceous, rotational faulting resulted in the erosion of sediments in the footwalls and deposition of sediments in the hangingwalls (Fig. 3.3), with the most intense rotational movements occurring within the Hidra High. Structural extension ceased during the Early Cretaceous with the onset of passive thermal subsidence. During the sag phase, which has lasted from the Cretaceous to present day, the Norwegian Mandal Formation and UK equivalent Kimmeridgian Clay Formation were brought to maturity and have acted as the source rock for much of the North Sea (Baird, 1986; Miller, 1990; Cooper et al., 1995).

3.4 STRATIGRAPHIC FRAMEWORK

The Ula Formation (Vollset and Doré, 1984) is an Upper Jurassic (Kimmeridgian-Oxfordian) succession that was deposited on Middle Jurassic or Triassic sediments (Stewart, 1993). Within the study area, an unconformity is common at the base of the Ula Formation and is detectable by the presence of a *Glossifungities*-demarcated surface. The Ula Formation is part of the Tyne Group and is commonly interbedded with the Haugesund, Farsund, and Mandal Formations (Vollset and Doré, 1984; Fraser et al., 2003) (Fig. 3.4). The name 'Ula' was first applied to the Ula Field following its discovery, and was named after a famous Norwegian sea pilot called Ulabrand (Home, 1987). Bailey et al. (1981) then applied the name 'Ula' to a sequence of Upper Jurassic sandstones overlying the non-marine Lower to Middle Jurassic Bryne Formation in the Ula Field. Since then, the name 'Ula' has been extended to a wider geographic area and stratigraphic range. The post-Paleozoic stratigraphic nomenclature for the Ula Formation is based on that of Deegan and Scull (1977) and modified by Vollset and Doré (1984).

3.5 DATABASE AND METHODOLOGY

The Ula Formation was studied in four wells (7/12-6, 2/9-3, 2/1-6, and 1/3-3; Fig. 3.1) with roughly 380 m of core and well-log coverage. Sedimentological data used to interpret depositional facies included: grain-size, sorting, bedding contacts, thicknesses, primary and secondary physical structures, lithologic constituents, mineralogical accessories, and identification of important stratigraphic surfaces. Ichnological data comprises description of ichnogenera, cross-cutting relationships, and bioturbation intensity. Bromley and Ekdale (1984, 1986) established how the cross-cutting relationships of trace fossils could be used to determine the tiering profiles of vertical rock successions (i.e., shallow tier trace fossils being cross-cut deeper-tier trace fossils). These are important because colonization style and

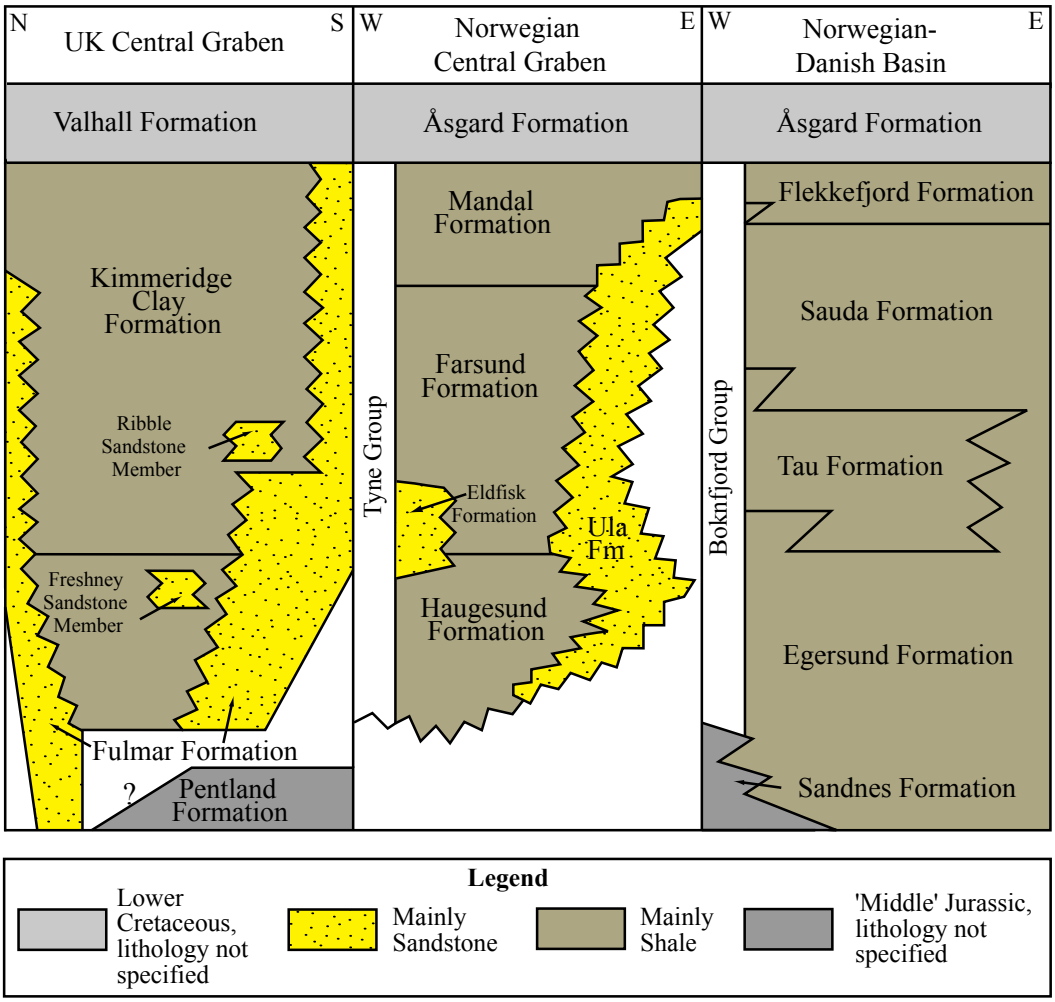

Figure 3.4: Upper Jurassic stratigraphic correlation chart for the Ula Formation and equivalents in the southern North Sea. Modified after Fraser et al. (2003).

subsequent cross-cutting relationships of trace fossils aid in facies interpretation and recognition of major stratigraphic surfaces (e.g., Taylor and Gawthorpe, 1993; MacEachern et al., 1998; Pemberton et al., 2004). Bioturbation intensity (hereafter denoted BI) involves the allocation of a grade of bioturbation and varies from absent (BI of 0 or 0% intensity) to complete (BI of 6 or 100% intensity) (Fig. 3.5). Measurement of the bioturbation intensity was adapted from Bann et al. (2004), from the original concepts of Reineck (1963) and Taylor and Goldring (1993).

3.6 RESULTS

Deposits of Facies Association 1 (FA1), as represented by Facies 1 and 2, contain massive to finely laminated silts and silty mudstone. Thirteen ichnogenera, representing a distal to proximal *Cruziana* ichnofacies, were observed in FA1.

Grade	Percent Bioturbated	Classification	Visual Representation
0	0 %	Bioturbation absent	
1	1 to 4 %	Sparse bioturbation, bedding distinct, few discrete trace fossils	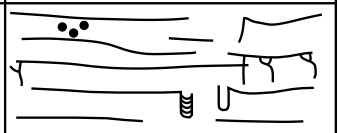
2	5 to 30 %	Uncommon bioturbation, bedding distinct, low trace fossil density	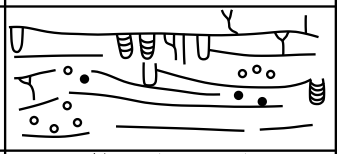
3	31 to 60 %	Moderate bioturbation, bedding boundries sharp, trace fossils discrete	
4	61 to 90 %	Common bioturbation, bedding boundries indistinct, high trace fossil density with common overlap	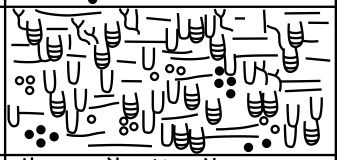
5	91 to 99 %	Abundant bioturbation, bedding completely disturbed (just visible)	
6	100 %	Complete bioturbation (total biogenic homogenization of sediment)	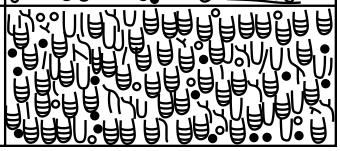

Figure 3.5: Schematic representation of Bioturbation Intensity (BI). The BI values are a function of the relative degree of burrowing versus identifiable physical sedimentary values. Adapted from Bann et al. (2004), from the original concepts of Reineck (1963) and Taylor and Goldring (1993).

Facies Association 2 (FA2) is represented by sandstones that are fine- to medium-grained and highly bioturbated. Although typically devoid of identifiable physical sedimentary structures, rare structures include high- and low-angle cross-beds and trough cross stratification. In a contrast to FA1, only four ichnogenera were observed in FA2 with *Ophiomorpha* being the most dominant. FA2 represents a proximal *Cruziana* to *Skolithos* ichnofacies and is represented by Facies 3 through 6. A detailed core description showing FA1 and FA2 is presented in wells 7/12-6 (Fig. 3.6) and 1/3-3 (Fig. 3.7).

3.6.1 Facies 1: Moderately to Weakly Bioturbated Silty Mudstone

3.6.1.1 Description

Facies 1 consists of bioturbated claystones and mudstones that contain 20 to

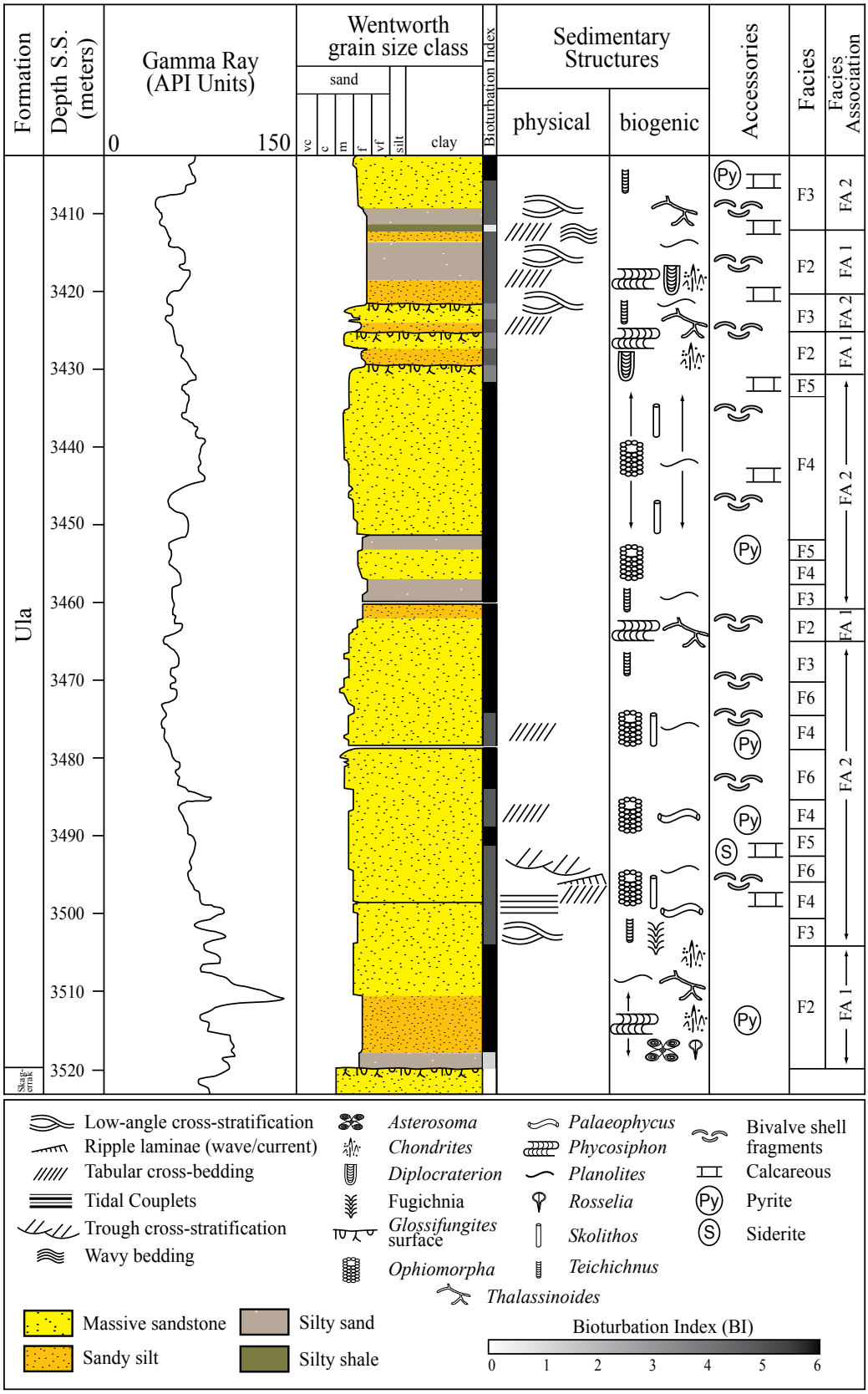

Figure 3.6: Lithology column for the Upper Jurassic Ula Formation and upper most Late Triassic Skagerrak Formation in subsurface well 7/12-6.

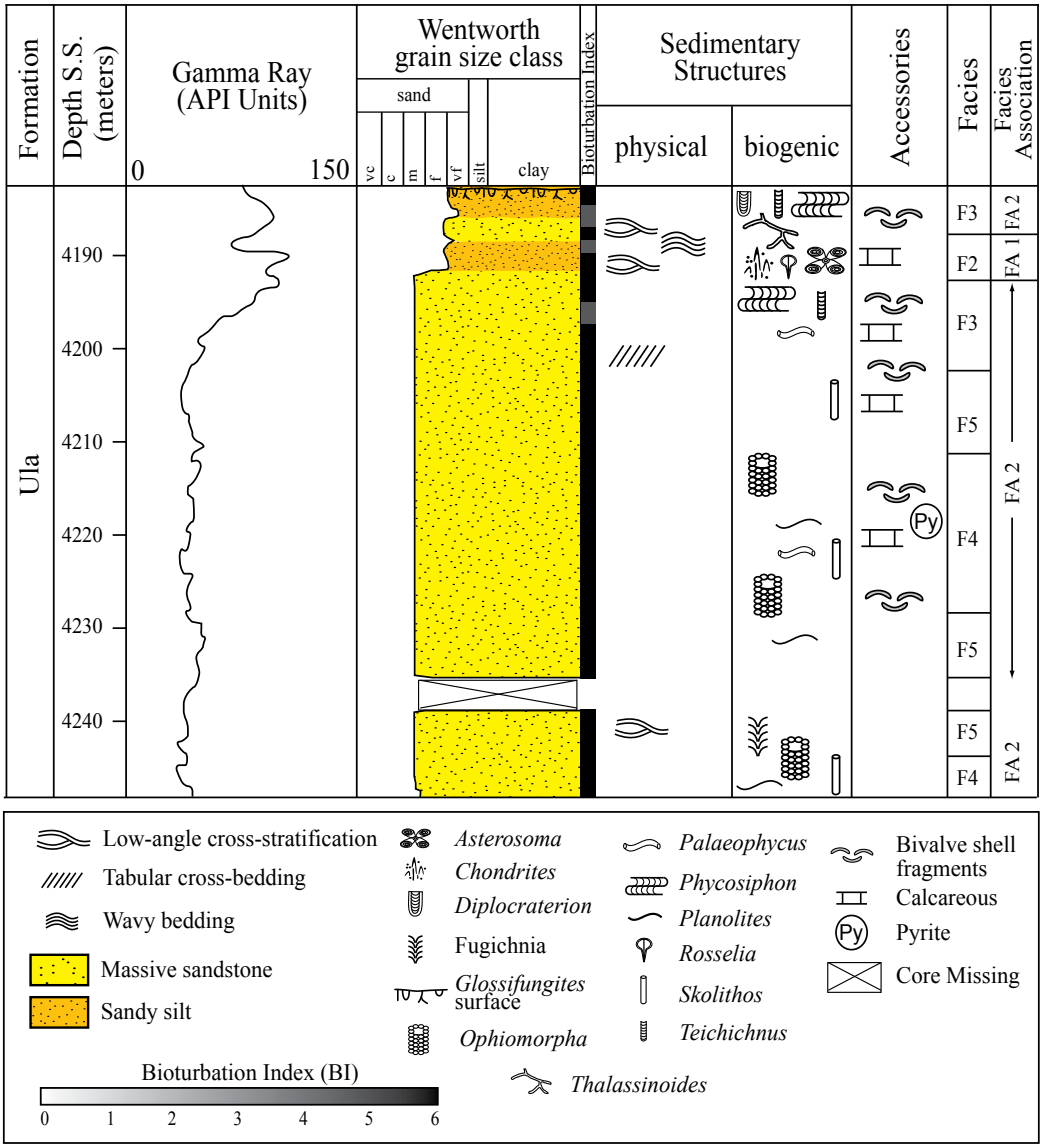

Figure 3.7: Lithology column for the Upper Jurassic Ula Formation in subsurface well 1/3-3.

40% admixed very fine sand and siltstone. Lithologic accessories may include rare bivalve and fish fragments, and pyrite nodules that are disseminated throughout the interval. The interval has a sharp contact at its base and is commonly recognized through the presence of a *Glossifungites*-demarcated surface of erosion. Facies 1 defines the base of upward-coarsening sedimentary succession. Facies 1 gradationally underlies Facies 2 with a thickness ranging from decimeter to meter scale. Rare, thin planar laminae of sandstone occur sporadically throughout the interval. Biogenic reworking is common throughout the entire facies, with a variable BI ranging from 0 to 3. The interval is burrowed with a monospecific to low-diversity trace fossil suite and the trace fossils are evident as both indistinct mottles and clearly defined

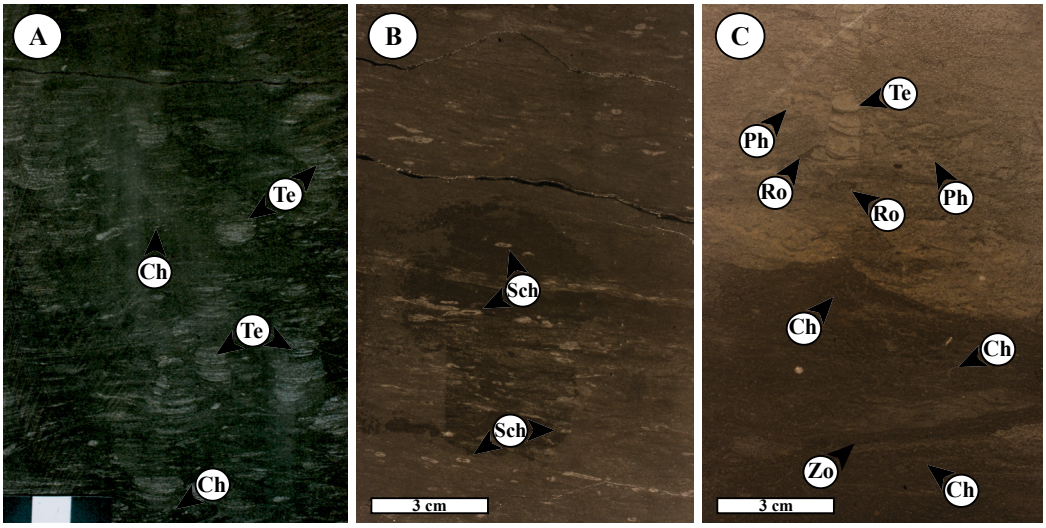

Figure 3.8: Depositional facies of the offshore (FA1). **(A)** Silty mudstones pervasively bioturbated by *Teichichnus* (Te) with subordinate *Chondrites* (Ch). Core 2/9-3, depth 4520.10m. **(B)** Monospecific assemblage of *Schaubcylindrichnus freyi* (Sch) within silty mudstone. Core 2/1-6, depth 4391.35m. **(C)** A tempestite truncating lower offshore silty mudstones that contain *Chondrites* (Ch), a single *Zoophycos* (Zo), and indistinct burrow mottling. The fine-grained tempestite contains *Phycosiphon* (Ph), *Rosselia* (Ro), and *Teichichnus* (Te). Core 2/1-6, depth 4197.25m.

traces. Recognizable trace fossils include *Chondrites*, *Cosmoraphe*, *Helminthopsis*, *Planolites*, *Teichichnus*, and *Schaubcylindrichnus freyi* (Fig. 3.8A-B).

3.6.1.2 Interpretation

The fine-grained nature of Facies 1 indicates a low-energy depositional environment that was beyond the influence of most current or wave processes. The thin sandstone laminae, however, reflect exceptional storm events and are characteristic of distal tempestites (Einsele, 2000). Subsequently, these tempestites were partially reworked by small, opportunistic organisms during fair weather conditions resulting in the indistinct mottling. The preservation potential of distal tempestites is quite high, owing to emplacement well below fair-weather wave base where typical waves and tides are not capable of modifying them (MacEachern and Pemberton, 1992). The presence of moderately diverse trace fossil assemblages produced by deposit-feeding and grazing/foragers behaviors of the distal *Cruziana* ichnofacies reflects deposition in an open marine lower offshore environment (MacEachern et al., 2007a). Monospecific *Chondrites* suites may indicate reduced dissolved oxygen in the sediment column with depth (Bromley and Ekdale, 1984; Ekdale and Mason, 1988). Occasional nodules of pyrite in the matrix support this interpretation (Berner, 1985).

3.6.2 Facies 2: Thoroughly Bioturbated Silty to Sandy Mudstones

3.6.2.1 Description

Facies 2 consists of primarily silty to sandy mudstones that is interbedded with occasional very fine-grained sandstone beds that makes up 20% of Facies 2. The sandstone thicknesses range from 5 to 10 cm (Fig. 3.8C), whereas the silty to sandy mudstones form successions that range up to 2 m. Facies 2 is gradationally interbedded with Facies 1 as well as Facies 3 and 4 of FA2. Additionally, the contacts between Facies 2 and the aforementioned facies are typically bioturbated. Rare pyrite nodules and carbonaceous debris are common lithological accessories. Planar parallel laminations and low-angle cross stratification occur in greater abundance near the top of the interval especially within the coarser sandstones. The degree of bioturbation within the facies is extremely high (BI 4 to 6), and generally obliterates the primary physical structures. The most abundant trace fossil is *Phycosiphon*, which is not distinguished from its junior synonymous trace fossil *Anconichnus* (see Wetzel and Bromley (1994) for more discussion). Subordinate elements include *Chondrites, Teichichnus, Rosselia, Asterosoma,* subvertical to vertical *Diplocraterion habichi,* and *Thalassinoides* (Fig. 3.9A-B). Notably, there are numerous examples within Facies 2 of deeper tier trace fossils overprinting shallower tier trace fossils (e.g., *Chondrites* cross-cutting *Rosselia*).

3.6.2.2 Interpretation

The fine-grained nature of the sediments, combined with a high degree of bioturbation, reflects sedimentation in an upper offshore setting (MacEachern and Pemberton 1992; Pemberton et al., 1992). Exclusion of a potential prodeltaic setting is indicated by the lack of features characteristic of rapid sedimentation (i.e., convolute bedding, ball and pillow structures). Furthermore, the ichnological suite in Facies 2 is dominated by a diverse and abundant expression of grazing- and deposit-feeding traces representative of the archetypal *Cruziana* ichnofacies in a fully marine offshore setting (MacEachern et al., 2007a). Deltaic trace fossil assemblages, in contrast, reflect the activities of a stressed infaunal community and are commonly of lower-diversity (Gingras et al., 1998; Bann and Fielding, 2004).

Facies 2 contains numerous examples of cross-cutting relationships. Studies of *Phycosiphon* have shown that it may be either a shallow-tier, medium-tier, or deep-tier trace fossil (Ekdale and Bromley, 1991; Wetzel and Uchman, 2001). Within Facies 2, *Phycosiphon* is commonly cross-cut by most other ichnogenra, thereby suggesting that the *Phycosiphon* producers must have been one the first

to colonize the substrate. As diversity increased, deeper-tier burrowers such as *Chondrites* cross-cut *Phycosiphon*. *Chondrites* are typically interpreted as a deeper-tier trace fossil (Bromley, 1990), although actual burrow depth within the substrate is probably dependent on the depth of the redox-discontinuity layer (Goldring et al., 1991). In many of the cores, *Phycosiphon* is also typically cross-cut by mid-tier trace fossils such as *Thalassinoides* and *Diplocraterion habichi*, suggesting possible penecontemporaneous erosion (Goldring et al., 1991).

3.6.3 Facies 3: Highly bioturbated Very Fine to Fine-Grained Sandstones

3.6.3.1 Description

Facies 3 is a very fine to lower fine-grained sandstone that coarsens upwards and has a detrital silt component (5 to 30%). Lithological accessories include dispersed fossil fragments, rare bivalve fragments, mica flakes, glauconitic material, and scattered fecal pellets. Facies 3 intervals are gradational with Facies 2, 4, and 5, and have thicknesses that range up to 3 m. Physical sedimentary structures are rare, and are only present as remnant low-angle parallel laminations. Bioturbation intensities reach up to 90% (BI ranging between 4 to 6), and the most abundant trace fossil is *Teichichnus zigzag* (Fig. 3.9C). These *Teichichnus zigzag* burrows can reach up to 15 cm in height and width, and are a discernible trace fossil due to their discrete margins. Secondary trace fossils include *Planolites*, *Palaeophycus*, *Thalassinoides*, and *Asterosoma*. *Phycosiphon*, an abundant trace fossil in the underlying succession (Facies 2), occurs sparsely throughout Facies 3 and becomes exceedingly rare at the top of the section.

3.6.3.2 Interpretation

The fine-grained nature of Facies 3, combined with a paucity of sedimentary structures, indicates that sedimentation was exceeded by the rate of infaunal reworking. Coarsening upward sequences, combined with moderate to intense levels of bioturbation (BI 4 to 6), suggest that Facies 3 was deposited in an upper offshore to lower shoreface environment (MacEachern and Pemberton, 1992). Remnant low-angle parallel laminations are interpreted as hummocky cross-stratification (HCS), as defined by Harms et al. (1975). The thicker successions of sand sized sediment are likely to have been derived from the upper and middle shoreface through possible storm events. Due to a likely infrequent nature of storm events, these sandy event beds were subsequently bioturbated during fair-weather periods (MacEachern and Pemberton, 1992).

The presence of a moderately diverse trace fossil assemblage, produced primarily by deposit feeding organisms in low- to moderate-energy conditions, suggests a proximal *Cruziana* ichnofacies (MacEachern et al., 2007a). *Teichichnus zigzag* reflects repeated burrowing episodes by an infaunal deposit feeding community that colonized event beds during periods of fair-weather conditions or non-deposition. This is reflected in the broad spreite of the *Teichichnus zigzag* that represents lateral migrations of the causative burrow (Frey and Bromley, 1985). The reduction in *Phycosiphon* is believed to be due to the reduction in clay and silt material (Bednarz and McIlroy, 2009) and gradual increase in depositional energy.

3.6.4 Facies 4: Heavily Bioturbated, Fine-Grained Sandstones

3.6.4.1 Description

Facies 4 is composed of highly bioturbated, lower to upper fine-grained sandstones that are moderately to well sorted. Sedimentary structures, although rare, include sporadically distributed trough cross-bedding and low-angle planar cross-stratification. Gradationally interstratified with Facies 3, 5, 6, and 7 at various intervals, the typical thickness for Facies 4 ranges between 0.5 m and 5 m. Micaceous debris and whispy concentrations of mud likely represent fecal material. Bioturbation intensities, although variable, typically range from 4 to 6. Large *Ophiomorpha* and *Siphonichnus* dominate the trace fossil suite. *Siphonichnus* commonly contains sediment infill that is cleaner and coarser from the surrounding matrix (Fig. 3.9D). Furthermore, the burrow lining of *Siphonichnus* is quite thick, and commonly contains re-burrowing. Identifiable trace fossils are commonly limited to *Planolites* within these burrow linings. *Ophiomorpha* can be subdivided into *Ophiomorpha irregulaire* and *Ophiomorpha nodosa* based on morphology (Fig. 3.9E-G). *Ophiomorpha irregulaire* is often located within clean to slightly ‘muddy’ sandstones and is associated with abundant mottling of the background sediment. *Ophiomorpha nodosa* occurs within clean sandstones and are commonly ovoid shaped (5 cm wide and up to 30 cm long), and contain well-defined pelleted walls. Subordinate trace fossils include *Planolites*, rare *Thalassinoides* and diffuse *Teichichnu*s.

3.6.4.2 Interpretation

A restricted suite of dwelling structures dominates the resident ichnocoenosis within Facies 4 and represents a stressed expression of the *Skolithos* ichnofacies (MacEachern et al., 2007a). The local existence of hummocky and swaley cross-

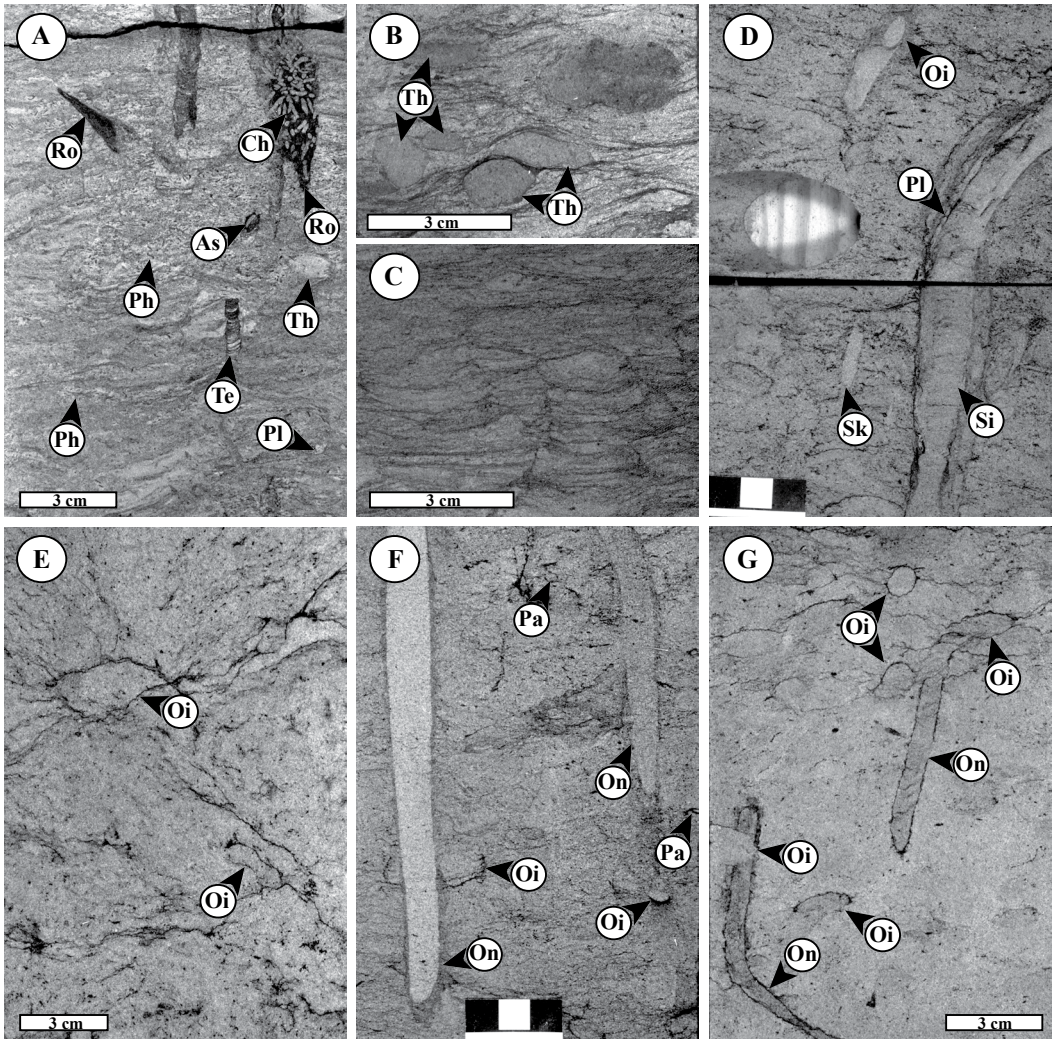

Figure 3.9: Trace fossil distributions of the facies in the upper offshore (FA1) to lower/middle shoreface (FA2). **(A)** A thin tempestite passes into thoroughly burrowed upper offshore siltstone containing *Phycosiphon* (Ph), *Teichichnus* (Te), *Asterosoma* (As), *Rosselia* (Ro), and *Chondrites* (Ch). An example of deeper-tier *Chondrites* (Ch) cross-cutting *Rosselia* (Ro) occurs near the top of the photo. Core 1/3-3, depth 4192.70m. **(B)** Low-diversity assemblage of burrowed mottled silty mudstone truncated by a fine-grained tempestite. The tempestite contains distinct *Thalassinoides* (Th) and thin mudstone lenses. Core 1/3-3, depth 4183.50m. **(C)** Argillaceous, very fine-grained sandstones within an upper offshore-lower shoreface complex containing bell-shaped patches of laminated sand interpreted to represent *Teichichnus zigzag*. Core 1/3-3, depth 4181.90m. **(D)** Lower shoreface complex of burrow mottled fine-grained sandstones. Identifiable ichnofossils include *Siphonichnus* (Si), *Ophiomorpha irregulaire* (Oi), and *Skolithos* (Sk). Core 2/1-6, depth 4328.65m. **(E)** Fine-grained sandstone containing fine mud streaks and irregular shaped horizontal burrows interpreted to represent *Ophiomorpha irregulaire* (Oi). Reflective of lower-energy conditions within the lower shoreface complex. Core 2/1-6, depth 4217.75m. **(F)** Massive, heavily lined vertical *Ophiomorpha nodosa* (On) cross-cutting a burrow mottled fabric containing *Ophiomorpha irregulaire* (Oi) and *Palaeophycus* (Pa). Reflective of high-energy conditions in the lower/middle shoreface. Core 2/1-6, depth 4319.80m. **(G)** Low-diversity assemblage of *Ophiomorpha irregulaire* (Oi) and *Ophiomorpha nodosa* (On) within fine-grained sandstones. Core 2/1-6, depth 4304.20m.

stratification suggests elevated wave activity and possible storm deposits (Harms et al., 1975; Leckie and Walker, 1982). Given the highly bioturbated nature of the beds, the storms probably represented low frequency, but moderate to potentially high-energy events within a lower to middle shoreface setting (MacEachern, 1994; Pemberton et al., 2001). In intervals where the high-energy storms are pronounced, the diversity of deposit feeding structures declined markedly. For example, Howard (1975) noted that *Ophiomorpha* trace fossils tend to shift from a horizontal to vertical orientation during higher-energy conditions. In storm-dominated intervals in Facies 4, only deeply penetrating structures, particularly *Ophiomorpha nodosa*, were recorded. In comparison, the thin nature of burrow walls observed within *Ophiomorpha irregulaire* ichnofossils, as opposed to the thicker burrow linings of *Ophiomorpha nodosa*, suggest intervals of lower-energy conditions (Martin and Pollard, 1996). Much of the silt content lining the burrow walls of *Ophiomorpha nodosa* is believed to be in the form of fecal pellets as opposed to primary suspension fallout of clays (Frey et al., 1978).

The presence of *Siphonichnus*, a bivalve trace fossil, indicates that the bivalve was well suited for keeping pace during intervals of higher sedimentation (Gingras et al., 2008). Given the large size of the *Siphonichnus* (i.e., up to 30 cm long in some intervals), it is likely that long periods of stability at the sediment water interface were punctuated by periodic storm events (Gingras et al., 2008).

3.6.5 Facies 5: Highly Bioturbated 'Massive' Sandstone

3.6.5.1 Description

Facies 5 is an upper fine- to lower medium-grained sandstone that is well sorted and dominantly sub-rounded. Silt content is sparse, and often only present as disseminated fecal pellets or organic matter. Facies 5 is the most widespread facies of FA 2, and is gradational with Facies 3, 4 and 6 with thicknesses ranging up to 3 m. Sedimentary structures include low-angle planar lamination and rare trough cross-stratification. Biogenic reworking of the sediment is high (BI 5 to 6), and generally results in the bedding taking on a massive appearance. Most of the bioturbation is attributed to cryptic reworking of the sediment, and identifiable ichnofossils only include rare examples of *Ophiomorpha*, *Planolites*, and fugichnia.

3.6.5.2 Interpretation

The majority of bioturbation in Facies 5 is interpreted to represent the activities of microorganisms such as meiofauna and amphipods (Howard and Frey,

1975; Bromley, 1996; Pemberton et al., 2008). This is interpreted by the presence of fugichnia (escape trace fossils) and cryptic bioturbation. Fugichnia records the attempts of organisms to burrow up through storm beds in order to reach the new sediment interface (Fig. 3.10A) (MacEachern, 1994). Studies in modern tropical environments have shown that the activities of organisms can result in the complete homogenization of the sediment in only a couple days (Bromley, 1996). Howard and Frey (1975) showed that many of the prolific bioturbated sections in modern shorefaces and estuaries (Georgia, United States) did not exhibit distinct traces. Instead, most of the ubiquitous biogenic texture was produced by amphipods.

It must also be noted that the intensity and uniformity of bioturbation in the sandstones, combined with a general lack of primary sedimentary structures, suggest either limited storm-influence or considerable time between storm events. Following any storm event, microorganisms were likely first to recolonize the substrate and reorganize the sediment in into a massive appearing sandstone within days (Bromley, 1996). Furthermore, in middle shoreface settings, substrates are commonly well oxygenated and non-cohesive. Microorganisms therefore have the ability to colonize the substrate at great depths below the sediment-water interface (Pemberton et al., 2001). Recognition of planar cross-bedding (Fig. 3.10B), indicative of tractive processes such as migration of subaqueous sand dunes and unidirectional ripples, suggests deposition within a middle to upper shoreface setting (Buatois et al., 1999).

3.6.6 Facies 6: Medium-grained, Cross-Stratified Sandstone

3.6.6.1 Description

Facies 6 is a medium-grained sandstone interbedded with clast-supported pebbles and shell deposits. The sandstone itself is upper fine- to medium-grained size, sub rounded in character, and moderately to locally well sorted. Sedimentary structures include low- and high-angle cross-stratification and trough cross-bedding (Fig. 3.10C). Intervals of this facies consist of amalgamated sharp based, sandstone bodies in which the lower scoured contacts are overlain by thin-shelled bivalves (Fig. 3.10D-E), variable lags of pebbles (Fig. 3.10F), and other bioclastic debris. The pebble lags range from 5 to 10 cm in thickness and are composed of fragments that are poorly sorted, angular to sub-rounded, and between 1 and 2 cm across. The shell deposits are composed primarily of bivalves and occupy intervals up to 5 cm thick. Within the clast and shell deposits, bioturbation is very low (BI ranging between 0 and 1), whereas in the sandstone the degree of bioturbation is

slightly higher (BI 0 to 2), with evidence of *Ophiomorpha* and fugichnia. There is also evidence of rare tidal reworking, with tubular tidalites being preserved within the burrows (Fig. 3.11A) as well as examples of tidal bundles (Fig. 3.11B). Grain size profiles appear blocky, but a subtle coarsening upward trend to medium sand is discernable. These bioturbated sandstone beds are decimeter to meter scale in thickness, and collectively form a gradational interval with Facies 4 and 5.

3.6.6.2 Interpretation

The presence of trough cross-bedding, low and high-angle planar cross-stratification, and reduction in trace fossils suggests a middle to upper shoreface setting (Pemberton et al., 1992; Raychaudhuri and Pemberton, 1992). Rare, sporadically distributed trace fossils are a feature of upper shoreface successions (e.g., MacEachern and Pemberton, 1992). This is because continuously migrating bedforms commonly limit animal colonization (Howard, 1975, MacEachern and Pemberton, 1992).

Upper shoreface facies are generally the coarsest part of most coastal systems and are characterized by high-angle planar and trough cross-bedding (Clifton, 2005). Cross stratification is typical of the bar forms migrating shoreward and amalgamating into the foreshore. During storm events, the sand is remobilized and transported back into the offshore (e.g., F1 and F2). The presence of pebbles and shell beds are interpreted as erosional lags in the shoreface profile (Clifton, 2005). The amalgamation of sandstone bodies indicates storm currents as the principle creator of the shoreface deposits.

Although uncommon, evidence also exists to suggest that tides influenced sedimentation within Facies 6. For example, tubular tidalites represent burrows infilled with asymmetric sedimentary couplets, that is, open burrows that trapped tidal lamination (defined in Gingras et al., 2012). Other examples of tidal sedimentation include rare neap-spring tides (i.e., tidal bundles, *sensu* Boersma, 1969).

3.7 FACIES ASSOCIATION 1 (FA1): SUMMARY

Facies of FA1 range from sandstones containing complete bioturbation to silty mudstones that are devoid of burrowing. The primary physical structures of the sandstone and siltstones (e.g., thin planar laminae) are consistent with a distal tempestite (storm-bed) interpretation in a setting lying seaward of fair-weather wave base (MacEachern and Pemberton, 1992). Many of the tempestite beds record the waning stage of storm action on the substrate, characterized by normal grading,

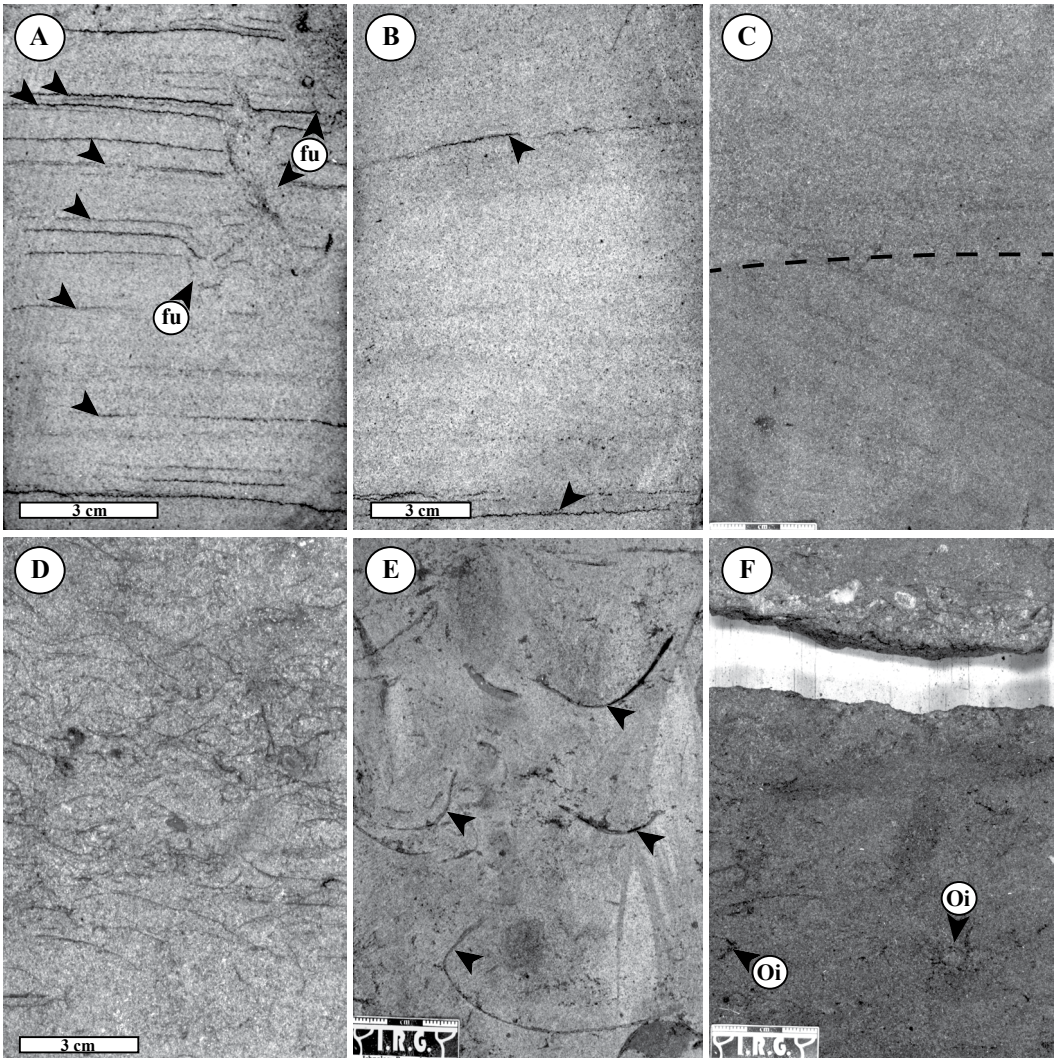

Figure 3.10: Facies of the middle to upper shoreface complex (FA2). **(A)** Lower medium-grained sandstone containing stylolites (black arrows) that became modified thereafter by fugichnia (fu). Core 1/3-3, depth 4239.80m. **(B)** Lower medium-grained sandstone that contains low-angle planar cross-stratification. Interval is cryptically bioturbated. Core 2/1-6, depth 4254.73m. **(C)** High-angle medium-grained sandstone containing planar cross-bedding that is erosionally overlain by trough cross-stratified, medium-grained sandstone. Core 7/12-6, 3483.35m. **(D)** Abundant bivalve shell debris within a massive bedded medium-grained sandstone. Core 7/12-6, depth 3484.43m. **(E)** Massive convex upward bivalve shell fragments (black arrows) located within a silty medium-grained sandstone. Core 7/12-6, depth 3442.00m. **(F)** Low-angle planar cross-stratified, medium-grained sandstone containing rare *Ophiomorpha irregulaire* (Oi). Interval overlain by a sharp based conglomerate containing sub-rounded to sub-angular pebble deposits and bivalve fragments. Core 7/12-6, 3483.00m.

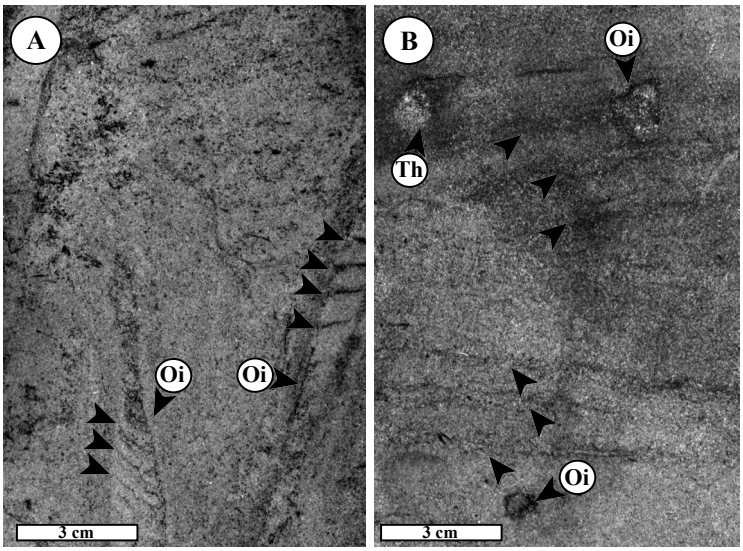

Figure 3.11: Sedimentary and biogenic structures indicative of tidal sedimentation within FA2. **(A)** Tubular tidalites (black arrows) localized within *Ophiomorpha nodosa* (On) ichnofossils. Well 1/3-3, depth 4220.50m. **(B)** Tidal bundles (i.e., neap-spring tides) within a medium-grained sandstone. Background mottling includes distinct *Ophiomorpha irregulaire* (Oi) and *Thalassinoides* (Th) ichnofossils. Well 7/12-6, depth 3494.24m.

and suspension fallout of silts and muds following storm abatement. The presence of silty and sandy material within an offshore setting in the Ula Formation is also believed to be partially a result of sediment derived from FA2 during storm-initiated sediment gravity flows.

Sediment gravity flows are a turbulent mixture of sediment and water flowing under the influence of gravity (Tucker, 2001). They are dynamically interesting because of their non-linear interaction of sediment mixing, entrainment, and suspension (Parsons et al., 2007). Initiation of a sediment gravity flow commonly occurs through an increase of the gravity force acting on a given slope (Bridge and Demicco, 2008). Increasing the slope angle can increase the downslope component of gravity force acting on a mass of sediment. Slope angles can be modified through: (i) deposition of sediment at the top of the slope; (ii) undercutting of sediment at the base of the slope; (iii) high-energy storms; and (iv) tsunamis (i.e., tectonics) (Bridge and Demicco, 2008). Storm waves, in particular, have long wavelengths and thereby have the ability to rework fair-weather deposits (MacEachern and Pemberton, 1992). As a result, storm waves can deposit their eroded material either in the supratidal zone (coastal storm sand) or, as a result of backflow, basinward in deeper water (i.e., FA1).

3.8 FACIES ASSOCIATION 2 (FA2): SUMMARY

MacEachern and Pemberton (1992) characterized three types of shorefaces based on the intensity and frequency of storms: (i) intense; (ii) moderate; and (iii) weak. Highest-energy shorefaces are composed of storm beds with minimal bioturbation. Intermediate energy shorefaces consist of a series of laminated and burrowed horizons. The bioturbated intervals represent re-colonization of storm beds by opportunistic and finally fair-weather ichnofauna. Low-energy shorefaces are intensely bioturbated through a diverse series of ichnofauna and have minimal preservation of storm beds (MacEachern and Pemberton, 1992; Pemberton et al., 2001). The Ula Formation is interpreted to reflect the weak to moderate energy shoreface profiles outlined in MacEachern and Pemberton (1992) (Fig. 3.12).

Within FA2, the low-angle parallel laminated sandstones are interpreted to represent hummocky cross-stratification and swaley cross-stratification indicative of storm waves (Harms et al., 1975; Leckie and Walker, 1982). The occurrence of escape trace fossils within the storm beds (e.g., fugichnia) records the presence of organisms entrained within or buried by the event bed, which attempt to regain the new sediment-water interface. The erosional amalgamation of successive tempestites accounts for the paucity of biogenic structures within F6. This is reflected by only the remnants of deeply penetrating *Ophiomorpha nodosa* being preserved from the opportunistic and resident fair-weather suite (MacEachern, 1994).

Although uncommon, evidence also exists to suggest tides could have influenced sedimentation within the Ula Formation. One example is tubular tidalites that were found within vertically lined trace fossils interpreted to represent *Ophiomorpha nodosa* (Fig. 3.11A). Tubular tidalites represent burrows infilled with asymmetric sedimentary couplets, that is, open burrows that trapped tidal lamination (Gingras et al., 2012). Such laminations were first described in Pleistocene *Psilonichnus* trace fossils at Willapa Bay, Washington by Gingras et al. (2000). Other examples of tidal sedimentation within this study include tidal bundles (*sensu* Boersma, 1969) within Facies 6 (Fig. 3.11B).

Historically, documentation of tidal deposits has been uncommon within Upper Jurassic sediments in the Central Graben. Steep shelf gradients and narrow intertidal zonation resulted in tidal currents having restricted lateral extent and therefore poor preservation potential. However, Howell et al. (1996) documented draped cross-beds interpreted to represent tidal origin within estuarine deposits of the Fulmar Formation in the offshore UK. Active salt withdrawal during the Upper Jurassic, resulting in intermittent reduction of tectonic slope, could have provided

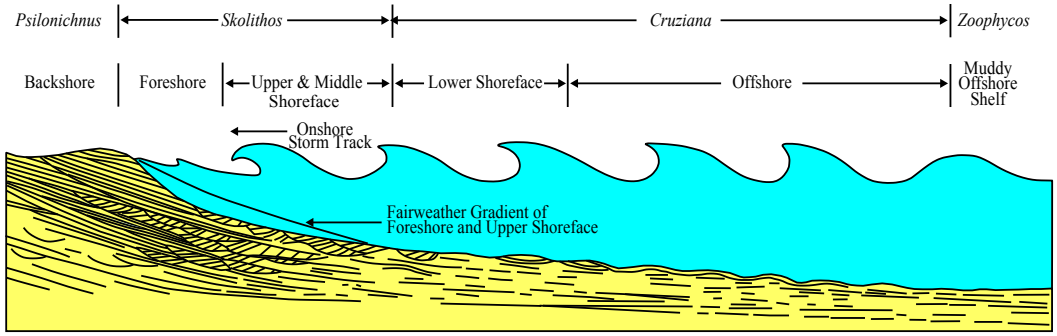

Figure 3.12: Schematic illustration of an idealized shoreface succession during a major storm. Incision of the upper shoreface and foreshore sediments are common. Modified after Gowland (1996).

an excellent opportunity for preservation of tidal activity within the Ula Formation. An additional hypothesis may be that these tidal sediments were deposited in a barred coastline or structurally embayed coast line with limited wave energy. Extensive faulting, combined with halokinesis, could have created structural embayments that were protected from fair-weather wave energy that allowed for possible preservation of tidal structures.

3.9 DISCUSSION

3.9.1 Factors Impacting Storm Sedimentation within the Central Graben

The knowledge of the frequency and magnitude of storm events (e.g., tropical cyclones) that have occurred globally is relatively unknown throughout most of earth's history (Nott, 2004). Nevertheless, ichnological and sedimentological evidence in this study suggest that sedimentation within the Upper Jurassic in the Norwegian Central Graben was influenced by storm activity. To better understand the cause of these storm events, examination into the temperature trends and sea-level profiles during the Jurassic Period is required.

During much of the Jurassic Period, a greenhouse climate with warm temperatures prevailed (Chandler et al., 1992; Hallam, 1993; Sellwood et al., 2000). Within the Middle to Upper Jurassic, a cooling period at the Callovian-Oxfordian transition is followed by a global warming trend from the Oxfordian to the Kimmeridgian (Abbink et al., 2001; Dromart et al., 2003a, Dromart et al., 2003b; Lécuyer et al., 2003; Cecca et al., 2005) (Fig. 3.13). This increase in temperature resulted in an expansion of the tropical zone (Hallam, 1985). As a result, it is probable that a change in the frequency and intensity of storm events (e.g., tropical cyclones) would have occurred due to a fluctuation in temperatures.

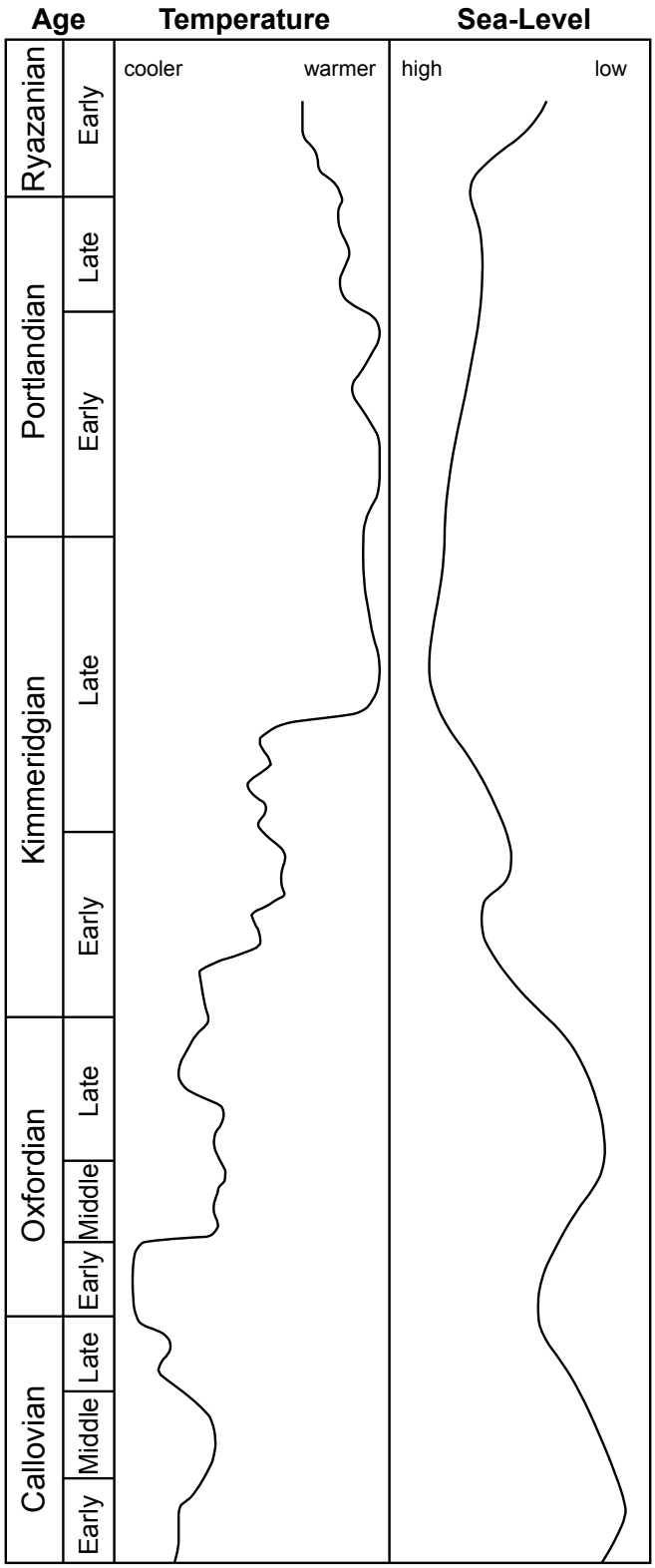

Figure 3.13: Temperature and sea-level curves for the Upper Jurassic. Modified after Abbink et al. (2001).

In addition to temperature changes, sea level transgression reached its maximum point during the Kimmeridgian due to continued extension and subsidence of the basin (Haq et al., 1988; Hallam, 1988) (Fig. 3.13). Shoreline retreat due to erosion would have been significant and remobilization of sediments in the form of tempestites likely occurred. Studies by List et al. (2006) and Nebel et al. (2012) along the coastline of the northeastern United States showed that shoreline retreat could average between 10 and 25 m following a major storm. As a result, the paucity of upper shoreface (and more particularly foreshore-backshore) deposits within FA2 is likely in part due to truncation and erosion by transgression and storm activity. Consequently, a transgressive surface of erosion (TSE) (i.e., ravinement surface, *sensu* Stamp, 1921) demarcated by a *Glossifungities* surface is common at the top of FA2.

At present, the exact number of storm events that occurred within the Ula Formation is unidentifiable. Nonetheless, the presence of highly bioturbated sediments suggests the frequency of storms would have been low to moderate (MacEachern and Pemberton, 1992). Examples of *Ophiomorpha nodosa* and *Siphonichnus* having lengths reaching up to 30 cm are present within the core dataset. This suggests that up to 30 cm of sediment could have been deposited during a single storm event. Similar storm deposit thicknesses are observable within the Fulmar Formation (Howell et al., 1996) and on modern shelves (e.g., Howard and Reineck, 1981; Wang, 1998). Furthermore, many examples of storm deposits in other Upper Jurassic intervals occur worldwide and include: (i) northern and eastern Ethiopia (Bosellini et al., 1997; Bosellini et al., 2001); (ii) southern Tanzania (Bussert and Aberhan, 2004); (iii) central and northern Morocco (Ager, 1974; Ait Addi, 2008); and (iv) northern United States (Brenner and Davies, 1973).

Given the evidence suggesting storm sedimentation, debate might also exist as to whether any deposits also reflect palaeotsunamis. Fundamentally, tsunamis are a reflection of long-period waves generated by submarine landslides, volcanic eruptions, asteroid impacts, or deep-ocean earthquakes (Morton et al., 2007). Within the Upper Jurassic, the presence of extensional rifting (Ziegler, 1982; Roberts et al., 1990; Gowers et al., 1993; Fraser et al., 2003) suggests tsunamis might have occurred. However, no concrete sedimentary signatures exist within the studied cores (e.g., sand sheets, boulder deposits, slump scours, overturned beds, debris flows, mass transport deposits) to imply paleotsunami deposits (Goff et al., 2011; Dominey-Howes et al., 2006). Possible reasons could be relative distance of the paleoshoreline from the epicenter of the earthquake. For example, many of the

large waves produced by tsunamis near the Pacific Rim are commonly reduced to small waves by the time they reach the shoreline of western North America (McCulloch, 1985). Furthermore, coastal records from the modern Pacific Ocean region suggest major tsunamis are rare (i.e., generally less than one per decade) and occur much less frequently than storm events (Morton et al., 2007). As such, most tsunami deposits, if deposited, were likely subjected post-depositional processes such as wave erosion that reduced their thickness and overall spatial distribution (e.g., Hori et al., 2007; McAdoo et al., 2008; Bahlburg and Spiske, 2012).

3.9.2 Influence of Basin Geometry on Sedimentation

At present, between 30 and 50% of the marine coastlines exist along or near an active margin coastline (e.g., Pacific coastline of North and South America) (Inman and Nordstrom, 1971). Within these areas, common morphological characteristics include deep submarine trenches and narrow continental shelves. This is in stark contrast to passive continental margins (e.g., Atlantic coastline of North America, northeastern Australia) wherein low-relief coastal plains and a wide continental shelf are common. As a result, shoreface environments in extensional basins, and especially their facies distributions, are greatly influenced by extensional faulting (Leeder and Gawthorpe, 1987; Gawthorpe and Hurst, 1993; Gawthrope et al., 1994; Ravnås and Steel, 1998; Mellere et al., 2005).

Tectonic processes in extensional basins influence sedimentation in several ways: (i) relative sea level; (ii) rapidly changing accommodation space; (iii) altering sediment supply; and (iv) altering the basin physiography (Gawthorpe et al., 1994). Regarding basin physiography, tectonic slopes generated through extensional basin development often include a steep, spatially restricted footwall scarp and a gently sloping hanging wall (Leeder and Gawthorpe, 1987). The angle of the tectonic slope exerts a fundamental control on geomorphology and sedimentation process.

The deposition of the studied sediments is the general result of wave- and gravity-driven onshore to offshore transport. Sediment was most likely derived from emerged highs comprised by Triassic sediments such as the Vestland Arch (Bjørnseth and Gluyas, 1995). Basinward transport of sand dominantly occurred as a result of high-energy, short-period waves generating strong, offshore and alongshore surges, typically directed through rip channels and longshore troughs similar to what has been observed along modern shorelines (Swift et al., 1985). Sands stranded in the offshore and shelf were sporadically mobilized following storm events and were most likely preserved as thinly bedded tempestites (e.g.,

FA1). Ultimately, tectonic and halokinetic subsidence led to the aggradation and preservation of FA1 and FA2 (as seen in Fig. 3.3).

3.9.3 Ichnological Trends: Storm-Dominated, Active Margin Coastline

It has been noted that wide shorelines commonly occur within low-angle, gently dipping coastal plains (Heward, 1981). Conversely, in areas with a narrow coastline, such as the Pacific coast of North America (Inman and Nordstrom, 1971; Storlazzi and Field, 2000), a narrow shoreline-attached foreshore would be predicted. Due to these differences in coastline morphology, the influence of waves on sediment transport and biogenic diversity will be different (Fig. 3.14).

Using the Ula Formation as an example of an active margin coastline, it can be observed that the backshore and foreshore (i.e., upper intertidal zone) are absent due a combination of factors such as high tectonic slope and wave erosion. In this content, it must also be noted that backshore and foreshore sediments are usually not preserved unless there is a rapid transgression that will cover and preserve the sediments with mudstones. Because sea-level transgression is believed to have coincided with elevated wave activity due to storms during the Upper Jurassic, it is likely that most of the upper intertidal sediments were removed through erosion during transgressions.

The upper shoreface (i.e., middle intertidal zone) within the Ula Formation is similar to that of other shoreface settings in that it is dominated by trough cross-bedding in both a onshore and offshore direction (Howard and Reineck, 1981). However, the ichnological characteristics of the upper shoreface within the Ula Formation appear to differ from those of low-angle shorefaces. In this study, the overall ichnological suite is characterized by sporadically distributed bioturbation and reduced diversity of ichnogenera in the *Skolithos* ichnofacies. This is similar to the expected trace fossil suites of low-angle shorefaces (MacEachern et al., 1999; Pemberton et al., 2001), which typically have a bioturbation intensity of 1 to 3 (Dashtgard et al., 2009). However, within the Ula Formation, greater ichnodiversity reduction occurs as compared to other low-angle shorefaces as they are either patchy burrowed (i.e., BI 0 to 2) or contain cryptic bioturbation (i.e., BI 5 to 6). Common elements of the *Skolithos* ichnofacies observed in the upper shoreface of the Ula Formation include *Planolites*, *Skolithos*, *Ophiomorpha*, and fugichnia. Much of the reduction in ichnogenera within the upper shoreface is likely due to the persistent reworking of sediments through storm waves.

Sedimentologically, the lower shoreface within this study is dominated by

current and oscillation generated structures. In the finer grained sandstones, wave and combined flow ripples, along with hummocky cross-stratification, are present, although high levels of bioturbation obscure their detection. Interbedded within these finer-grained sediments are medium-grained sandstones containing current-generated trough cross-bedding and low-angle planar cross-bedding. Although most shorefaces display a high level of infaunal reworking (e.g., BI 3 to 5 in low-angle shorefaces (Dashtgard et al., 2009) versus BI 4 to 6 in this study), the *Skolithos* ichnofacies extends markedly into the lower shoreface within the Ula Formation. Elements of the *Skolithos* ichnofacies common to the Ula Formation in the lower shoreface include *Ophiomorpha* and *Siphonichnus*. Typically proximal, *Ophiomorpha nodosa* commonly cross-cut characteristically distal (or lower-energy) *Ophiomorpha irregulaire* (e.g., Fig. 3.10E-F), indicating fluctuating energy conditions. This, in combination with sporadically distributed wave-generated structures, attests to an influence of storm currents during deposition. The Ula Formation shoreface sediments therefore depart from the generalized facies models based on the oscillatory and shoaling wave processes that is predicted under fair-weather conditions (Clifton et al., 1971; Walker and Plint, 1992; Reading, 1996; Clifton, 2005).

The offshore limit within the Ula Formation is gradational and the storm-wave base is predicted as the transitional point between the offshore (FA1) and shoreface (FA2). In this study, above the storm-wave base the seafloor is subjected to both fair-weather and storm-generated currents. Beyond this point, hydraulic reworking of the seafloor is sporadic and limited to episodic tempestities. Within the proximal end of the lower shoreface in the Ula Formation, elements of the distal *Skolithos* ichnofacies become integrated with elements of the *Cruziana* ichnofacies. The offshore deposits of within this study and other low-angle shorefaces are very similar in that both are occupied by the *Cruziana* ichnofacies (e.g., *Asterosoma*, *Phycosiphon*, *Rosselia*, *Teichichnus*). However, within the Ula Formation, persistent energy fluctuations within the offshore environment through storm-generated currents typically inhibited grazing behaviors within the *Cruziana* ichnofacies. The dominance of permanent dwellings of deposit-feeding ichnofossils (i.e., *Palaeophycus*, *Rosselia*, *Thalassinoides*) is therefore a reflection of increased sedimentation within a deeper-water setting. In contrast, owing to the diminished influence of storm surges beyond the fair-weather wave base, food resources commonly accumulate on the sea floor in low-angle shorefaces (Pemberton *et al*., 2001), thereby leading to a predominance of grazers and deposit-feeding organisms.

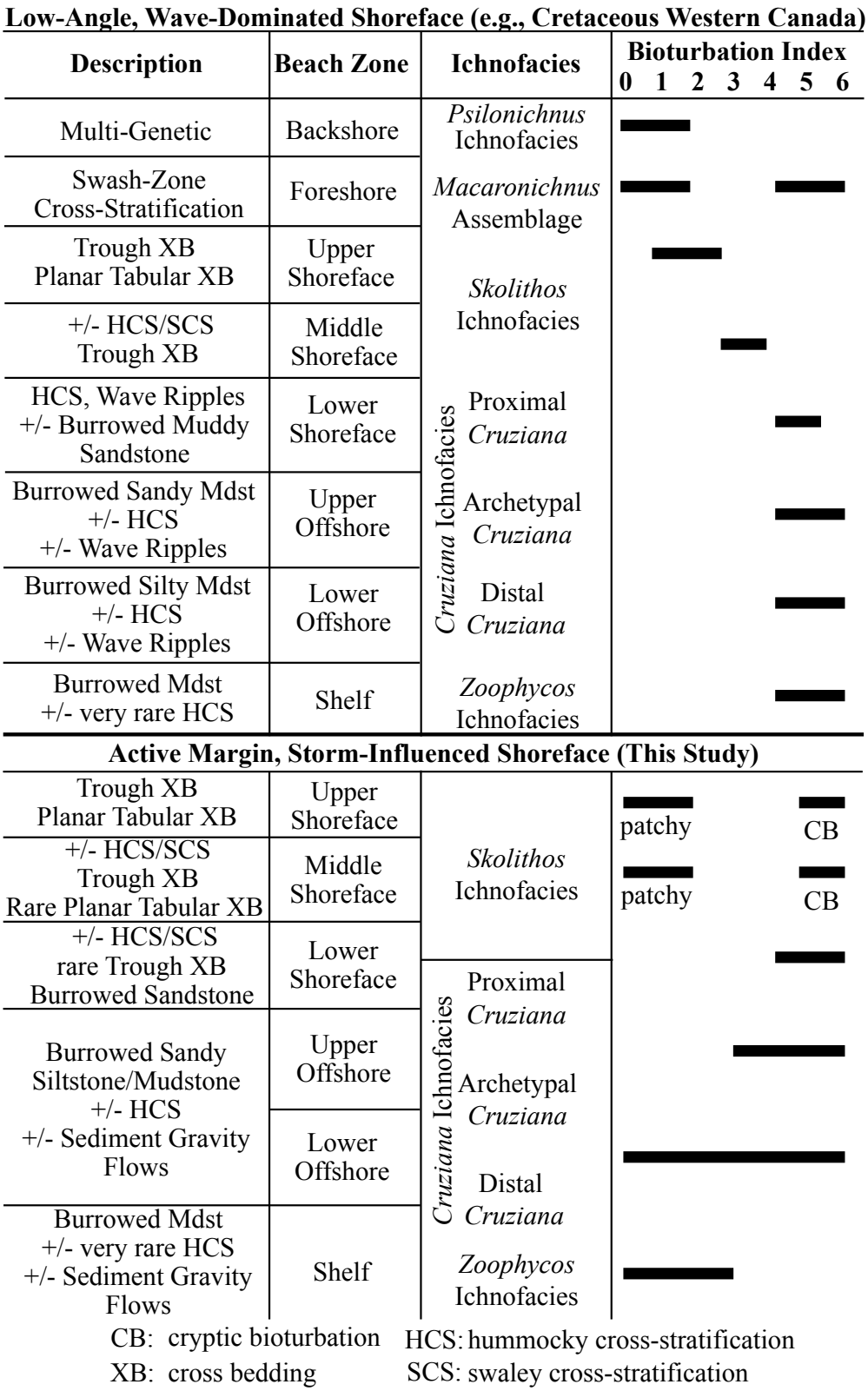

Figure 3.14: Comparison of ichnological assemblages in low-angle shorefaces (e.g., Western Canadian Sedimentary Basin: MacEachern et al. (1999); Dashtgard et al. (2009)) and storm-influenced, active margin successions (e.g., Ula Formation, Norwegian Central Graben: this study).

3.9.4 Sequence Stratigraphy

Ichnofacies classification allows for recognition of stratigraphic surfaces such as bounding discontinuities, unconformities, marine flooding surfaces (MFS) and transgressive surfaces of erosion (TSE) (MacEachern et al., 1992). Recognition of these surfaces is critical to providing clearer resolution of depositional environments and allocyclic controls on depositional systems (MacEachern et al., 1992). Key stratal surfaces within the Ula Formation are reflected primarily through the presence of MFS and TSE.

MFS are typically, but not always, sharp and abrupt stratigraphic horizons across which there is evidence of an increase in water depth without significant erosion (Van Wagoner et al., 1988). MFS can be recognized through the presence of *Glossifungites* ichnofacies. Trace fossils present in the *Glossifunigites* assemblages have several diagnostic characteristics (MacEachern et al., 1992; Gingras et al., 2000; MacEachern et al., 2007c), including: (i) sharply-defined walls; (ii) scratch marks in the burrow walls; (iii) ichnofossils that cross-cut the palimpset trace fossil assemblage; and (iv) burrow infill that consists of sediment that is distinct from which comprises the firmground. Commonly associated with semilithified or firm substrate formed either by subaerial exposure or by burial and subsequent exhumation (e.g., MacEachern et al., 1992; Gingras et al., 2000; Pemberton et al., 2001; MacEachern et al., 2007c), there is also the recording of *Glossifungites* ichnofacies with other non-erosional surfaces such as MFS.

Within the Ula Formation cores, *Diplocraterion* (most notably *Diplocraterion habichi*) is the most common trace fossil at MFS (Fig. 3.15). *Diplocraterion*

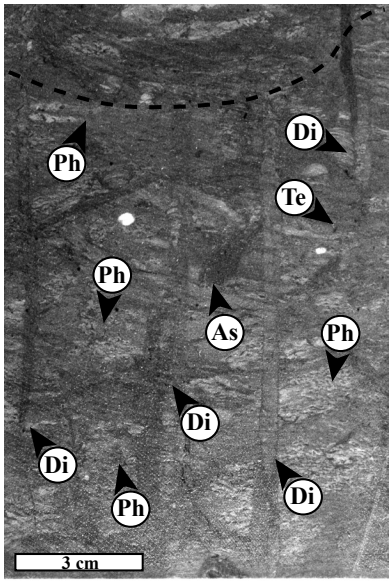

Figure 3.15: An example of a maximum flooding surface (MFS). Deeply penetrating *Diplocraterion habichi* (Di) cross-cutting a *Cruziana* ichnofacies assemblage within Facies 2 that consists of *Phycosiphon* (Ph), *Teichichnus* (Te), and *Asterosoma* (As). The *Diplocraterion habichi* are interpreted to demarcate a marine flooding surface (MFS). Core 1/3-3, depth 4182.45m.

habachi, a commonly monospecific ichnocoenosis, is represented through the presence of long, slender, u-shaped burrows formed by suspension-feeders (Dam, 1990). Heinberg and Birkelund (1984) suggested that the long tubes were formed as protective shelters against unstable conditions on the sea floor. *Diplocraterion hahachi* commonly overprints background *Cruziana* ichnofacies within the cores (e.g., Facies 2) and are therefore regarded as omission suites at transgressive surfaces (MacEachern et al., 1992; Pemberton et al., 2004). Similar examples include Lower to Middle Jurassic sediments from the Halten Terrace in the mid-Norwegian continental shelf (Taylor and Gawthorpe, 1993) and sediments from the Neill Klinter Formation of Jameson Land, East Greenland (Dam, 1990).

3.10 CONCLUSIONS

The Upper Jurassic Ula Formation located along the northeastern margin of the Norwegian Central Graben reflects a storm-influenced shoreface succession. Core logging revealed two reoccurring facies associations: offshore (FA1) and shoreface (FA2). Ichnological analysis of FA1 revealed that the trace fossil suites developed under fair-weather conditions contained a high-diversity and abundance of deposit feeding trace fossils, with excellent development of tiering structures and widespread distribution. Evidence of distal tempestites within FA1 includes thin planar laminae and localized reductions in ichnofossil abundances.

Trace fossil suites found within FA2 display low- to moderate-diversity in trace fossils and an overall dominance of dwelling-structures. The occurrence of storm events commonly precludes the development of diverse communities within FA2. Nonetheless, moderate to extensive bioturbation of the shoreface sediments (e.g., cryptic bioturbation) suggests the overall energy conditions were low to moderate and the presence of higher-energy storm events are occasional. The importance of understanding these animal-sediment interactions within the Ula Formation therefore serves to highlight the significance of ichnology towards reconstructions of depositional environments within the geological rock record.

3.11 REFERENCES CITED

Abbink, O.A., Targaron, J., Brinkhuis, H., and Visscher, H., 2001, Late Jurassic to earliest Cretaceous paleoclimatic evolution of the southern North Sea: Global and Planetary Change, v. 30, p. 231-256.

Ager, D.V., 1974, Storm deposits in the Jurassic of the Moroccan High Atlas: Palaeogeography, Palaeoclimatology, Palaeoecology, v. 15, p. 83-93.

Ait Addi, A., 2008, Storm deposits: Evidence of event sedimentation in the Bajocian of the Central High Atlas, Morocco: Volumina Jurassica, v. 6, p, 23-32.

Bahlburg, H., and Spiske, M., 2012, Sedimentology of tsunami inflow and backflow deposits: Key differences revealed in a modern example: Sedimentology, v. 59, p. 1063-1086.

Bailey, C.C., Price, I., and Spencer, A.M., 1981, The Ula Field, Block 7/12, Norway: *in* Norwegian Symposium on Exploration. Norwegian Petroleum Society (NPF), Article 18, 26 p.

Baird, R.A., 1986, Maturation and source rock-evaluation of Kimmeridge Clay, Norwegian North Sea: American Association of Petroleum Geologists Bulletin, v. 70, p. 1-11.

Bann, K.L., and Fielding, C.R., 2004, An integrated ichnological and sedimentological comparison of non-deltaic shoreface and subaqueous delta deposits in Permian reservoir units of Australia: *in* McIlroy, D., ed., The Application of Ichnology to Palaeoenvironmental and Stratigraphic Analysis. Geological Society, London, Special Publication, v. 228, p. 273-310.

Bann, K.L., Fielding, C.R., MacEachern, J.A., and Tye, S.C., 2004, Differentiation of estuarine and offshore marine deposits using integrated ichnology and sedimentology: Permian Pebbly Beach Formation, Sydney Basin, Australia: *in* McIlroy, D., ed., The Application of Ichnology to Palaeoenvironmental and Stratigraphic Analysis. Geological Society, London, Special Publication, v. 228, p. 179-211.

Barrell, J., 1912, Criteria for the recognition of ancient delta deposits: Geological Society of America Bulletin v. 23, p. 377-446.

Bednarz, M., and McIlroy, D., 2009, Three-dimensional reconstruction of "Phycosiphoniform" burrows: Implications for identification of trace fossils in core: Palaeontologia Electronica, v. 12, p. 1-15.

Berner, R.A., 1985, Sulphate reduction, organic matter decomposition and pyrite formation: Philosophical Transactions of the Royal Society of London Series A, v. 315, 25-38.

Bjørnseth, H.M., and Gluyas, J.G., 1995, Petroleum exploration in the Ula Trend: *in* Hanslien, S., ed., Petroleum Exploration in Norway: Proceedings of the Norwegian Petroleum Conference. Norwegian Petroleum Society (NPF), Special Publication 4, Elsevier, Amsterdam, p. 85-96.

Boersma, J.R., 1969, Internal structures of some tidal megaripples on a shoal in the Westerschelde estuary, the Netherlands: Geologie en Mijnbouw, v.48, 409-414.

Bosellini, A., Russo, A., Fantozzi, P.L., Assefa, G., and Solomon, T., 1997, The Mesozoic succession of the Mekelle outlier (Tigre Province, Ethiopia): Memorie di Scienze Geologiche, v. 49, p. 95-116.

Bosellini, A., Russo, A., and Assefa, G., 2001, The Mesozoic succession of Dire Dawa, Harar Province, Ethiopia: Journal of African Earth Sciences, v. 32, p. 403-417.

Brenner, R.L., and Davies, D.K., 1973, Storm-generated coquinoid sandstone: Genesis of high-energy marine sediments from the Upper Jurassic of Wyoming and Montana: Geoological Society of America Bulletin, v. 84, p. 1685-1698.

British Petroleum (BP) Energy., 2013, BP Norway English- Fields Operated by BP: Available at http://www.bp.com/subsection.do?categoryId=9003421&contentId=7008709 (Accessed on June 27, 2013).

Bridge, J.S., and Demicco, R.V., 2008, Earth Surface Processes, Landforms and Sediment Deposits. Cambridge University Press, Cambridge, 815 p.

Bromley, R.G., and Ekdale, A.A., 1984, *Chondrites*: A trace fossil indicator of anoxia in sediments: Science, v. 224, p. 872-874.

Bromley, R.G., and Ekdale, A.A., 1986, Composite ichnofabrics and tiering of burrows: Geological Magazine, v. 123, p. 59-65.

Bromley, R.G., 1990, Trace Fossils: Biology and Taphonomy. Unwin Hyman, London, United Kingdom, 280 p.

Bromley, R.G., 1996, Trace Fossils: Biology, Taphonomy and Applications, Second Edition. Chapman and Hall, London, United Kingdom, 361 p.

Brown, A., Mitchell, A.W., Nilssen, I.R., Stewart, I.J., and Svela, P.T., 1992, Ula Field: Relationship and hydrocarbon distribution: *in* Larsen, R.M., Brekke, H., Larsen, B.T., and Talleraas, E., eds., Structural and Tectonic Modeling and its Application to Petroleum Geology. Norwegian Petroleum Society (NPF), Special Publication 1, Elsevier, Amsterdam, p. 409-420.

Buatois, L.A., Mángano, M.G., and Carr, T.R., 1999, Sedimentology and ichnology of Paleozoic estuarine and shoreface reservoirs, Morrow Sandstone, Lower Pennsylvanian of southwest Kansas, USA: Kansas Geological Survey, Bulletin 243, Current Research in Earth Sciences. Available at: http://www.kgs.ukans. edu/Current /1999/ buatois1.html (Accessed on June 27, 2013).

Bussert, R., and Aberhan, M., 2004, Storms and tsunamis: Evidence of event sedimentation in the Late Jurassic Tendaguru Beds of southeastern Tanzania: Journal of African Earth Sciences, v. 39, p. 549-555.

Cecca, F., Martin-Garin, B., Marchand, D., Lathuiliere, B., and Bartolini, A., 2005, Paleoclimatic control of biogeographic and sedimentary events in Tethys and peri-Tethys areas during the Oxfordian (Late Jurassic): Palaeogeography, Palaeoclimatology, Palaeoecology, v. 222, p. 10-32.

Chandler, M.A., Rind, D., and Ruedy, R., 1992, Paleoclimate during the Early Jurassic: GCM simulations and the sedimentary record of paleoclimate: Geological Society of America Bulletin, v. 104, p. 543-59.

Christie, P.A.F., and Sclater, J.G., 1980, An extensional origin for the Buchan and Witchground graben in the North Sea: Nature, v. 283, p. 729-732.

Clifton, H.E., 2005, Coastal sedimentary facies: *in* Schwartz, M.L., ed., Encyclopedia of Coastal Science. Springer-Verlag, Dordrecht, The Netherlands, p. 270-278.

Clifton, H.E., Hunter, R.E., and Phillips, R.L., 1971, Depositional structures and processes in the nonbarred high-energy nearshore: Journal of Sedimentary Petrology, v. 41, p. 651-670.

Cooper, B.S., Barnard, P.C., and Telnaes, N., 1995, The Kimmeridge Clay Formation of the North Sea: *in* Katz, B.J., ed., Petroleum Source Rocks. Springer, New York, New York, p. 89-110.

Coward, M.P., Dewey, J., Hempton, M., Holroyd, J., and Mange, M.A., 2003, Tectonic evolution: *in* Evans, D., Graham, C., Armour, A., and Bathurst, P., eds., The Millennium Atlas: Petroleum Geology of the Central and Northern North Sea. Geological Society, London, United Kingdom, p. 17-33.

Dam, G., 1990, Palaeoenvironmental significance of trace fossils from the shallow marine Lower Jurassic Neill Klinter Formation, East Greenland: Palaeogeography, Palaeoclimatology, Palaeoecology, v. 79, p. 221-248.

Dashtgard, S.E., Gingras, M.K., and MacEachern, J.A., 2009, Tidally modulated shorefaces: Journal of Sedimentary Research, v. 79, p. 793-807.

Deegan, C.E., and Scull, B.J., 1977, A proposed standard lithostratigraphic nomenclature for the Central and Northern North Sea: Norwegian Petroleum Directorate Bulletin, no. 1, 36 pp.

Dominey-Howes, D.T.M., Humphreys, G.S., and Hesse, P.P., 2006, Tsunami and palaeotsunami depositional signatures and their potential value in understanding the late-Holocene tsunami record: The Holocene, v. 16, p. 1095-1107.

Donato, J.A., and Tully, M.C., 1981, A regional interpretation of the North Sea gravity data: *in* Illing, L.V., and Hobson, G.D., eds., Petroleum Geology of the Continental Shelf of North-West Europe. Heyden and Son, London, United Kingdom, p. 65-75.

Dromart, G., Garcia, J.-P., Gaumet, F., Picard, S., Rousseau, M., Atrops, F., Lécuyer, C., and Shepard, S.M.F., 2003a, Perturbation of the carbon cycle at the Middle/ Late Jurassic transition: Geological and geochemical evidence: American Journal of Science, v. 303, 667-707.

Dromart, G., Garcia, J.-P., Picard, S., Atrops, F., Lécuyer, C., and Shepard, S.M.F., 2003b, Ice age at the Middle-Late Jurassic transition?: Earth and Planetary Science Letters, v. 213, p. 205-220.

Einsele, G., 2000, Sedimentary Basin: Evolution, Facies and Sediment Budget, Second Edition. Springer-Verlag, Berlin, Heidelberg, 792 p.

Ekdale, A.A., and Mason, T.R., 1988, Characteristic trace-fossil associations in oxygen-poor sedimentary environments: Geology, v. 16, p. 720-723.

Ekdale, A.A., and Bromley, R.G., 1991, Analysis of composite ichnofabric: An example in uppermost Cretaceous chalk of Denmark: Palaios, v. 6, p. 232-249.

Fraser, S.I., Robinson, A.M., Johnson, H.D., Underhill, J.R., Kadolsky, D.G.A., Connell, R., Johannesen, P., and Ravnås, R., 2003, Upper Jurassic: *in* Evans, D., Graham, C., Armour, A., and Bathurst, P., eds., The Millennium Atlas: Petroleum Geology of the Central and Northern North Sea. Geological Society, London, United Kingdom, p. 157-189.

Frey, R.W., and Seilacher, A., 1980, Uniformity in marine invertebrate ichnology: Lethaia, v. 13, p.183-207.

Frey, R.W., and Bromley, R., 1985, Ichnology of American chalks: The Selma Group (Upper Cretaceous), western Alabama: Canadian Journal of Earth Sciences, v. 22, p. 801-828.

Frey, R.W., and Pemberton, S.G., 1985, Biogenic structures in outcrops and cores. I: Approaches to ichnology: Bulletin of Canadian Petroleum Geology, v. 33, p. 72-115.

Frey, R.W., Howard, J.D., and Pryor, W.A., 1978, *Ophiomorpha*: Its morphologic, taxonomic, and environmental significance: Palaeogeography, Palaeoclimatology, Palaeoecology, v. 23, p. 199-229.

Gawthorpe, R.L., and Hurst, J.M., 1993, Transfer zones in extensional basins: Their structural style and influence on drainage development and stratigraphy. Journal of the Geological Society, London, v. 150, p. 1137-1152.

Gawthorpe, R.L., Fraser, A.J., and Collier, R.E.L., 1994, Sequence stratigraphy in active extensional basins: Marine and Petroleum Geology, v. 11, p. 642-658.

Gingras, M.K., and MacEachern, J.A., 2012, Tidal ichnology of shallow-water clastic settings: *in* Davis, Jr., R.A., and Dalrymple, R.W., eds., Principles of Tidal Sedimentology. Springer, New York, New York, p. 57-77.

Gingras, M.K., MacEachern, J.A., and Pemberton, S.G., 1998, A comparative analysis of the ichnology of wave and river dominated allomembers of the Upper Cretaceous Dunvegan Formation: Bulletin of Canadian Petroleum Geology, v. 46, p. 51-73.

Gingras, M.K., Pemberton, S.G., and Saunders, T., 2000, Firmness profiles associated with tidal-creek deposits: The temporal significance of *Glossifungites* assemblages: Journal of Sedimentary Research, v. 70, p. 1017-1025.

Gingras, M.K., Bann, K.L., MacEachern, J.A., Waldron, J., and Pemberton, S.G., 2007, A conceptual framework for the application of trace fossils: *in* MacEachern, J.A., Bann, K.L., Gingras, M.K., and Pemberton, S.G., eds., Applied Ichnology. Society of Economic Paleontologists and Mineralogists (SEPM), Short Course Notes, no. 52, p. 1-26.

Gingras, M.K., Dashtgard, S.E., MacEachern, J.A., and Pemberton, S.G., 2008, The biology of shallow-marine ichnology: A modern perspective*:* Aquatic Biology, v. 2, p. 255-268.

Glennie, K.W., Highman, J., and Stemmerik, L., 2003, Permian: *in* Evans, D., Graham, C., Armour, A., and Bathurst, P., eds., The Millennium Atlas: Petroleum Geology of the Central and Northern North Sea. Geological Society, London, United Kingdom, p. 91-103.

Gluyas, J.G., 1997, Poroperm prediction for reserves growth exploration: Ula Trend, Norwegian North Sea: *in* Kupecz, J.A., Gluyas, J.G., and Bloch, S., eds., Reservoir Quality Prediction in Sandstones and Carbonates. American Association of Petroleum Geologists, Memoir no. 69, p. 201-210.

Gluyas, J.G., Byskov, K., and Rothwell, N., 1992, A year in the life of Gyda production: *in* Advances in Reservoir Technology. Conference Proceedings, IBC, London, United Kingdom, p. 187-202.

Goff, J., Chagué-Goff, C., Dominey-Howes, D., McAdoo, B., Cronin, S., Bonté-Grapetin, M., Nichol, S., Horrocks, M., Cisternas, M., Lamarche, G., Pelletier, B., Jaffe, B., and Dudley, W., 2011, Palaeotsunamis in the Pacific Islands: Earth Science Reviews, p. 107, p. 141-146.

Goldring, R., Pollard, J.E., and Taylor, A.M., 1991, *Anconcihnus horizontalis*: A pervasive ichnofabric-forming trace fossil in post-Paleozoic offshore siliciclastic facies: Palaios, v. 6, p. 250-263.

Gowers, M.B., Holtar, E., and Swensson, E., 1993, The structure of the Norwegian Central Trough (Central Graben area): *in* Parker, J.R., Petroleum Geology of Northwest Europe: Proceedings of the 4th Conference. Geological Society, London, p. 1245-1254.

Gowland, S., 1996, Facies characteristics and depositional models of highly bioturbated shallow marine siliciclastic strata: An example from the Fulmar Formation (Late Jurassic), UK Central Graben: *in* Hurst, A., Johnson, H.D., Burley, S.D., Canham, A.C., and Mackertich, D.S., eds., Geology of the Humber Group: Central Graben and Moray Firth, UKCS. Geological Society, London, Special Publication, v. 114, p. 185-214.

Hallam, A., 1985, A review of Mesozoic climates: Journal of the Geological Society, London, v. 142, p. 433-445.

Hallam, A., 1988, A re-evaluation of the Jurassic eustasy in the light of new data and the revised Exxon curve: *in* Wilgus, C.K., Hastings, B.S., Kendall, C.G.S.C., Posamentier, H.W., Ross, C.A., and Van Wagoner, J.C., eds., Sea Level Changes- An Integrated Approach. Society of Economic Paleontologists and Mineralogists (SEPM) Special Publication, v. 42, p. 261-273.

Hallam, A., 1993, Jurassic climates as inferred from the sedimentary and fossil record: Philosophical Transactions of the Royal Society of London Series B, v. 341, p. 287-296.

Harms, J.C., Southard, J.B., Spearing, D.R., and Walker, R.G., 1975, Depositional environments as interpreted from primary sedimentary structures and stratification sequences: Society of Economic Paleontologists and Mineralogists (SEPM), Short Course Notes, no. 2, Dallas, Texas, 161 p.

Haq, B.U., Hardenbol, J., and Vail, P.R., 1988, Mesozoic and Cenozoic chronostratigraphy and cycles of sea-level change: *in* Wilgus, C.K., Hastings, B.S., Kendall, C.G.S.C., Posamentier, H.W., Ross, C.A., and Van Wagoner, J.C., eds., Sea Level Changes- An Integrated Approach. Society of Economic Paleontologists and Mineralogists (SEPM) Special Publication, v. 42, p. 71-108.

Heinberg, C., and Birkelund, T., 1984, Trace fossil assemblages and basin evolution of the Vardekløft Formation (Middle Jurassic, Central East Greenland): Journal of Paleontolology, v. 58, p. 362-397.

Heward, J.D., 1981, A review of wave-dominated clastic shoreline deposits: Earth Science Reviews, v. 17, 223-276.

Hodgson, N.A., Farnsworth, J., and Fraser, A.J., 1992, Salt-related tectonics, sedimentation and hydrocarbon plays in the Central Graben, North Sea, UKCS: *in* Hardman, R.F.P., ed., Exploration Britain: Geological Insights for the Next Decade. Geological Society, London, Special Publication, v. 67, p. 31-63.

Home, P.C., 1987, Ula: *in* Spencer, A.M., Campbell, C.J., Hanslien, S.H., Nelson, P.H., Nysaether, E., and Ormaasen, E.G., Geology of the Norwegian Oil and Gas Fields. Graham and Trotman, London, United Kingdom, p. 143-152.

Hori, K., Kuzumoto, R., Hirouchi, D., Umitsu, M., Janjirawuttikul, N., and Patanakanog, B., 2007, Horizontal and vertical variation of 2004 Indian tsunami deposits: An example of two transects along the western coast of Thailand: Marine Geology, v. 239, p. 163-172.

Howard, J.D., 1975, The sedimentological significance of trace fossils: *in* Frey, R.W., The Study of Trace Fossils. Springer-Verlag, New York, New York, p. 131-146.

Howard, J.D., and Reineck, H.E., 1972, Georgia coastal region, Sapelo Island, U.S.A.: Sedimentology and biology IV: Physical and biogenic sedimentary structures of the nearshore shelf: Senckenbergiana Maritima, v. 4, p. 81-123.

Howard, J.D., and Reineck, H.E., 1981, Depositional facies of high-energy beach to offshore sequence: Comparison with the low-energy sequence: American Association of Petroleum Geologists Bulletin, v. 65, p. 807-830.

Howard, J.D., and Frey, R.W., 1975, Estuaries of the Georgia Coast, U.S.A.: sedimentology and biology. II. Regional animal-sediment characteristics of Georgia Estuaries: Senckenbergiana Maritima, v. 7, p. 33-103.

Howell, J.A., Flint, S.S., and Hunt, C., 1996, Sedimentological aspects of the Humber Group (Upper Jurassic) of the South Central Graben, UK North Sea: Sedimentology, v. 43, p. 89-114.

Inman, D.L., and Nordstrom, C.E., 1971, On the tectonic and morphologic classification of coasts: The Journal of Geology, v. 79, p. 1-21.

Johnson, D.W., 1919, Shore Processes and Shoreline Development. John Wiley, New York, New York, 584 p.

Johnson, H.D., Mackay, T.A., and Stewart, D.J., 1986, The Fulmar Oil-field (Central North Sea): Geological aspects of its discovery, appraisal and development: Marine and Petroleum Geology, v. 3, p. 99-125.

Leckie, D.A., and Walker, R.G., 1982, Storm- and tide-dominated shorelines in Cretaceous Moosebar-Lower Gates interval: Outcrop equivalents of Deep Basin gas trap in Western Canada: American Association of Petroleum Geologists Bulletin, v. 66, p. 138-157.

Lécuyer, C., Picard, S., Garcia, J.-P., Sheppard, S.M.F., Grandjean, P., and Dromart, G., 2003, Thermal evolution of Tethyan surface waters during the Middle-Late Jurassic: evidence from $\delta^{18}O$ values of marine fish teeth: Paleoceanography, v. 18, p. 1076-1091.

Leeder, M.R., and Gawthorpe, R.L., 1987, Sedimentary models for extensional tilt-block/half-graben basins: *in* Coward, M.P., Dewey, J.F., and Hancock, P.L., eds., Continental Extensional Tectonics. Geological Society, London, Special Publication, v. 28, p. 139-152.

Lemiski, R.T., Hovikoski, J., Pemberton, S.G., and Gingras, M., 2011, Sedimentological, ichnological and reservoir characteristics of the low-permeability, gas-charged Alderson Member (Hatton gas field, southwest Saskatchewan): Implications for resource development: Bulletin of Canadian Petroleum Geology, v. 59, p. 27-53.

List, J.H., Farris, A.S., and Sullivan, C., 2006, Reversing storm hotspots on sandy beaches: Spatial and temporal characteristics: Marine Geology, v. 226, p. 261-279.

MacEachern, J.A., 1994, Integrated ichnological-sedimentological models: Applications to the sequence stratigraphic and paleoenvironmental interpretation of the Viking and Peace River formations, west-central Alberta: University of Alberta PhD Thesis, Unpublished, 618 p.

MacEachern, J.A., and Pemberton, S.G., 1992, Ichnological aspects of Cretaceous shoreface successions and shoreface variability in the Western Interior Seaway of North America: *in* Pemberton, S.G., ed., Applications of Ichnology to Petroleum Exploration. Society of Economic Paleontologists and Mineralogists (SEPM), Core Workshop, no. 17, Calgary, Alberta, p. 57-84.

MacEachern, J.A., Raychaudhuri, I., and Pemberton, S.G., 1992, Stratigraphic applications of the *Glossifungites* ichnofacies: Delineating discontinuities in the rock record: *in* Pemberton, S.G., ed., Applications of Ichnology to Petroleum Exploration. Society of Economic Paleontologists and Mineralogists (SEPM), Core Workshop, no. 17, Calgary, Alberta, p. 169-198.

MacEachern, J.A., Zaitlin, B.A., and Pemberton, S.G., 1998, High resolution sequence stratigraphy of early transgressive incised shoreface and early transgressive valley/embayment deposits of the Viking Formation, Joffre Field, Alberta, Canada: American Association of Petroleum Geologists Bulletin, v. 82, p. 729-756.

MacEachern, J.A., Zaitlin, B.A., and Pemberton, S.G., 1999, A sharp-based sandstone of the Viking Formation, Joffre Field, Alberta, Canada: Criteria for recognition of transgressively incised shoreface complexes: Journal of Sedimentary Research, v. 69, p. 876-892.

MacEachern, J.A., Bann, K.L., and Gingras, M.K., and Pemberton, S.G., 2007a, The ichnofacies paradigm: High-resolution paleoenvironmental interpretation of the rock record: *in* MacEachern, J.A., Bann, K.L., Gingras, M.K., and Pemberton, S.G., eds., Applied Ichnology. Society of Economic Paleontologists and Mineralogists (SEPM), Short Course Notes, no. 52, p. 27-64.

MacEachern, J.A., Pemberton, S.G., Bann, K.L., and Gingras, M.K., 2007b, Departures from the archetypal ichnofacies: Effective recognition of environmental stress in the rock record: *in* MacEachern, J.A., Bann, K.L., Gingras, M.K., and Pemberton, S.G., eds., Applied Ichnology. Society of Economic Paleontologists and Mineralogists (SEPM), Short Course Notes, no. 52, p. 65-92.

MacEachern, J.A., Gingras, M.K., Bann, K., Dafoe, L.T., and Pemberton, S.G., 2007c, Applications of ichnology to high-resolution genetic stratigraphic paradigms: *in* MacEachern, J.A., Bann, K.L., Gingras, M.K., and Pemberton, S.G., eds., Applied Ichnology. Society of Economic Paleontologists and Mineralogists (SEPM), Short Course Notes, no. 52, p. 93-127.

Martin, M.A., and Pollard, J.E., 1996, The role of trace fossil (ichnofabric) analysis in the development of depositional models for the Upper Jurassic Fulmar Formation of the Kittiwake Field (Quadrant 21, UKCS): *in* Hurst, A., Johnson, H.D., Burley, S.D., Canham, A.C., and Mackertich, D.S., eds., Geology of the Humber Group: Central Graben and Moray Firth, UKCS. Geological Society, London, Special Publication, v. 114, p. 163-183.

McAdoo, B.G., Fritz, H.M., Jackson, K.L., Kalligeris, N., Kruger, J., Bonte-Grapentin, M., Moore, A.L., Rafiau, W.B., and Billx, D., 2008, Solomon Islands Tsunami, one year later: Eos, Transactions American Geophysical Union, v. 89, p. 169-170.

McCulloch, D.S., 1985, Evaluating tsunami potential: *in* Ziony, J.I., ed., Evaluating Earthquake Hazards in the Los Angeles Region- An Earth Science Perspective. United States Geological Survey Professional Paper 1360, p. 375-413.

McKenzie, D., 1978, Some remarks on the development of sedimentary basins: Earth and Planetary Science Letters, v. 40, p. 25-32.

Mellere, D., Zecchin, M., and Perale, C., 2005, Stratigraphy and sedimentology of fault-controlled backstepping shorefaces, middle Pliocene of Crotone Basin, Southern Italy: Sedimentary Geology, v. 176, p. 281-303.

Miller, R.G., 1990, A paleoceanographic approach to the Kimmeridge Clay Formation: *in* Huc, A.Y., ed., Deposition of Organic Facies: American Association of Petroleum Geologists, Studies in Geology, v. 30, p. 13-26.

Morton, A.W., Gelfenbaum, G., and Jaffe, B.E., 2007, Physical criteria for distinguishing sandy tsunami and storm deposits using modern examples: Sedimentary Geology, v. 200, p. 184-207.

Nebel, S.H., Trembanis, A.C., and Barber, D.C., 2012, Shoreline analysis and barrier island dynamics: Decadal scale patterns from Cedar Island, Virginia: Journal of Coastal Research, v. 28, p. 332-341.

Nott, J., 2004, Palaeotempestology: The study of prehistoric tropical cyclones- A review and implications for hazard assessment: Environment International, v. 30, p. 433-447.

Parsons, J.D., Friedrichs, C.T., Mohrig, D., Traykovski, P., Imran, J., Syvitski, J.P. M., Parker, G., Puig, P., Buttles, J.L., and Garcia, M.H., 2007, The mechanics of marine sediment gravity flows: *in* Nittrouer, C.A., Austin, J.A, Field, M.E., Kravitz, J.H., Syvitski, J.P.M, and Wiberg, P.L, eds., Continental Margin Sedimentation: From Sediment Transport to Sequence Stratigraphy. Blackwell Scientific Ltd., London, United Kingdom, p. 275-338.

Pemberton, S.G., and Gingras, M.K., 2005, Classification and characterizations of biogenically enhanced permeability: American Association of Petroleum Geologists Bulletin, v. 89, p. 1493-1517.

Pemberton, S.G., MacEachern, J.A., and Frey, R.W., 1992, Trace fossil facies models: Environmental and allostratigraphic significance: *in* Walker, R.G., and James, N.P., eds., Facies Models: Response to Sea Level Change. Geological Association of Canada, St. John's, Newfoundland, p. 47-72.

Pemberton, S.G., Spila, M., Pulham, A.J., Saunders, T., MacEachern, J.A., Robbins, D., and Sinclair, I.K., 2001, Ichnology and Sedimentology of Shallow to Marginal Marine Systems: Ben Nevis and Avalon Reservoirs, Jeanne D'Arc Basin. Geological Association of Canada, St. John's, Newfoundland, 343 p.

Pemberton, S.G., MacEachern, J.A., and Saunders, T.D.A., 2004, Stratigraphic applications of substrate-specific ichnofacies- delineating discontinuities in the rock record: *in* McIlroy, D., ed., The Application of Ichnology to Palaeoenvironmental and Stratigraphic Analysis. Geological Society, London, Special Publication, v. 228, p. 29-62.

Pemberton, S.G., MacEachern, J.A., Gingras, M.K., and Saunders, T.D.A., 2008, Biogenic chaos: Cryptobioturbation and the work of sedimentologically friendly organisms: Palaeogeography, Palaeoclimatology, Palaeoecology, v. 270, p. 273-279.

Plint, A.G., 2010, Wave- and storm-dominated shoreline and shallow-marine systems: *in* James, N.P., and Dalrymple, R.W., eds., Facies Models 4. Geological Association of Canada, St. John's, Newfoundland, p. 167-199.

Ravnås, R., and Steel, R.J., 1998, Architecture of marine rift-basin successions: American Association of Petroleum Geologists Bulletin, v. 82, p. 110-146.

Raychaudhuri, I., and Pemberton, S.G., 1992, Ichnologic and sedimentological characteristics of open-marine to storm-dominated restricted marine settings within the Viking/Bow Island Formations, south-central Alberta: *in* Pemberton, S.G., ed., Applications of Ichnology to Petroleum Exploration. Society of Economic Paleontologists and Mineralogists (SEPM), Core Workshop, no. 17, Calgary, Alberta, p. 119-139.

Reading, H.G., 1996, Sedimentary Environments- Processes, Facies and Stratigraphy, Third Edition. Blackwell Scientific Ltd., London, United Kingdom, 688 p.

Reineck, H.E., 1963, Sedimentgefüge im Bereich der südlichen Nordsee: Abhandlungen der Senckenbergischen Naturforschenden Gesellschaft, v. 505, p. 1-138.

Roberts, A.M., Price, J.D., and Olsen, T.S., 1990, Late Jurassic half-graben control on the siting and structure of hydrocarbon accumulations UK/Norwegian Central Graben: *in* Hardman, F.R.P., and Brooks, J., Tectonic Events Responsible for Britain's Oil and Gas Reserves. Geological Society, London, Special Publication, v. 55, p. 229-257.

Seilacher, A., 1964, Biogenic sedimentary structures: *in* Imbrie, J., and Newell, N., eds., Approaches to Paleoecology. Wiley, New York, New York, p. 296-316.

Seilacher, A., 1967, Bathymetry of trace fossils: Marine Geology, v. 5, p. 413-428.

Sellwood, B.W., Valdes, P.J., and Price, G.D., 2000, Geological evaluation of multiple GCM simulations of Late Jurassic palaeoclimate: Palaeogeography, Palaeoclimatology, Palaeoecology, v. 156, p. 147-160.

Spencer, A.M., Home, P.C., and Wiik, V., 1986, Habitat of hydrocarbons in the Jurassic Ula Trend, Central Graben, Norway: *in* Spencer, A.M., ed., The Habitat of Hydrocarbons on the Norwegian Continental Shelf. Graham and Trotman, London, United Kingdom, p. 111-127.

Stamp, L.D., 1921, On cycles of sedimentation in the Eocene strata of the Anglo-Franco-Belgian basin. Geological Magazine, v. 58, p. 108-114, 146-157, 194-200.

Stewart, I.J., 1993, Structural controls on the Late Jurassic shelf system, Ula Trend, Norwegian North Sea: *in* Parker, J.R., Petroleum Geology of Northwest Europe: Proceedings of the 4th Conference. Geological Society, London, p. 469-483.

Storlazzi, C.D., and Field, M.E., 2000, Sediment distribution and transport along a rocky, embayed coast: Monterey Peninsula and Carmel Bay, California: Marine Geology, v. 170, p. 289-316.

Swift, D.J.P., Niederoda, A.W., Vincent, C.E., and Hopkins, T.S., 1985, Barrier island evolution, middle Atlantic shelf, U.S.A.: Part 1: Shoreface dynamics. Marine Geology, v. 63, p. 331-361.

Taylor, A.M. and Gawthorpe, R.L., 1993, Application of sequence stratigraphy and trace fossil analysis to reservoir description: Examples from the Jurassic of the North Sea: *in* Parker, J.R., Petroleum Geology of Northwest Europe: Proceedings of the 4th Conference. Geological Society, London, p. 317-336.

Taylor, A.M., and Goldring, R., 1993, Description and analysis of bioturbation and ichnofabric. Journal of the Geological Society, London, v. 150, p. 141-148.

Tucker, M.E., 2001, Sedimentary Petrology: An Introduction to the Origin of Sedimentary Rocks, Third Edition. Blackwell Scientific Ltd., London, United Kingdom, 262 p.

Tonkin, N.S., McIlroy, D., Meyer, R., and Moore-Turpin, A., 2010, Bioturbation influence on reservoir quality: A case study from the Cretaceous Ben Nevis Formation, Jeanne d'Arc Basin, offshore Newfoundland, Canada. American Association of Petroleum Geologists Bulletin, v. 94, p. 1059-1078.

Van Wagoner, J.C., Posamentier, H.W., Mitchum, R.M., Vail, P.R., Sarg, J.F., Loutit, T.S., and Hardenbol, J., 1988, An overview of sequence stratigraphy and key definitions: *in* Wilgus, C.K., Hastings, B.S., Kendall, C.G.S.C., Posamentier, H.W., Ross, C.A., and Van Wagoner, J.C., eds., Sea Level Changes- An Integrated Approach. Society of Economic Paleontologists and Mineralogists (SEPM) Special Publication, v. 42, p. 39-45.

Vollset, J., and Doré, A.G., 1984, A revised Triassic and Jurassic lithostratigraphic nomenclature for the Norwegian North Sea: Norwegian Petroleum Directorate Bulletin, no. 3, 53 p.

Walker, R.G., and Plint, A.G., 1992, Wave- and storm-dominated shallow marine systems: *in* Walker, R.G., and James, N.P., Facies Models: Response to Sea Level Change. Geological Association of Canada, St. John's, Newfoundland, p. 219-238.

Wang, W., 1998, Beach rocks and storm deposits on the beaches of Hong Kong. Science in China (Series D), v. 41, p. 369-376.

Wetzel, A., and Bromley, R.G., 1994, *Phycosiphon incertum* revisited: *Anconichnus horizontalis* is its junior subjective synonym. Journal of Paleontology, v. 68, p. 1396-1402.

Wetzel, A., and Uchman, A., 2001, Sequential colonization of muddy turbidites in the Eocene Beloveža Formation, Carpathians, Poland: Palaeogeography, Palaeoclimatology, Palaeoecology, v. 168, p. 173-188.

Whiteman, A.J., Naylor, D., Pegrum, R.M., and Rees, G., 1975, North Sea troughs and plate tectonics: Tectonophysics, v. 26, p. 39-54.

Zanella, E., and Coward, M.O., 2003, Structural Framework: *in* Evans, D., Graham, C., Armour, A., and Bathurst, P., eds., The Millennium Atlas: Petroleum Geology of the Central and Northern North Sea. Geological Society, London, United Kingdom, p. 45-59.

Ziegler, P.A., 1982, Geological Atlas of Western and Central Europe. Shell International Petroleum Maatschappij B.V., Amsterdam, 130 p.

CHAPTER 4: PETROPHYSICAL CHARACTERIZATION OF BIOTURBATED SANDSTONE RESERVOIRS: UPPER JURASSIC ULA FORMATION, NORWEGIAN NORTH SEA, EUROPE*

4.1 INTRODUCTION

The understanding of fluid flow within an interval (reservoir or aquifer) has evolved considerably in recent decades. Variables such as cementation, diagenesis, fracturing, and lithology have been documented as controlling factors influencing fluid recovery and permeability distribution within a reservoir (Ringrose et al., 1993; Pickup et al., 1995; Macaulay et al., 2001; Ringrose et al., 2005; Taylor et al., 2010). More recently, bioturbation has been recognized as an agent influencing permeability and porosity distributions within geological media (Dawson, 1978; Gingras et al., 1999; Gingras et al., 2004; Pemberton and Gingras, 2005; Gingras et al., 2007; Spila et al., 2007; Cunningham et al., 2009; Knaust, 2009; Tonkin et al., 2010; Lemiski et al., 2011; Cunningham et al., 2009; Gingras et al., 2012; Polo, 2013; La Croix et al., 2013). Recent efforts have shown that elements such as burrow geometry and burrow connectivity, and their associated two- and three-dimensional character, have a profound influence on permeability and porosity distributions within a reservoir (Gingras et al., 1999; Gingras et al., 2002a; Gingras et al.; 2002b; Knaust, 2012; La Croix et al., 2012).

To better comprehend the relationship between burrow morphology, bioturbation intensity (i.e., volume of sediment occupied by burrows), and burrow connectivity, spot-permeametry measurements and numerical modeling are undertaken in this chapter. By assigning porosity (thin sections) and permeability values (spot-permeametry data) to two different host-rock bedding fabrics (laminated and massive appearing bedding) and burrow elements (*Ophiomorpha*), the impact of bioturbation on single-phase fluid flow can be simulated using SBED computer software (Dabek and Knepp, 2011; SBED Geomodeling, 2011). From these numerical models, a conceptual framework for assigning absolute permeability to bioturbated reservoir media can be developed.

For this study, the bioturbated fabrics come from the Upper Jurassic (Kimmeridgian-Oxfordian) Ula Formation of the Norwegian Central Graben (Fig. 4.1). The Ula Formation is an important interval for hydrocarbons in the oil-rich

* A version of this chapter has been submitted for publication in *AAPG Bulletin* as "Petrophysical Characterization of Bioturbated Reservoir Sandstone Facies in the Upper Jurassic Ula Formation, Norwegian North Sea, Europe" by Greg M. Baniak, Murray K. Gingras, Beverly A. Burns, and S. George Pemberton.

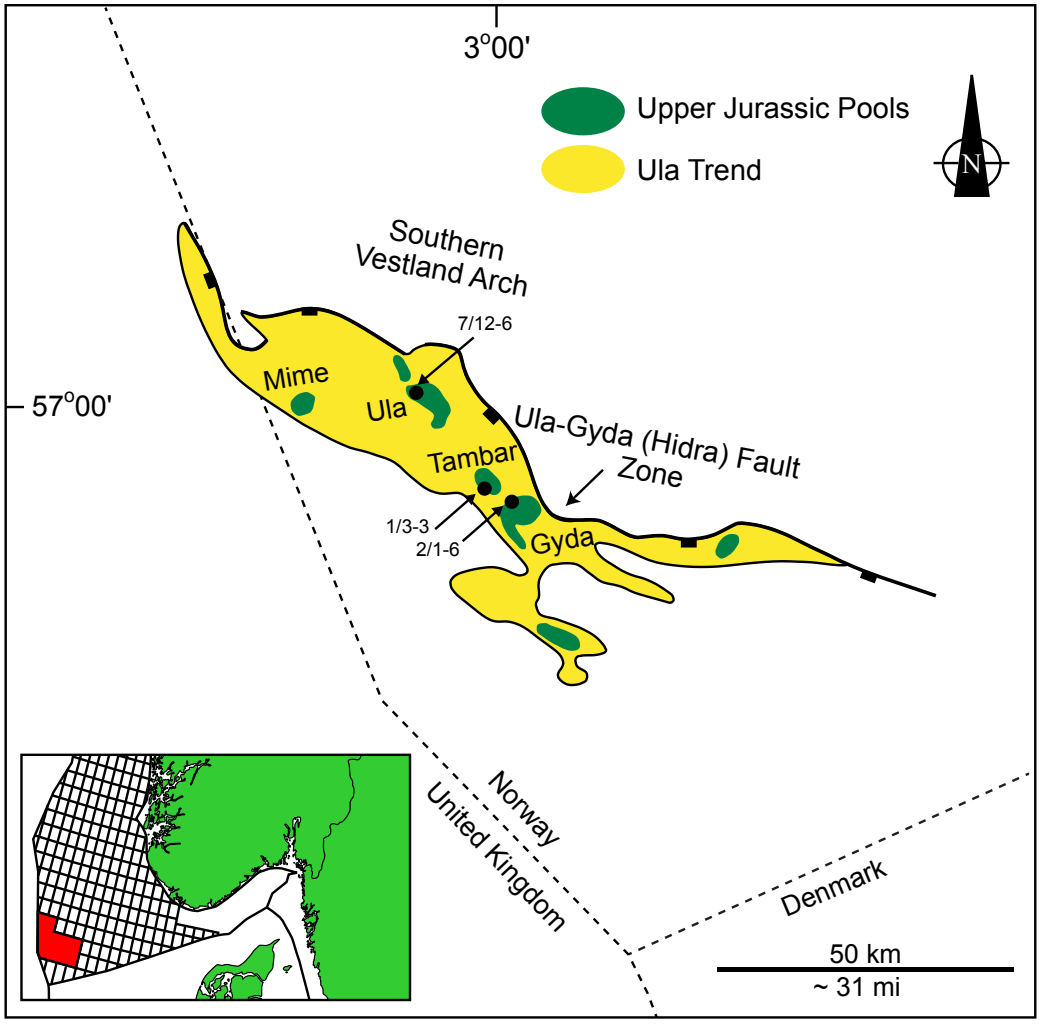

Figure 4.1: Location map of the Ula Trend and main Upper Jurassic oil fields in the southern Norwegian Central Graben. The location of the Ula Trend in comparison to Norwegian offshore drilling area is denoted by red boxes in the inset located in the bottom left corner of the diagram. Figure modified from Gluyas (1997).

Ula Trend (Spencer et al., 1986; Home, 1987), with production occurring from highly faulted, thickly bedded sandstones. The sandstones are moderately to highly bioturbated, with trace fossil distribution controlled by physico-chemical stresses such as sedimentation rate and water turbidity (see Chapter 3). *Ophiomorpha*-associated and cryptically bioturbated fabrics commonly occur within the reservoir producing intervals. The purpose of this chapter is to analyze the main reservoir intervals within the Ula Formation and document which ones are characterized by bioturbation. From this, analytical and numerical models will be used to evaluate the influence of bioturbation on reservoir quality by using lithologies derived from conventional core analysis, permeabilities derived from spot-permeametry measurements, and porosities derived from thin sections.

4.2 PREVIOUS RESEARCH ON BIOGENIC PERMEABILITY

Organisms such as earthworms, amphipods, and meiofauna alter the sorting characteristics and diagenetic composition of the substrate (Meadows and Tait, 1989; Green et al., 1992; Bastardie et al., 2003; Katrak and Bird, 2003). In many circumstances, the burrows are infilled with sediment that differs lithologically and geochemically from the surrounding sedimentary media (Over, 1990; Konhauser and Gingras, 2011; Petrash et al., 2011). As a result, enhancement or reduction of the permeabilities and porosities relative to the unburrowed surrounding matrix occurs. In scenarios of biogenic permeability enhancement, development of either dual-porosity or dual-permeability flow networks occur (Gingras et al., 2004, Pemberton and Gingras 2005; Gingras et al., 2007; Gingras et al., 2012). Dual-porosity fabrics represent intervals wherein contrasts in permeability between the burrows and matrix are less than two orders of magnitude (Gingras et al., 2007; Gingras et al., 2012). Under such scenarios, fluid flow will occur comparatively equally from the matrix and burrows. Dual-permeability fabrics represent intervals wherein the contrast in permeability between the matrix and burrows is greater than three orders of magnitude (Gingras et al., 2004, Gingras et al., 2007, Gingras et al., 2012). In these reservoirs, a well-defined contrast in permeability fields develop and fluid flow will occur predominantly from the highest permeable fabrics while the lower permeable fabrics will interact with the flow conduits through diffusion.

Building upon the different characteristics of flow media, and their stratigraphic context, Pemberton and Gingras (2005) developed a classification outline to catalogue biogenic permeability. Five interrelated classifications were presented and include: (1) surface-constrained textural-heterogeneities; (2) non-surface-constrained textural heterogeneities; (3) weakly defined textural heterogeneities; (4) cryptic textural heterogeneities; and (5) diagenetic textural heterogeneities (Fig. 4.2). In the Ula Formation, weakly defined textural heterogeneities and cryptic textural heterogeneities have been identified. Weakly defined textural heterogeneities represent a dual-porosity fabric (Pemberton and Gingras, 2005; Gingras et al., 2007; Gingras et al., 2012) as sand-filled burrows occur within a matrix composed of very fine- to fine-grained sand. Examples of trace fossils include *Ophiomorpha*, *Planolites*, *Skolithos*, and *Thalassinoides*, with *Ophiomorpha* being the most common example in this study. Cryptic bioturbation represents minute disruption of sedimentary fabric by microorganisms and *Macaronichnus*-like trace fossils (Gingras et al., 2002b; Gordon et al., 2010). As a result, homogenization of the sedimentary fabric commonly occurs and dual-porosity fabrics may form.

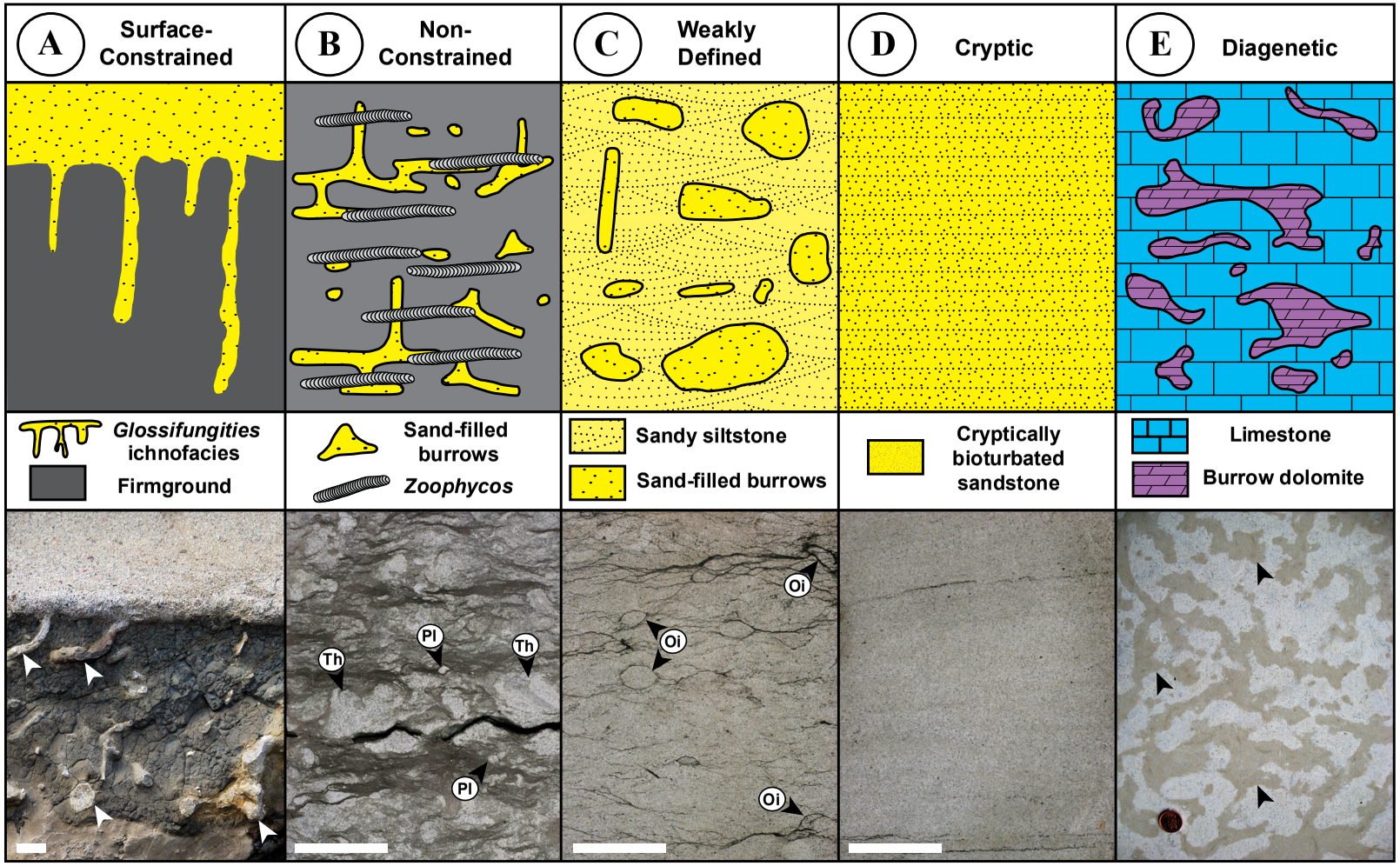
A
Surface-Constrained
B
Non-Constrained
C
Weakly Defined
D
Cryptic
E
Diagenetic
Glossifungities ichnofacies
Firmground
Sand-filled burrows
Zoophycos
Sandy siltstone
Sand-filled burrows
Cryptically bioturbated sandstone
Limestone
Burrow dolomite
Th
Pl
Th
Pl
Oi
Oi
Oi

Figure 4.2 (above): Examples of each class of biogenic flow media from drill cores and outcrops. Scale bars are 3 cm unless noted otherwise. **(A)** Surface-constrained discrete heterogeneities. Example of an Eocene outcrop from New Zealand. Sand-filled burrows (arrows) projecting into a firmground mudstone represent a *Glossifungities* surface. **(B)** Non-constrained discrete heterogeneities. Example from Upper Cretaceous Lysing Formation, Norwegian Sea, Europe. Sand-filled *Thalassinoides* (Th) and *Planolites* (Pl) within a siltstone matrix. **(C)** Weakly defined textural heterogeneities. Example from Upper Jurassic Ula Formation, Norwegian North Sea. Monospecific assemblage of sand-filled *Ophiomorpha irregulaire* (Oi) within a fine-grained sandstone matrix. **(D)** Cryptic biogenic heterogeneities. Example from Upper Jurassic Ula Formation, Norwegian North Sea. **(E)** Diagenetic textural heterogeneities. Example from outcropping Ordovician Tyndall Stone (Selkirk Member/Yeoman Formation), Western Canada. Arrows indicate dolomitized burrow mottling adjacent to cream-colored fossiliferous lime wackestone matrix. Penny used for scale. Figure modified from Gingras et al. (2012).

4.3 STUDY AREA AND GEOLOGICAL SETTING

The Ula Trend is located within the northeastern corner of the Norwegian Central Graben. The Central Graben represented a major rift sequence that was initiated in the Permian and lasted until the early Cretaceous (Ziegler, 1982; Roberts et al., 1990; Gowers et al., 1993). The Ula Formation was deposited during the final stage of rifting during the Upper Jurassic and subsequently underwent thermal subsidence during the Early Cretaceous (Zanella and Coward, 2003).

Figure 4.3 shows a stratigraphic chart of the Norwegian Central and United Kingdom Central Graben. The Ula Formation is overlain conformably by the Lower Cretaceous shales of the Asgaard Formation and underlain unconformably by either Triassic or Lower Jurassic sediments. Within the Upper Jurassic, the Ula Formation is commonly interbedded with the shales of the Mandal, Farsund, and Haugesund Formations (Fraser et al., 2003). It is believed that hydrocarbons began generating from the Upper Jurassic Mandal Formation beginning in the Late Cretaceous from the deeper parts of the Central Graben (Taylor et al., 1999). Regionally, the Ula Formation correlates with the siliciclastic Fulmar Formation in the United Kingdom Central Graben (Fraser et al., 2003).

The sandstones within the studied cores range from very-fine to medium-grained, and are commonly moderately- to well-sorted. The thickest accumulations of sandstones commonly occur on the downthrown side of basin-bounding faults (Brown et al., 1992). Apart from a few studies (Bailey et al., 1982; Bergan et al., 1989), sparse sedimentological or ichnological data exist on the Ula Formation. Conversely, the highly bioturbated sandstones of the Fulmar Formation have received greater attention (Johnson et al., 1986; Gowland, 1996; Martin and Pollard, 1996; Spaak et al., 1999). Recent work by Baniak et al. (in press) suggests a storm-influenced, shoreface setting for the Ula Formation (see Chapter 3).

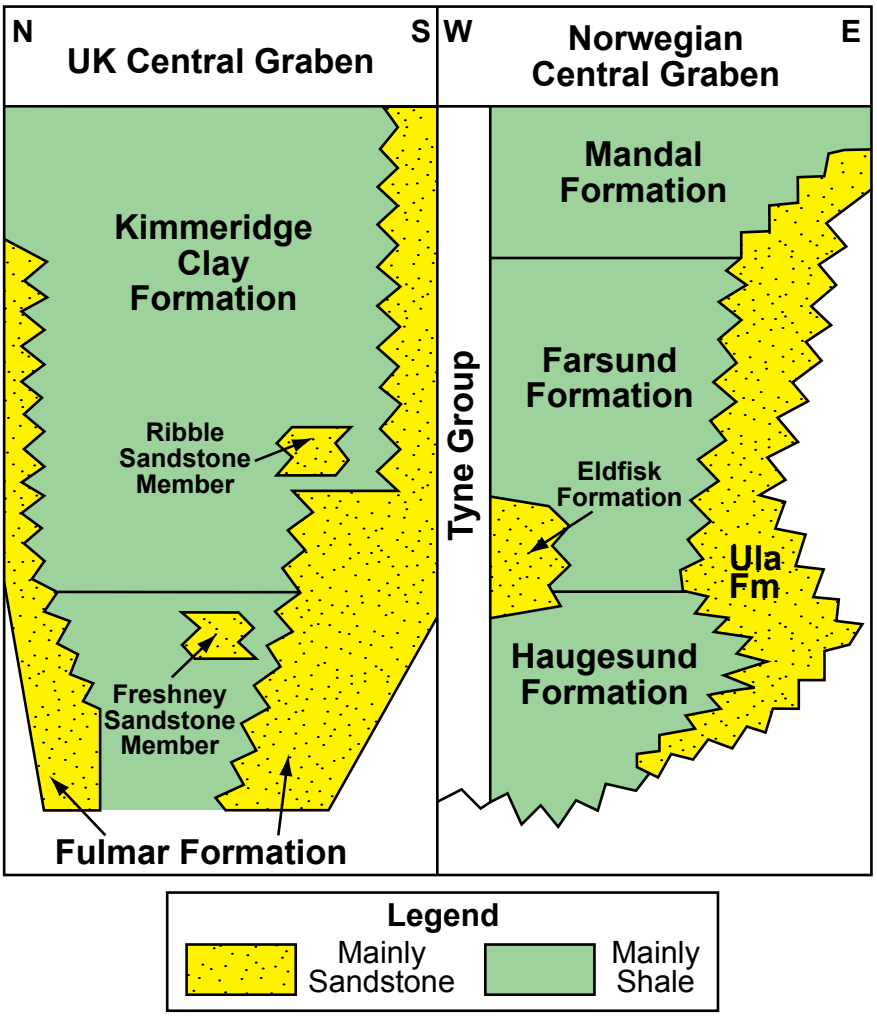

Figure 4.3: Upper Jurassic stratigraphy of the southern Central Graben in Europe. Figure modified from Fraser et al. (2003).

4.4 METHODS

Using slabbed core samples recovered from two wells in the Ula Trend (7/12-6 and 1/3-3), five methods were used to evaluate the influence of bioturbation on reservoir quality. The slabbed cores were analyzed from a sedimentological and ichnological perspective, with evaluation including assessment of bioturbation intensities (BI), mineralogy, sedimentary structures, biogenic structures, grain-size, and lithological accessories. Bioturbation intensity, hereafter denoted BI, is used to evaluate the overall amount of biogenic reworking of the primary sedimentary fabric and varies from absent (BI of 0 or 0% intensity) to complete (BI of 6 or 100% intensity) (Reineck, 1963; Taylor and Goldring, 1993; Bann et al., 2004). Within the Ula Formation, reservoir intervals with weakly defined textural heterogeneities commonly have a BI ranging from 2 to 6 and are commonly represented by

examples of *Ophiomorpha*. On the other hand, cryptically bioturbated reservoir intervals within the Ula Formation have a BI of 6.

The surfaces of slabbed cores were mapped into 0.5 cm grids and permeability measurements were obtained using a Core Laboratories PDPK 400 Pressure-Decay Profile Permeameter located at the University of Alberta (Core Laboratories Instruments, 1996). The permeability measurements were unstressed and collected under horizontal air permeabilities. A second set of permeability data is also used for comparison with the results from the PDPK 400 Permeameter. These permeabilities were obtained by evaluating old well reports (commonly 1980's vintage) supplied by oil companies to the Norwegian Petroleum Directorate (NPD). Because oil companies collected these permeability results independently, they can be used as a secondary source to confirm the permeability measurements and interpretations.

Assessment of the measured burrow and matrix permeabilities were made using arithmetic-, harmonic-, and geometric-averaging permeability techniques. Thin sections were cut from the slabbed core to study lithological and porosity contrasts between the matrix and trace fossils. The thin sections were also impregnated with blue epoxy to highlight porosity (measured using point counting). As with the permeability measurements, the porosity measurements were made under laboratory conditions and were therefore unstressed. Numerical modeling of sedimentary bedding and ichnological configurations is then completed using SBED software to better understand the importance of trace fossils on permeability distribution within the Ula Formation.

4.4.1 Spot-Permeametry Measurement

The Core Laboratories PDPK 400 Pressure-Decay Profile Permeameter measures the permeabilities of a sample with a measurement range of 0.001 millidarcy (mD) to greater than 30 darcy (Jones, 1994; Core Laboratories Instruments, 1996; Lemiski et al., 2011; Polo, 2013; La Croix et al., 2013). A 0.46 cm probe rubber tip was sealed against the flat core surface using a pneumatic cylinder. Nitrogen gas injected through the probe was recorded as a function of time. The maximum pressure-decay time for each measurement was 30 seconds. For each point, three measurements were taken to provide an average permeability. Following data collection, the averaged permeability values were plotted on the core photographs and contoured using Surfer 9 gridding and contouring software (Rockware ®, Inc., 2009). Upon generation, the contours maps were modified in Adobe Illustrator to highlight the nature of the permeability domains within the burrows.

4.4.2 Average Permeability

Using the permeability measurements derived from the spot-permeameter, a detailed characterization of the whole sample permeability is completed. Three permeability-averaging techniques (arithmetic, harmonic, and geometric) are commonly used to determine an average permeability that is equivalent to a homogenous system (Muskat, 1937; Warren and Price, 1961; Bear, 1972; Freeze and Cherry, 1979; Weber and van Geuns, 1990). The arithmetic-average permeability (Eq. 1) is used to determine the average permeability of a system with layered-parallel beds that have different permeabilities and can be characterized as:

$$k_{arithmetic} = \sum_{i=1}^{n} \frac{k_i d_i}{d} \quad (1)$$

where k_i is the permeability of each layer, d_i is the individual layer thickness, and d the total thickness. The harmonic-average permeability (Eq. 2) estimates the bulk vertical permeability occurring perpendicular to the layered media:

$$k_{harmonic} = \frac{1}{\sum_{i=1}^{n} \frac{d_i}{k_i d}} \quad (2)$$

The final method is the geometric-average permeability (Eq. 3), which is representative of isotropic system where fluid flow occurs in all directions in a randomized nature:

$$\ln (k_{geometric}) = \sum_{i=1}^{n} \frac{\ln(k_i) d_i}{d} \quad (3)$$

Using these three aforementioned equations, graphs of burrowing intensity versus permeability in an idealized unit volume can be constructed for each core sample analyzed (e.g., La Croix et al., 2013). In this chapter, the graphs will contain end-member permeability measurements as determined from the spot-permeametry dataset. In this context, the highest spot-permeametry measurements commonly occurred within the burrows while the lowest spot-permeametry measurements values occurred within the matrix. As such, d_i/d is used to represent the volume in the sample occupied by the burrows. The three highest values of measured permeability values within a bioturbated sample were therefore averaged together to approximate the idealized permeability of a bioturbated end member (i.e., 100% bioturbation, 6 BI, or $d_i/d = 1.0$). On the other hand, the three lowest permeability values located in the matrix are taken to represent the matrix permeability (i.e., 0%

bioturbation, 0 B.I., or $d_t/d = 0.0$). Visual observation of permeability distribution within the burrows and matrix is used to identify the three highest and three lowest values. The three permeability measurements used to average the burrow and matrix permeability were commonly localized in the same area in the core sample and were generally within 10 to 15% of one another. This suggests that these permeability member values were a good approximation of the permeabilities associated with the burrows and matrix within the sample.

4.4.3 Numerical Modeling

Categorization of fluid flow within bioturbated models is studied using SBED software (Wen et al., 1998). SBED software allows the incorporation of common burrow morphologies (plug-shaped, irregularly branching) and burrow ichnogenera (*Skolithos*, *Ophiomorpha*) into a range of bedding structures and lithologies at varying densities (Dakek and Knepp, 2011). For this study, two process-oriented model templates (laminated sandstones and massive appearing sandstones) were used. The permeabilities and porosities used for numerical modeling are based on the values and measurements obtained during spot-permeametry and thin section analysis (see 'Observation' section below) and oil company well reports obtained from the NPD website. For the sake of clarity and simplicity, a constant permeability and porosity value is used for the mud beds, sediment matrix, and burrows in each numerical model.

The laminated sandstone model had sand intervals with defined permeabilities of 20 mD and porosities of 12%. The mud layers within the laminated model are defined with permeabilities of 0.100 mD and porosities of 1%. The massive appearing sandstone model contained two alternating sand intervals with different values. One sandstone type is defined with permeabilities of 40 mD and porosities of 12% and the other sandstone type had defined permeabilities of 20 mD and porosities of 10%.

Ophiomorpha burrows were populated within both model templates and were assigned variable dimensions, orientations, and bioturbation intensities (as is commonly observed within the Ula Formation). The *Ophiomorpha* burrows were constructed with lengths ranging from 1 to 10 cm, diameters of 1.0 cm, and linings of 0.10 cm. The permeabilities and porosities within the *Ophiomorpha* burrows (100 mD and 20%, respectively) were consistent throughout the two models, and the burrow rims had a constant permeability of 30 mD.

A 3D grid is constructed with dimensions of 30 x 30 x 30 cm and discretized

such that each grid cell size is 0.30 x 0.30 x 0.30 cm. SBED Geomodeling uses a combination of Gaussian simulation and vector-based movement of geometric surfaces through space and time to produce a stochastic model (Wen et al., 1998). An absolute permeability is calculated by SBED software for each model, while incorporating the effects of small-scale heterogeneities such as mud beds, using a flow-simulation-based numerical method (SBED Geomodeling, 2011). The flow-simulation-based numerical method can be applied to permeability grids simulating single-phase fluid flow. In this study, built-in SBED solver uses a multi-scale mixed finite-element method, and handles full permeability tensors using fixed boundary conditions. Fixed (no-flow) boundary conditions dictate that fluid flows only across two end surfaces normal to pressure gradient and that no fluid flows across the other four end surfaces parallel to the pressure gradient (SBED Geomodeling, 2011). Using SBED single phase flow-based upscaling with fixed boundary conditions, the arithmetic-, harmonic-, and geometric-averaged permeabilities are calculated for each model.

4.5 OBSERVATIONS

4.5.1 Reservoir Facies

The Ula Formation can be subdivided into three main facies intervals based on lithology, sedimentary structures, and trace fossil assemblages (Fig. 4.4 and 4.5). Facies 1 represents a highly-bioturbated, fine-grained sandstone (Fig. 4.4A). Sedimentary structures are rare, but where present include trough cross bedding and low-angle planar laminations. Representing a *Cruziana* to *Skolithos* ichnofacies (Seilacher 1967; Frey and Pemberton, 1985; MacEachern et al., 2007a), common trace fossils include *Ophiomorpha nodosa*, *Ophiomorpha irregulaire*, and *Siphonichnus*. *Ophiomorpha nodosa* is composed of tubular tunnels and shafts (roughly 5 cm thick, up to 30 cm long vertically) and contain well-defined pelleted walls. *Ophiomorpha irregulaire* is generally narrower and sub-vertical to horizontal in orientation in comparison to *Ophiomorpha nodosa.* Due to the burrows commonly containing a sediment infill that differs from the surrounding matrix, Facies 1 represents an example of a weakly defined textural heterogeneity.

Facies 2 represents a highly-bioturbated, massive appearing sandstone (Fig. 4.4B). Composed of upper fine- to lower medium-grained sandstones, sedimentary structures are generally rare and only include sporadic low-angle planar laminations and trough cross-bedding. Examples of macro burrows are also commonly absent, and limited to rare examples of *Ophiomorpha*, *Planolites*, and fugichnia. Instead,

Core Photo	Facies Classification	Lithology and Accessories	Sedimentary Structures	Ichnology
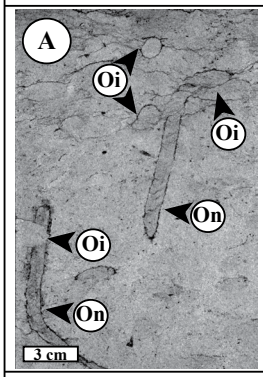	1. Highly-bioturbated, fine-grained sandstone Represents a weakly defined textural heterogeneity	Lower to upper fine-grained sandstone Fecal peloids and micaceous debris	Trough cross bedding Low-angle planar laminations	*Ophiomorpha nodosa*, *Ophiomorpha irregulaire*, and *Siphonichnus* BI 4-6
	2. Highly-bioturbated, 'massive sandstone' Represents a cryptic textural heterogeneity	Upper fine- to lower medium-grained sandstones Fecal peloids and organic matter debris	Rare trough cross bedding Rare low-angle planar laminations	Rare *Ophiomorpha*, *Planolites*, and fugichnia Dominant fabric is crytpic bioturbation BI 5-6
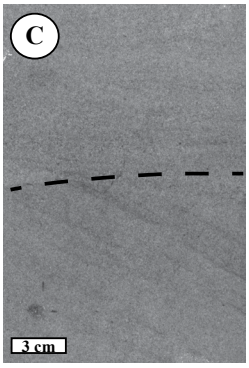	3. Poorly-bioturbated, cross-stratified sandstones Represents a non-biogenically modified interval	Upper-fine to lower-medium grained sandstones Thin-shelled bivalves, pebble lags, and bioclastic debris.	High-angle planar cross-stratification Trough cross-bedding. Tidal bundles Tubular tidalites	Rare *Ophiomorpha* and fugichnia BI 0-1

Figure 4.4: Outline of the three main reservoir facies within the Ula Formation, with a summary of their lithologies, sedimentary structures, and trace fossil assemblages. **(A)** Example of a low-diversity assemblage of *Ophiomorpha irregulaire* (Oi) and *Ophiomorpha nodosa* (On). Facies 1 represents a weakly defined heterogeneity. Core 2/1-6, depth 4304.20 m. **(B)** Example of lower medium-grained sandstone that is cryptically bioturbated and contains faint low-angle planar cross-stratification. Facies 2 represents a cryptic textural heterogeneity. Core 2/1-6, depth 4254.73m. **(C)** Example of a planar cross-bedded sandstone that overlays a trough cross-bedded sandstone (hashed line demarcates erosional surface). Facies 3 represents a non-biogenically modified interval. Core 7/12-6, 3483.35 m.

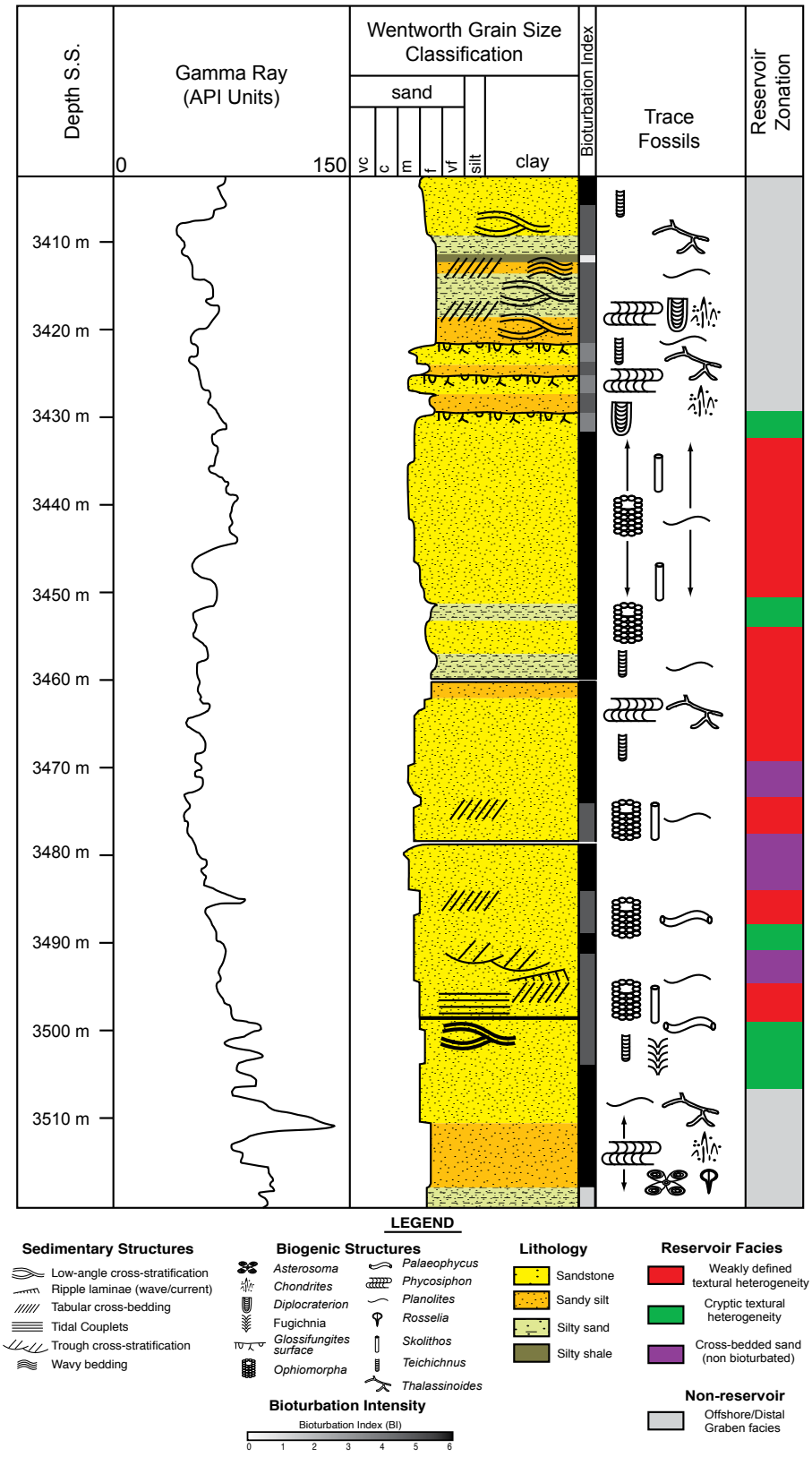

Figure 4.5: A lithology log and associated reservoir facies for subsurface well 7/12-6. Roughly 80% of the reservoir is influenced by bioturbation, with weakly defined textural heterogeneities being the most prominent. Modified from Baniak et al. (in press).

bioturbation is cryptic in nature (Howard and Frey, 1975; Pemberton et al., 2008) and is the dominant element in causing a massive appearing sandstone. Facies 2 therefore represents an example of a cryptic textural heterogeneity.

Facies 3 represents a poorly-bioturbated, cross-stratified sandstone (Fig. 4.4C). Composed of upper-fine to lower-medium grained sandstones, sedimentary structures include high-angle planar cross-stratification and trough cross-bedding. Evidence of tidal sedimentation also exists, with tidal bundles and tubular tidalites (Gingras et al., 2000; Gingras et al., 2002c) being present. Bioturbation is rare (BI 0-1) and only includes sporadic *Ophiomorpha* and fugichnia. Since Facies 3 represents an example of non-biogenically modified reservoir interval, it is not further analyzed in this chapter.

4.5.2 Petrology

Thin sections analyzed indicate the Ula Formation is composed primarily of very fine- to fine-grained sand. The framework minerals are dominated by quartz (70-80%), with secondary amounts of plagioclase (10-15%), micas (5-10%), and accessory minerals (0-5%). The similarity in composition to other wells in the Ula Trend (e.g., 7/8-3; Harris, 2006) can be attributed to a constant depositional environment and point source (i.e., Southern Vestland Arch) across the basin during sedimentation (Gluyas, 1997). The grains are subangular to subrounded, moderately to well sorted, and can be classified texturally as subarkosic (after Dott, 1964). Quartz is the dominant cement (rare dolomite and feldspar being the others) and plays a large role in reservoir quality (Nedkvitne et al., 1993; Oxtoby et al., 1995).

Due to levels of bioturbation, the original laminated fabric of the rock is commonly destroyed. In this context, the most porous sandstones typically occur within the burrows. The relationship between porosity heterogeneities is a consequence of factors that include bioturbation, with primary (i.e., selective grain emplacement and alignment) and secondary (i.e., differential cementation) features being noted.

Within Facies 1, porosity values are commonly enhanced within the burrows (Fig. 4.6A-C). The *Ophiomorpha* burrows have porosities ranging from 10 to 20% and the surrounding sandstone matrix has porosities of 5 to 10 %. Because the burrow fill is passive and unrelated to the host sediment, it can be either of lower or higher porosity. In the Ula Formation, the *Ophiomorpha* burrows are typically of higher porosity. However, Tonkin et al. (2010) showed porosity reduction can occur within *Ophiomorpha* as well.

In Facies 2, porosity enhancement occurs within the more cryptically bioturbated regions (Fig. 4.6D-E). The majority of the intervals in Facies 2 appear to be created by microorganisms as opposed to *Macaronichnus*-like trace fossils. Evidence has suggested that microorganisms commonly occur in colonies on sand grains (Meadows and Anderson, 1968). The sporadic colonization of microorganisms could possibly be related to their preferential attachment to grains (i.e., quartz and feldspar) that adhere bacteria and diatoms (Mills and Maubrey, 1981; Krejci and Lowe, 1986) or due to differences in microtopography of the sand grains (Krinsley and Funnell, 1965). It is therefore possible that these sand grains became cleaned, or possibly coated, by the microorganisms in a manner that prevented cementation.

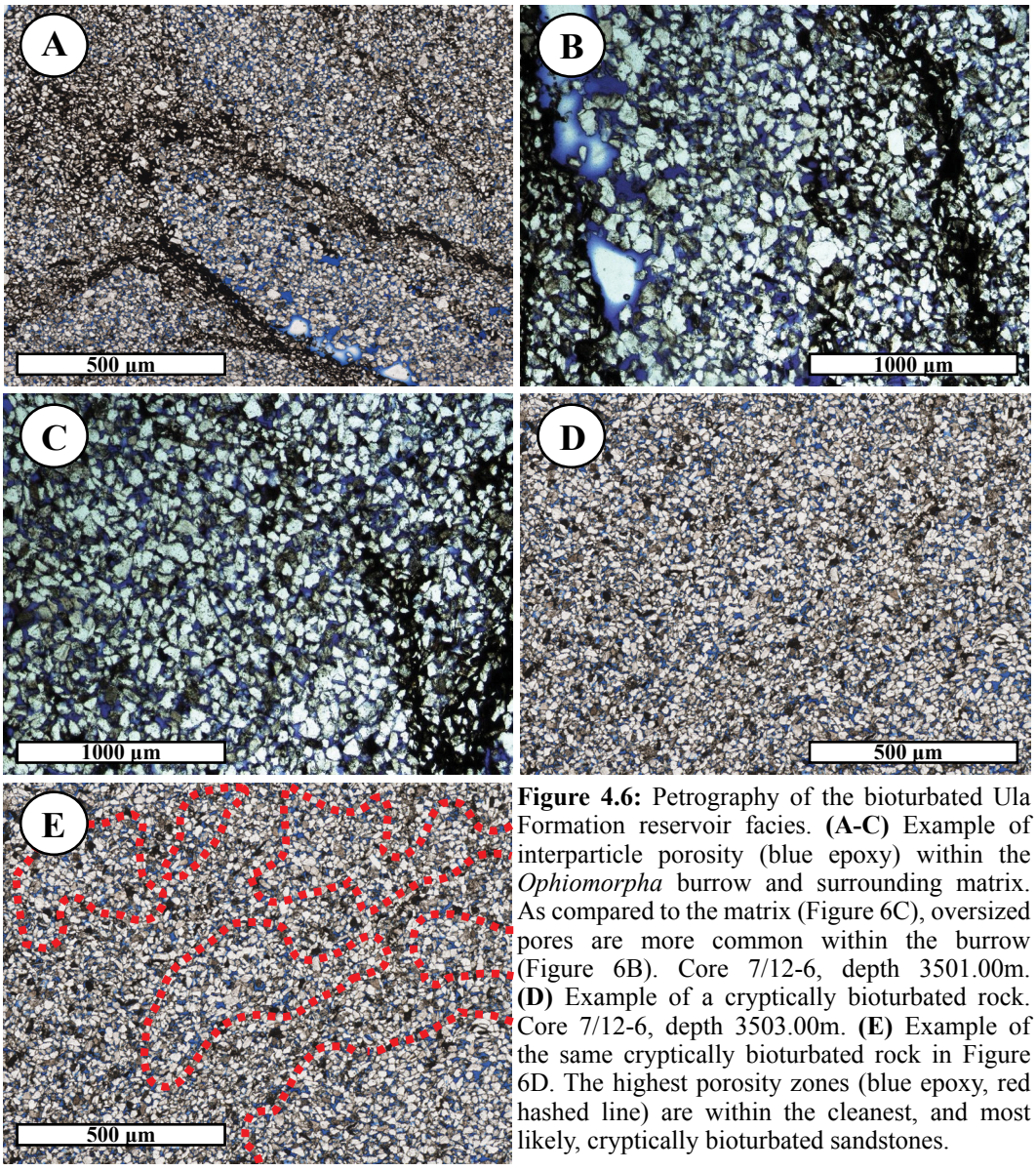

Figure 4.6: Petrography of the bioturbated Ula Formation reservoir facies. **(A-C)** Example of interparticle porosity (blue epoxy) within the *Ophiomorpha* burrow and surrounding matrix. As compared to the matrix (Figure 6C), oversized pores are more common within the burrow (Figure 6B). Core 7/12-6, depth 3501.00m. **(D)** Example of a cryptically bioturbated rock. Core 7/12-6, depth 3503.00m. **(E)** Example of the same cryptically bioturbated rock in Figure 6D. The highest porosity zones (blue epoxy, red hashed line) are within the cleanest, and most likely, cryptically bioturbated sandstones.

4.5.3 Spot-Permeametry

Spot-permeametry measurements discussed below are samples derived from Facies 1 (weakly defined textural heterogeneity) and Facies 2 (cryptic textural heterogeneity). The core photographs annotated with the spot-permeametry measurement locations and values, along with their corresponding contour maps, are presented in Figures 7, 8, and 9. These three figures also include plots of bioturbation intensity versus measured permeability values. The three curves in each plot show the arithmetic, harmonic, and geometric means of permeability. These three permeability equations were calculated on the relative proportions of fluid flow associated with the burrows and matrix, respectively. Superimposed onto each plot are measured permeability values obtained from well reports available on the NPD website.

4.5.3.1 Weakly defined textural heterogeneities

Figure 4.7A shows a sample displaying 100% bioturbation (BI 6) with *Ophiomorpha irregulaire* being the dominant burrow. Biogenically reworked sandstones with wispy concentrations of clay and peloidal material categorize the surrounding sediment. The upper limit of permeability (associated with the *Ophiomorpha irregulaire*) was measured at 152 mD. On the other hand, where fluid flow occurs within the surrounding sediment, measured permeability is 18 mD. The contour map shows that most of the highest permeabilities in the sample occur within the sub-horizontal *Ophiomorpha irregulaire*. The closest permeability data point available for comparison occurs within a highly bioturbated sandstone at depth 3440.91 m. This permeability measurement, roughly 1.90 m from permeability measurements made in this study, is available on the NPD website in the B.P. Petroleum Development Limited Special Core Analysis Study for well 7/12-6. It has a full diameter core sample air permeability value of 140 mD (blue star in Fig. 4.7B).

Characterization of absolute permeability for the data point obtained from the B.P. Core Analysis Study suggests it would be best approximated with the arithmetic mean of permeability in our model. Likewise, the core sample used in this study appears to be best approximated using the arithmetic mean due to the volume of bioturbation (BI 6) and overall horizontal orientation of the burrows. However, the arithmetic permeability only averages 88.18 mD at BI 6 (red star in Fig. 4.7B) instead of an idealized 152 mD (green star in Fig. 4.7B). Due to small-scale heterogeneities within the individual flow units, such as peloidal mud

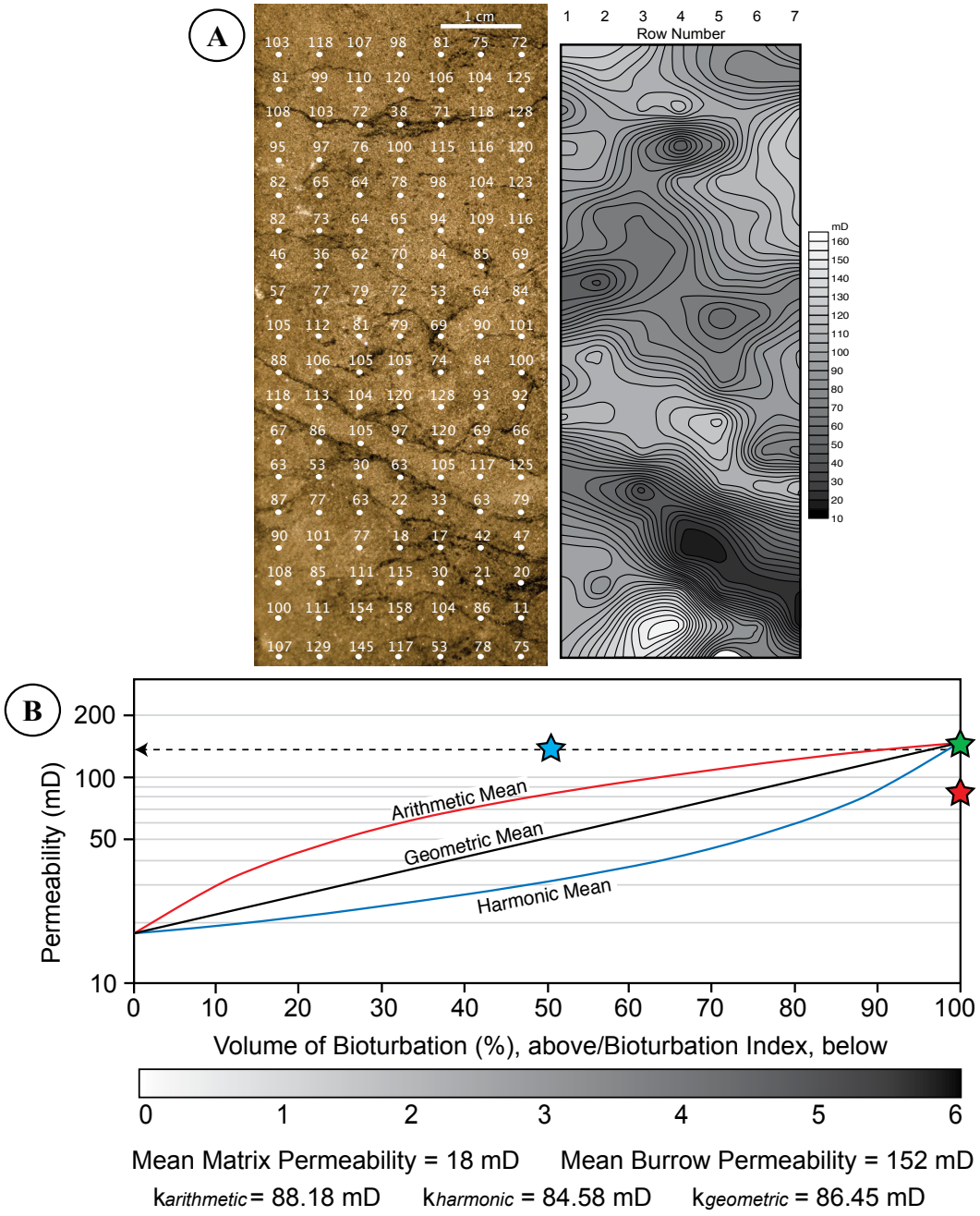

Figure 4.7: Spot-permeametry and associated bulk permeability analysis (geometric, arithmetic, and harmonic means) of a weakly defined textural heterogeneity. Well 7/12-6, depth 3439.00 m. **(A)** Example of an *Ophiomorpha irregulaire* within a highly bioturbated substrate (BI 6). Spot-permeameter measurements and a supplementary contour map highlight the permeability trends within the core sample. The highest permeabilities are present within the *Ophiomorpha irregulaire* and cleanest sandstones that have minor amounts of mud. **(B)** Due to heterogeneities (i.e., burrow mud linings), the arithmetic mean is only 88.18 mD at 100% bioturbation (red star) as opposed to the idealized 152 mD at 100% bioturbation intensity (green star). The whole core sample permeability obtained from B.P. Core Analysis at depth 3440.91 m is 140 mD (blue star). Figure modified from Gingras et al. (2012).

and wispy clay, localized reductions in permeability occur. Nevertheless, high bioturbation intensities contributed to a higher absolute permeability by providing continuous flow paths and increasing the overall amount of higher permeable flow media (Gingras et al., 1999; La Croix et al., 2012). As a result, the permeability fields may be comparably isotropic at BI 6 (e.g., Weaver and Schultheiss, 1983; Gingras et al., 1999).

In a second sample (Fig. 4.8A), bioturbation intensity is low (BI 1-2 or roughly 30% bioturbation by volume) and limited to a vertical *Ophiomorpha nodosa*. Spot-permeameter measurements indicate the most common range in permeability for the matrix is from 26 to 65 mD. The *Ophiomorpha nodosa* has a common permeability range of 56 to 85 mD (Fig. 4.8B). The matrix-associated permeability (0% bioturbation) has a measured average value of 18 mD. The upper limit of permeability associated with the *Ophiomorpha nodosa* is measured at 111 mD.

The permeability data point available for comparison occurs roughly in the same interval (4221.70 m) for well 1/3-3 as used in this study (4221.75 m). This permeability measurement, available on the NPD website in Elf Petroleum Norge AS Core Report for well 1/3-3, has a value of 195 mD (blue star in Fig. 4.8C) and is obtained from a core plug. It must be noted, however, that this core plug was taken from an adjacent core slab from the one used in this study. From core photos available on the NPD website, it appears that the core plug was taken from the bioturbated sandstone.

The arithmetic mean for the core sample used in this study has a value of roughly 48 mD at 30% bioturbation intensity (green star in Fig. 4.8C) and is very close to the 52.61 mD predicted by the arithmetic mean for the reservoir. Conversely, the harmonic mean is only 27 mD at 30% bioturbation. The separation in permeability between the arithmetic and harmonic mean is due to the fact the many burrow networks become connected between 10 and 30% bioturbation (La Croix et al., 2012). Furthermore, the matrix also contains regions of high permeabilities (Fig. 4.8A-B) that also contribute to bedding-parallel fluid flow. Analysis of the core plug permeability obtained from the Elf Petroleum Norge AS Core Report suggests it would be best approximated with the arithmetic mean of permeability in our model.

Despite numerous burrows likely being connected at 30% bioturbation, the presence of monospecific *Ophiomorpha nodosa* within the sample suggests that many burrows likely still remain unconnected in areas of lower bioturbation intensities. Fluid will therefore likely diffuse from these burrows into the

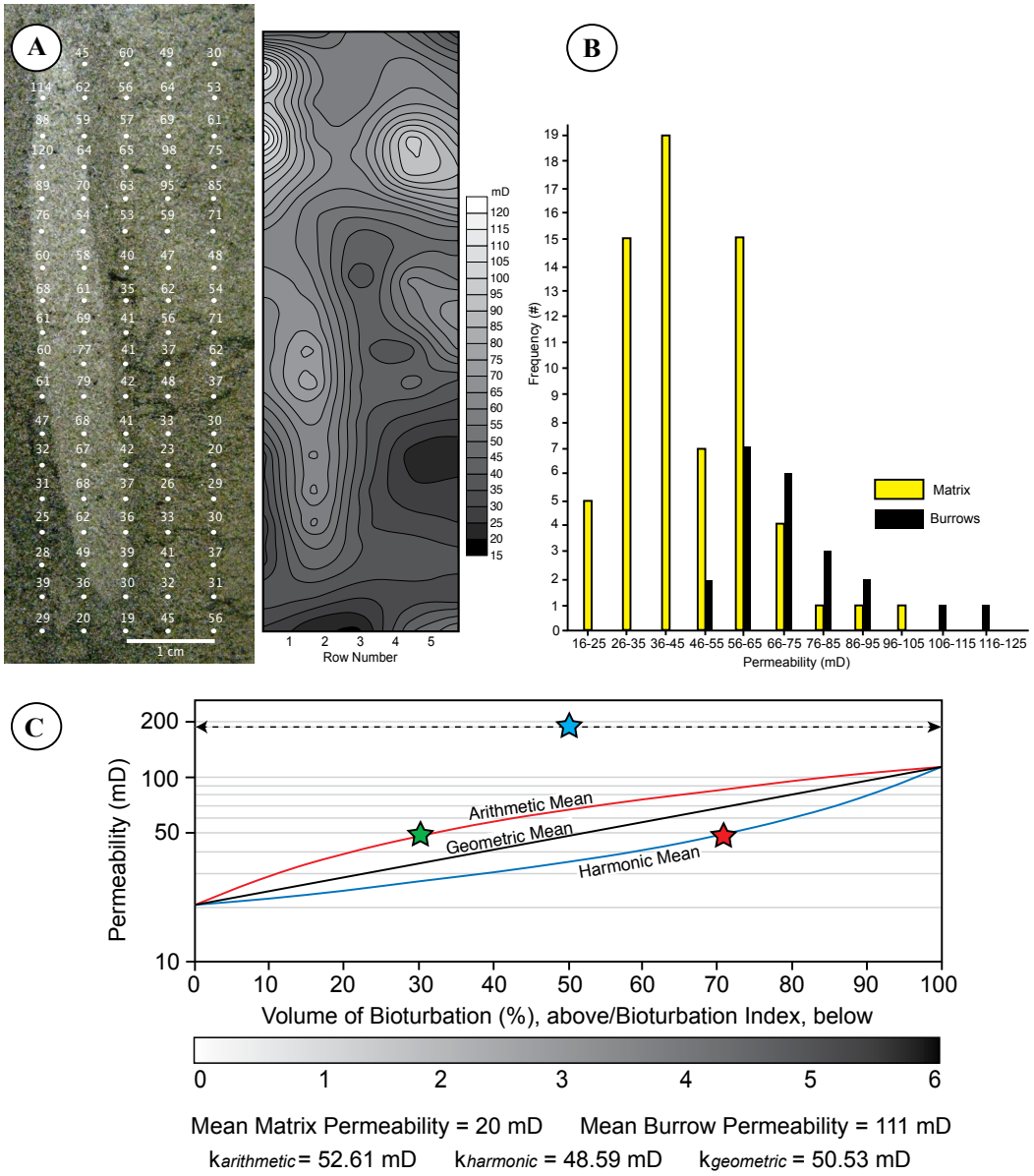

Figure 4.8: Spot-permeametry and associated bulk permeability analysis (geometric, arithmetic, and harmonic means) of a weakly defined textural heterogeneity. Well 1/3-3, depth 4221.75 m. **(A)** Example of a vertical oriented *Ophiomorpha nodosa* within a fine-grained sandstone. Spot-permeameter measurements and a supplementary contour map show that the highest permeabilities occur within the *Ophiomorpha nodosa*. **(B)** Histogram of the spot-permeametry measurements. Over 80% of the permeabilities for the matrix range from 26 to 65 mD and over 70% of the permeabilities for the *Ophiomorpha nodosa* range from 56 to 85 mD. The permeability values suggest an overall localized enhancement of permeability within the *Ophiomorpha nodosa*. **(C)** The permeability is best represented by the arithmetic mean (green star) as opposed to a harmonic mean at 30% bioturbation. The harmonic mean does not accurately predict the absolute permeability of the reservoir until ~70% bioturbation (50.53 mD, red star), when the vertical burrows likely become fully connected (Weaver and Schultheiss, 1983; Gingras et al., 1999). The core plug sample permeability obtained from Elf Petroleum Norge AS Core Report at depth 4221.70 m is 195 mD (blue star).

surrounding sandstone matrix during production. As a result, the harmonic mean does not accurately predict the absolute permeability of the reservoir until roughly 70% bioturbation (50.53 mD, red star in Fig. 4.8C), indicating moderate to high levels of bioturbation (i.e., 50 to 80% bioturbation by volume) are needed to fully connect the vertical burrows (Weaver and Schultheiss, 1983; Gingras et al., 1999).

4.5.3.2 Cryptic textural heterogeneity

In the sample displaying cryptic textural heterogeneity (Fig. 4.9A), total destruction of the original sedimentary fabric occurred and resulted in a massive appearing sandstone. Due to the spot-permeameter probe tip only having a diameter of 0.46 cm, it does not have the ability to exactly measure the permeability of the micro-scale burrows. The spot-permeameter, however, is able to give an approximation of permeabilities occurring within the burrows and matrix. Within our core sample, spot-permeametry measurements reveled a relatively uniform distribution of permeability measurements (Fig. 4.9B). In this context, the lowest mean permeability in the core sample was 161 mD while the highest mean permeability in the core sample was 288 mD. The closest permeability data point for comparison occurs at depth 3498.72 m for well 7/12-6, roughly 4.30 m from the permeability measurements made in this study. This full diameter core sample air permeability measurement, available on the NPD website in B.P. Petroleum Development Limited Special Core Analysis Study for well 7/12-6, has value of 583 mD (blue star in Fig. 4.9C) and occurs within cryptically bioturbated sandstones.

Because cryptic burrows are highly interconnected, permeability dead zones are rare and fluid flow is isotropic. The arithmetic, harmonic and geometric means are therefore similar throughout the entire core sample (Fig. 4.9C). Comparison with the permeability data point obtained from the B.P. Core Analysis suggests extremely permeable sands within the Ula Formation can occur in cryptically bioturbated intervals. Due to cryptically bioturbated reservoirs having no preferential flow direction, they are most accurately assessed using the geometric mean.

4.5.4 Numerical Modeling of Bioturbated Fabrics

Single-phase fluid flow, and thereby absolute permeability measurements, is simulated in two sedimentary fabrics: laminated sandstones and massive appearing sandstones. *Ophiomorpha* burrows were populated at different bioturbation intensities (1, 3, and 5) for each model and SBED numerical modeling recorded the arithmetic-, harmonic-, and geometric-averaged permeabilities. The reason

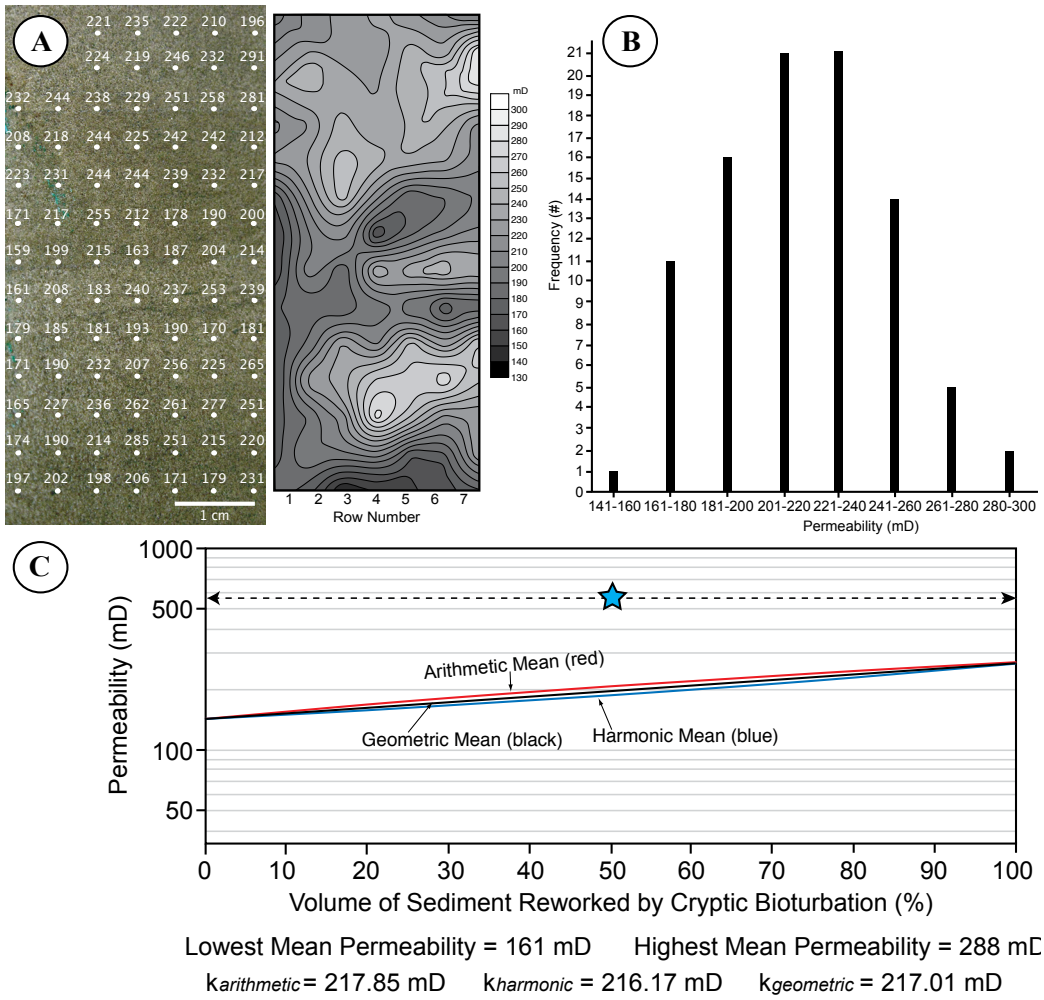

Figure 4.9: Spot-permeametry and associated bulk permeability analysis (geometric, arithmetic, and harmonic means) of a cryptic textural heterogeneity. Well 1/3-3, depth 3503.00 m. **(A)** Spot-permeameter measurements and a supplementary contour map of a fine-grained sandstone that has cryptic bioturbation. The highest permeabilities on the contour map are inferred to represent areas of higher levels of sediment reworking by microorganisms. **(B)** Histogram of the spot-permeametry measurements. With over 90% of the permeabilities ranging from 161 to 260 mD, an overall homogenization of permeabilities occurred due to cryptic bioturbation. **(C)** Due to cryptic bioturbation, the geometric mean would be the most accurate to characterize absolute reservoir permeability. The whole core sample permeability obtained from B.P. Core Analysis at depth 3498.72 m is 583 mD (blue star). Figure modified from Gingras et al. (2012).

different bioturbation intensities were used is two fold: (i) to show the influence bioturbation has on absolute permeability at different burrowing volumes, and (ii) because the Ula Formation commonly contains a wide variation in bioturbation intensities within the shoreface sandstones.

4.5.4.1 Laminated Sandstones Numerical Model

Computer simulations indicate that moderate to high levels of bioturbation are needed to increase the harmonic permeability in laminated sandstones (Table

4.1A). At low bioturbation intensities (BI 1 and 3), the harmonic permeabilities are essentially equivalent (1.17 and 1.77 mD, respectively). At BI 5, the harmonic permeability increased marginally to 15.23 mD. At lower bioturbation intensities, fewer *Ophiomorpha* burrows are present within the model and low-permeability horizontal mud layers act as a baffle inhibiting vertical fluid flow (Fig. 4.10A-B). With an increase in bioturbation intensity, interpenetrations of vertical burrow networks occur and effectively help transmit fluids across the mud layers (Fig. 4.10C) (Weaver and Schultheiss, 1983; Gingras et al., 1999; La Croix et al., 2012).

The arithmetic mean exhibited the greatest range in permeability with changes in bioturbation intensities (Table 4.1A). A rise in BI from 1 to 3 increased the arithmetic permeability from 19.33 mD to 43.03 mD, and when changed to BI 5, the permeability increased to 81.26 mD. An increase in arithmetic permeability is attributable to continuous flow paths being formed across the flow medium in both vertical and horizontal directions due to higher BI (Fig. 4.10B-C).

These numerical modeling results are consistent with *Ophiomorpha* systems that are generally interconnected in the bedding-parallel direction (Frey et al., 1978). Vertical *Ophiomorpha* burrow interpenetrations are commonly limited, however, and typically only shift from a horizontal to vertical orientation during higher-energy events (Howard, 1975). As a result, permeability fields within laminated sandstones are dominantly anisotropic with a bedding-parallel flow at low bioturbation intensities (BI 1-2). With successive time between storm events a lam-scram appearance can develop (Pemberton et al., 1992; Pemberton and MacEachern, 1997) and bioturbation intensities will commonly increase (BI 3-6). In these scenarios, permeability fields will exhibit localized isotopic fluid flow in ichnocoenoses exhibiting dense populations of *Ophiomorpha* burrows.

4.5.4.2 Massive Appearing Sandstones Numerical Model

Computer simulations reveal that little difference exists between the arithmetic-, harmonic-, and geometric-averaged permeabilities at BI 1 (Table 4.1B). Within the numerical model, interconnectivity exists between the alternating sand layers and there are no internal flow barriers, such as mud lenses, that inhibit fluid flow (Fig. 4.11A). The numerical model therefore acts as a cryptically bioturbated system wherein it is best characterized by the geometric mean. Furthermore, although considerable permeability contrasts exist between the *Ophiomorpha* and surrounding sand, unconnected burrow networks and low bioturbation intensities result in only minor influences on overall bulk reservoir permeability.

At higher levels of bioturbation (BI 3-5), the massive appearing sandstone becomes overprinted with *Ophiomorpha* burrows. The presence of highly connected burrow systems within the model resulted in a box work conduit system (Fig. 4.11B-C), in which all the entire system (burrows and matrix) contributed to fluid flow (Gingras et al., 1999). These results suggest that as bioturbation intensity and burrow connectivity increases, formerly isolated burrow conduits become linked (Gingras et al., 1999; La Croix et al., 2012) and help increase bulk reservoir permeability.

4.6 DISCUSSION

Thin sections, permeability measurements, and numerical modeling show that the most permeable and porous fabrics within the Ula Formation are associated with highly bioturbated rock fabrics. In occurrences where burrow connectivity exist, the overall enhancement of vertical and horizontal permeabilities occurs. Consequently, these burrow heterogeneities can be modeled to allow for a more robust evaluation of permeability trends and impact on resource and reservoir quality.

Laminated Sandstones

(A)	$k_{arithmetic}$	$k_{harmonic}$	$k_{geometric}$
BI 1	19.33	1.17	13.28
BI 3	43.02	1.77	24.86
BI 5	81.26	15.23	69.32

Massive Appearing Sandstones

(B)	$k_{arithmetic}$	$k_{harmonic}$	$k_{geometric}$
BI 1	31.97	27.17	29.26
BI 3	54.48	36.19	44.13
BI 5	84.78	65.45	76.73

Table 4.1: Numerical modeling values of absolute bulk permeability (geometric, arithmetic, and harmonic means) within two different sedimentary bedding fabrics (laminated and massive appearing) at different bioturbation intensities (BI 1, 3, and 5). All values are in millidarcies. **(A)** Numerical modeling of laminated sandstones. Absolute vertical permeability (harmonic mean) is unchanged at low bioturbation intensities, while horizontal permeability (arithmetic mean) is markedly enhanced with an increase in bioturbation intensity. **(B)** Numerical modeling of massive appearing sandstones. Both the vertical permeability (harmonic mean) and horizontal permeability (arithmetic mean) are enhanced with an increase in bioturbation intensity.

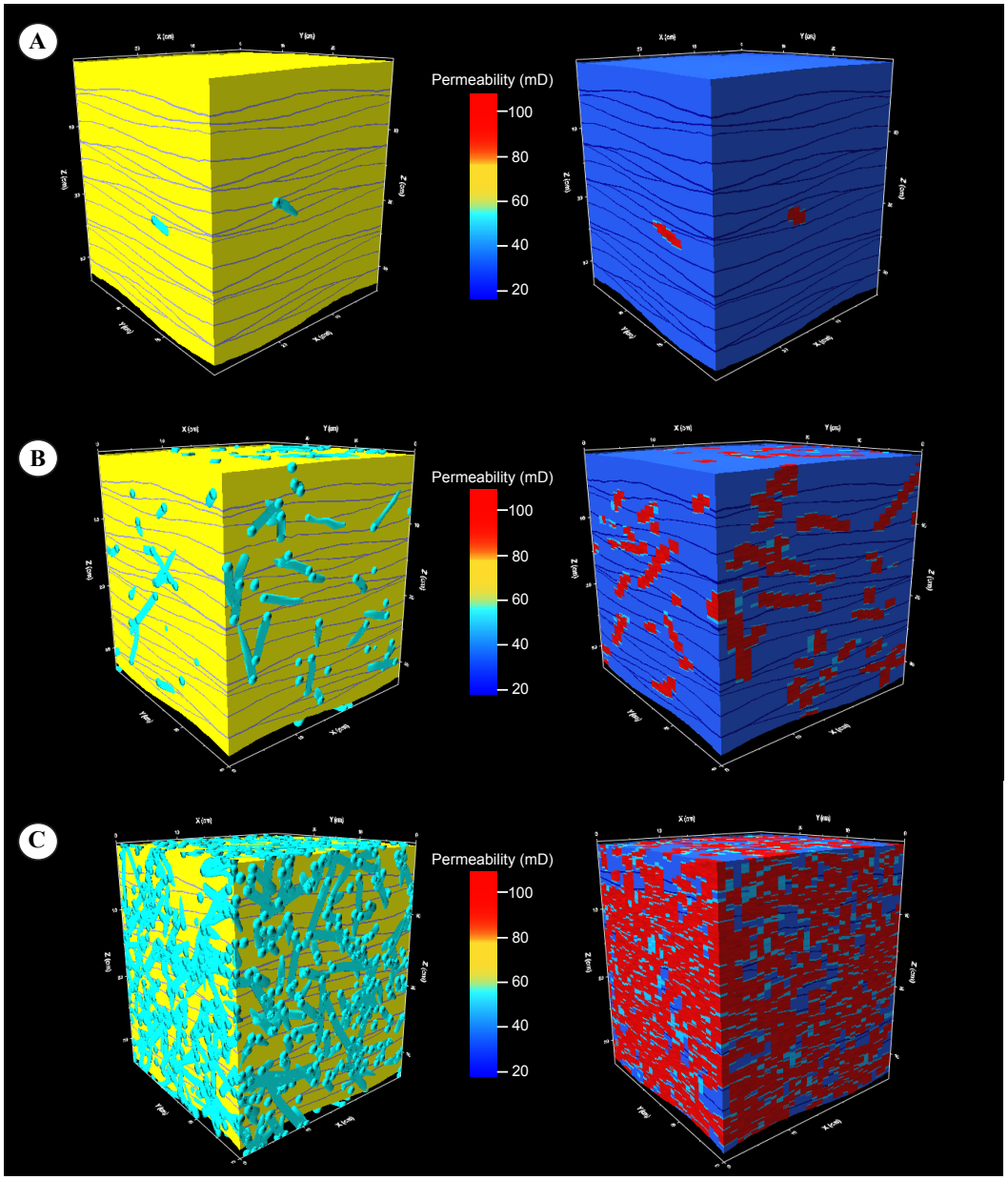

Figure 4.10: Computer modeling of laminated sandstones. On the left are examples of laminated sandstones with different volumes of *Ophiomorpha* populated within the model. On the right are the associated permeability contrasts. **(A)** Bioturbation intensity 1. **(B)** Bioturbation intensity 3. **(C)** Bioturbation intensity 5.

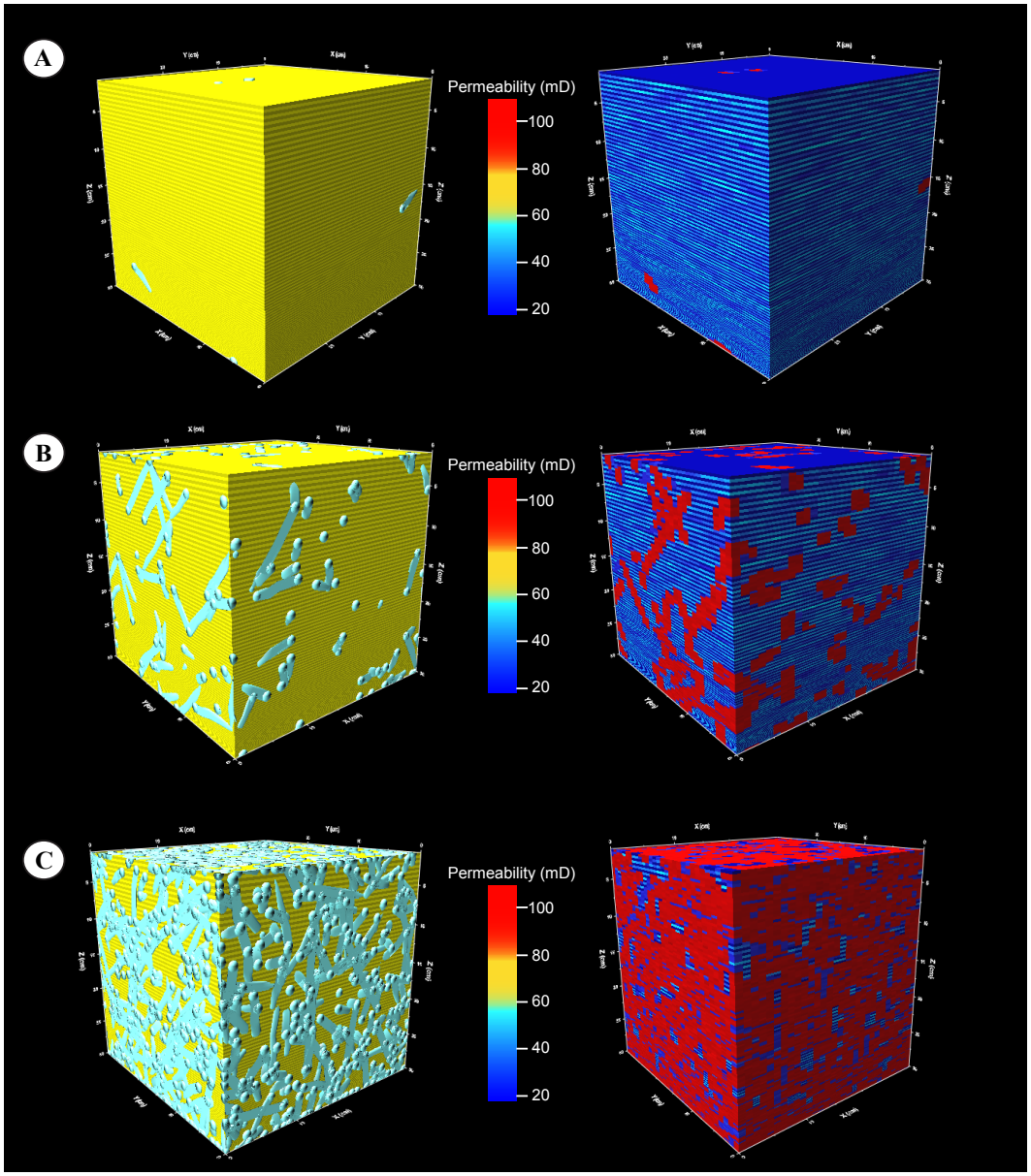

Figure 4.11: Computer modeling of a massive appearing sandstone that has two alternating sand intervals. On the left are examples of the massive sandstones with different volumes of *Ophiomorpha* populated within the model. On the right are the associated permeability contrasts. **(A)** Bioturbation intensity 1. **(B)** Bioturbation intensity 3. **(C)** Bioturbation intensity 5.

4.6.1 Assessment of Permeability Trends Using Ichnofacies Models

As shown in Chapter 3, ichnofacies models provide geologists with the proper framework to identify different groupings of ichnofossils based on organism behavior to different physico-chemical stresses (e.g., salinity, oxygenation, temperature). In this context, every bioturbated interval worldwide contains an ichnofacies expression that has a unique combination of vertical, sub-vertical, and horizontal trace fossils. The arithmetic, harmonic, and geometric means can therefore be used in combination with ichnofacies models to help better describe fluid flow within bioturbated reservoirs.

The arithmetic mean characterizes fluid movement through the most continuous and interconnected flow networks. In the Ula Formation, the arithmetic mean represents fluid migration pathways through highly bioturbated rock fabrics. An expression of the distal *Skolithos* ichnofacies that is gradational with proximal expressions of the *Cruziana* ichnofacies is a good example of a rock fabric that can be characterized using the arithmetic mean. Distal expressions of the *Skolithos* ichnofacies are associated with silty and muddy sandstone substrates, whereas proximal expressions of the *Cruziana* ichnofacies are associated with muddy sandstone, silty sandstone, and sandy siltstone substrates (MacEachern et al., 2007a). Typically common in reduced shoreface energy settings, ichnofossil orientation of the distal *Skolithos*-proximal *Cruziana* ichnofacies are sub-vertical to horizontal and bioturbation intensities are commonly very high (BI 4-5; Dashtgard et al., 2009). Trace fossils such as *Ophiomorpha irregulaire* and *Thalassinoides*, among others, are good examples of highly interconnected burrow networks that be best characterized using the arithmetic mean.

The harmonic mean characterizes vertical permeability conduits cross-cutting layers in perfectly stratified media. It best exemplifies reservoirs that contain isolated burrow conduits wherein fluid will move perpendicular to the sediment layering in order to connect with higher permeable conduits. Fluid movement is therefore commonly confined to the matrix (i.e., non-bioturbated sediment). Depending on burrow permeability, fluid will either diffuse from the burrows into the matrix or remain trapped within the burrow. The archetypal *Skolithos* ichnofacies is a good example to be used by the harmonic mean in shoreface environments. Archetypal *Skolithos* ichnofacies are typically developed in slightly muddy to clean, moderately- to well-sorted, loose or shifting particulate (sand-prone) substrates (MacEachern et al., 2007a). In addition, trace fossil orientations are dominantly vertical forms (Howard, 1975; Vossler and Pemberton, 1988) and commonly

display low bioturbation intensities (BI 1-3; Dashtgard et al., 2009). Bioturbation intensities are generally reduced due to environmental stresses such as storm waves and rapid sedimentation (Pemberton et al., 1992; Pemberton and MacEachern, 1997; MacEachern et al., 2007b). Trace fossils such as *Ophiomorpha nodosa* and *Skolithos*, among others, are good examples of vertical burrow networks that would be best characterized using the harmonic mean.

The geometric mean best characterizes intervals with extreme bioturbation intensities, with the best example being cryptic bioturbation. Within cryptically bioturbated intervals, the primary bedding structures are commonly preserved despite complete bioturbation. Similar phenomenon is also seen in some macro-burrows such as *Macaronichnus segregatis*, where the burrowing process does not result in the total destruction of the sedimentary fabric (Gingras et al., 2002b; Gordon et al., 2010). As a result, cryptic bioturbation serves to reduce heterogeneities associated with background sedimentation and create a more homogenous flow network. In highly bioturbated systems with macro burrows, such as *Ophiomorpha*, numerous burrow flow paths are formed in both horizontal and vertical directions. Isotropic flow units will therefore begin forming and the arithmetic and harmonic means become comparable to the geometric mean.

4.6.2 Impact on Resource and Reservoir Quality

Bulk absolute reservoir permeability is estimated in this study using the arithmetic, harmonic, and geometric means. The arithmetic and harmonic means represent idealized end-member permeabilities within homogenous intervals and thereby capture all possible bulk permeabilities of the reservoir. In practice, heterogeneities within the substrate, such as diagenetic cements, cemented fractures, and mud lenses, among many others, normally provide obstacles to fluid flow. Numerical modeling of reservoirs suggests most bulk permeabilities occur between the end-member harmonic and arithmetic means and somewhere near the geometric mean (Renard and de Marsily, 1997).

Within intervals containing weakly defined textural heterogeneities, fluid flow occurs predominately bedding-parallel and is best characterized using the arithmetic mean (Fig. 4.12A). Due to flow barriers such as laminated muds, increases in absolute vertical burrow permeability do not occur until a BI of 3 or greater. With increased bioturbation intensities, isotropic flow units begin developing as all burrows systems become interconnected. As a result, the arithmetic and harmonic means become comparable to the geometric mean. It is worth mentioning that at

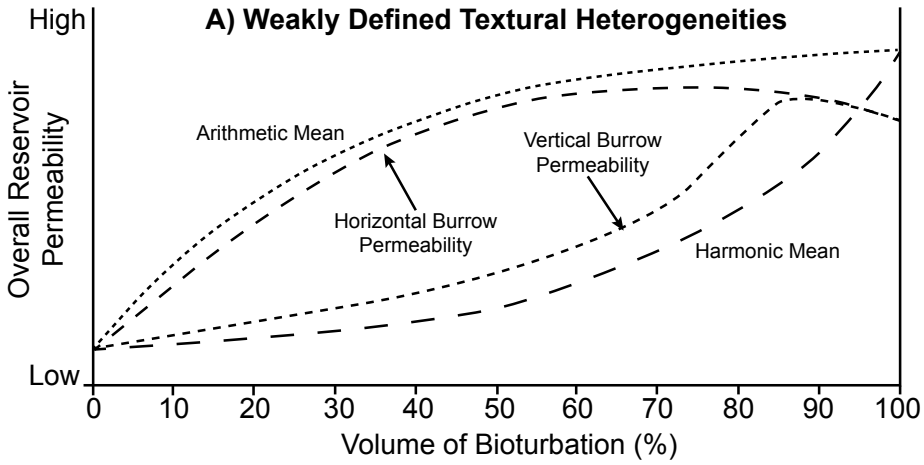
A) Weakly Defined Textural Heterogeneities
High
Low
Overall Reservoir Permeability
Arithmetic Mean
Vertical Burrow Permeability
Horizontal Burrow Permeability
Harmonic Mean
0
10
20
30
40
50
60
70
80
90
100
Volume of Bioturbation (%)

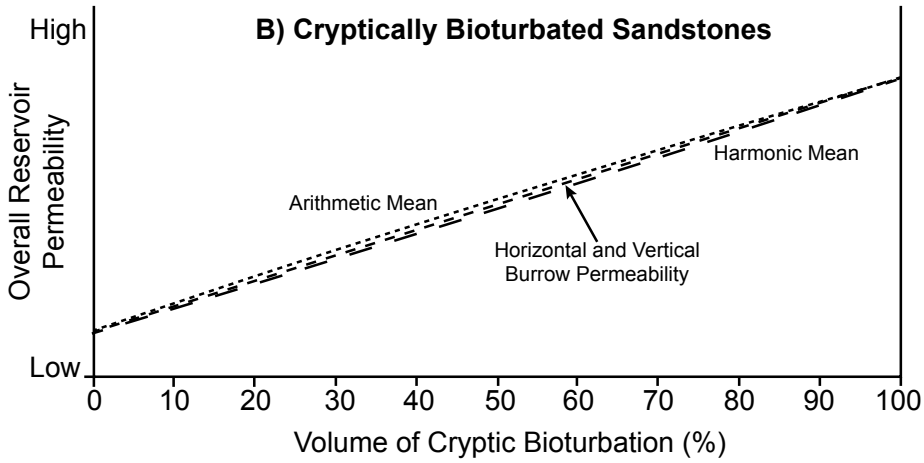
B) Cryptically Bioturbated Sandstones
High
Low
Overall Reservoir Permeability
Harmonic Mean
Arithmetic Mean
Horizontal and Vertical Burrow Permeability
0
10
20
30
40
50
60
70
80
90
100
Volume of Cryptic Bioturbation (%)

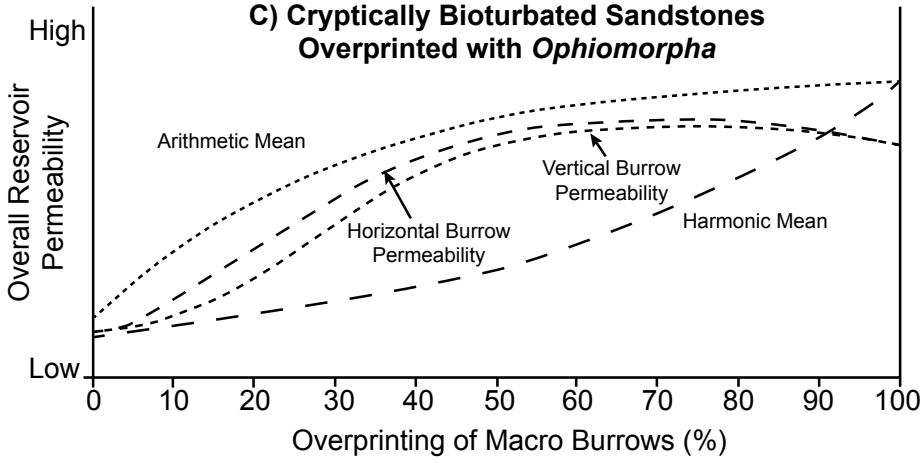
C) Cryptically Bioturbated Sandstones
Overprinted with *Ophiomorpha*
High
Low
Overall Reservoir Permeability
Arithmetic Mean
Vertical Burrow Permeability
Horizontal Burrow Permeability
Harmonic Mean
0
10
20
30
40
50
60
70
80
90
100
Overprinting of Macro Burrows (%)

Figure 4.12 (above): Conceptualized characterizations of horizontal and vertical burrow permeability trends within intervals with weakly defined textural heterogeneities and cryptic textural heterogeneities, using data from spot-permeametry measurements and numerical models. **(A)** In intervals with weakly defined textural heterogeneities, absolute vertical burrow permeability does not increase until moderate to high levels of bioturbation are achieved. Horizontal burrow permeability follows very closely to the arithmetic mean of the reservoir. At extreme bioturbation intensities, heterogeneities (e.g., laminated muds) become incorporated into the burrow flow pathways. As a result, the horizontal and vertical burrow permeabilities decrease slightly from the idealized arithmetic and harmonic permeabilities. **(B)** In cryptically bioturbated intervals, horizontal and vertical permeabilities are roughly equal. **(C)** In cryptically bioturbated rocks overprinted with macro burrows (e.g., *Ophiomorpha*), anisotropy occurs due to difference in horizontal and vertical burrow permeabilities of the macro burrows. At extreme bioturbation intensities, isotropy occurs again and slight decreases in bulk permeability can occur due to the incorporation of lower permeable sands into the burrow flow pathways.

extreme bioturbation intensities (BI 6), heterogeneities within the substrate become incorporated into the fluid pathways. As a result, absolute permeabilities slightly deviate away from the idealized the arithmetic, harmonic, and geometric means.

In cryptically bioturbated intervals, absolute horizontal and vertical permeabilities are best approximated using the geometric mean (Fig. 4.12B). When an overprinting of *Ophiomorpha* burrows occurs (Fig. 4.11B-C), anisotropy develops due the difference in permeabilities between the *Ophiomorpha* and cryptically bioturbated sands (Fig. 4.12C). At extreme bioturbation intensities, isotropy forms again as the horizontal and vertical permeabilities become roughly equal within the sample. Due to extreme bioturbation, the sandstones from the cryptically bioturbated units, along with heterogeneities from the *Ophiomorpha* burrow linings, become incorporated into the *Ophiomorpha* burrow fluid pathways. As a result, localized reductions in overall bulk permeability from the idealized arithmetic, harmonic, and geometric means can occur.

In the Ula Formation, Facies 1 and Facies 2 act as dual-porosity systems (Fig. 4.13A). The greatest fluid flux will occur through the highest permeability zones (typically the burrows) and fluid flow interaction with the matrix will be moderate to extensive (Fig. 4.13B-C) (Gingras et al., 2004, Pemberton and Gingras, 2005; Gingras et al., 2007; Gingras et al., 2012). In scenarios where the sandstones are populated with low volumes of *Ophiomorpha* (e.g., BI 1), fluid transmissivity will most likely occur through the matrix (Fig. 4.14A). Because the *Ophiomorpha* burrows are unconnected, fluid will likely diffuse from the burrows into the matrix as production occurs. When an increase in *Ophiomorpha* burrows occur (e.g., BI 3-5), the burrow systems become interconnected and begin to dominate the reservoir fabric (Frey et al., 1978; Weaver and Schultheiss, 1983; Gingras et al., 1999; La Croix et al., 2012). Under these conditions, the *Ophiomorpha* burrows will likely begin to act as the primary conduits for fluid flow (Fig. 4.14B-C).

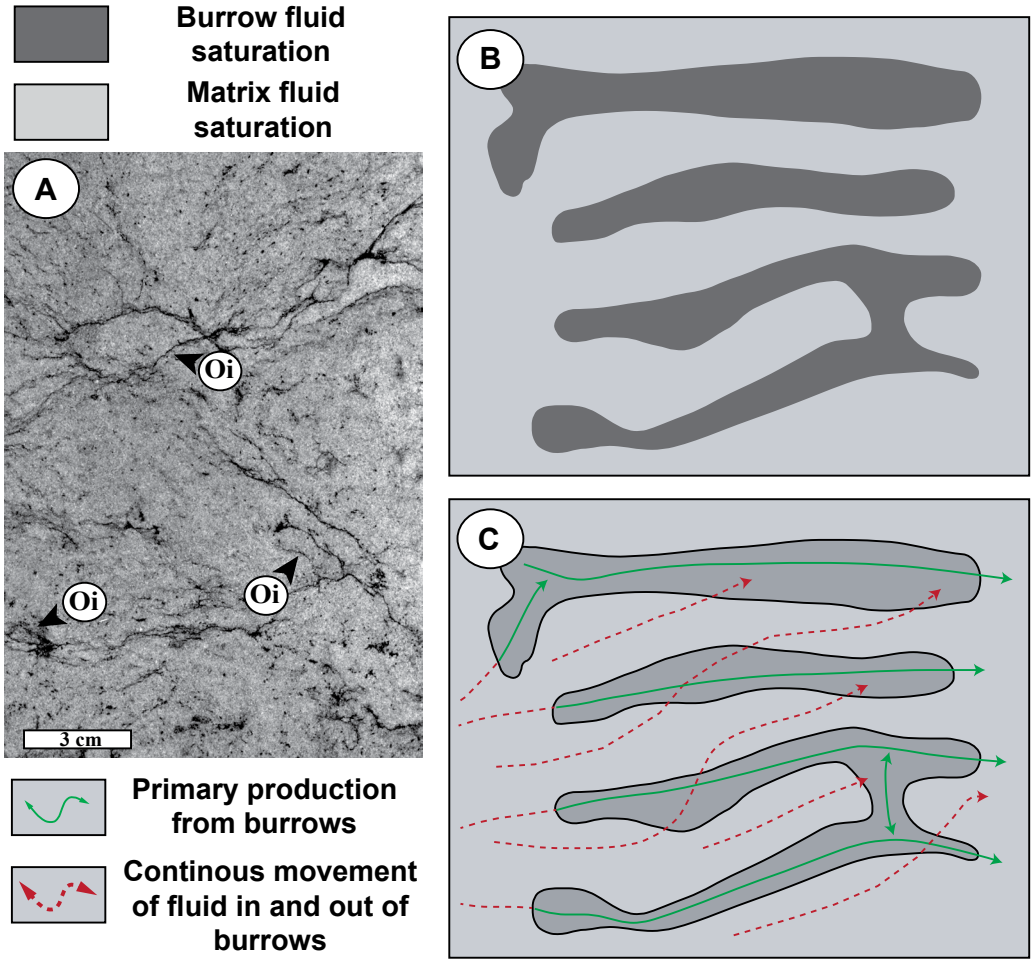

Figure 4.13: A schematic of a fluid flow within a dual-porosity reservoir. **(A)** Example of a slabbed core showing sand-filled *Ophiomorpha irregulaire* (Oi) within a sandstone matrix. Represents an example of a weakly defined textural heterogeneity. **(B)** Oil saturation is typically saturated along the most permeable conduits (i.e., burrows). **(C)** During fluid production, fluid flow will occur through both the matrix and burrows as a result of the similar permeabilities. Figure modified from Gingras et al. (2012).

4.7 CONCLUSIONS

To better understand fluid flow within bioturbated siliciclastic reservoirs, thin sections, spot-permeametry measurements, and numerical modeling was completed on subsurface cores from the Upper Jurassic Ula Formation of the Norwegian Central Graben. Within the reservoir intervals, examples of *Ophiomorpha* and cryptically bioturbated sandstones dominate the bioturbated assemblages. The *Ophiomorpha* burrows have elevated permeabilities and porosities relative to the surrounding sediment and represent examples of weakly defined textural heterogeneities. Cryptic bioturbation caused a reduction in heterogeneities and homogenization of permeability and porosity occurred as a result.

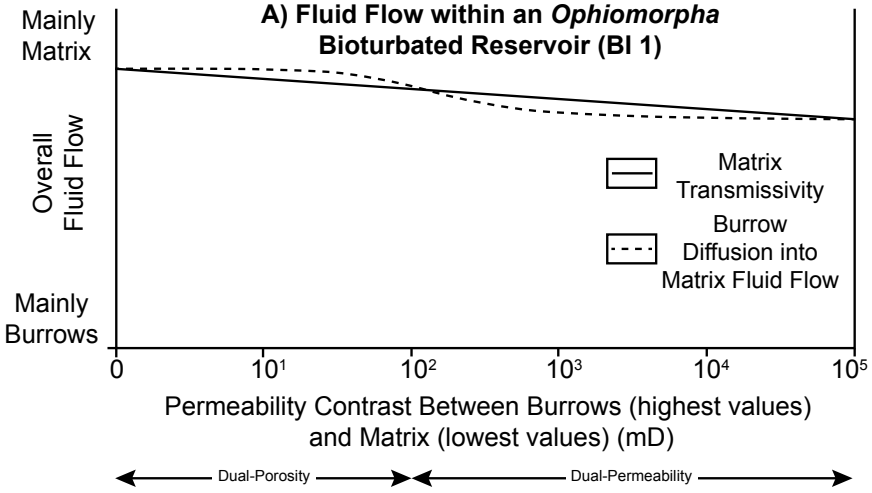
A) Fluid Flow within an *Ophiomorpha* Bioturbated Reservoir (BI 1)
Mainly Matrix
Overall Fluid Flow
Mainly Burrows
Matrix Transmissivity
Burrow Diffusion into Matrix Fluid Flow
0
10^1
10^2
10^3
10^4
10^5
Permeability Contrast Between Burrows (highest values) and Matrix (lowest values) (mD)
Dual-Porosity
Dual-Permeability

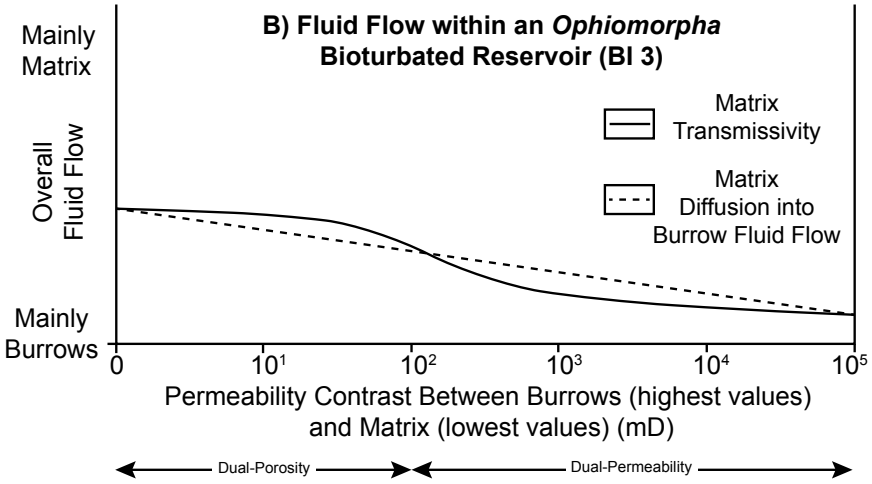
B) Fluid Flow within an *Ophiomorpha* Bioturbated Reservoir (BI 3)
Mainly Matrix
Overall Fluid Flow
Mainly Burrows
Matrix Transmissivity
Matrix Diffusion into Burrow Fluid Flow
0
10^1
10^2
10^3
10^4
10^5
Permeability Contrast Between Burrows (highest values) and Matrix (lowest values) (mD)
Dual-Porosity
Dual-Permeability

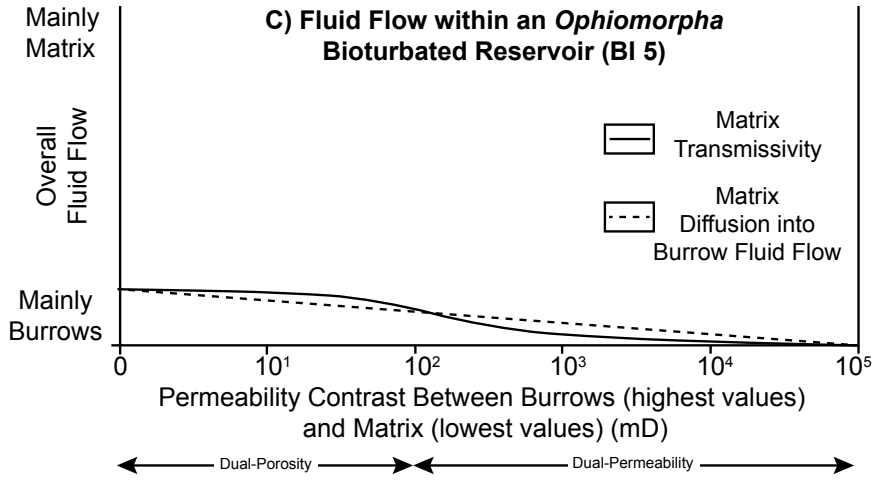
C) Fluid Flow within an *Ophiomorpha* Bioturbated Reservoir (BI 5)
Mainly Matrix
Overall Fluid Flow
Mainly Burrows
Matrix Transmissivity
Matrix Diffusion into Burrow Fluid Flow
0
10^1
10^2
10^3
10^4
10^5
Permeability Contrast Between Burrows (highest values) and Matrix (lowest values) (mD)
Dual-Porosity
Dual-Permeability

Figure 4.14 (above): Conceptual fluid production from a dual-porosity and dual-permeability reservoir with *Ophiomorpha* populated at three different bioturbation intensities (BI 1, 3, and 5). **(A)** At BI 1, *Ophiomorpha* burrows are unconnected. As a result, fluid flow occurs predominately from the sandstone matrix in both dual-porosity and dual-permeability reservoirs. Due to low bioturbation intensities, the *Ophiomorpha* burrows act as secondary fluid pathways and drain into the producing matrix. **(B)** At BI 3, *Ophiomorpha* burrows are moderately to well connected. The matrix and burrows will contribute relatively equally to fluid production in dual-porosity intervals. In intervals exhibiting extreme permeability contrasts (i.e., dual-permeability), the *Ophiomorpha* burrows will act as the primary fluid conduits. **(C)** At BI 5, *Ophiomorpha* burrows are fully connected. As a result, fluid flow occurs predominately from the burrows in both dual-porosity and dual-permeability reservoirs.

Using arithmetic, harmonic, and geometric numerical models, the bulk permeability of the bioturbated intervals are evaluated. The arithmetic mean represented intervals dominated by horizontal to sub-vertical burrows or high bioturbation intensities. An expression of the distal *Skolithos* to proximal *Cruziana* ichnofacies represents a good example of a fabric that can be characterized using the arithmetic mean. The harmonic mean characterized intervals dominated by vertical burrows or low bioturbation intensities. An expression of the archetypal *Skolithos* ichnofacies represents a good example of a fabric that can be characterized using the harmonic mean. The geometric mean best characterized intervals overprinted with cryptic bioturbation or high degrees of bioturbation by macro burrows (e.g., *Ophiomorpha*).

Numerical modeling of *Ophiomorpha* populated within two different sedimentary fabrics (laminated sandstones and massive appearing sandstones) indicated that the dominant influences on absolute permeability and fluid flow are burrow connectivity, burrow permeability, and bioturbation intensity. At low bioturbation intensities, isolated burrow conduits exist and absolute reservoir permeability increases only marginally. With increased bioturbation intensities, enhancement in absolute horizontal and vertical permeability occurs due to a higher amount of continuous flow paths and increased amount of permeable flow media. High levels of bioturbation are especially important in scenarios where flow barriers, such as mud lenses, act as aquitards and restrict fluid flow between permeable layers.

The bioturbated zones within the Ula Formation serve to represent an important element to recovering fluids from the reservoir intervals. Due to the dual-porosity nature of the Ula Formation, both the matrix and burrows act as components contributing towards fluid flow. In moderate to pervasively bioturbated intervals (BI 3-6), the burrows can be considered the primary fluid flow conduits as they have considerable influence on the overall absolute bulk permeability within the reservoir.

4.8 REFERENCES CITED

Bailey, C.C., Price, I., and Spencer, A.M., 1981, The Ula Field, Block 7/12, Norway: *in* Norwegian Symposium on Exploration. Norsk Petroleumsforening (NPF), Article 18, 26 p.

Baniak, G.M., Gingras, M.K., Burns, B.A., and Pemberton, S.G., in press, A paleogeographic reconstruction of a highly bioturbated, fault-influenced shoreface (FIS) deposit: Upper Jurassic Ula Formation, Norwegian North Sea: Sedimentology.

Bann, K.L., Fielding, C.R., MacEachern, J.A., and Tye, S.C., 2004, Differentiation of estuarine and offshore marine deposits using integrated ichnology and sedimentology: Permian Pebbly Beach Formation, Sydney Basin, Australia: *in* McIlroy, D., ed., The Application of Ichnology to Palaeoenvironmental and Stratigraphic Analysis. Geological Society, London, Special Publication, v. 228, p. 179-211.

Bastardie, F., Capowiez, Y., de Dreuzy, J.R., and Cluzeau, D., 2003, X-ray tomographic and hydraulic characterization of burrowing by three earthworm species in repacked soil cores: Applied Soil Ecology, v. 24, p. 3-16.

Bear, J., 1972, Dynamics of Fluids in Porous Media. Elsevier, New York, New York, 746 p.

Bergan, M., Tørudbakken, B., and Wandås, B., 1989, Lithostratographic correlation of Upper Jurassic sandstones within the Norwegian Central Graben: Sedimentological and tectonic implications: *in* Collinson, J.D., ed., Correlation in Hydrocarbon Exploration. Norwegian Petroleum Society (NPF), Graham and Trotman, London, United Kingdom, p. 243-251.

Brown, A., Mitchell, A.W., Nilssen, I.R., Stewart, I.J., and Svela, P.T., 1992, Ula Field: Relationship and hydrocarbon distribution: *in* Larsen, R.M., Brekke, H., Larsen, B.T., and Talleraas, E., eds., Structural and Tectonic Modeling and its Application to Petroleum Geology. Norwegian Petroleum Society (NPF), Special Publication 1, Elsevier, Amsterdam, p. 409-420.

Core Laboratories Instruments., 1996, Profile Permeameter PDPK-400 Operations Manual, 40 p.

Cunningham, K.J., Sukop, M.C., Huang, H., Alvarez, P.F., Curran, H.A., Renken, R.A., and Dixon, J.F., 2009, Prominence of ichnologically influenced macroporosity in the karst Biscayne aquifer: Stratiform "super-k" zones: Geological Society of America Bulletin, v. 121, p. 164-180.

Cunningham, K.J., Sukop, M.C., and Curran, H.A., 2012, Carbonate aquifers: *in* Knaust, D., and Bromley, R.G., eds., Trace Fossils as Indicators of Sedimentary Environments. Developments in Sedimentology 64, Elsevier, Amsterdam, p. 869-896.

Dabek, L.B., and Knepp, R., 2011, Bioturbation and its effects on permeability in wave-dominated shoreface rocks of the Spring Canyon Member, Blackhawk Formation, Utah, USA: American Association of Petroleum Geologists, Search and Discovery Article # 50425, 10 p.

Dashtgard, S.E., Gingras, M.K., and MacEachern, J.A., 2009, Tidally modulated shorefaces: Journal of Sedimentary Research, v. 79, p. 793-807.

Dawson, W.C., 1978, Improvement of sandstone porosity during bioturbation: American Association of Petroleum Geologists Bulletin, v. 62, p. 508-509.

Dott, R.H., 1964, Wacke, graywacke and matrix; what approach to immature sandstone classification?: Journal of Sedimentary Petrology, v. 34. p. 625-632.

Fraser, S.I., Robinson, A.M., Johnson, H.D., Underhill, J.R., Kadolsky, D.G.A., Connell, R., Johannesen, P., and Ravnås, R., 2003, Upper Jurassic: *in* Evans, D., Graham, C., Armour, A., and Bathurst, P., eds., The Millennium Atlas: Petroleum Geology of the Central and Northern North Sea. Geological Society, London, United Kingdom, p. 157-189.

Freeze, R.A., and Cherry, J.A., 1979, Groundwater: Prentice-Hall, New Jersey, 604 p.

Frey, R.W., and Pemberton, S.G., 1985, Biogenic structures in outcrops and cores. I: Approaches to ichnology: Bulletin of Canadian Petroleum Geology, v. 33, p. 72-115.

Frey, R.W., Howard, J.D., and Pryor, W.A., 1978, *Ophiomorpha*: Its morphologic, taxonomic, and environmental significance: Palaeogeography, Palaeoclimatology, Palaeoecology, v. 23, p. 199-229.

Gingras, M.K., Pemberton, S.G., Mendoza, C.A., and Henk, F., 1999, Assessing the anisotropic permeability of *Glossifungites* surfaces: Petroleum Geoscience, v. 5, p. 349-357.

Gingras, M.K., Pemberton, S.G., and Saunders, T., 2000, Firmness profiles associated with tidal-creek deposits: The temporal significance of *Glossifungites* assemblages: Journal of Sedimentary Research, v. 70, p. 1017-1025.

Gingras, M.K., MacMillan, B., and Balcom, B.J., 2002a, Visualizing the internal physical characteristics of carbonate sediments with magnetic resonance imaging and petrography: Bulletin of Canadian Petroleum Geology, v. 50, p. 363-369.

Gingras, M.K., MacMillan, B., Balcom, B.J., Saunders, T., and Pemberton, S.G., 2002b, Using magnetic imaging and petrographic techniques to understand the textural attributes and porosity distribution in *Macaronichnus*-burrowed sandstone: Journal of Sedimentary Research, v. 72, p. 552-558.

Gingras, M.K., Räsänen, M., Pemberton, S.G., and Romero, L.P., 2002c, Ichnology and sedimentology reveal depositional characteristics of bay-margin parasequences in the Miocene Amazonian foreland basin: Journal of Sedimentary Research, v. 72, p. 871-883.

Gingras, M.K., Mendoza, C.A., and Pemberton, S.G., 2004, Fossilized worm-burrows influence the resource quality of porous media: American Association of Petroleum Geologists Bulletin, v. 88, p. 875-883.

Gingras, M.K., Pemberton, S.G., Henk, F., MacEachern, J.A., Mendoza, C.A., Rostron, B., O'Hare, R., and Spila, M.V., 2007, Applications of ichnology to fluid and gas production in hydrocarbon reservoirs: *in* MacEachern, J.A., Bann, K.L., Gingras, M.K., and Pemberton, S.G., eds., Applied Ichnology. Society of Economic Paleontologists and Mineralogists (SEPM), Short Course Notes, no. 52, p. 129-143.

Gingras, M.K., Baniak, G., Konhauser, K.O., La Croix, A., Lemiski, R., Mendoza, C., Pemberton, S.G., Polo, C., and Zonneveld, J.-P., 2012, Porosity and permeability in bioturbated sediments: *in* Knaust, D., and Bromley, R.G., eds., Trace Fossils as Indicators of Sedimentary Environments. Developments in Sedimentology 64, Elsevier, Amsterdam, p. 837-868.

Gluyas, J.G., 1997, Poroperm prediction for reserves growth exploration: Ula Trend, Norwegian North Sea: *in* Kupecz, J.A., Gluyas, J.G., and Bloch, S., eds., Reservoir Quality Prediction in Sandstones and Carbonates. American Association of Petroleum Geologists, Memoir no. 69, p. 201-210.

Gordon, J.B., Pemberton, S.G., Gingras, M.K., and Konhauser, K.O., 2010, Biogenically enhanced permeability: A petrographic analysis of *Macaronichnus segregatus* in the Lower Cretaceous Bluesky Formation, Alberta, Canada: American Association of Petroleum Geologists Bulletin, v. 94, p. 1779-1795.

Gowers, M.B., Holtar, E., and Swensson, E., 1993, The structure of the Norwegian Central Trough (Central Graben area): *in* Parker, J.R., Petroleum Geology of Northwest Europe: Proceedings of the 4th Conference. Geological Society, London, p. 1245-1254.

Gowland, S., 1996, Facies characteristics and depositional models of highly bioturbated shallow marine siliciclastic strata: An example from the Fulmar Formation (Late Jurassic), UK Central Graben: *in* Hurst, A., Johnson, H.D., Burley, S.D., Canham, A.C., and Mackertich, D.S., eds., Geology of the Humber Group: Central Graben and Moray Firth, UKCS. Geological Society, London, Special Publication, v. 114, p. 185-214.

Green, M.A., Aller, R.C., and Aller, J.Y., 1992, Experimental evaluation of the influences of biogenic reworking on carbonate preservation in nearshore sediments: Marine Geology, v. 107, p. 175-181.

Harris, N.B., 2006, Low porosity haloes at stylolites in the feldspathic Upper Jurassic Ula Formation, Norwegian North Sea: An integrated petrographic and chemical mass-balance approach: Journal of Sedimentary Research, v. 76, p. 444-459.

Home, P.C., 1987, Ula: *in* Spencer, A.M., Campbell, C.J., Hanslien, S.H., Nelson, P.H., Nysaether, E., and Ormaasen, E.G., eds., Geology of the Norwegian Oil and Gas Fields. Graham and Trotman, London, United Kingdom, p. 143-152.

Howard, J.D., 1975, The sedimentological significance of trace fossils: *in* Frey, R.W., The Study of Trace Fossils. Springer-Verlag, New York, New York, p. 131-146.

Howard, J.D., and Frey, R.W., 1975, Estuaries of the Georgia Coast, U.S.A.: sedimentology and biology. II. Regional animal-sediment characteristics of Georgia Estuaries: Senckenbergiana Maritima, v. 7, p. 33-103.

Johnson, H.D., Mackay, T.A., and Stewart, D.J., 1986, The Fulmar oil-field (central North Sea): Geological aspects of its discovery, appraisal and development: Marine and Petroleum Geology, v. 3, p. 99-125.

Jones, S.C., 1994, A new, fast, accurate pressure-decay probe permeameter: Society of Petroleum Engineers Journal, v. 9, p. 193-199.

Katrak, G., and Bird, F.L., 2003, Comparative effects of the large bioturbators, *Trypaea australiensis* and *Heloecius cordiformis*, on intertidal sediments of western port, Victoria, Australia: Marine and Freshwater Research, v. 54, p. 701-708.

Knaust, D., 2009, Ichnology as a tool in carbonate reservoir characterization: A case study from the Permian-Triassic Khuff Formation in the Middle East: GeoArabia, v. 14, p. 17-38.

Knaust, D., 2012, Methodology and techniques: *in* Knaust, D., and Bromley, R.G., eds., Trace Fossils as Indicators of Sedimentary Environments. Developments in Sedimentology 64, Elsevier, Amsterdam, p. 245-271.

Konhauser, K.O., and Gingras, M.K., 2011, Are animal burrows a major sedimentary sink for metals?: Ichnos, v. 18, p. 1-3.

Krejci, M.E., and Lowe, R.L., 1986, Importance of sand grain mineralogy and topography in determining micro-spatial distribution of epipsammic diatoms: Journal of the North American Benthological Society, v. 5, p. 211-220.

Krinsley, D.H., and Funnell, B.M., 1965, Environmental history of quartz sand grains from the lower and middle Pleistocene of Norfolk, England: Quarterly Journal of the Geological Society, v. 121, p. 435-456.

La Croix, A.D., Gingras, M.K., Dashtgard, S.E., and Pemberton, S.G., 2012, Computer modeling bioturbation: The creation of porous and permeable fluid-flow pathways: American Association of Petroleum Geologists Bulletin, v. 96, p. 545-556.

La Croix, A.D., Gingras, M.K., Pemberton, S.G., Mendoza, C.A., MacEachern, J.A., and Lemiski, R.T., 2013, Biogenically enhanced reservoir properties in the Medicine Hat Gas Field, Alberta, Canada: Marine and Petroleum Geology, v. 43, p. 464-477.

Lemiski, R.T., Hovikoski, J., Pemberton, S.G., and Gingras, M.K., 2011, Sedimentological, ichnological and reservoir characteristics of the low-permeability, gas-charged Alderson Member (Hatton gas field, southwest Saskatchewan): Implications for resource development: Bulletin of Canadian Petroleum Geology, v. 59, p. 1-28.

MacEachern, J.A., Bann, K.L., and Gingras, M.K., and Pemberton, S.G., 2007a, The ichnofacies paradigm: High-resolution paleoenvironmental interpretation of the rock record: *in* MacEachern, J.A., Bann, K.L., Gingras, M.K., and Pemberton, S.G., eds., Applied Ichnology. Society of Economic Paleontologists and Mineralogists (SEPM), Short Course Notes, no. 52, p. 27-64.

MacEachern, J.A., Pemberton, S.G., Bann, K.L., and Gingras, M.K., 2007b, Departures from the archetypal ichnofacies: Effective recognition of environmental stress in the rock record: *in* MacEachern, J.A., Bann, K.L., Gingras, M.K., and Pemberton, S.G., eds., Applied Ichnology. Society of Economic Paleontologists and Mineralogists (SEPM), Short Course Notes, no. 52, p. 65-92.

Macaulay, C.I., Beckett, D., Braithwaite, K., Bliefnick, D., and Philps, B., 2001, Constraints on diagenesis and reservoir quality in the fractured Hasdrubal field, offshore Tunisia: Journal of Petroleum Geology, v. 24, p. 55-78.

Martin, M.A., and Pollard, J.E., 1996, The role of trace fossil (ichnofabric) analysis in the development of depositional models for the Upper Jurassic Fulmar Formation of the Kittiwake Field (Quadrant 21, UKCS): *in* Hurst, A., Johnson, H.D., Burley, S.D., Canham, A.C., and Mackertich, D.S., eds., Geology of the Humber Group: Central Graben and Moray Firth, UKCS. Geological Society, London, Special Publication, v. 114, p. 163-183.

Meadows, P. S., and Anderson, J.G., 1968, Micro-organisms attached to marine sand grains: Journal of the Marine Biological Association of the United Kingdom, v. 48, p. 161-175.

Meadows, P.S., and Tait, J., 1989, Modification of sediment permeability and shear strength by two burrowing invertebrates: Marine Biology, v. 101, p. 75-82.

Mills, A.L., and Maubrey, R., 1981, Effect of mineral composition on bacterial attachment to submerged rock surfaces: Microbial Ecology, v. 7, p. 315-322.

Muskat, M., 1937, The Flow of Homogeneous Fluids Through Porous Media. McGraw-Hill, New York, New York, 763 p.

Nedkvitne, T., Karlsen, D.A., Bjorlykke, K., and Larter, S.R., 1993, Relationship between diagenetic evolution and petroleum emplacement in the Ula Field, North Sea: Marine and Petroleum Geology, v. 10, p. 255-270.

Over, D.J., 1990, Trace metals in burrow walls and sediments, Georgia Bight, USA: Ichnos, v. 1, p. 31-41.

Oxtoby, N.H., Mitchell, A.W., and Gluyas, J.G., 1995, The filling and emptying of the Ula oilfield: Fluid inclusion constraints: *in* Cubitt, J.M., and England, W.A., eds., The Geochemistry of Reservoirs. Geological Society, London, Special Publication, v. 86, p. 141-157.

Pemberton, S.G., and MacEachern, J.A., 1997, Ichnological signature of storm deposits: The use of trace fossils in event stratigraphy: *in* Brett, C. E., and Baird, G.C., eds., Paleontological Events: Stratigraphic, Ecological, and Evolutionary Implications. Columbia University Press, New York, p. 73-109.

Pemberton, S.G., and Gingras, M.K., 2005, Classification and characterizations of biogenically enhanced permeability: American Association of Petroleum Geologists Bulletin, v. 89, p. 1493-1517.

Pemberton, S.G., MacEachern, J.A., and Ranger, M.J., 1992, Ichnology and event stratigraphy: The use of trace fossils in recognizing tempestites: *in* Pemberton, S.G., ed., Applications of Ichnology to Petroleum Exploration. Society of Economic Paleontologists and Mineralogists (SEPM), Core Workshop, no. 17, Calgary, Alberta, p. 85-117.

Pemberton, S.G., MacEachern, J.A., Gingras, M.K., and Saunders, T.D.A., 2008, Biogenic chaos: Cryptobioturbation and the work of sedimentologically friendly organisms: Palaeogeography, Palaeoclimatology, Palaeoecology, v. 270, p. 273-279.

Petrash, D.A., Lalonde, S.V., Gingras, M.K., and Konhauser, K.O., 2011, A surrogate approach to studying the chemical reactivity of burrow mucous linings in marine sediments: Palaios, v. 26, p. 594-600.

Pickup, G.E., Ringrose, P.S., Corbett, P.W.M., Jensen, J.L., and Sorbie, K.S., 1995, Geology, geometry and effective flow: Petroleum Geoscience, v. 1, p. 37-42.

Polo, C., 2013, Bioturbation and resource quality: A case study of the Upper Cretaceous Lysing and Nise Formations, Ellida and Midnatsoll fields area, Norwegian Sea: University of Alberta Master's Thesis, Unpublished, 155 p.

Reineck, H.E., 1963, Sedimentgefüge im Bereich der südlichen Nordsee: Abhandlungen der Senckenbergischen Naturforschenden Gesellschaft, v. 505, p. 1-138.

Ringrose, P.S., Sorbie, K.S., Corbett, P.W.M., and Jensen, J.L., 1993, Immiscible flow behaviour in laminated and crossbedded sandstones: Journal of Petroleum Science and Engineering, v. 9, p. 103-124.

Ringrose, P., Nordahl, K., and Wen, R., 2005, Vertical permeability estimation in heterolithic tidal deltaic sandstones: Petroleum Geoscience, v. 11, p. 29-36.

Renard, P., and de Marsily, G., 1997, Calculating equivalent permeability: A review: Advances in Water Resources, v. 20, p. 253-278.

Roberts, A.M., Price, J.D., and Olsen, T.S., 1990, Late Jurassic half-graben control on the siting and structure of hydrocarbon accumulations UK/Norwegian Central Graben: *in* Hardman, F.R.P., and Brooks, J., Tectonic Events Responsible for Britain's Oil and Gas Reserves. Geological Society, London, Special Publication, v. 55, p. 229-257.

Rockware ®, Inc., 2009, Surfer 9.0: Gridding and Contouring Software.

SBED Geomodeling., 2011, SBED upscaling algorithms: How does SBED upscale petrophysical properties?: Geomodeling Technology Corp., 23 p.

Seilacher, A., 1967, Bathymetry of trace fossils: Marine Geology, v. 5, p. 413-428.

Spaak, P., Almond, J., Salahudin, S., Mohd Salleh, Z., and Tosun, O., 1999, Fulmar: A mature field revisited: *in* Fleet, A.J., and Boldy, S.A.R., eds., Petroleum geology of Northwest Europe: Proceedings of the 4th Conference. Geological Society, London, p. 1098-1100.

Spencer, A.M., Home, P.C., and Wiik, V., 1986, Habitat of hydrocarbons in the Jurassic Ula Trend, Central Graben, Norway: *in* Spencer, A.M., ed., The Habitat of Hydrocarbons on the Norwegian Continental Shelf. Graham and Trotman, London, United Kingdom, p. 111-127.

Spila, M.V., Pemberton, S.G., Rostron, B., and Gingras, M.K., 2007, Biogenic textural heterogeneity, fluid flow and hydrocarbon production: Bioturbated facies Ben Nevis Formation, Hibernia field, offshore Newfoundland: *in* MacEachern, J.A., Bann, K.L., Gingras, M.K., and Pemberton, S.G., eds., Applied Ichnology. Society of Economic Paleontologists and Mineralogists (SEPM), Short Course Notes, no. 52, p. 363-380.

Taylor, A.M., and Goldring, R., 1993, Description and analysis of bioturbation and ichnofabric: Journal of the Geological Society, London, v. 150, p. 141-148.

Taylor, M.S.G., Leroy, A., and Forland, M., 1999, Hydrocarbon systems modelling of the Norwegian Central Graben fairway trend: *in* Fleet, A.J., and Boldy, S.A.R., eds., Petroleum geology of Northwest Europe: Proceedings of the 5th Conference. Geological Society, London, p. 1325-1338.

Taylor, T.R., Giles, M.R., Hathon, L., Diggs, T.N., Braunsdorf, N.R., Birbiglia, G.V., Kittridge, M.G., Macaulay, C.I., and Espejo, I.S., 2010, Sandstone diagenesis and reservoir quality prediction: Models, myths, and reality: American Association of Petroleum Geologists Bulletin, v. 94, p. 1093-1132.

Tonkin, N.S., McIlroy, D., Meyer, R., and Moore-Turpin, A., 2010, Bioturbation influence on reservoir quality: A case study from the Cretaceous Ben Nevis Formation, Jeanne d'Arc Basin, offshore Newfoundland, Canada. American Association of Petroleum Geologists Bulletin, v. 94, p. 1059-1078.

Vossler, S.M., and Pemberton, S.G., 1988, *Skolithos* in the Upper Cretaceous Cardium Formation: An ichnofossil example of opportunistic ecology: Lethaia, v. 21, p. 351-362.

Warren, J.E., and Price, H.S., 1961, Flow in heterogeneous porous media: Society of Petroleum Engineers Journal, v. 1, p. 153-169.

Weaver, P.P.E., and Schultheiss, P.J., 1983, Vertical open burrows in deep-sea sediments 2 m in length: Nature, v. 329, p. 329-331.

Weber, K.J., and van Geuns, L.C., 1990, Framework for constructing clastic reservoir simulation models: Journal of Petroleum Technology, v. 42, p. 1248-1253, 1296-1297.

Wen, R., Martinius, A.W., Næss, A., and Ringrose, P., 1998, Three-dimensional simulation of small-scale heterogeneity in tidal deposits- a process-based stochastic simulation method: *in* Buccianti A., Nardi G., Potenza R., eds., Proceedings of 4th Annual Conference of the International Association for Mathematical Geology, p. 129-134.

Zanella, E., and Coward, M.O., 2003, Structural Framework: *in* Evans, D., Graham, C., Armour, A., and Bathurst, P., eds., The Millennium Atlas: Petroleum Geology of the Central and Northern North Sea. Geological Society, London, United Kingdom, p. 45-59.

Ziegler, P.A., 1982, Geological Atlas of Western and Central Europe. Shell International Petroleum Maatschappij B.V., Amsterdam, 130 p.

CHAPTER 5: RESERVOIR CHARACTERIZATION OF BURROW-MOTTLED DOLOMITES: UPPER DEVONIAN WABAMUN GROUP, PINE CREEK GAS FIELD, CENTRAL ALBERTA, CANADA

5.1 INTRODUCTION

In carbonate depositional environments, organisms commonly alter the chemical and physical composition of the substrate through activities such as sediment compaction, sediment sorting, and by adding extracellular polysaccharides (i.e., EPS or mucous) to the sediment (Bromley, 1996; Gingras et al., 2007a; Petrash et al., 2011). A common by-product of bioturbation within carbonate settings, among many others, can include the precipitation of dolomite within and adjacent to the burrow itself (e.g., Brown and Farrow, 1978; Gunatilaka et al., 1987). In this context, burrow-associated dolomites have become an increasingly important topic as recent studies have demonstrated that dolomitized burrows can act as primary or secondary pathways for fluid movement within subsurface aquifers and reservoirs. Examples include the Upper Ordovician Yeoman Formation in Saskatchewan, Canada (Pak et al., 2001; Gingras et al., 2004a), Middle Mississippian Debolt Formation in Alberta, Canada (Packard et al., 2004; Chapters 2 and 6), and the Upper Jurassic Arab-D reservoir interval in Saudi Arabia (Pemberton and Gingras, 2005; Swart et al., 2005; Lindsay et al., 2006).

In their study of bioturbated carbonate sediments, Gingras et al. (2004a) examined the tortuosities and hydraulic interactions of bioturbated Tyndall Stone (Red River Formation, Western Canada) using dispersivity and spot-permeametry techniques. Based upon the distribution of permeable-burrow pathways and extensive interaction of fluid flow between the burrows and matrix, Gingras et al. (2004a) concluded that the Tyndall Stone contained both dual-permeability and dual-porosity fluid flow media.

Dual-permeability fabrics are defined as reservoirs wherein the contrast in permeability between the matrix and burrows is greater than three orders of magnitude (e.g., burrow permeability of 1000 mD and matrix permeability of 1 mD). In such systems, fluid flow occurs predominantly within the burrow fabrics and the low-permeability matrix interacts with the flow pathways through diffusion. Dual-porosity fabrics represent flow-media wherein the permeability contrast

---

* A version of this chapter has been accepted for publication in *Marine and Petroleum Geology* as "Reservoir Characterization of Burrow-Associated Dolomites in the Upper Devonian Wabamun Group, Pine Creek Gas Field, Central Alberta, Canada" by Greg M. Baniak, Murray K. Gingras, and S. George Pemberton.

between the burrows and matrix is within two orders of magnitude (e.g., burrow permeability of 10 mD and matrix permeability of 1 mD). Due to the similarity in permeabilities, fluid flow occurs in relatively equal proportions from the matrix and burrows (Gingras et al., 2007b, Gingras et al., 2012).

Building upon the different characteristics of bioturbated flow media presented in Gingras et al. (1999) and Gingras et al. (2004a), Pemberton and Gingras (2005) proposed a classification scheme for permeability distributions in bioturbated siliciclastics and carbonates. Within carbonates, diagenetic textural heterogeneities are the most commonly encountered type of biogenic permeability modification (e.g., Rameil, 2008; Corlett and Jones; Baniak et al., in press) (Fig. 5.1). Diagenetic textural heterogeneities therefore represent both dual-permeability and dual-porosity fabrics, as dolomitized burrows of varying permeabilities occur within a low-permeability lime-mud matrix.

The purpose of this chapter is to present the reservoir characteristics of dolomitized burrow fabrics within the Wabamun Group located in the Pine Creek gas field in central Alberta, Canada. Using conventional core analysis and petrographic thin sections as a foundation, the core samples are imaged using micro-CT and helical-CT to highlight the complexity in bioturbation in two- and three-dimensions (2D and 3D). Assessment of permeability contrasts between the dolomitized burrows and lime-mud matrix are made using spot-permeametry techniques. From these processed images and permeability measurements, quantification of fluid flow within bioturbated fabrics is completed using analytical and numerical modeling techniques.

5.2 STUDY AREA AND DEPOSITIONAL SETTING

The Pine Creek gas field is located from Townships 56-58 and Ranges 19-20 west of the fourth meridian in central Alberta, Canada (Fig. 5.2), roughly 110 km east of the Canadian Rocky Mountains. Natural gas production has exceeded 550 million cubic feet as of December 2012, with production occurring at depths greater than 3000 m. The composition of the natural gas is wet to dry with approximately 2 to 5% wet gas and around 30% hydrogen sulfide concentrations (Green and Mountjoy, 2005).

Occurring throughout the Western Canadian Sedimentary Basin, the Upper Devonian (Famennian) Wabamun Group is equivalent to the outcropping Palliser Formation and subsurface Three Forks Group in southern Saskatchewan and Manitoba (Fig. 5.3). Within central Alberta, the Wabamun Group is deposited

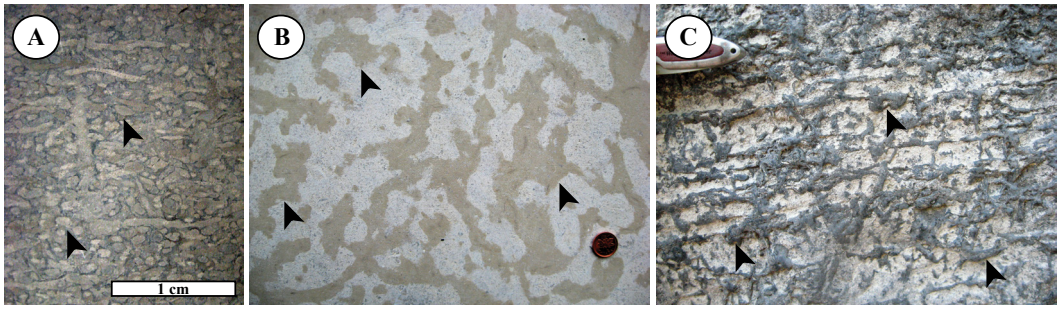

Figure 5.1: Examples of bioturbated carbonate rocks with diagenetic textural heterogeneities from the geologic rock record. **(A)** A highly bioturbated monospecific assemblage of dolomitized Planolites burrows (black arrows) from the Middle Mississippian Debolt Formation, Dunvegan gas field, north-western Alberta, Canada. Well 9-18-81-4W6M, depth 1412.15m. **(B)** A fossiliferous, cream-colored limestone with buff-colored dolomitic mottling (black arrows) from the Upper Ordovician Tyndall Stone. This photograph of Tyndall Stones comes from a university building located on the University of Alberta campus in Edmonton, Alberta, Canada. **(C)** Cross-sectional view of highly connected dolomitized burrow networks (black arrows) from the Palliser Formation, Jura Creek outcrop, south-western Alberta, Canada. Pocketknife used for scale.

conformably above the Winterburn Group (Graminia Formation) and is overlain unconformably by the Mississippian Exshaw Formation. Within the Pine Creek gas field, and surrounding areas, the Wabamun Group is commonly subdivided into five units (Halbertsma and Meijer-Drees, 1987; and Halbertsma, 1994). In order from oldest to youngest, the five units include Dixonville Unit, Whitelaw Unit, Normandville Unit, Cardinal Lake Unit, and the Big Valley Formation. Within the Pine Creek gas field, most of the natural gas production occurs from the Normandville Unit (Fong et al., 2001).

Bond and Kominz (1991) have suggested a pulse of intraplate stress in the cratonic margins and cratonic interiors of North America resulted in accelerated tectonic subsidence throughout the Upper Devonian in western Canada. Sedimentation within the Fammenian was controlled by eustatic sea level transgressions and tectonic subsidence (Halbertsma and Meijer-Drees, 1987). Within the Fammenian of western Alberta, two major transgressive episodes are recorded (Burrowes and Krause, 1987; Halbertsma and Meijer-Drees, 1987). The Dixonville Unit and Whitelaw Unit were deposited during the first major transgression, while the Normandville Unit reflected a near still-stand (Halbertsma and Meijer-Drees, 1987). During the second transgression, an accelerated rise in sea level resulted in an open marine depositional setting and fossiliferous limestones of the Cardinal Lake Units and Big Valley Formation were deposited across much of Alberta (Burrowes and Krause, 1987). A disconformity separates the Big Valley Formation from the Exshaw Formation (Richards and Higgins, 1988).

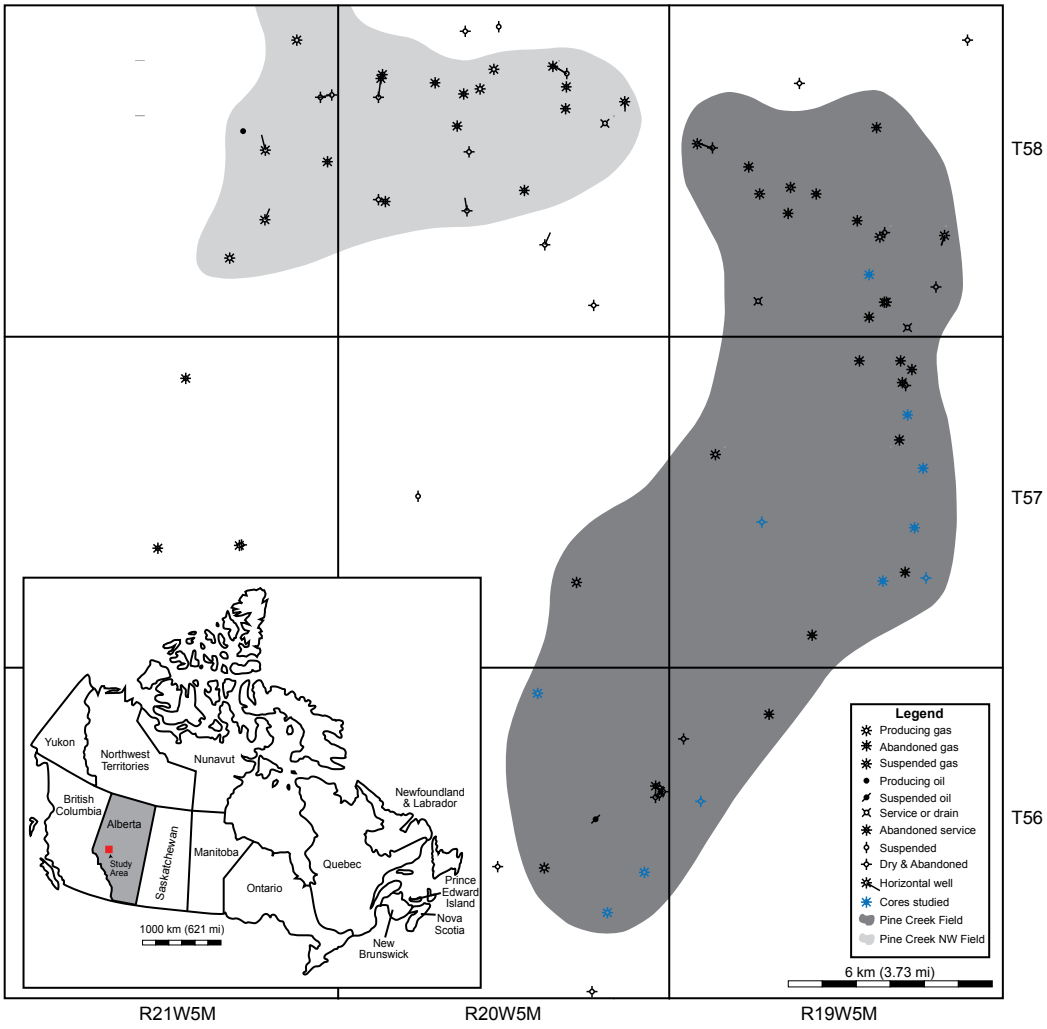

Figure 5.2: Location map of the Pine Creek gas field in central Alberta, Canada. The wells demarcated in blue represent wells with cored intervals in the Wabamun Group and that were evaluated in this study.

5.3 METHODS

Using slabbed core samples recovered from eleven subsurface wells in the Pine Creek gas field (Fig. 5.2), the sedimentological, ichnological, and petrophysical properties (i.e., porosity and permeability) of the bioturbated fabrics were assessed. The cores were evaluated to identify lithologies, primary and secondary physical structures, bioturbation, and mineralogical accessories. Characterization of the amount of burrow-associated dolomite was completed visually by looking at slabbed core samples. The percentage of burrow dolomite varies from absent (0% burrow dolomite) to thorough (80 to 100% burrow dolomite) within the core samples. Thin sections were also used to evaluate allochems (e.g., fossils, peloids) and diagenetic cements.

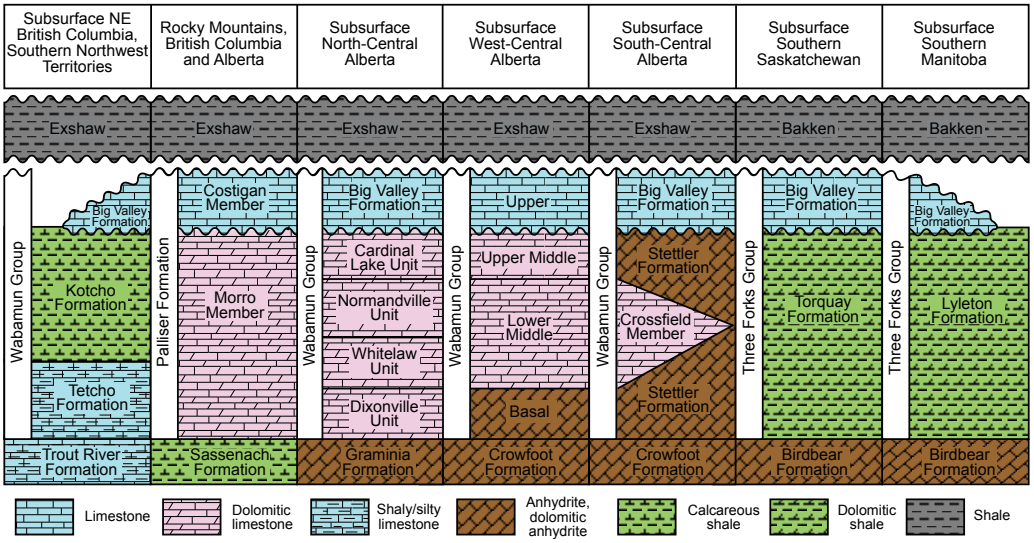

Figure 5.3: Upper Devonian (Famennian) stratigraphy of Western Canada. The Wabamun Group is equivalent to the Palliser Formation in the Canadian Rocky Mountains and the Three Forks Group in southern Saskatchewan and Manitoba. Figure modified from deWit and McLaren (1950), Andrichuck (1960), Halbertsma and Meijer Drees (1987), Halbertsma (1994), and Peterhänsel (2003).

Following core analysis, bioturbated core samples were selected for 2D and 3D imaging (micro-CT and helical-CT) and spot-permeametry analysis. Numerical flow simulations of dual-porosity and dual-permeability fabrics were then completed to better understand the properties of the burrow-associated flow media.

5.3.1 Two- and Three-Dimensional (2D and 3D) Sample Imaging

5.3.1.1 X-ray Computed Microtomography (micro-CT)

For micro-CT scanning, a SkyScan 1172 Desktop X-ray microtomograph was used (Fig. 5.4A). The core sample size used for imaging is approximately 2.5 cm in height and 1.0 cm in width. The X-ray point source was operated at 110 kV and 250 μA. Aluminum-copper and aluminum filters were applied, when necessary, to reduce beam hardening and allow for clearer images. The transmission X-ray images were acquired as the core sample on the stage rotated through 180^{o} at 0.5^{o} increments (Fig. 5.4B).

Upon generation, the 2D cross-sectional projections were opened using NRecon software (SkyScan, 2005). The NRecon software was used to reconstruct the images and correct for beam hardening, ring artifacts, and provide alignment optimization. The application of CT-Analyser software was used to open the reconstructed dataset of the 2D image projections (SkyScan, 2005). From these 2D image projections, a range of coefficients was selected to build 3D reconstructions of the sample.

5.3.1.2 Helical Computed Tomography (CT)

For helical CT scanning, an Aquilion 64-Slice Helical Scanner was used (Fig. 5.4C). The core sample size used is approximately 12 cm in height and 8 cm in width. Commonly used for medical and dental purposes (e.g., Silverman et al., 1995; Sebastià et al., 2001; Wang et al., 2012), the helical CT has been applied in recent years to new disciplines such as geology (e.g., Schreurs et al., 2003; Zhang et al., 2008). For this study, the helical CT was operated at point source of 110 kV and 250 μA. The core sample was scanned with a calibrated viewing point of 180 mm and matrix reconstructed viewing area of 512 x 512 pixels, resulting in an image resolution of 0.35 mm per voxel.

Unlike the micro-CT, which acquires individual 2-D slices of the sample as it rotates through 180^{o} on the rotary stage, the helical CT acquires a volume of data with the core sample in one position. Acquisition of complete core data images using the helical CT is due to slip-ring technology present within the helical CT scanner. Slip-ring technology is unique in that it allows for electrical power to be transferred from a stationary power source onto a continuously rotating gantry (Fig. 5.4D). As a result, during a helical scan the patient table moves through the gantry at a continuous and constant speed while the X-ray source performs a continuous rotating scan (Brink et al., 1994; Bushberg et al., 2002). Scanning of the core sample is therefore continuous and completed within minutes. Upon completion of scanning, the volume data was reconstructed using OsiriX software.

5.3.2 Permeability Measurements

A Core Laboratories PDPK 400 Pressure-Decay Profile Permeameter was used to measure permeabilities in the core samples (Fig. 5.4E). Using a 0.46 cm probe with a rubber tip, nitrogen gas (N_2) is injected through the probe into the rock sample and recorded as a function of time (Fig. 5.4F). The permeability of each measurement is recorded on a computer and has a measurement range from 0.001 millidarcy (mD) to greater than 30 darcy (Jones, 1994; Lemiski et al., 2011; Polo, 2013; La Croix et al., 2013). For each core sample, 0.5 x 0.5 cm grids were mapped to ensure the largest collection of permeability measurements were obtained within an area. Three permeability measurements were taken and averaged for each test location. Following the collection of permeability measurements, contour maps were generated to show the distribution of the permeability domains within the bioturbated intervals.

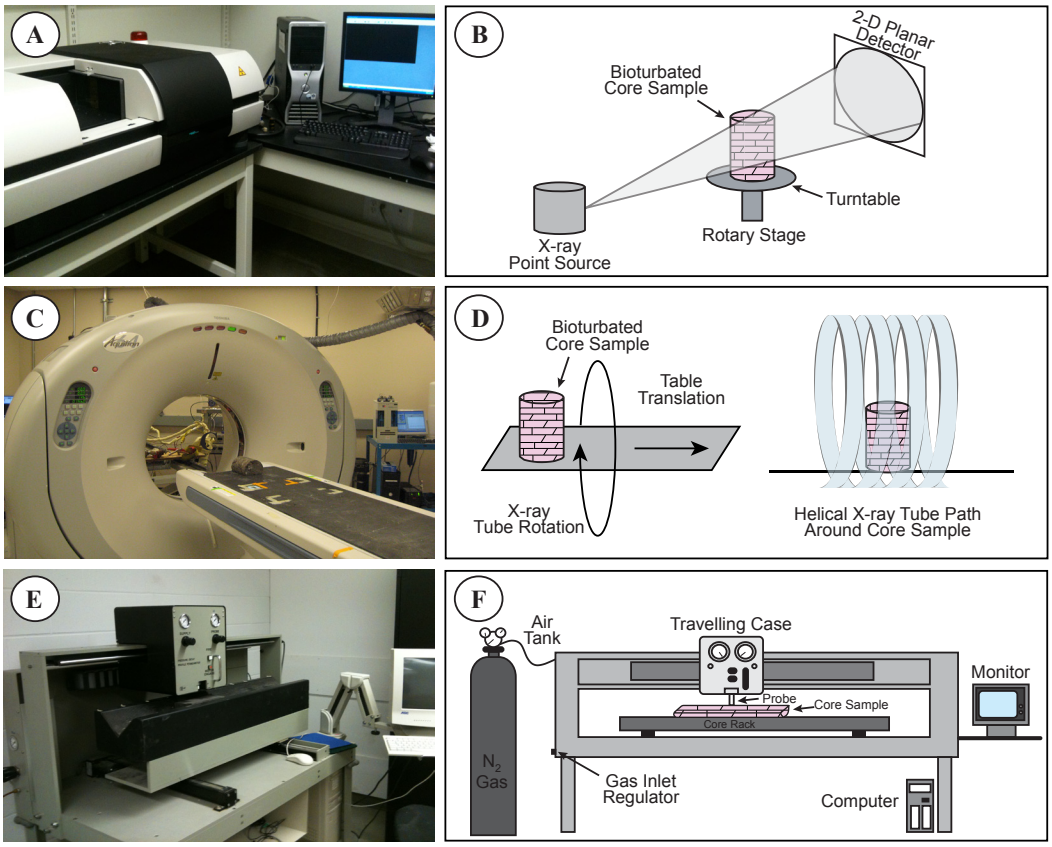

Figure 5.4: Equipment used to acquire images of the core samples and measure permeability. **(A)** SkyScan 1172 Desktop X-ray microtomograph. **(B)** The core sample rotates on a stage between a static X-ray source and a detector. The images of the sample are acquired as a series of 2D projections that are then processed on the computer using SkyScan software. **(C)** Aquilion 64-Slice Helical Scanner. **(D)** The X-ray tube rotates around the core sample as the core sample and table are moved through the gantry. As a result of these two simultaneous motions, the X-ray tube travels in a helical path around the core sample. Modified from Bushburg et al. (2002). **(E)** Core Laboratories PDPK 400 Pressure-Decay Profile Permeameter. **(F)** A core sample is placed onto the sliding core rack and a probe injects nitrogen gas into the core sample. Modified from Lemiski (2010).

5.3.3 Evaluation of Absolute Bulk Reservoir Permeability

5.3.3.1 Analytical Methods

Using spot-permeability measurements as a framework, the bulk permeability of the samples was estimated. Absolute bulk permeability of a sample represents the permeability of a homogeneous sample in which fluid flow is uniform (i.e., linear, steady-state) under the same pressure and boundary conditions (Pickup et al., 1995). Using arithmetic, harmonic, and geometric means, the average permeability of the interval that is equivalent to a homogenous system can be calculated (Muskat, 1937; Warren and Price, 1961; Bear, 1972; Freeze and Cherry, 1979; Weber and van Geuns, 1990). The arithmetic-average permeability (Eq. 1) is used to determine the average bulk permeability along continuous parallel permeability domains:

$$k_{arithmetic} = \sum_{i=1}^{n} \frac{k_i d_i}{d} \quad (1)$$

where k_i is the permeability of each layer, d_i is the individual layer thickness, and d the total thickness. The harmonic-average permeability (Eq. 2) estimates the average bulk permeability where fluid flow occurs perpendicular to permeability domains units:

$$k_{harmonic} = \frac{1}{\sum_{i=1}^{n} \frac{d_i}{k_i d}} \quad (2)$$

The final method is the geometric-average permeability (Eq. 3), which is representative of isotropic system wherein fluid flow occurs across and along permeability domains in a randomized nature:

$$\ln (k_{geometric}) = \sum_{i=1}^{n} \frac{\ln(k_i) d_i}{d} \quad (3)$$

These three equations for determining absolute bulk permeability are convenient for rock samples that are homogeneous in character. However, localized deviations in fluid flow and bulk permeability occur in samples comprised of heterogeneities such as lamination, clay drapes, cemented fractures, and cements (Weber, 1986). Within bioturbated rocks, permeability distributions are distorted and contain a combination of non-bioturbated and bioturbated fluid flow domains. As a result, graphs of permeability versus total volume of burrow dolomite in an idealized unit volume can be constructed to account for these fluid flow heterogeneities (e.g., La Croix et al., 2013).

These graphs are constrained by end-member spot-permeametry measurements wherein the arithmetic mean characterizes fully connected burrow networks and the harmonic mean characterizes isolated burrow flow pathways (Gingras et al., 1999). In this study, d_i/d represents the volume occupied by the burrow-associated dolomite in the sample. The highest permeability measurements within the bioturbated fabrics always occurred within the dolomitized burrows. These three highest burrow permeabilities within a sample were used to approximate the bulk permeability of a completely bioturbated sample (i.e., 100% burrow dolomite or $d_i/d = 1.0$). On the other hand, the three lowest matrix permeabilities were taken from each sample to approximate the bulk permeability of a non-bioturbated sample (i.e., 0% burrow dolomite or $d_i/d = 0.0$). Upon completion of these analytical graphs, a

comparison with computer generated numerical flow models (outlined below) is performed to determine which end-member permeability best characterizes fluid flow within the Pine Creek gas field.

5.3.3.2 Numerical Flow Modeling

Fluid flow within the bioturbated fabrics was modeled numerically using SBED Geomodeling software (Wen et al., 1998). For this study, two process-oriented model templates (dual-porosity and dual-permeability) were used. For simplicity, the permeabilities of the burrows and matrix for each model template were made to be uniform. Permeability values obtained from the spot-permeameter were used as a framework. As such, the massive limestone mud matrix was set to 0.01 mD for both models. The dual-porosity model uses a fixed burrow permeability of 10 mD (i.e., two orders of magnitude difference between burrow and matrix) and the dual-permeability model uses a burrow permeability of 100 mD (i.e., three orders of magnitude difference between burrow and matrix).

Thalassinoides burrows were populated within the dual-porosity and dual-permeability templates at six different volumes of burrow-associated dolomite (20%, 35%, 50%, 65%, 80%, and 100%) and were assigned variable dimensions and orientations. *Thalassinoides* burrows were used as their morphology and dimensions are most similar to those observed within the Wabamun Group. The *Thalassinoides* burrows were constructed with lengths ranging from 1-10 cm and diameters of 0.1-1.0 cm.

A 3-D grid was constructed with dimensions of 30 x 30 x 30 cm and discretized such that each grid cell size was 0.30 x 0.30 x 0.30 cm. Using a process-oriented modeling approach, SBED Geomodeling combines Gaussian simulation with a vector-based movement of geometric surfaces through space and time to generate a stochastic model (Wen et al., 1998). Within this study, absolute permeability is calculated using a flow-simulation-based numerical method (SBED Geomodeling, 2011). The flow-simulation-based numerical method is applied to permeability grids simulating single-phase fluid flow. Fixed (no-flow) boundary conditions were used such that fluid flows only across two end surfaces normal to pressure gradient and that no fluid flows across the other four end surfaces parallel to the pressure gradient (SBED Geomodeling, 2011). Using SBED single phase flow-based upscaling with fixed boundary conditions, the arithmetic-, harmonic-, and geometric-averaged permeabilities are calculated.

5.4 RESULTS

5.4.1 Reservoir Facies

The Wabamun Group, and outcropping equivalent Palliser Formation, form part of an extensive shallow-water Upper Devonian carbonate platform and ramp succession that stretches across Alberta and into the Canadian Rocky Mountains. Within the Pine Creek gas field, Fong et al. (2001) and Green and Mountjoy (2005) briefly identified bioturbated mudstones-wackestones and peloidal grainstones-packstones characteristic of a proximal carbonate ramp as the primary reservoir facies. In this study, the Wabamun Group reservoir facies are further subdivided into four main facies: bioturbated mudstones-wackestones (Facies 1); peloidal packstones-grainstones (Facies 2); fossiliferous, peloidal packstone-grainstones (Facies 3) and peloidal grainstones (Facies 4). In this context of this chapter, the bioturbated mudstones-wackestones (Facies 1) form the primary reservoir intervals in the Pine Creek gas field and therefore represents the primary focus. Descriptions for Facies 2, Facies 3, and Facies 4 are provided as supplementary information.

Facies 1 comprises bioturbated mudstones-wackestones. Sedimentary structures are rare as burrow-associated dolomite is ubiquitous within Facies 1, commonly occupying between 40 and 80% of the overall volume. Texturally, the burrow fabrics within this study are similar to other Wabamun and Palliser burrow fabrics observed in subsurface wells and outcrops across western Canada (Beales, 1953; Halbertsma, 1994; Fong et al., 2001; Gingras et al., 2002; Peterhänsel, 2003; Green and Mountjoy, 2005). The dolomitized burrows in Facies 1 represent a mixture of architectures that range from tubes several millimeters to centimeters in diameter to an interconnected, boxwork of burrows. Although difficult to discern, the burrows within Facies 1 are most comparable to examples of *Thalassinoides* and *Palaeophycus* based on morphology and orientation.

The dolomite-filled burrows and adjacent ‘diagenetic halos’ (Gingras et al., 2004b) are filled with early planar-euhedral dolomite crystals (Fig. 5.5A-B). Due to a lack of internal structures, distinguishing the actual burrow from the diagenetic halo in core samples or thin sections is challenging. In any event, a sharp contact commonly exists between the burrow-associated dolomite (i.e., actual dolomitized burrow and adjacent diagenetic halo) and surrounding non-dolomitized lime mud matrix (Fig. 5.5C). The matrix between the burrows is non-dolomitized and comprised of lime mudstone-wackestone that contains disarticulated and fragmented allochems. Although this study does not try to put forth a paragenetic model, work by other authors (e.g., Gingras et al., 2004b; Rameil, 2008; Corlett and

Jones, 2012; Baniak et al., in press) have suggested that burrow environments (e.g., microbial sulfate reduction), and associated permeability pathways, play important roles in burrow-fabric dolomitization. Deposition of Facies 1 within a low-energy subtidal to intertidal carbonate ramp setting is probable and is consistent with previous interpretations made by Enos (1983), Harris et al. (1985), and Gischler and Lomando (1999).

Facies 2 is characterized by peloidal packstones-grainstones. The peloids vary from micritic to containing some traces of skeletal (echinoderm fragments, bivalves, ostracodes) or detrital material. Facies 2 includes peloids and micritized grains of different sizes and shapes ranging from 25 to 500 μm in diameter, and exceptionally up to 1000 μm in diameter (Fig. 5.5D-F). Beales (1956) suggested that the occurrence of skeletal fragments within the grains suggests lithification and agglutination of grains may have been assisted by the presence of organic matter. The different peloidal shapes, combined with extensive micritization, indicate that they were micritized *in situ* or shortly after deposition (Al-Saad and Sadooni, 2001).

Facies 3 is composed of fossiliferous, peloidal packstone-grainstone. Allochems include ostracods, calcareous algae (calcispheres), echinoderms, and peloids (Fig. 5.5G-H). The peloids are moderate to well sorted, spherical to sub-spherical, and commonly 100 to 400 μm in diameter. Allochems such as ostracods and echinoderms occur as fragmented to occasionally intact specimens, suggesting low to moderate energy levels. The overall abundance of allochems, combined with a low to moderate diversity fauna suite, denotes deposition within a semi-restricted to open marine subtidal setting. Localized deposition within a restricted to semi-restricted subtidal environment, such as a lagoon, is probable due to the presence of calcispheres (Kaźmierczak, 1976; Flügel, 2010).

Facies 4 is characterized by peloidal grainstones. The preserved peloids are rounded to sub-rounded, moderate to high in sphericity, and generally smaller than 50 μm in diameter, (Fig. 5.5I). The characteristic roundness and lack of internal structure specify a fecal origin (Bathurst, 1975; Land and Moore, 1980; Flügel, 1982). The preservation of the peloidal grainstones indicates deposition within a shallow, low-energy, restricted marine environment, which would lead to rapid lithification and preservation of the peloids (Enos, 1983; Qing and Nimegeers, 2008).

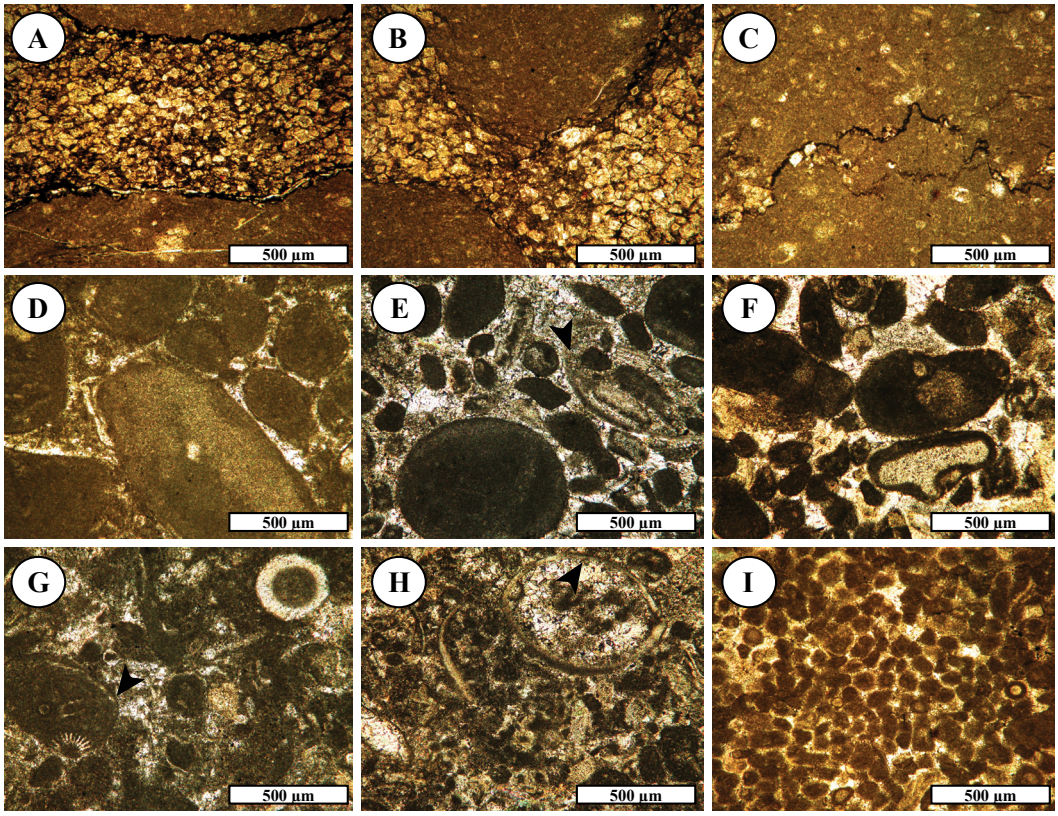

Figure 5.5: Thin section photomicrographs of the primary reservoir facies in the Pine Creek gas field. **(A-B)** Planar-euhedral dolomites infilling burrow networks in Facies 1. The contact between the dolomitized burrows and undolomitized lime mudstone-wackestone is sharp in both examples and is demarcated by low amplitude stylolites. Well 10-17-57-19W5M, depth 3208.48 m. **(C)** A undolomitized lime wackestone matrix in Facies 1 adjacent to dolomitized burrows (not shown). Porosity and permeability are typically very low within the lime wackestone matrix. Well 11-14-57-19W5M, depth 3079.52 m. **(D)** A moderate to well rounded peloidal packstone from Facies 2. The majority of grain sizes are larger than 100 µm and the bright areas represent unfilled pore spaces. Well 10-17-57-19W5M, depth 3223.96 m. **(E)** A peloidal packstone in Facies 2 with a rare ostracod shell fragment (black arrow). Majority of peloidal grain sizes are smaller than 100 µm and are moderately rounded. The massive peloids are well rounded. Most of the primary porosity is infilled with secondary calcite. Well 10-17-57-19W5M, depth 3223.96 m. **(F)** A moderate to well rounded peloidal packstone from Facies 2. The majority of the porosity has been infilled with calcite cement. Well 7-13-56-20W5M, depth 3485.19 m. **(G)** A highly fossiliferous, peloidal packstone in Facies 3 with poor to moderate intercrystalline porosity. Fossil fragments include calcareous algae (calcispheres) and echinoderms. The peloids are moderately rounded and contain traces of skeletal material (black arrow). Well 10-10-57-19W5M, depth 3182.58 m. **(H)** A fossiliferous, peloidal packstone from Facies 3. Most of the peloids are well rounded and smaller than 50 µm. An intact ostracod can be seen near the top (black arrow). Most of the porosity is infilled with secondary calcite. Well 10-17-57-19W5M, depth 3215.70 m. **(I)** A well rounded and well sorted peloidal grainstone from Facies 4 that has excellent porosity. Well 10-17-57-19W5M, depth 3195.40 m.

5.4.2 X-ray Computed Microtomography (micro-CT)

Volume rendered 2D and 3D images from micro-CT scanning is presented along with the corresponding core sample photograph for a core sample from Facies 1 (Fig. 5.6A). At 34 µm resolution, the 2D cross-sectional slices show the overall volumes of burrow dolomite and matrix calcite vary considerably at various levels throughout the scanned core sample (Fig. 5.6B). Corresponding 3D volumes exposed an interconnected network of dolomitized burrows, with the total volume of burrow-associated dolomite and burrow interconnectivity varying considerably throughout the sample. As a result, the micro-CT model appears to suggest that the localized distribution of higher permeabilities within the Wabamun Group is highly variable and commonly constrained to intervals of higher bioturbation intensities.

5.4.3 Helical Computer Tomography (CT)

Three-dimensional volumes of a bioturbated core sample from Facies 1 (Fig. 5.7A), scanned with the helical CT, are presented in Figures 5.7B-C. The 3D images show a complex distribution of burrow-associated dolomite throughout the core sample. When viewed perpendicular to the top of the core sample (Fig. 5.8A-C), 2D cross-sectional slices reveal a mixture of vertical and horizontally connected burrows of various dimensions and orientations. Likewise, 2D cross-sectional slices parallel to the top of the core sample (Fig. 5.9A-C) display an intricate

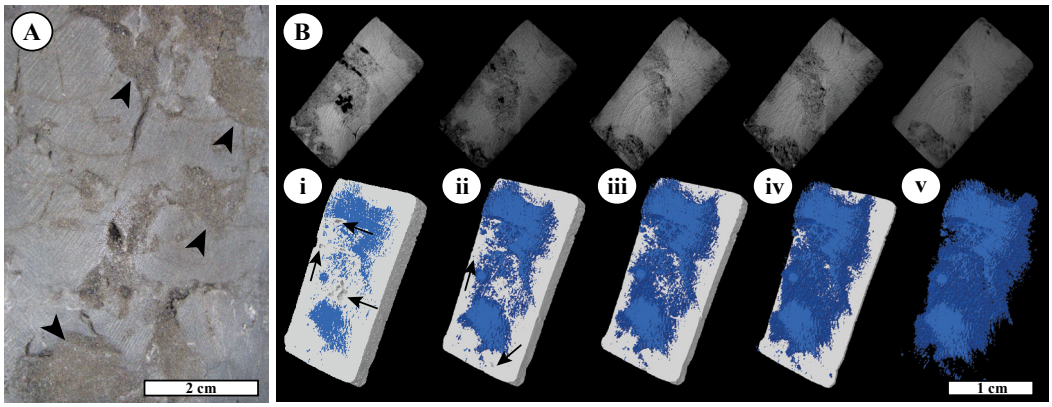

Figure 5.6: Wabamun core sample and associated micro-CT analysis for Facies 1. **(A)** Core sample with dolomite-filled trace fossils (light brown, black arrows) and non-dolomitized lime mudstone matrix (light grey). Well 10-10-57-19W5M, depth 3180.32m. **(B)** Example of five micro-CT scans (i to v) in 2D (above) and corresponding 3D images at 34 µm resolution (below). The 2D cross-sectional slices at the top (i to v) correspond with the 3D images (below). The core sample in Fig. 5.6A was scanned using an aluminum-copper filter. As a result, clearer definition of the dolomitic burrows (light grey), limestone matrix (dark grey), and porous vugs (black) in the 2D cross-sections can be made. On the bottom, the matrix (light grey) is removed from the 3D images starting from the left (i) and moving right (v). As the matrix is removed from the 3D image, increases in burrow (blue) density and burrow interconnectivity throughout the sample occur. The porous vugs in the matrix are represented as unfilled holes (black arrows).

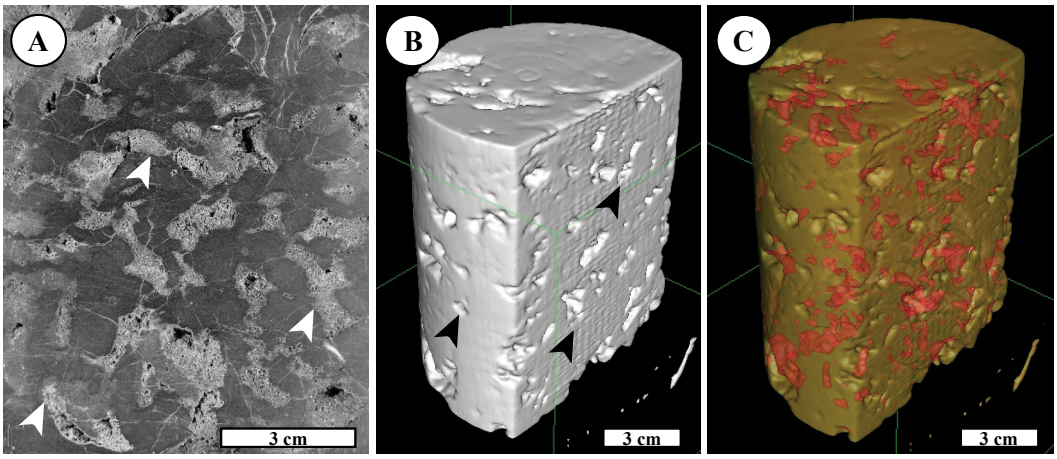

Figure 5.7: Wabamun core sample (Facies 1) and associated helical-CT analysis. **(A)** Core sample scanned with helical-CT. Well 11-26-57-19W5M, 3012.80m. The dolomitized burrows (white arrows; lighter colored rock) are present within a non-dolomitized lime mud matrix (darker, non-mottled rock). **(B)** 3D visualization of the core sample in Fig. 5.7A. The black arrows highlight macropores associated with burrow dolomitization. **(C)** 3D visualization of macropores associated with burrow dolomitization within the core sample. The burrow-associated dolomite is highlighted in red color and the lime mud matrix in lime green color.

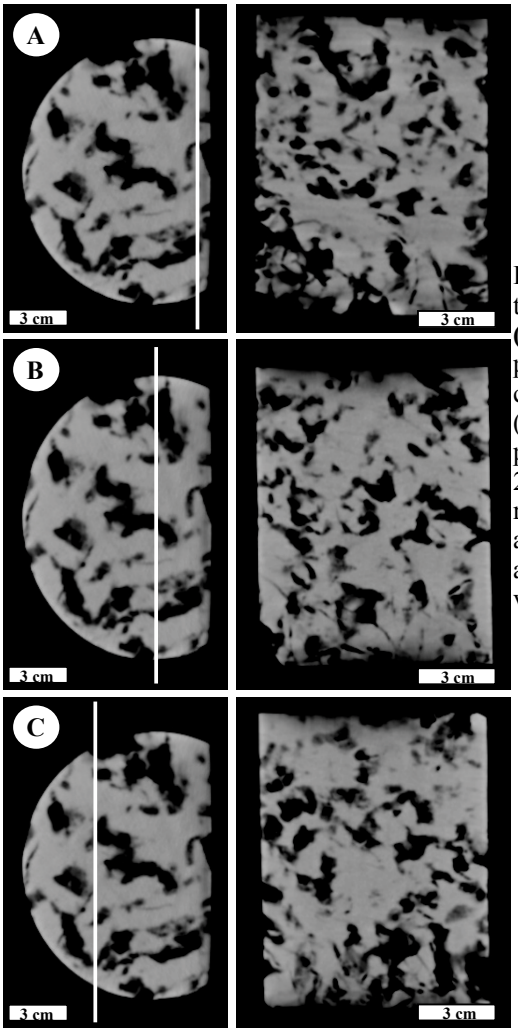

Figure 5.8: 2D helical-CT scans perpendicular to the top of the bioturbated core sample (Facies 1). **(A-C)** On the left hand side are three identical 2D photos (top of core) indicating where perpendicular cross-sectional slices were taken for 2D CT analysis (vertical white line). Using three successive perpendicular slices through the core sample, 2D images of the burrow dolomite (dark colored regions) and lime mud matrix (light grey color) are visualized (right hand side). The distribution and size of the burrow dolomite (horizontally and vertically) is heterogeneous and complex.

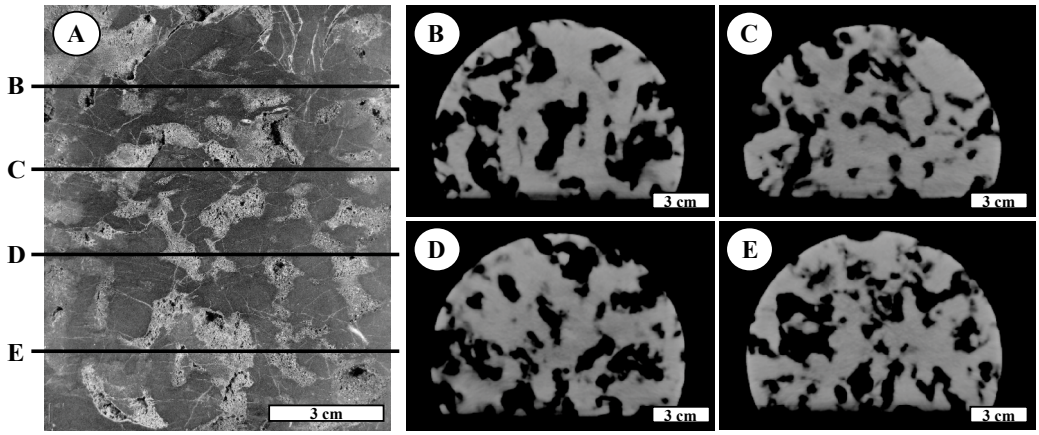

Figure 5.9: Bioturbated core sample (Facies 1) and associated 2D cross-sectional slices parallel to top of core using helical-CT. **(A)** Photograph of the slabbed core sample and the associated four areas (Fig. 5.9B-E) where parallel cross-sectional slices were taken for 2D CT analysis. **(B-E)** Four 2D cross-sectional slices from the core sample that demonstrate the chaotic and heterogeneous nature of the dolomitized burrows (dark colored regions).

distribution of burrow sizes and orientations. Within both the perpendicular and parallel views, horizontal and sub-vertical connectivity among the burrows is more common than the vertical connectivity. The helical CT images therefore demonstrate the complexity in bioturbation associated the Wabamun Group. As a result, the distribution of permeable conduits within the Wabamun Group is heterogeneous and challenging to evaluate based solely on core photographs and thin sections.

5.4.4 Permeability Estimation Using Spot-Permeametry Data

Photographs annotated with spot-permeability test locations and the corresponding permeability measurements for two core samples from Facies 1 are presented in Figures 5.10 and 5.11. Core sample 1 represents an example of a dual-porosity flow network. Core sample 2 represents an example of a dual-permeability flow network. Each figure includes a contoured plot, demonstrating the distribution of permeability within each sample, and histograms outlining the distribution of permeability within the burrows and matrix. Also included are graphs of overall burrow dolomite versus permeability for each core sample. The three curves presented in each plot indicate the harmonic, geometric, and arithmetic means of permeability, as calculated on the basis of relative proportions of fluid flow associated with the burrows and matrix, respectively.

5.4.4.1 Core Sample 1: 11-26-57-19W5M (3010.81 m)

Permeability measurements range from 0.04 mD (matrix) to 9.8 mD (burrows) and reflect a dual-porosity flow network (Fig. 5.10A). Sample 1 contains roughly

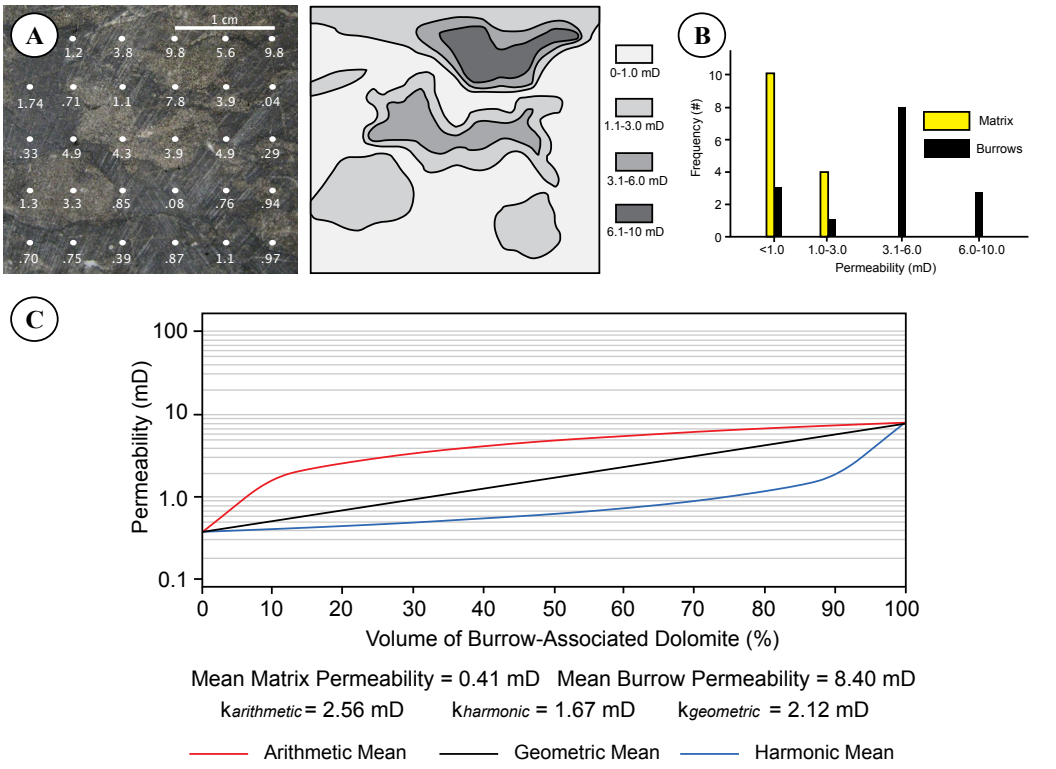

Figure 5.10: Spot-permeametry and associated bulk permeability analysis (geometric, arithmetic, and harmonic means) of a dual-porosity flow network. Core sample comes from Facies 1, Well 11-26-57-19W5M, depth 3010.81 m. **(A)** A moderately bioturbated (50% burrow-associated dolomite) lime mudstone-wackestone. Spot-permeameter measurements and a supplementary contour map show that the highest permeabilities occur within the dolomitized burrows. **(B)** Histogram of the spot-permeametry measurements. Majority of matrix permeabilities measurements occur below 1 mD while 80% of the burrow permeabilities occur between 1 and 10 mD. **(C)** Bulk reservoir permeability is best characterized by the geometric mean at 50% burrow dolomite.

50% burrow-associated dolomite and a lime mudstone-wackestone characterizes the surrounding matrix. The contour map shows the highest permeabilities being concentrated within the dolomitized burrows, with the burrows having a common permeability range of 1 to 10 mD (Fig. 5.10B).

The graph of permeability versus overall volume of burrow dolomite (Fig. 5.10C) indicates that the lower bounding permeability value (i.e., 0% burrow dolomite or 100% fluid flow through the matrix) is 0.41 mD. Conversely, the permeability associated with completely bioturbated sections of the sample (i.e., 100% burrow dolomite or 100% fluid flow through the burrows) is 8.40 mD. The reservoir permeability averaged by the harmonic mean is approximately 0.60 mD at 50% burrow dolomite and is within one order of magnitude to the 2.12 mD predicted by the harmonic mean for Sample 1. The geometric mean at 50% burrow dolomite is approximately 1.9 mD and is nearly equal to the 2.12 mD predicted by the geometric mean for sample 1. For the arithmetic mean, reservoir permeability is

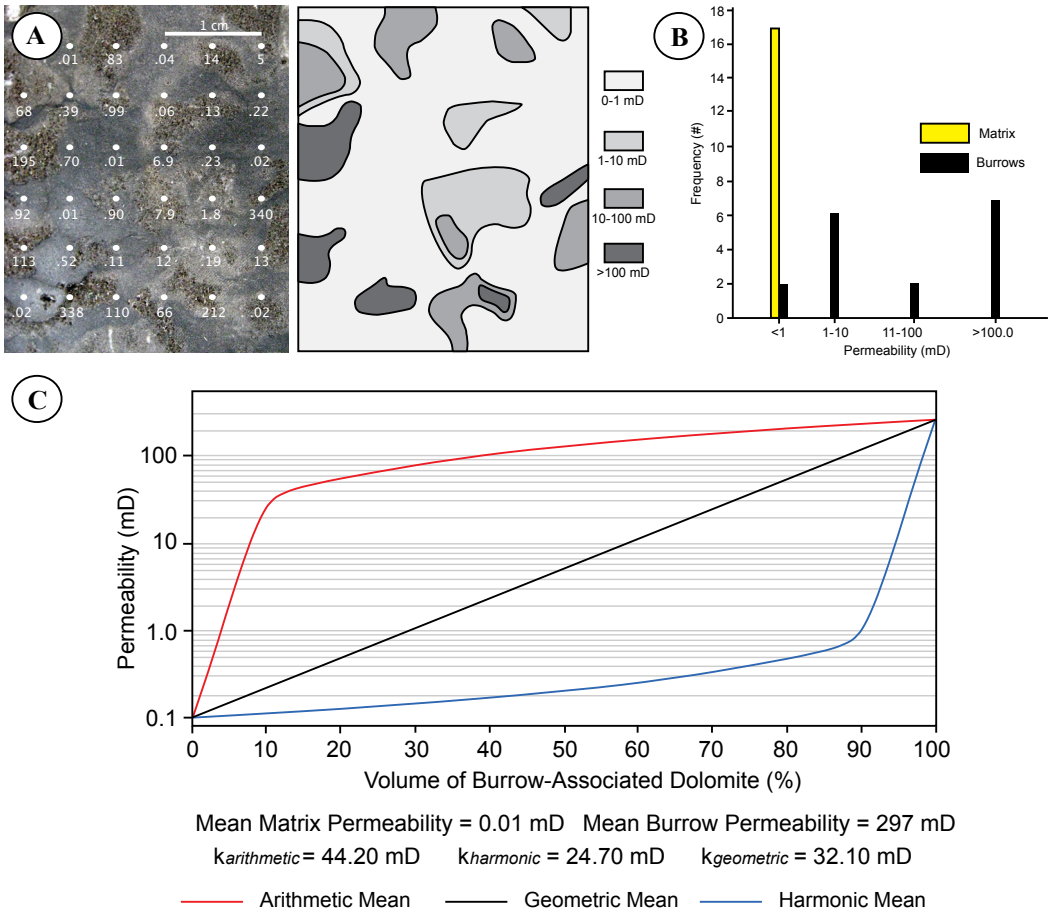

Figure 5.11: Spot-permeametry and associated bulk permeability analysis (geometric, arithmetic, and harmonic means) of a dual-permeability flow network. Core sample comes from Facies 1, Well 9-11-56-20W5M, depth 3450.95 m. **(A)** A moderately bioturbated (50% burrow-associated dolomite) lime mudstone-wackestone. Spot-permeameter measurements and a supplementary contour map show that the highest permeabilities occur within the dolomitized burrows, with extreme cases of super-permeability (i.e., > 100 mD) occurring locally. **(B)** Histogram of the spot-permeametry measurements. All of the matrix permeabilities measurements occur below 1 mD while almost 90% of the burrow permeabilities occur above 10 mD. **(C)** At 50% burrow dolomite and above, bulk reservoir permeability is best approximated using the arithmetic mean.

approximately 2.5 mD at 50% burrow dolomite and is within one order of magnitude to the 5.0 mD predicted by the arithmetic mean for Sample 1.

5.4.4.2 Core Sample 2: 9-11-56-20W5M (3450.95 m)

In Core Sample 2, permeability measurements range from 0.01 mD (matrix) to 338 mD (burrows) (Fig. 5.11A). Comparable to Sample 1, the volume of burrow-associated dolomite in Sample 2 is also moderate (50%) and the matrix is also characterized by a lime mudstone-wackestone. A significant portion of Sample 2 exhibits permeabilities ranging between 0.01 and 10 mD (Fig. 5.11B). As a whole, the entire matrix is characterized by permeabilities less than 1 mD while the dolomitized burrows generally have permeabilities greater than 1 mD. As a result,

these regions of the sample are reflective of a dual-porosity flow network. On the other hand, localized, highly permeable units greater than 100 mD are concentrated within the dolomitized burrows and are reflective of a dual-permeability flow network (Fig. 5.11A-B).

Permeability values obtained from sample 2 indicate the matrix-associated permeability (i.e., 0% burrow dolomite) is 0.01 mD. The upper limit of permeability associated with the dolomitized burrows is 297 mD. The reservoir permeability averaged by the arithmetic mean at 50% burrow dolomite is approximately 100 mD and is within one order of magnitude to the 44.20 mD predicted by the arithmetic mean for Sample 1 (Fig. 5.11C). The geometric mean at 50% burrow dolomite is approximately 5.0 mD and is also within one order of magnitude to the 24.70 mD predicted by the geometric mean for sample 1. The reservoir permeability averaged by the harmonic mean at 50% burrow dolomite is approximately 0.02 mD and is quite different to the 24.70 mD predicted by the harmonic mean for Sample 2.

5.4.5 Permeability Estimation using Numerical Fluid Flow Simulation

Single-phase fluid flow was simulated in two different flow media models: dual-porosity and dual-permeability. *Thalassinoides* burrows of various dimensions and sizes were populated at six different volumes (20%, 35%, 50%, 65%, 80%, and 100%) for each model and SBED numerical modeling recorded the arithmetic-, harmonic-, and geometric-averaged permeabilities along with the bulk vertical and horizontal permeabilities.

5.4.5.1 Dual-Porosity Numerical Model

Computer simulations indicate that extreme levels of bioturbation are needed to increase the harmonic permeability within the massive mudstone (Fig. 5.12A). The harmonic permeability (0.10 mD) is therefore nearly equivalent to the matrix permeability at low levels of bioturbation (10 to 25% burrow dolomite). Consequently, the bulk horizontal and vertical permeabilities typically fall between the harmonic and geometric means between 20 and 35% bioturbation (Fig. 5.12A). In models with 50% bioturbation, the bulk horizontal (1.65 mD) and vertical permeabilities (1.90 mD) transition and occur between the arithmetic and geometric means. At moderate to high levels of bioturbation (65 to 80% burrow dolomite), increased abundances of burrow networks result in the bulk horizontal and vertical permeabilities being best approximated using the arithmetic mean.

5.4.5.2 Dual-Permeability Numerical Model

Within the dual-permeability model, considerable permeability contrasts exists between the *Thalassinoides burrows* and surrounding low-permeability muds (Fig. 5.13A-C). Within the numerical model, the bulk horizontal and vertical permeabilities are best approximated using the geometric mean at moderate to low levels of bioturbation (10 to 50% burrow dolomite) (Fig. 5.12B). At higher levels of bioturbation (50 to 80%), the massive mudstone becomes overprinted with higher permeability *Thalassinoides* burrows. As a result, the arithmetic mean increases considerably and reaches up to 98.6 mD at 80% burrow dolomite (Fig. 5.12B). Consequently, the bulk horizontal and vertical permeabilities are best approximated using the arithmetic mean at moderate to high bioturbation intensities.

5.5 DISCUSSION

Thin section analysis, permeability measurements, and sample imaging have shown that the most permeable and porous units within the Pine Creek gas field are associated with dolomitized burrows (Facies 1). These dolomitized burrows can be modeled to allow for a more detailed evaluation of permeability trends and resource and reservoir quality within the Pine Creek gas field.

5.5.1 Assessment of Bulk Reservoir Permeability

The character of the burrow-associated dolomite has an important effect on bulk permeability, with micro-CT and helical-CT imaging indicating that the dimensions and orientations of the burrows are spatially complex. Similar textural fabric complexities have been observed by Gingras et al. (2002) in samples from the Wabamun Group outcrop equivalent Palliser Formation using MRI (magnetic resonance imaging) and SPRITE (single-point ramped imaging with T_1 enhancement) imaging techniques. Within this chapter, imaging methods indicate that the burrows are moderately to well connected in the horizontal plane in scenarios where total bioturbation ranges from 30 to 80%. On the other hand, vertical interconnectivity among the burrow dolomites is typically restricted to intervals associated with extreme bioturbation (70 to 100% burrow dolomite).

Analytical graphs of burrow-associated dolomite versus permeability show the range of possible solutions of bulk permeability in dual-porosity (Fig. 5.10C) and dual-permeability media (Fig. 5.11C). Numerical flow simulations for dual-porosity systems show that bulk permeability is best estimated using the arithmetic mean at high to extreme volumes of burrow dolomite (65 to 80%). Conversely,

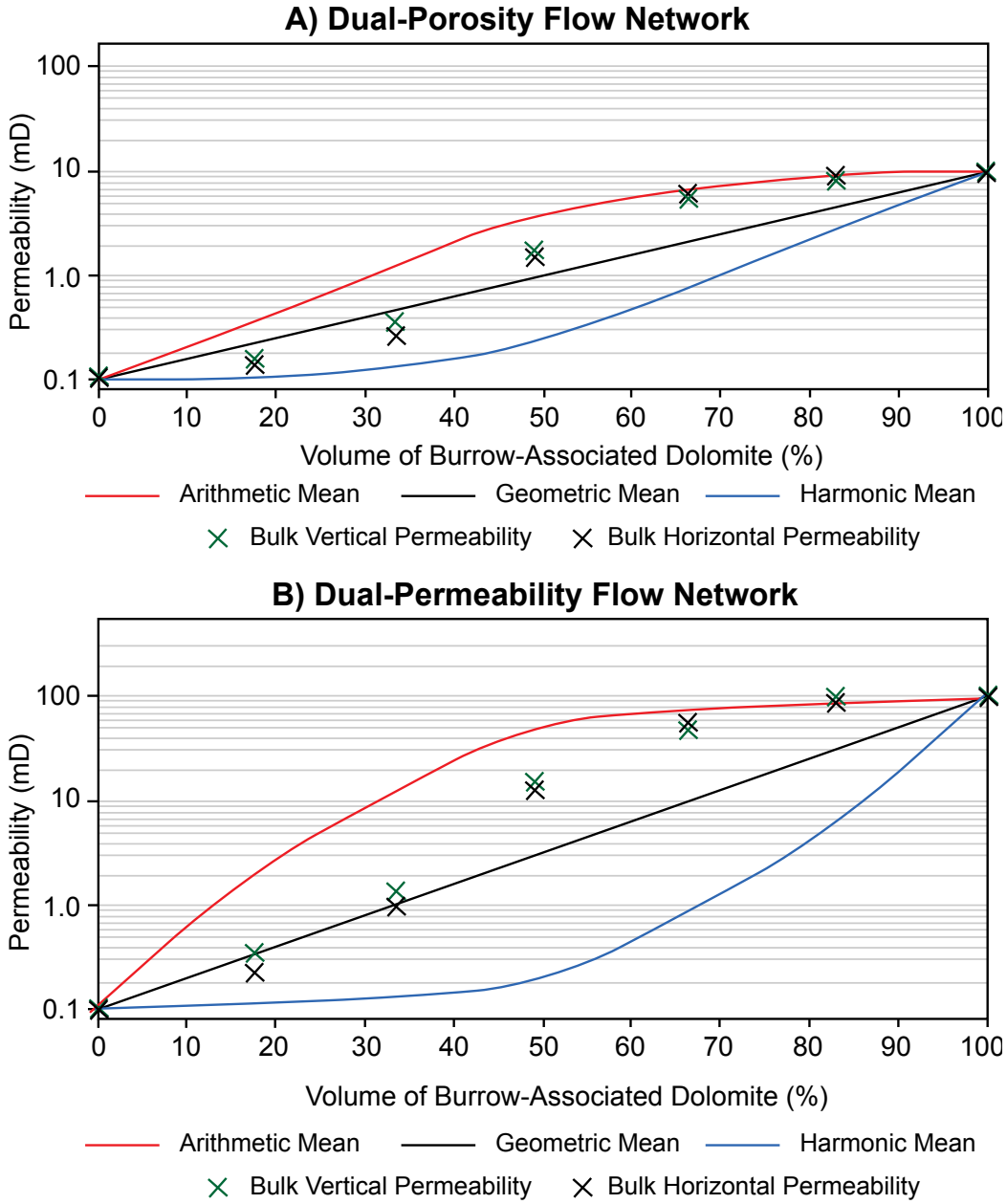

Figure 5.12: Numerical fluid flow simulations of the geometric, arithmetic, and harmonic means along with the bulk horizontal and vertical permeabilities in dual-porosity and dual-permeability carbonate flow networks. **(A)** At 10 to 25% burrow dolomite, the bulk horizontal and vertical permeabilities are best characterized by the harmonic mean in dual-porosity systems. At 25 to 65% burrow dolomite, the bulk horizontal and vertical permeabilities are best approximated using the geometric mean. At 65 to 80% burrow dolomite, the bulk horizontal and vertical permeabilities are best approximated using the arithmetic mean. **(B)** Within dual-permeability systems, bulk horizontal and vertical permeabilities are best approximated using the geometric mean between 10 and 50% burrow dolomite. At 50 to 80% burrow dolomite, the bulk horizontal and vertical permeabilities are best approximated using the arithmetic mean.

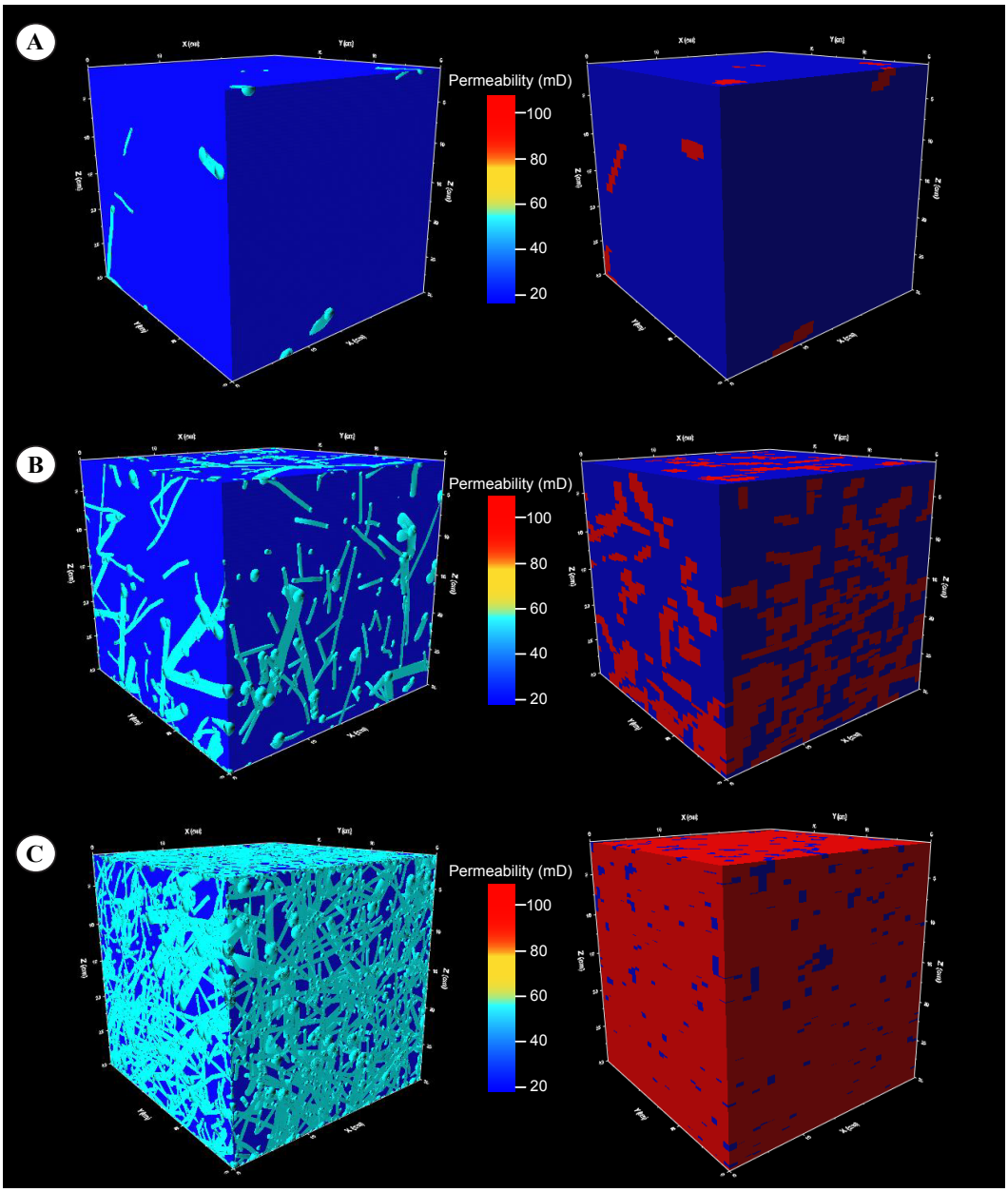

Figure 5.13: Computer modeling of dual-permeability flow media. On the left are examples of massive mudstones with different volumes and dimensions of *Thalassinoides* populated within the model. On the right are the 3D spatial distributions of permeabilities for the three volumes shown on the left. **(A)** Low bioturbation intensities (20% bioturbation). **(B)** Moderate bioturbation intensities (50% bioturbation). **(C)** High bioturbation intensities (80% bioturbation).

bulk permeability is best estimated using the harmonic mean at low volumes of burrow dolomite (10 to 25%) and geometric mean at low to moderate volumes of burrow dolomite (25 to 65%) (Fig. 5.12A). In dual-permeability systems, similar relationships are observable (Fig. 5.12B) as bulk permeability is best estimated using the arithmetic mean at moderate to high volumes of burrow dolomite (50 to 80%) and the geometric means at low to moderate volumes of burrow dolomite (10 to 50%).

The slight difference in arithmetic-, harmonic-, and geometric-averaged permeabilities for dual-porosity and dual-permeability numerical flow models can be attributed to a difference in permeabilities between the burrows and matrix. Within dual-porosity systems, higher volumes of burrow dolomite are required increase the overall bulk permeability of the sample due to the similarities in permeabilities between the matrix and burrows. As a result, the geometric mean best characterizes bulk reservoir permeability within dual-porosity systems exhibiting low to moderate levels of bioturbation (25 to 65% burrow dolomite). This relationship was also seen in Core Sample 1 (Fig. 5.10A-C), where the bulk reservoir permeability was best approximated using the geometric mean at 50% burrow dolomite. On the other hand, extreme contrasts in permeabilities occur between the burrows and matrix in dual-permeability models. As a result, the geometric mean best characterizes bulk reservoir permeability up to 50% burrow dolomite. After this point, the arithmetic mean begins to best characterize bulk reservoir permeability within dual-permeability systems. This relationship is also observable in Core Sample 2 (Fig. 5.11A-C), where bulk reservoir permeability transitions from being best approximated using the geometric mean to the arithmetic mean at around 50% burrow dolomite.

5.5.2 Characterization of Permeability Trends

Within the lime mudstone-wackestone matrix in Facies 1, permeabilities between 0.01 and 0.1 mD are common and thereby make it a tight gas reservoir (Holditch, 2006; Smith et al., 2009). In this context, significant volumes of natural gas that are stored within the matrix are commonly produced through the fabric-selective burrow dolomite due to its high permeabilities. As a result, Ichnofossil Hosted Tight Gas (IHG) is a new term proposed in this chapter to demarcate tight gas reservoirs wherein natural gas is produced predominately from the low permeability matrix via burrow networks.

Using subsurface well 9-11-56-20W5 from the Pine Creek gas field as an

example, IHG intervals can exceed 10 m in thickness and provide excellent, if subtle, drilling targets (Fig. 5.14A-B). Importantly, porosity is generally higher in the described IHG successions and is easily recognizable on geophysical well-logs (e.g., sonic and density) (Fig. 5.14C). The dolomitized burrow fabrics will therefore provide the primary flow pathways.

Because of the spatial complexity associated with bioturbation and permeability distribution within IHG reservoirs, production decline is interpreted to be high and chaotic as the burrows become drained of natural gas (Fig. 5.14D). This chaotic production decline is best explained by comparing the exchange of natural gas between the dolomitized burrows and lime mudstone matrix. Within their study of the Tyndall Stone, Gingras et al. (2004a) noted that natural gas moves rather freely throughout the burrow networks and only slowly into and out of the low-permeability matrix. This relationship is likely in part due to the fact that the frictional resistance to fluid flow within the dolomitized burrows is less than that of the surrounding limestone matrix.

Once the majority of primary natural gas has been produced from the burrows (i.e., natural gas originally stored within the burrows and not the matrix), it is likely that movement of natural gas from the matrix into the burrows will occur at a much slower rate. Production decline will likely therefore occur at a more predictable rate within an IRG interval, thereby allowing for many decades of continuous production from a single well. Similar production trends are observable across the Pine Creek gas field where production is interpreted to occur primarily from IHG intervals (Fig. 5.15A-C).

5.5.3 Conceptual Framework for IHG Reservoirs

In IHG reservoirs with low volumes of burrow-associated dolomite (Fig. 5.16A), natural gas will most likely diffuse slowly from the matrix into the isolated burrow dolomites. However, the overall majority of the natural gas will remain stored within the matrix regardless of burrow permeability. This is because under normal conditions (i.e., no secondary fracturing), the matrix permeability is too low to permit economic production rates. In intervals of higher volumes of burrow-associated dolomite, bulk reservoir permeability is enhanced (Fig. 5.16B-C). Under such scenarios, the burrows increase the overall amount of flow media present without fracturing and provide additional new flow paths through burrow interpenetration (Gingras et al., 1999; La Croix et al., 2012). With an increase in burrow-associated dolomites, interpenetrations of vertical and horizontal burrow

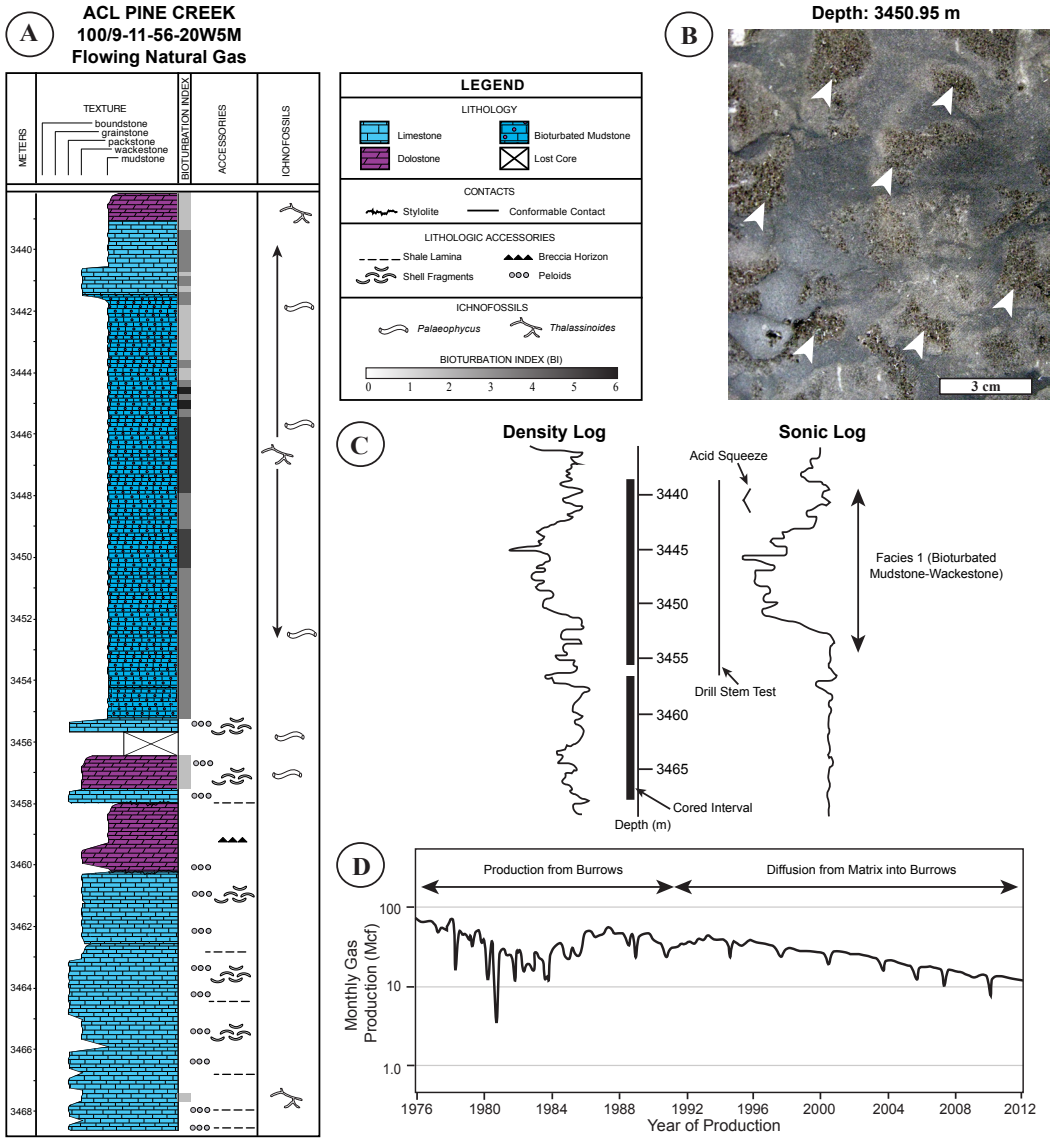

Figure 5.14: Example of an IHG reservoir in Facies 1 with accompanying geophysical well-logs and production history. **(A)** Litholog of Well 9-11-56-20W5M. Within the cored interval, a 12 m IHG zone occurs and is interpreted as the primary drilling target. **(B)** Example of a reservoir rock from the IHG interval. White arrows denote the dolomitized burrows. **(C)** Geophysical well-logs through the cored interval. Within both the density and sonic logs, large increases in porosity are observable in the IHG interval. Note the perforation and drill-stem tests occur preferentially within the IHG interval. **(D)** Production history of Well 9-11-56-20W5M. Production of natural gas from the burrows is interpreted to have high decline rates. Upon depletion from the burrows, movement of natural gas from the matrix into the burrows is believed to occur at a much slower rate.

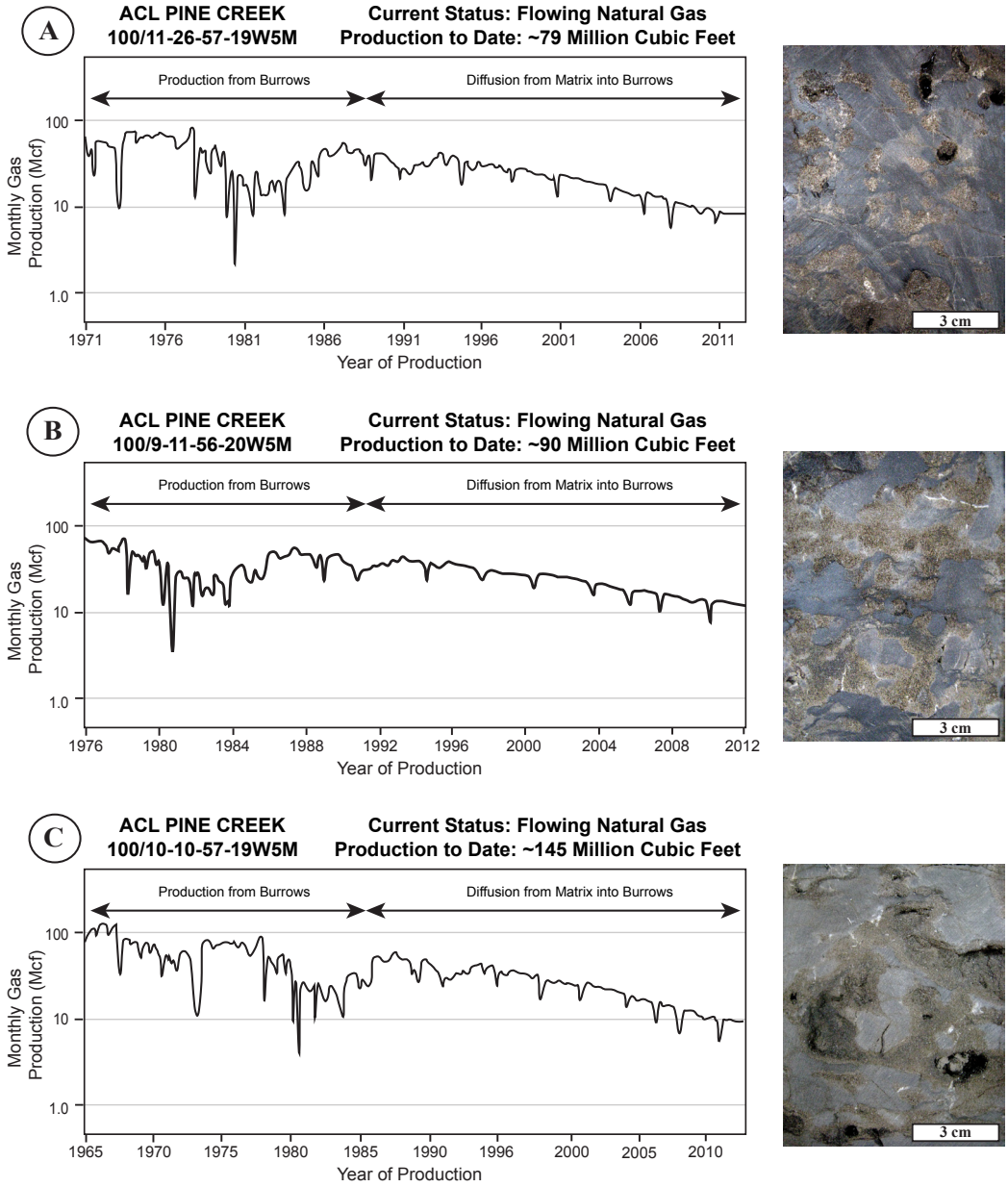

Figure 5.15: Production histories, and associated examples of reservoir rocks, for wells in the Pine Creek gas field wherein natural gas production is interpreted to occur predominately from IHG intervals. **(A-C)** Within most IHG reservoirs, production from bioturbated intervals is interpreted to result in high decline rates and fluctuating spikes in production. When movement of natural gas from the matrix into the burrows occurs, it is interpreted that a more constant and slower decline in production will occur.

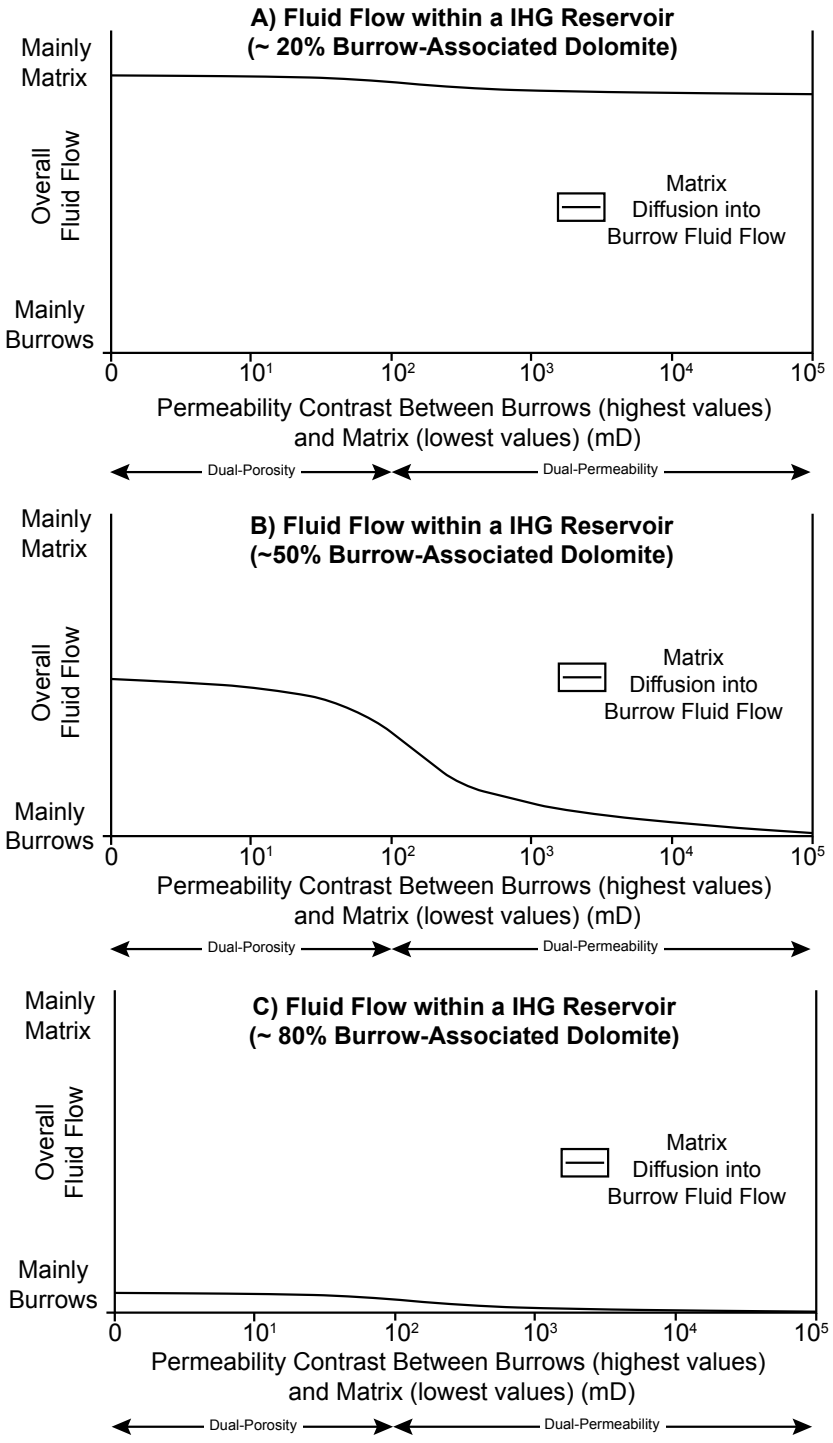

Figure 5.16: Conceptual fluid flow production from an IHG reservoir at three different volumes of burrow-associated dolomite. **(A)** At volumes of 20% burrow dolomite, the burrows are unconnected and occur sporadically within the reservoir. As a result, the majority of the natural gas remains stored within the low-permeability matrix in both dual-porosity and dual-permeability reservoirs. **(B)** At volumes of 50% burrow dolomite, the dolomitized burrows are moderately to well connected. In both dual-porosity and dual-permeability reservoirs, the burrows will act as the primary fluid pathways and natural gas will move slowly from the matrix into the burrows. **(C)** At volumes of 80% burrow dolomite, the dolomitized burrows are fully connected. As a result, production occurs predominately from the burrows and contribution from the matrix is negligible.

networks occur and ultimately help transmit fluids from the lower permeability matrix (Weaver and Schultheiss, 1983; Gingras et al., 1999; La Croix et al., 2012). Reservoir permeability enhancement and vertical transmissivity of natural gas is therefore centralized within the bioturbated intervals (Gingras et al., 1999; Gingras et al., 2007b; Gingras et al., 2012). As such, these dolomitized burrows have the ability to make IHG reservoirs more accessible through the creation of permeable pathways within the lower-permeability matrix.

5.6 CONCLUSIONS

Bioturbated reservoir facies from the Wabamun Group in the Pine Creek gas field of central Alberta, Canada were analyzed to assess the effects of fabric-selective burrow dolomite on permeability distribution and reservoir quality. Within the bioturbated reservoir fabrics (Facies 1), burrow dolomites exhibit permeabilities (1 to 350 mD) that range between two and four orders of magnitude greater than the surrounding non-bioturbated lime mudstone-wackestone matrix (commonly less than 1 mD). Due to the moderate to extreme contrasts in permeabilities between the burrows and matrix, the burrows are interpreted to act as the primary flow pathways within the Pine Creek gas field. Ichnofossil Hosted Tight Gas (IHG) is a new term introduced to demarcate similar reservoir intervals within the geological rock record.

Numerical modeling and spot-permeametry analysis revealed that the dominant influences on fluid flow and bulk permeability are burrow connectivity, burrow and matrix permeability, and total burrow volume. Imaging techniques (micro-CT and helical-CT) revealed that the burrow orientations and dimensions are highly complex spatially. As a whole, horizontal connectivity among burrows was more common than vertical connectivity. Fluid flow within the burrow fabrics is therefore dominantly anisotropic and commonly confined to a bedding-parallel flow direction. In this context, the geometric mean is found to best represent dual-porosity systems at moderate volumes of burrow dolomite (25 to 65%) and dual-permeability systems at low to moderate volumes of burrow dolomite (10 to 50%). On the other hand, the arithmetic mean is found to best represent dual-porosity systems at high volumes of burrow dolomite (65 to 80%) and dual-permeability systems at moderate to high volumes of burrow dolomite (50 to 80%). To this end, we assert that IHG reservoirs contain great potential and provide new resource opportunities within not only the Pine Creek gas field, but globally as well.

5.7 REFERENCES CITED

Al-Saad, H., and Sadooni, F.N., 2001, A new depositional model and sequence stratigraphic interpretation for the upper Jurassic Arab "D" reservoir in Qatar: Journal of Petroleum Geology, v. 24, p. 243-264.

Andrichuck, J.M., 1960, Facies analysis of upper Devonian Wabamun Group in west-central Alberta, Canada: American Association of Petroleum Geologists Bulletin, v. 44, p. 1651-1681.

Beales, F.W., 1953, Dolomitic mottling in Palliser (Devonian) Limestone, Banff and Jasper National Parks, Alberta: American Association of Petroleum Geologists Bulletin, v. 37, p. 2281-2293.

Beales, F.W., 1956, Conditions of deposition of Palliser (Devonian) limestone of southwestern Alberta: American Association of Petroleum Geologists Bulletin, v. 40, p. 848-870.

Bear, J., 1972, Dynamics of Fluids in Porous Media. Elsevier, New York, New York, 746 p.

Bond, G.C., and Kominz, M.A., 1991, Disentangling Middle Paleozoic sea level and tectonic events in cratonic margins and cratonic basins of North America: Journal of Geophysical Research, v. 96, p. 6619-6639.

Brink, J.A., Heiken, J.P., Wang, G., McEnery, K.W., Schlueter, F.J., and Vannier, M.W., 1994, Helical CT: Principles and technical considerations: RadioGraphics, v. 14, p. 887-893.

Bromley, R.G., 1996, Trace Fossils: Biology, Taphonomy and Applications, Second Edition. Chapman and Hall, London, United Kingdom, 361 p.

Brown, B.J., and Farrow, G.E., 1978, Recent dolomite concretions of crustacean burrow origin from Loch Sunart, west coast of Scotland: Journal of Sedimentary Petrology, v. 48, p. 825-834.

Burrowes, O.G., and Krause, F.F., 1987, Overview of the Devonian system: Subsurface western Canada basin: *in* Krause, F.F., and Burrowes, O.G., eds., Devonian Lithofacies and Reservoir Styles in Alberta, Second International Symposium on the Devonian System, Core Conference Guide. Canadian Society of Petroleum Geologists, Calgary, Alberta, p. 1-20.

Bushberg, J.T., Seibert, J.A., Leidholdt, E.M. Jr., and Boone, J.M., 2002, The Essential Physics of Medical Scanning, Second Edition. Lippincott, Williams and Wilkins, Baltimore, Maryland, 933 p.

Corlett, H.J., and Jones, B., 2012, Petrographic and geochemical contrasts between calcite- and dolomite-filled burrows in the Middle Devonian Lonely Bay Formation, Northwest Territories, Canada: Implications for dolomite formation in Paleozoic burrows: Journal of Sedimentary Research, v. 82, p. 648-663.

de Wit, R., and McLaren, D.J., 1950, Devonian sections in the Rocky Mountains between Crowsnest Pass and Jasper, Alberta: Geological Survey of Canada, Paper 50-23, 66 p.

Enos, P., 1983, Shelf environment: *in* Scholle, P.A., Bebout, D.G., and Moore, C.H., eds., Carbonate Depositional Environments. American Association of Petroleum Geologists, Memoir no. 33, p. 267-295.

Flügel, E., 1982, Microfacies Analysis of Limestones. Springer-Verlag, Berlin, 633 p.

Flügel, E., 2010, Microfacies of Carbonate Rocks: Analysis, Interpretation and Application, Second Edition. Springer-Verlag, Berlin, 976 p.

Fong, G., Hunter, I.G., and Bloy, G.R., 2001, Burrow-mottled carbonates in the Devonian Wabamun Formation, Pine Creek gas field, Alberta, Canada. Canadian Society of Petroleum Geologists, Conference Abstracts. Available at http://www.cspg.org/documents/Conventions/Archives/Annual/2001/C-142.pdf (Accessed on July 17, 2013).

Freeze, R.A., and Cherry, J.A., 1979, Groundwater. Prentice-Hall, New Jersey, 604 p.

Gingras, M.K., Pemberton, S.G., Mendoza, C.A., and Henk, F., 1999, Assessing the anisotropic permeability of *Glossifungites* surfaces: Petroleum Geoscience, v. 5, p. 349-357.

Gingras, M.K., MacMillan, B., and Balcom, B.J., 2002, Visualizing the internal physical characteristics of carbonate sediments with magnetic resonance imaging and petrography: Bulletin of Canadian Petroleum Geology, v. 50, p. 363-369.

Gingras, M.K., Mendoza, C.A., and Pemberton, S.G., 2004a, Fossilized worm burrows influence the resource quality of porous media: American Association of Petroleum Geologists Bulletin, v. 88, p. 875-883.

Gingras, M.K., Pemberton, S.G., Muelenbachs, K., and Machel, H., 2004b, Conceptual models for burrow-related, selective dolomitization with textural and isotopic evidence from the Tyndall Stone, Canada: Geobiology, v. 2, p. 21-30.

Gingras, M.K., Bann, K.L., MacEachern, J.A., Waldron, J., and Pemberton, S.G., 2007a, A conceptual framework for the application of trace fossils: *in* MacEachern, J.A., Bann, K.L., Gingras, M.K., and Pemberton, S.G., eds., Applied Ichnology. Society of Economic Paleontologists and Mineralogists (SEPM), Short Course Notes, no. 52, p. 1-26.

Gingras, M.K., Pemberton, S.G., Henk, F., MacEachern, J.A., Mendoza, C.A., Rostron, B., O'Hare, R., and Spila, M.V., 2007b, Applications of ichnology to fluid and gas production in hydrocarbon reservoirs: *in* MacEachern, J.A., Bann, K.L., Gingras, M.K., and Pemberton, S.G., eds., Applied Ichnology. Society of Economic Paleontologists and Mineralogists (SEPM), Short Course Notes, no. 52, p. 129-143.

Gingras, M.K., Baniak, G., Konhauser, K.O., La Croix, A., Lemiski, R., Mendoza, C., Pemberton, S.G., Polo, C., and Zonneveld, J.-P., 2012, Porosity and permeability in bioturbated sediments: *in* Knaust, D., and Bromley, R.G., eds., Trace Fossils as Indicators of Sedimentary Environments. Developments in Sedimentology 64, Elsevier, Amsterdam, p. 837-868.

Gischler, E., and Lomando, A.J., 1999, Recent sedimentary facies of isolated carbonate platforms, Belize-Yucatan system, Central America: Journal of Sedimentary Research, v. 69, p. 747-763.

Green, D.G., and Mountjoy, E.W., 2005. Fault and conduit controlled burial dolomitization of the Devonian west-central Alberta Deep Basin: Bulletin of Canadian Petroleum Geology, v. 53, p. 101-129.

Gunatilaka, A., Al-Zamel, A., Shearman, D.J., and Reda, A., 1987, A spherulitic fabric in selectively dolomitized siliciclastic crustacean burrows, northern Kuwait: Journal of Sedimentary Petrology, v. 57, p. 922-927.

Halbertsma, H.L., 1994, Devonian Wabamun Group of the Western Canada Sedimentary Basin: *in* Mossop, G.D., and Shetsen, I., eds., Atlas of the Western Canada Sedimentary Basin. Canadian Society of Petroleum Geologists and Alberta Research Council, p. 203-220.

Halbertsma, H.L., and Meijer Drees, N.C., 1987, Wabamun limestone sequences in north-central Alberta: *in* Krause, F.F., and Burrowes, O.G., eds., Devonian Lithofacies and Reservoir Styles in Alberta, Second International Symposium on the Devonian System, Core Conference Guide. Canadian Society of Petroleum Geologists, Calgary, Alberta, p. 21-37.

Harris, P.M., Moore, C.H., and Wilson, J.L., 1985, Carbonate depositional environments. Modern and ancient. Part 2: Carbonate platforms: Colorado School of Mines Quarterly, v. 80, p. 1-60.

Holditch, S., 2006, Tight gas sands: Journal of Petroleum Technology, v. 58, p. 86-90.

Jones, S.C., 1994, A new, fast, accurate pressure-decay probe permeameter: Society of Petroleum Engineers Journal, v. 9, p. 193-199.

Kaźmierczak, J., 1976, Volvocacean nature of some Palaeozoic non-radiosphaerid calcispheres and parathuramminid "foraminifera": Acta Palaeontologica Polonica, v. 21, p. 245-258.

La Croix, A.D., Gingras, M.K., Dashtgard, S.E., and Pemberton, S.G., 2012, Computer modeling bioturbation: the creation of porous and permeable fluid-flow pathways: American Association of Petroleum Geologists Bulletin, v. 96, p. 545-556.

La Croix, A.D., Gingras, M.K., Pemberton, S.G., Mendoza, C.A., MacEachern, J.A., and Lemiski, R.T., 2013, Biogenically enhanced reservoir properties in the Medicine Hat Gas Field, Alberta, Canada: : Marine and Petroleum Geology, v. 43, p. 464-477.

Lemiski, R.T., 2010, Sedimentology, ichnology, and resource characteristics of the low-permeability Alderson Member, Hatton Gas Pool, Southwest Saskatchewan, Canada: University of Alberta M.Sc. Thesis, Unpublished, 131 p.

Lemiski, R.T., Hovikoski, J., Pemberton, S.G., and Gingras, M.K., 2011, Sedimentological, ichnological and reservoir characteristics of the low-permeability, gas-charged Alderson Member (Hatton gas field, southwest Saskatchewan): Implications for resource development: Bulletin of Canadian Petroleum Geology, v. 59, p. 1-28.

Lindsay, R.F., Cantrell, D.L., Hughes, G.W., Keith, T.H., Mueller III, H.W., and Russell, S.D., 2006, Ghawar Arab-D reservoir: Widespread porosity in shoaling-upward carbonate cycles, Saudi Arabia: *in* Harris, P.M., and Weber, L.J., eds., Giant Hydrocarbon Reservoirs of the World: From Rocks to Reservoir Characterization and Modeling. American Association of Petroleum Geologists, Memoir no. 88, Society of Economic Paleontologists and Mineralogists (SEPM) Special Publication, p. 97-147.

Muskat, M., 1937, The Flow of Homogeneous Fluids Through Porous Media. McGraw-Hill, New York, New York, 763 p.

Pak, R., Pemberton, S.G., and Gingras, M.K., 2011, Reservoir characterization of burrow-mottled carbonates: The Yeoman Formation of southern Saskatchewan-preliminary report: Summary of Investigations, Geological Survey, Saskatchewan Energy and Mines, Misc. Report 1, p. 10-13.

Peterhänsel, A., 2003, Depositional dynamics of a giant carbonate platform- the Famennian Palliser Formation of western Canada: University of Saskatchewan PhD Thesis, Unpublished, 220 p.

Petrash, D.A., Lalonde, S.V., Gingras, M.K., and Konhauser, K.O., 2011, A surrogate approach to studying the chemical reactivity of burrow mucous linings in marine sediments: Palaios, v. 26, p. 594-600.

Pickup, G.E., Ringrose, P.S., Corbett, P.W.M., Jensen, J.L., and Sorbie, K.S., 1995, Geology, geometry and effective flow: Petroleum Geoscience, v. 1, p. 37-42.

Polo, C., 2013, Bioturbation and resource quality: a case study of the Upper Cretaceous Lysing and Nise Formations, Ellida and Midnatsoll fields area, Norwegian Sea: University of Alberta M.Sc. Thesis, Unpublished, 155 p.

Qing, H., and Nimegeers, A.R., 2008, Lithofacies and depositional history of Midale carbonate-evaporite cycles in a Mississippian ramp setting, Steelman-Bienfait area, southeastern Saskatchewan, Canada: Bulletin of Canadian Petroleum Geology, v. 56, p. 209-234.

Rameil, N., 2008, Early diagenetic dolomitization and dedolomitization of Late Jurassic and earliest Cretaceous platform carbonates: A case study from the Jura Mountains (NW Switzerland, E France): Sedimentary Geology, v. 212, p. 70-85.

Richards B.C., and Higgins, A.C., 1988, Devonian-Carboniferous Boundary Beds of the Palliser and Exshaw Formations at Jura Creek, Rocky Mountains, Southwestern Alberta: *in* McMillan, N.J., Embry, A.F., and Glass, D.J., eds., Devonian of the World: Proceedings of the 2nd International Symposium on the Devonian System, Volume II. Canadian Society of Petroleum Geologists, Memoir no. 14, p. 319-412.

Sebastià, C., Quiroga, S., Boyé, R., Cantarell, C., Fernandez-Planas, M., and Alvarez, A., 2011, Helical CT in renal transplantation: Normal findings and early and late complications: RadioGraphics, v. 21, p. 1103-1117.

Schreurs, G., Hänni, R., Panien, M., and Vock, P., 2003, Analysis of analogue models by helical X-ray computed tomography: Geological Society, London, Special Publication, v. 215, p. 213-223.

Silverman, P.M., Cooper, C.J., Weltman, D.I., and Zeman, R.K., 1995, Helical CT: practical considerations and potential pitfalls: RadioGraphics, v. 15, p. 25-36.

SkyScan., 2005, SkyScan 1172 desktop x-ray microtomograph instruction manual, 53 p.

Swart, P.K., Cantrell, D.L., Westphal, H., Handford, C.R., and Kendall, C.G., 2005, Origin of Dolomite in the Arab-D Reservoir from the Ghawar Field, Saudi Arabia: Evidence from petrographic and geochemical constraints: Journal of Sedimentary Research, v. 75, p. 476-491.

Wang, G., Li, J., Khadka, A., Hsu, Y., Li, W., and Hu, J., 2012, CAD/CAM and rapid prototyped titanium for reconstruction of ramus defect and condylar fracture caused by mandibular reduction: Oral Surgery, Oral Medicine, Oral Pathology and Oral Radiology, v. 113, p. 356-361.

Warren, J.E., and Price, H.S., 1961, Flow in heterogeneous porous media: Society of Petroleum Engineers Journal, v. 1, p. 153-169.

Weaver, P.P.E., and Schultheiss, P.J., 1983, Vertical open burrows in deep-sea sediments 2 m in length: Nature, v. 329, p. 329-331.

Weber, K.J., 1986, How heterogeneity affects oil recovery: *in* Lake, L.W., and Carroll, Jr., H.B., eds., Reservoir Characterization. Academic Press, New York, New York, p. 487-544.

Weber, K.J., and van Geuns, L.C., 1990, Framework for constructing clastic reservoir simulation models: Journal of Petroleum Technology, v. 42, p. 1248-1253, 1296-1297.

Wen, R., Martinius, A.W., Næss, A., and Ringrose, P., 1998, Three-dimensional simulation of small-scale heterogeneity in tidal deposits- a process-based stochastic simulation method: *in* Buccianti A., Nardi G., Potenza R., eds., Proceedings of 4th Annual Conference of the International Association for Mathematical Geology, p. 129-134.

Zhang, J., Yingfeng, M., Gao, L., Yongjie, L., and Congwu, Y., 2008, Observing core fissures with multiple helical CT technology: Fault-Block Oil and Gas Field, v. 3, p. 52-54.

CHAPTER 6: SABKHA AND BURROW-MEDIATED DOLOMITIZATION: MISSISSIPPIAN DEBOLT FORMATION, NORTHWESTERN ALBERTA, CANADA*

6.1 INTRODUCTION

The study of dolomite has a long and extensive history, dating back to the pioneering work of Giovanni Arduino and Déodat Gratet de Dolomieu in the 18th century. Despite being an abundant mineral in the rock record, dolomite distribution is limited in modern sedimentary environments. Kinetic energy barriers such as high hydration energies of the magnesium ion (Mg^{2+})(Markham et al., 2002), low concentration and activities of the carbonate ion (CO_3^{2-}), and the presence of sulfate ions (Morrow, 1982; Budd, 1997) are all major inhibiting factors in abiotic dolomite precipitation. Despite this knowledge, replicating dolomite precipitation under modern physico-chemical conditions in the laboratory has proven futile (McKenzie, 1991; Land, 1998). The formation of dolomite and the nature of the dolomitizing fluids remains controversial and is widely referred to as the 'dolomite problem' (Gunatilaka, 1987; Arvidson and Mackenzie, 1999; Machel, 2004). Classic models such as evaporative pumping, hydrothermal circulation, seepage reflux, sabkha, seawater convection, burial diagenesis, and subsurface mixing have been invoked to explain dolomitization within the rock record (Hsü and Siegenthaler, 1969; Morrow, 1982; Machel and Mountjoy, 1986; Warren, 2000; Machel, 2004).

In this context, burrow-associated diagenesis has recently emerged as another model for shallow-burial dolomitization. This is due to textural and compositional heterogeneities (e.g., concentration of extracellular polysaccharides in burrow walls and contrasts in permeability) associated with biogenic sedimentary structures (Gingras et al., 2004; Rameil, 2008; Corlett and Jones, 2012). Although occurrences of dolomitized burrows within the rock record are very common (see Table 6.1), the timing and cause of dolomitization associated with the burrows can be difficult to determine.

Within modern environments, microbial sulfate reduction (MSR) plays an integral role in the precipitation of dolomite at near-surface temperatures (Vasconcelos et al., 1995; Warthmann et al. 2000; van Lith et al., 2003; Krause et al., 2012). Examples include the hypersaline lagoons of Lagoa Vermelha and

* A version of this chapter has been accepted for publication in *Ichnos* as "Sabkha and Burrow-Mediated Dolomitization in the Mississippian Debolt Formation, Northwestern Alberta, Canada" by Greg M. Baniak, Larry Amskold, Kurt O. Konhauser, Karlis Muehlenbachs, S. George Pemberton, and Murray K. Gingras.

Brejo do Espinho, northeastern coast of Brazil (Vasconcelos et al., 1995, 2005; Vasconcelos and Mackenzie, 1997; Warthmann et al. 2005) and the ephemeral lakes of the Coorong Region of South Australia (Wright and Wacey, 2005; Wacey et al., 2007). Such studies are invaluable as they help outline the manner in which microbes influence the physiochemical parameters that can help mediate early dolomitization within modern sediments.

The focus of this chapter is the Mississippian (Visean) Debolt Formation located in the Dunvegan gas field of northwestern Alberta (Fig. 6.1). Located at depths greater than 1400 m, the Dunvegan gas field has in place reserves of 3.4 x 10^{10} m^3 to 4.5 x 10^{10} m^3 (1.2 to 1.6 trillion cubic feet) (Al-Aasm and Packard, 2000; Packard et al., 2004). These reserves make the Dunvegan gas field the second largest carbonate-hosted non-reefal gas field in the Western Canadian Sedimentary Basin (Al-Aasm and Packard, 2000). Reservoir production occurs primarily from highly porous microsucrosic dolomites occurring within the bioturbated fabrics (Packard et al., 2004). The preferred dolomitization of the burrow fabrics suggests

Formation/Interval	Age	Location	Description	Reference
Irene Bay and Thumb Mountain Formation	Upper Ordovician	Nunavut, Canada	*Palaeophycus*? *Thalassinoides*?	Morrow, 1978
Red River and Yeoman Formation	Upper Ordovician	Manitoba/ Saskatchewan, Canada	*Chondrites* *Palaeophycus* *Thalassinoides*	Kendall, 1977a Pak and Pemberton, 2003 Gingras et al., 2004
Steamboat Point Member (Bighorn Dolomite)	Upper Ordovician	Wyoming, United States	*Thalassinoides*	Zenger, 1992 Zenger, 1996 Holland and Patzkowsky, 2009
Børglum River Formation	Upper Ordovician	Northern Greenland	*Thalassinoides*	Jin et al., 2008 Jin et al., 2012
Elk Point Formation	Middle Devonian	Manitoba, Canada	*Palaeophycus*? *Thalassinoides*?	Chow and Longstaffe, 1995
Lonely Bay Formation	Middle Devonian	Northwest Territories, Canada	*Palaeophycus*? *Thalassinoides*?	Corlett and Jones, 2012
Palliser Formation/ Wabamun Group	Upper Devonian	Alberta, Canada	*Chondrites* *Palaeophycus* *Thalassinoides*	Beales, 1953 Peterhänsel, 2003 Baniak (Chapter 5)
Debolt Formation	Middle Mississippian	Alberta, Canada	*Chondrites* *Planolites* *Quebecichnus*	Packard et al., 2004 Baniak (Chapter 2)
Midale Formation	Middle Mississippian	Saskatchewan, Canada	*Chondrites* *Planolites* *Zoophycos*	Keswani, 1999 Nimegeers and Qing, 2002
Arab-D Reservoir (Ghawar Field)	Upper Jurassic	Eastern Saudi Arabia	*Glossifungities* (*Thalassinoides*)	Pemberton and Gingras, 2005 Swart et al., 2005 Lindsay et al., 2006
Jura Mountains	Upper Jurassic/ Lower Cretaceous	NW Switzerland/ Eastern France	*Palaeophycus*? *Thalassinoides*?	Rameil, 2008
Na'ur Formation/ Fuheis Formation	Upper Cretaceous	Western Jordan	*Thalassinoides*	Abed and Schneider, 1980

Table 6.1: Selected examples of dolomitized burrows, along with their age and location, in the geological rock record.

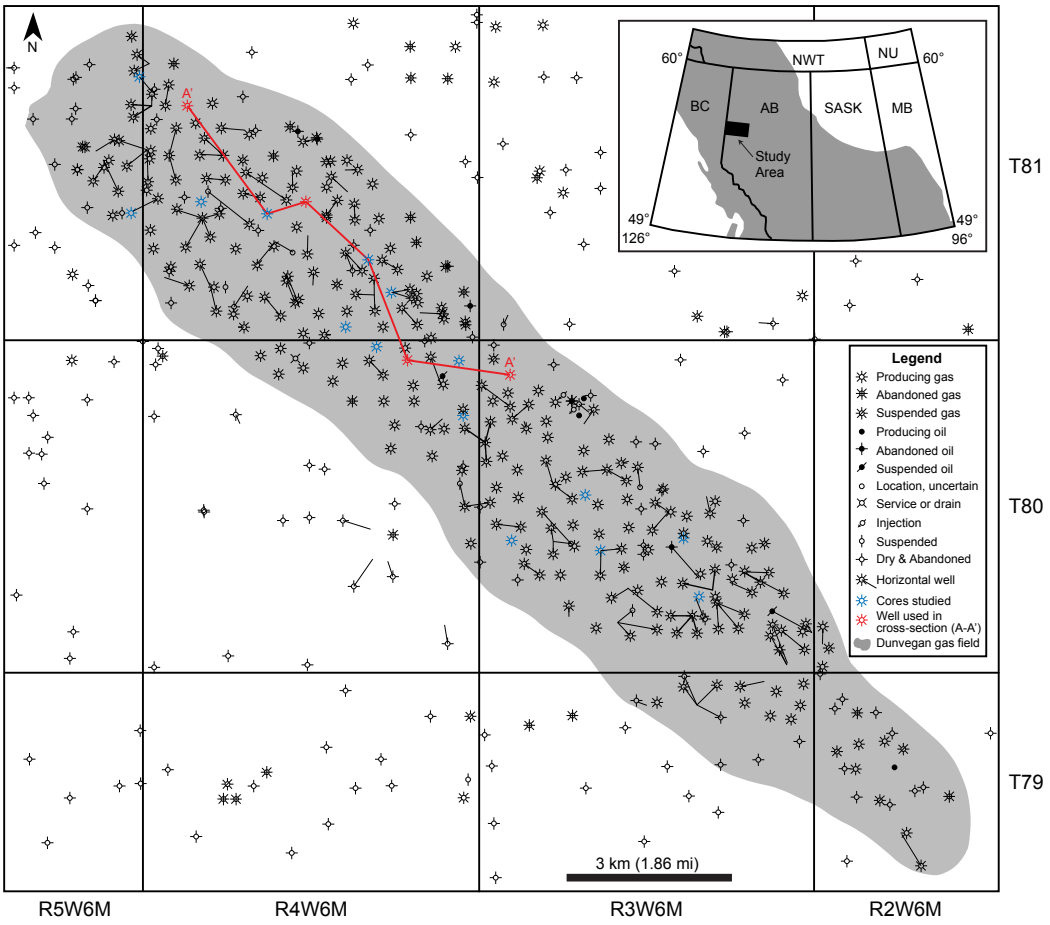

Figure 6.1: Location map of the Dunvegan gas field in northwestern Alberta that produces from the Mississippian (Visean) Debolt Formation. In the study area, 15 cored wells (demarcated in blue) were studied. The wells used in the cross-section (A-A', Fig. 6.5) are demarcated in red.

certain parameters (e.g., the presence of MSR, low oxygenation, high salinity) must have existed. The purpose of this chapter is to therefore document the lithofacies and their paleogeographic distribution within the Dunvegan gas field. From this, an understanding of the environmental settings that helped mediate dolomitization within the burrows will be analyzed by integrating lithologic, petrographic, and isotopic analysis.

6.2 IMPACT OF BIOTURBATION ON SUBSTRATE BIOGEOCHEMISTRY

Infaunal invertebrates, such as crustaceans, insects, and earthworms, commonly modify sediment through particle remobilization and grazing (Aller, 1994, Bromley, 1996, Gingras et al., 2007a). A common by-product of bioturbation is the introduction of labile organic matter, such as mucous secretions and fecal

material, into the substrate (Steward et al., 1996; Hauck et el., 2008; Pak et al., 2010). Mucous secretions, for instance, represent ideal microenvironments for microbes, as many of the burrows are lined with organic materials such as extracellular polysaccharides (i.e., microbial exopolymer secretions) and glycoprotein mucin (Konhauser and Gingras, 2007; Lalonde et al., 2010; Konhauser and Gingras, 2011; Petrash et al., 2011). For example, Gunnarsson *et al.* (1999a) observed that elevated concentrations of a tetrachlorobiphenyl commonly occurred in the thin mucous layer covering the burrow linings of the polychaete *Neries diversicolor* compared to the surrounding bulk sediment. Similar observations were also made by Gunnarsson *et al.* (1999b) for the linings of disk chamber and arm burrows of the brittle star *Amphiura filiformis*. These microbial exopolymer secretions (EPS) are important, as they are able to bind organic compounds of both high and low molecular weight (Decho, 1990). EPS therefore comprises a significant portion of organic carbon within sediment (Confer and Logan, 1998) and acts as a reactive interface for the sorption of dissolved matter and secondary mineral precipitation (Mayer et al. 1999, Gunnarsson et al., 1999a; Gunnarsson et al., 1999b; Konhauser and Gingras, 2007, Konhauser and Gingras, 2011).

The eventual decomposition of EPS and other organic material within bioturbated environments is critical in driving sedimentary metabolic reactions (Fig. 6.2). Typically, any organic carbon present usually becomes paired to a sequence of terminal electron accepting processes, with the more energetically favored reactions proceeding first (Froelich et al., 1979; Canfield et al., 1993; Chapelle et al., 1995). However, these idealized biogeochemical reactions within sediments (e.g., Freolich et al., 1979) can become disrupted through activities within the substrate (e.g., bioturbation) (Aller, 1982; Kristensen, 2000; Needham et al., 2004). At present, it is unclear how much bioturbation alters these biogeochemical reactions and therefore requires further research. As a result of the decomposition of EPS, these geochemical reactions are commonly microbially mediated and include (after Froelich et al., 1979 and Konhauser, 2007):

[1] *Aerobic respiration:*

CH_2O (organic carbon) + $O_2 \rightarrow CO_2 + H_2O$

[2] *Nitrate reduction:*

$2CH_2O + NO_3^- + 2H^+ \rightarrow 2CO_2 + NH_4^+ + H_2O$

[3] *Mn(IV)-oxide reductive dissolution:*

$CH_2O + 2MnO_{2(s)} + 4H^+ \rightarrow CO_2 + 2Mn^{2+} + 3H_2O$

[4] *Fe(III)-oxyhydroxide reductive dissolution:*

$CH_2O + 4FeOOH_{(s)} + 8H^+ \rightarrow CO_2 + 4Fe^{2+} + 7H_2O$

[5] *Sulfate reduction:*

$2CH_2O + SO_4^{2-} + H^+ \rightarrow HS^- + 2CO_2 + 2H_2O$

[6] *Methanogenesis:*

$2CH_2O \rightarrow CH_4 + CO_2$

Notably, the oxidation (or mineralization) of organic carbon leads to an increase in alkalinity (represented as CO_2) and an increase in pH (reactions 2 through 5). Studies of pore waters in deep-sea sediments (e.g., Froelich et al., 1979) and anoxic basins (e.g., Reeburgh, 1980) have shown that the most energetically favorable redox reactions occur first and concentrations of electron acceptors such as O_2 and NO_3 are typically the first to become depleted. Sulfate reduction (reaction 5) and methanogenesis (reaction 6) are therefore later-stage redox reactions. Consequently, high concentrations of organic carbon are required to consume these earlier terminal electron acceptors before the onset of the later reactions can occur. The contemporaneous bacterial mineralization of organic carbon and increase in pH will also help favor the formation of a carbonate ion due to the hydration of CO_2 to carbonic acid (H_2CO_3) and subsequent deprotonation reactions (i.e., $H_2CO_3 \rightarrow HCO_3^- + H^+ \rightarrow CO_3^{2-} + 2H^+$).

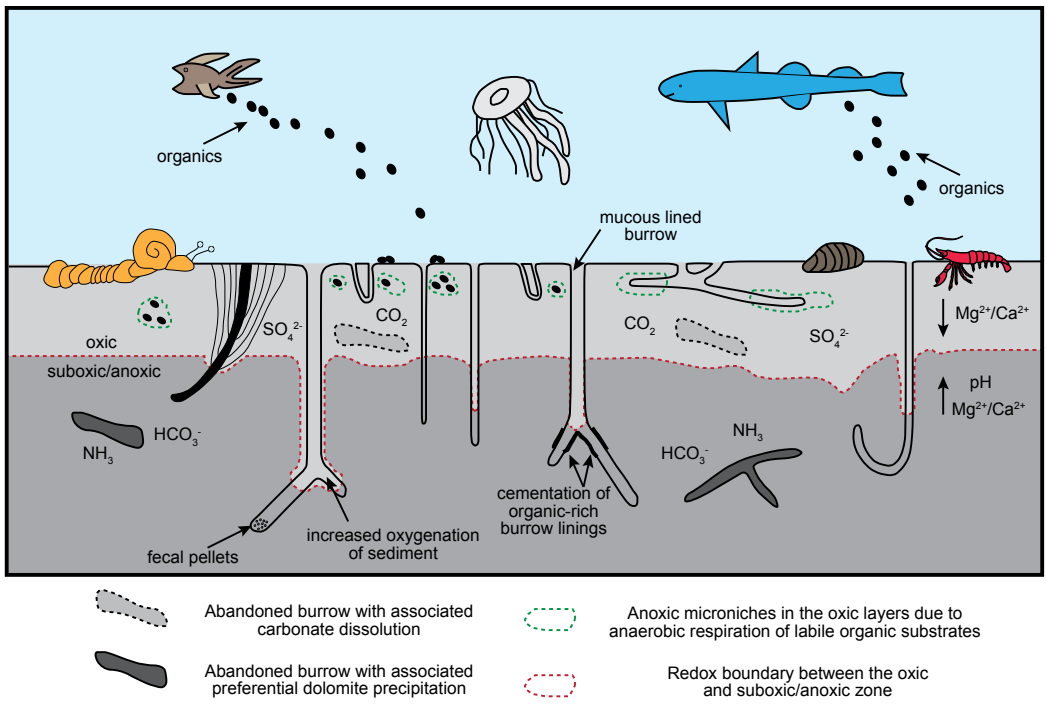

Figure 6.2: Illustration of the geochemical characteristics of the oxic and anoxic zones in a bioturbated substrate. Modified from Gingras et al. (2004) and Konhauser and Gingras (2007).

Modern studies by Garrison and Luternauer (1971) and Gunatilaka et al. (1987) have shown that organic material present within animal burrows helps promote the precipitation of dolomite. Given the ubiquitous presence of organic material within most burrows environments, development of a reducing microenvironment can occur (Gingras et al., 2004). Within reducing sediment, sulfate-reducing bacteria are present and are able to remove dolomite-inhibiting sulfate anions. As a result, liberation of the Mg^{2+} cation from the SO_4^{2-}-Mg^{2+} ion pair occurs, thereby increasing the availability of the free Mg^{2+} cations for early dolomite precipitation (van Lith et al., 2003). Elevated concentrations of sulfide have been measured in modern burrows (Waslenchuk et al., 1983), suggesting that sulfate reduction is indeed occurring within or adjacent to burrow systems.

6.3 REGIONAL GEOLOGICAL SETTING

During the Carboniferous Period in western Canada, the principal tectonic features were the Prophet Trough, Peace River Embayment, Cratonic Platform, Williston Basin, and Yukon Fold Belt (Richards, 1989). The Debolt Formation, and stratigraphic equivalents, is deposited primarily within the Prophet Trough and Peace River Embayment in British Columbia and Alberta (Fig. 6.3). The Prophet Trough is a downfaulted margin (i.e., distal foreland basin) that extends from the northern Yukon and Alaska southward to join the Antler Foreland Basin of the western United States (Richards, 1989; Richards et al., 1993; Richards et al., 1994). The Peace River Embayment (Douglas et al., 1970) can trace its origins to the structural evolution of the Peace River Arch (Cant, 1988; O'Connell et al., 1990). The Peace River Arch was a prominent east-northeast trending topographic high of Precambrian granites that were approximately 800 to 1,000 m above the regional elevation near the Alberta-British Columbia border during the early Paleozoic (Cant, 1988).

Despite providing expressible topographic relief from the Cambrian to Devonian, a combination of subsidence (compression and extension) and normal faulting (horst and graben structures) to the Peace River Arch during the mid-Devonian to Permian provided locations for sediments to accumulate (Cant, 1988; O'Connell et al., 1990). Because of subsidence and normal faulting, the Peace River Arch became a negative feature from the Mississippian to Jurassic (Hein, 1999). Isopach maps of northwestern Alberta show the Debolt Formation to be the thickest in areas interpreted to be bounded by extensional faults (Cant, 1988). The Peace River Embayment may have become connected to the Prophet

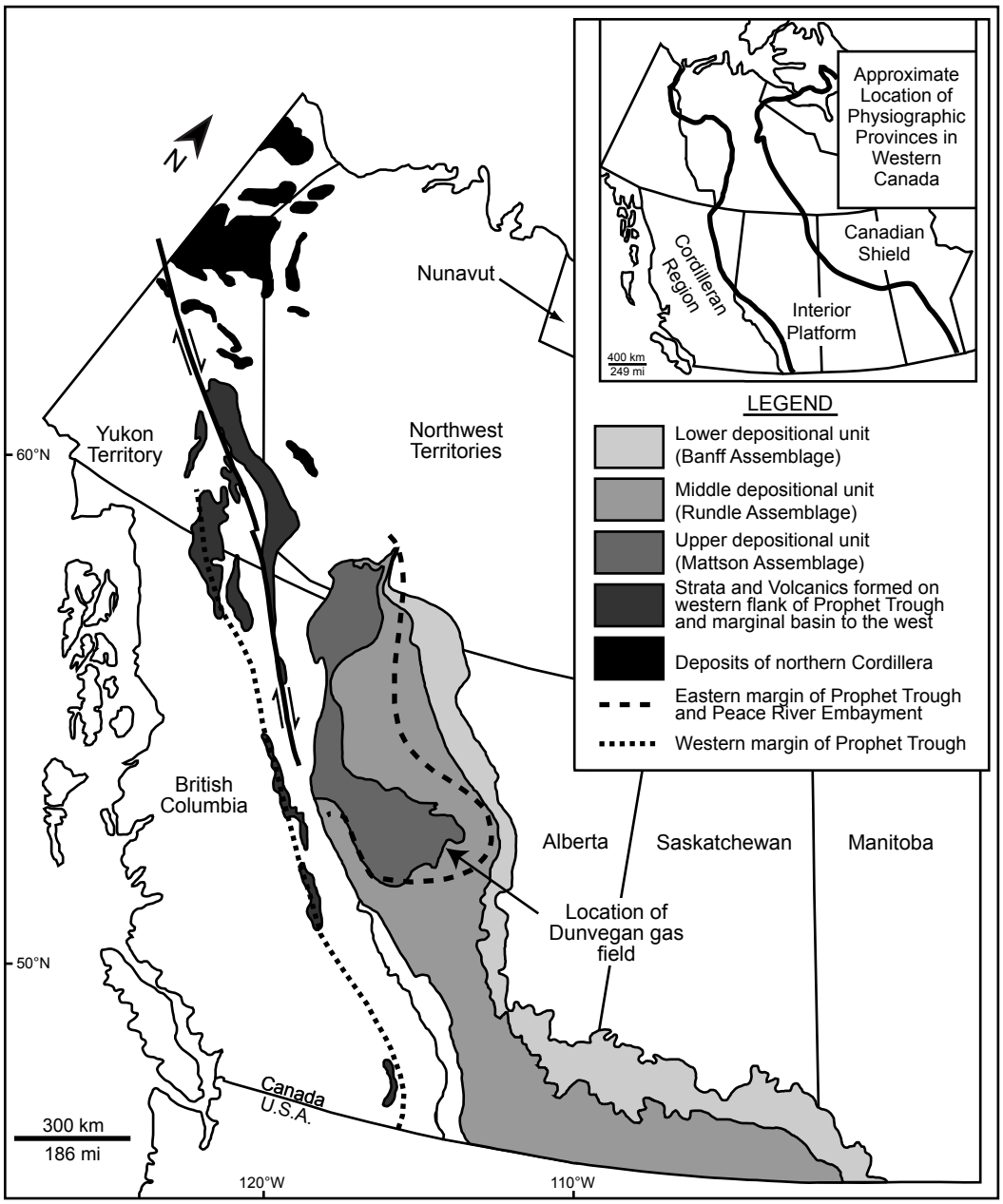

Figure 6.3: A map of western Canada showing the depositional limits for sedimentation during the Carboniferous Period. Non-highlighted areas denote positive regions where sediments are not preserved. The location of interest for this study is situated in the southeastern margin of the Peace River Embayment. The Debolt Formation corresponds to middle depositional unit (Rundle Assemblage) deposited during the Visean. Inset shows the main physiographic provinces of western Canada. Figure modified from Richards et al. (1993) and Richards et al. (1994).

Trough during the early- and middle-Tournaisian due to the faulting and regional subsidence that continued throughout the Carboniferous (Durocher and Al-Aasm, 1997). Connection with the Prophet Trough helped facilitate deposition of a thick Carboniferous succession within the embayment and across the western Canadian Cratonic Platform (O'Connell et al., 1990). Petroleum traps formed within the Dunvegan gas field as a result of these aforementioned events are both structural (two-way up-dip closures) and stratigraphic (anhydrite, shale accumulations, pinch-outs of dolomitized burrow intervals) (Cioppa et al., 2003).

6.4 STRATIGRAPHIC SETTING

The Carboniferous succession in the Peace River Embayment of northwestern Alberta and interior platform of northeastern British Columbia is subdivided into three main stratigraphic units. In chronological order, these units include: (i) lower to middle Tournaisian Banff Formation; (ii) middle Tournaisian to upper Visean Rundle Group; and (iii) upper Visean to Serpukhovian Stoddart Group (O'Connell, 1994) (Fig. 6.4). The Debolt Formation is Visean in age and belongs to the Rundle Group. Consisting primarily of carbonate and evaporitic facies, the Debolt Formation typically grades into deeper basinal facies towards the west (Richards, 1989; Durocher and Al-Aasm, 1997; Al-Aasm and Packard, 2000). Macauley (1958) was the first to subdivide the Debolt Formation into lower and upper members. Law (1981) later subdivided the Debolt Formation into five informal members in northeastern British Columbia. The Debolt Formation is 244 m thick at its type section in west-central Alberta and becomes progressively thinner near its southwestern depositional limit (Richards et al., 1993). Within the Peace River Embayment, the Debolt Formation overlies the Shunda Formation in the east and the Pekisko Shale (Formation F) in the west (Richards et al., 1993). The Golata Formation disconformably overlies the Debolt Formation throughout the embayment. The outcrop nomenclature of the Mount Head and Livingstone formations have been applied to internal zones of the Debolt Formation with varying degrees of success (Packard et al., 2004).

In general, the Debolt Formation records no less than 30 shoaling-upward hemicycles or $4^{th}/5^{th}$ order parasequences that can be correlated over many kilometers (Fig. 6.5) (Al-Aasm and Packard, 2000; Packard et al., 2004). These numerous packages are a reflection of the ongoing relative sea level oscillation in a shallow-water to littoral setting during the Visean. In Alberta, an early Visean transgression is recorded by the presence of protected-shelf carbonates in the basal

part of the Debolt Formation above the restricted-shelf carbonates of the Shunda Formation (Packard et al., 2004). The subsequent regression, recorded by anhydrite and restricted-shelf carbonates preserved in the upper Debolt Formation of west-central Alberta and east-central British Columbia, appears to have coincided with sedimentation of the regressive Wileman and Salter members of the Mount Head Formation (Richards et al., 1993). Towards the east and east-southeast into Alberta, the upper member of the Debolt Formation becomes anhydritic and displays sabkha cycles.

Reservoir zones in the Dunvegan gas field are located in the uppermost argillaceous unit (Al-Aasm and Packard, 2000). This argillaceous unit consists of a succession of stacked sabkha cycles of thinly interstratified carbonates, evaporites, and siliclastics (Al-Aasm and Packard, 2000). A stratigraphic cross-section (Fig. 6.5) along a transect through the Dunvegan gas field illustrates the cyclical nature of the sabkha cycles.

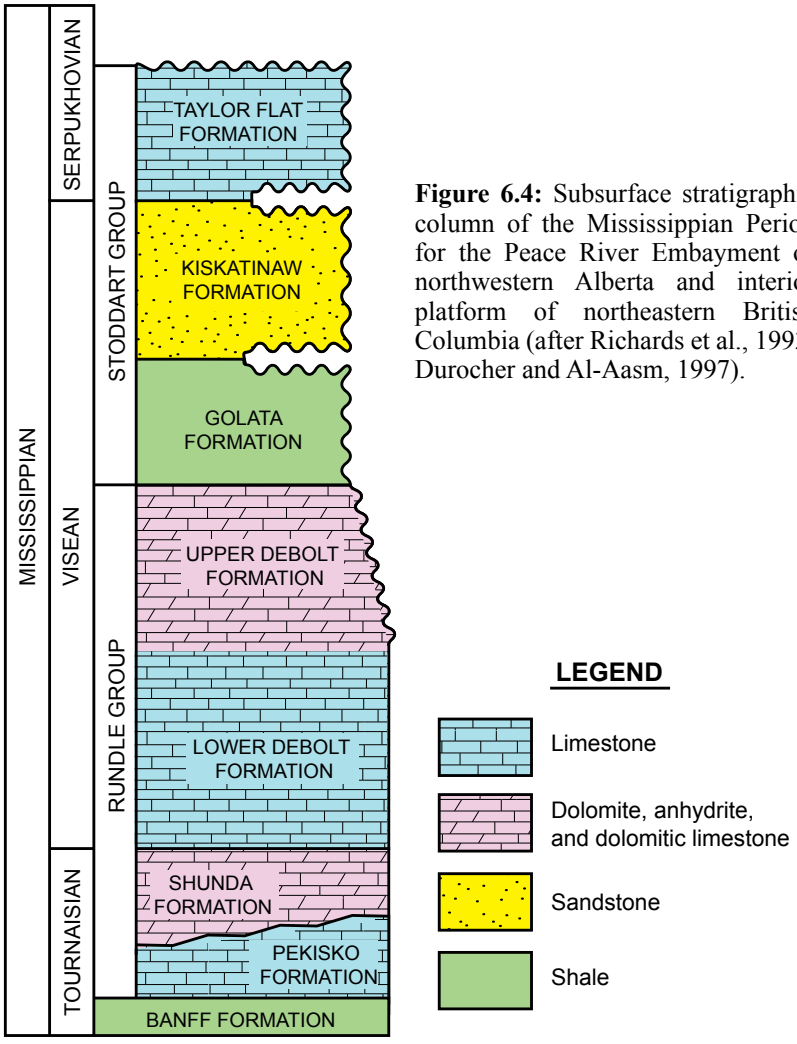

Figure 6.4: Subsurface stratigraphic column of the Mississippian Period for the Peace River Embayment of northwestern Alberta and interior platform of northeastern British Columbia (after Richards et al., 1993; Durocher and Al-Aasm, 1997).

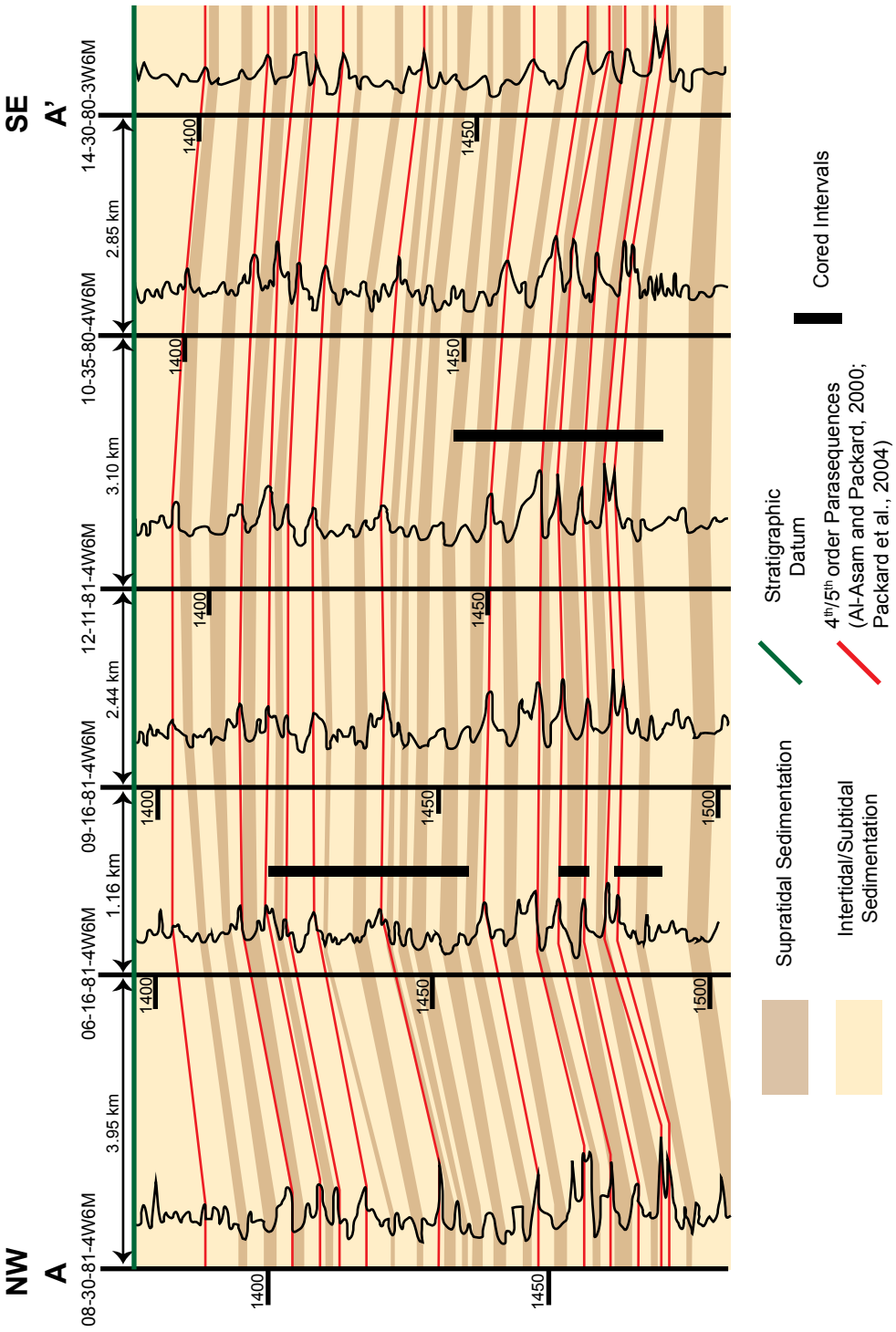

Figure 6.5: Stratigraphic cross-section of the Debolt Formation along the northwestern part of the Dunvegan gas field. All well-logs shown are gamma ray. Twelve parasequence surfaces are recognized in this cross-section and are commonly represented in core as thinly bedded shale surfaces. Within these parasequences are stacked sabkha facies that are gradational with tidal flat, lagoonal, and shoal sediments. The repetitive nature of these facies over a large stratigraphic interval indicates high levels of sea level oscillation (i.e., transgressive-regressive cycles) in a shallow-water ramp setting during the Visean.

6.5 DATABASE AND METHODS

In this study, fifteen drill cores from the Dunvegan gas field were examined (see Fig. 6.1) along with 30 thin sections. The thin sections from the drill core samples were examined under a polarizing microscope. Sedimentological characterization included identification of carbonate grains (e.g., ooids, pisoids, oncoids, and other allochems), fossils, bedding contacts, layer thicknesses, primary and secondary physical structures, lithologic constituents, and accessory minerals. Ichnological data comprised descriptions of ichnogenera, cross-cutting relationships, and bioturbation intensity.

Isotopic analyses ($\delta^{18}O$ and $\delta^{13}C$) were performed on the burrow fill and surrounding matrices. Samples for isotopic analysis were obtained from representative sections of slabbed core and were mechanically extracted using the engraver tip of a high-speed rotary drill. The samples were selectively obtained from locations where discrete burrows were present or where burrows were absent (i.e., matrix). In each case, 10 to 25 mg samples were excavated from a depth of around 1 to 2 mm. In the case of burrow samples, this occasionally necessitated sampling more than one burrow in an interval. Samples for the isotopic analysis of the calcite phase were obtained by reaction with 100% phosphoric acid (H_3PO_4) for one hour at 25°C using the technique of McCrea (1950). Samples for the isotopic analysis of the dolomite phase were obtained after an additional 24 hours in 100% H_3PO_4 at 50°C. Isotopic analyses were performed with a Finnigan-MAT 252 mass spectrometer operated in dual inlet mode. All isotopic values are reported in standard delta notation (δ) relative to PDB standards (Craig, 1957).

6.6 RESULTS

6.6.1 Facies Analysis

In this study, the Dunvegan gas field can be subdivided into six reoccurring facies intervals: nodular and bedded anhydrite (Facies 1); microbially-laminated mudstones (Facies 2); massive-patterned mudstone (Facies 3); bioturbated mudstone-wackestone (Facies 4); skeletal packstone-wackestone (Facies 5); and peloidal grainstone-packstone (Facies 6). Within the study area, Al-Aasm and Packard (2000) identified oxidized muds and highly bioturbated sediments as the main intervals with dolomite present. In this context, the bioturbated mudstones-wackestones (Facies 4) represents the primary focus for this study regarding petrographic and isotopic analysis.

6.6.1.1 Facies 1 (F1): Nodular and Bedded Anhydrite

Facies 1 consists of dense anhydrite and anhydritic-dolomite sediments that is non-bioturbated. The most commonly observed type of anhydrite is nodular, with mottled and cryptocrystalline fabrics and occasional dolostone stringers. Nodules vary from 1 to 6 cm in diameter and are ovoid to irregular in shape (Fig. 6.6A-B). Facies 1 is typically embedded within dolostone and commonly has thicknesses ranging from 10 to 30 cm. Expressions of anhydrite in sub-vertically elongated position, with crystals ranging up to 10 cm in length, are also present (Fig. 6.6C). Examples of more massive nodular anhydrite, reaching up to 2 m in thickness, also occur within F1. This unit contains larger nodules (up to 10 cm) and typically contains very little matrix. In areas, the nodules are present within, or juxtaposed, to stylolites or pressure dissolution seams (Fig. 6.6D). Examples of bedded anhydrite containing thin interbeds of dolostone are also present in localized areas. These bedded anhydrites range up to 10 m in thickness and preserve planar to wavy laminations. Where dolomite is present, it is typically expressed as millimeter- to centimeter-thick laminae or thin discontinuous beds.

The combination of different anhydrite morphologies suggests deposition within closely related environments along an arid marine coastline. Given the large range of nodular fabrics, it is likely that the nodular anhydrite is indicative of a sabkha environment. It is important to note, however, that not all nodular anhydrite is formed in a sabkha setting (Warren and Kendall, 1985). The presence of isolated masses of nodular (chicken-wire) anhydrite within other carbonates indicates displacive growth of gypsum and anhydrite in the upper zones of a sabkha (Warren and Kendall, 1985; Kendall, 2010). Similarly, examples of more massive nodular anhydrite indicate that they represent an overprinted subaqueous (salina) gypsum deposit (Kendall, 2010). The sub-vertical elongated morphology of anhydrite nodules further indicates subaqueous precipitation of gypsum in either shallow (less than 10 m) hypersaline lagoons or brine ponds adjacent to the sabkha (Warren and Kendall, 1985). Additional evidence of subaqueous sedimentation is provided by the bedded anhydrite with interbeds of dolostone. The nature of the anhydrite, with little evidence of subaerial exposure, implies diagenetic alteration of primary gypsum that chemically precipitated under subaqueous conditions (Hardie, 2003). The presence of stylolites and pressure dissolution seams in some examples implies that some nodular anhydrite may have formed during burial at depths of tens to several hundred meters (Machel and Burton, 1991; Machel, 1993).

6.6.1.2 Facies 2 (F2): Microbially Laminated Mudstones

Facies 2 consists of tan-colored, cryptocrystalline, microbially laminated carbonate mudstones (Fig. 6.6E). Present within these laminated mudstones are very fine, dark-brown to black, organic-rich laminae present in intervals that vary from 5 to 50 cm in thickness. Sedimentary structures include irregular to planar laminations and low-relief domal stromatolites (Fig. 6.6F). Petrography of F2 shows the presence of silt-sized to fine-grained sandstones within the matrix. These grains are typically sub-rounded to sub-angular and occasionally form bedded deposits. Subaerial exposure features include desiccation cracks and some fenestral (birds-eye) porosity. Skeletal fragments and bioturbation are extremely rare in F2.

Fenestral porosity, formed by a combination of gas bubbles and sediment shrinkage, are common occurrences in tidal-flat carbonates (Choquette and Prey, 1970). Combined with the presence of desiccation cracks, periodic subaerial exposure of the substrate is envisioned in F2. The presence of low-relief domal stromatolites also suggests deposition on high intertidal and supratidal sites and on tidal flats with protected shorelines (Logan, 1961; Davies, 1970; Taylor and Halley, 1974). Due to shoreline isolation, fluctuating salinities were probable, thereby presenting additional ecological stresses to the localized macrofauna. Because most eukaryotic organisms are unable to withstand high salinities or exposure to extreme salinity fluctuations (Franks and Stolz, 2009), the levels of bioturbation and overall fossil content are expectedly limited in F2.

As a result of extreme physico-chemical conditions, flat laminated microbial mats were able to flourish in the intertidal flats and hypersaline lagoons of the carbonate ramp (Nicholson et al., 1987; Stolz, 1990). The presence of organic laminae is attributable to the sharp geochemical interface present beneath the microbial mat (Krumbein and Cohen, 1977). Pore waters below the interface were anoxic and thus had a higher preservation potential for buried organic matter. The presence of siliciclastic material within the microbial mats is likely the result of sticky EPS produced by microorganisms (Krumbein, 1994). As shown in the Mellum Island, southern North Sea and southern coast of Tunisia (Gerdes et al., 2000), microbial mats coated with EPS have the ability to trap and bind sediment introduced into the tidal flats.

6.6.1.3 Facies 3 (F3): Massive Patterned Mudstone

Facies 3 is recognizable in core by its distinctive mottled fabric (Fig. 6.6G). In short, F3 is a cryptocrystalline dolomudstone that contains no visible burrows

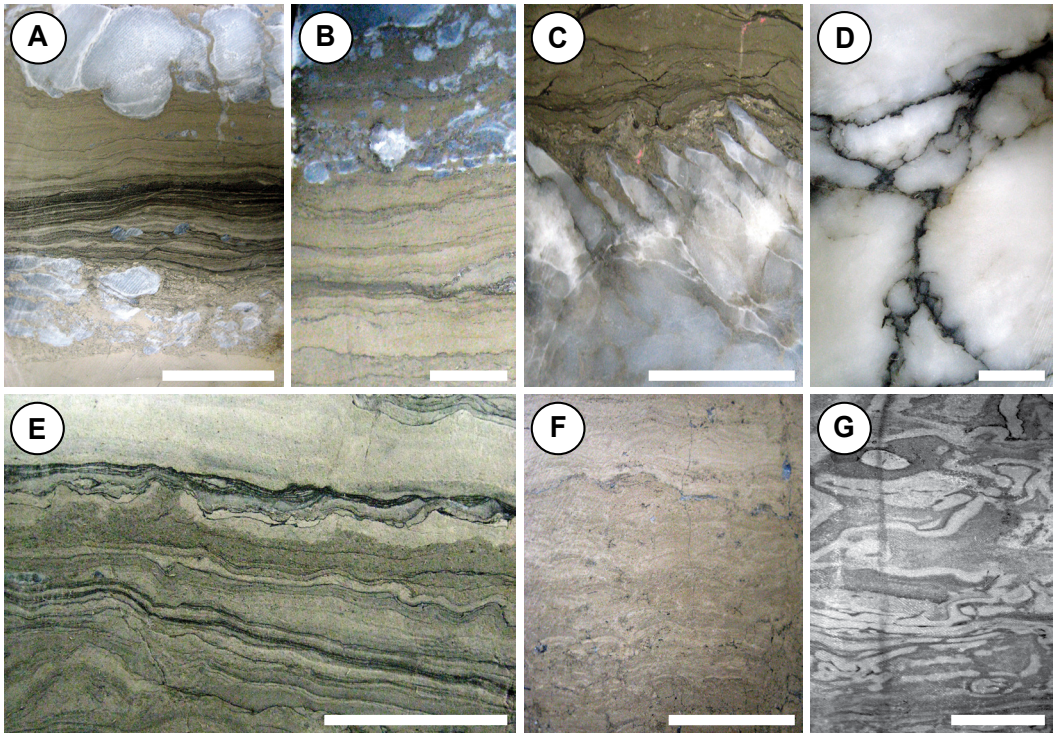

Figure 6.6: Core photographs of supratidal to intertidal facies in the Dunvegan gas field. All scale bars are 3 cm. **(A)** Eroded nodular anhydrite capped by planar to wavy black shale and laminated mudstone. The biolaminated mudstone is sharply overlain by nodular anhydrite. Well 12-11-81-4W6M, depth 1479.83m. **(B)** Laminated mudstone overlain by nodular anhydrite. Well 5-16-80-3W6M, depth 1478.10m. **(C)** Sub-vertically elongated nodular anhydrite in an argillaceous, brown-colored dolomitic mudstone matrix capped by massive appearing dolomudstone with dissolution seems. Well 7-18-80-3W6M, depth 1472.80m. **(D)** Nodular mosaic anhydrite of chicken-wire juxtaposed to stylolites and interstitial mud. Well 9-25-81-5W6M, depth 1601.50m. **(E)** Bio-laminations with wavy to contorted laminae, dark organic-rich partings, and stylolites. Well 7-3-81-4W6M, depth 1480.54m. **(F)** Domal stromatolites. Well 7-3-81-4W6M, depth 1487.65m. **(G)** Massive patterned cryptocrystalline mudstone with alternating dark- and light-colored fabrics. Well 7-15-80-3W6M, depth 1474.52m.

or fossiliferous material. Facies 3 ranges in thickness from 10 to 30 cm, with some thicker intervals present. The mottled fabric consists of a pattern of light- and dark-colored areas, with the concentration of pyrite crystals seen in the darker regions. Facies 3 is commonly gradational with anhydrite sequences (F1), microbially laminated carbonates (F2) and bioturbated mudstones-wackestones (F4), and is observable throughout the Dunvegan gas field.

The variable size, irregular shape, and indistinct contacts of the mottles suggest they are not related to burrowing. Instead, the alteration of light- and dark-colored fabrics represents a diagenetic feature wherein microcrystalline pyrite became concentrated in the darker regions (Dixon, 1976; Kendall, 1977b; Kirkham, 2004). Termed ‘patterned carbonate’ by Dixon (1976), the diagenetic origin of this unique fabric is attributable to the destruction of calcium sulfate nodules by sulfate-

reducing microorganisms, thereby leading to pyrite formation (Kendall, 1977b). Within reducing subenvironments, the formation of pyrite commonly requires pH values greater than 8.0 and salinities above 200‰ (Krumbein and Garrels, 1952). Such extreme conditions suggest sedimentation of F3 within a restricted supratidal to intertidal setting (Dixon, 1976), similar to those observed in the modern Persian Gulf (e.g., Butler, 1969). Furthermore, the cryptocrystalline dolomudstone suggests formation under hypersaline conditions with precipitation likely induced by sulfate-reducing bacteria (Kirkham, 2004).

6.6.1.4 Facies 4 (F4): Bioturbated Mudstone-Wackestone

Bioturbated dolomudstones-dolowackestones (60 to 100% of total reservoir volume) represent important reservoir strata within the Dunvegan gas field. Common assemblages include monospecific examples *Chondrites, Quebecichnus*, and *Planolites* (Fig. 6.7A-B). Other ichnofossils occasionally dispersed within F4 include moderately abundant *Thalassinoides* (Fig. 6.7C), rare *Arenicolites*, rare *Skolithos*, and very rare *Zoophycos*. Although no fossil fragments are visible in core, petrographic sections reveal low to moderate amounts of fossil content composed of benthic invertebrates and calcareous algae that have been completely reworked by bioturbation. Gradational with F2 and F3, F4 has thicknesses on the order of decimeter to meter scale.

The predominance of low-diversity ichnological assemblages is typical of ecological stresses, such as high salinity and low oxygenation, commonly present within lagoonal settings (MacEachern et al., 2007). For example, it has been shown that the ghost shrimp *Callianassa californiensis*, which make *Thalassinoides*-type burrows, is capable of tolerating fluctuating salinities (Thompson and Pritchard, 1969). Complex feeding traces (i.e., fodinichnia) are also abundant within oxygen-poor environments (Bromley and Ekdale, 1984; Ekdale, 1988; Ekdale and Mason, 1988). *Chondrites*, for example, is believed to be unique to anoxic conditions (Bromley and Ekdale, 1984). The presence of *Zoophycos* may reflect the activity of opportunistic organisms habituating poorly oxygenated communities (Ekdale, 1988; Ekdale and Lewis, 1991; Miller, 1991). Increased ichnodiversity present within some intervals in F4 (e.g., *Skolithos*, *Arenicolites*) could be the result of events such as fresh water influx that helped alleviate earlier stresses imparted on the ecosystem. Collectively, F4 represents a restricted, low-energy lagoon.

6.6.1.5 Facies 5 (F5): Skeletal Packstone-Wackestone

Facies 5 is a bioclastic packstone-wackestone composed of a diverse assemblage of fauna (Fig. 6.7D). Identifiable fossils include fragmented brachiopods, crinoids, bryozoans, and ostracodes. Also present are stylolites, pressure dissolution seams, and peloids. Grain sorting varies between different intervals, ranging from poorly- to well-sorted. The matrix is composed primarily of carbonate mud within the wackestone successions, and becomes increasing depleted of mud in the more well-sorted packstone-rich intervals. Either gradational or sharp contact with F2, F3, and F4, bed thicknesses in F5 range from 10 to 25 cm, although thicker intervals are present in areas.

The diversity of fossils suggests a normal-marine origin (James and Kendall, 1992). The well-sorted, fine-grained, bedded nature indicates that the skeletal material may have undergone earlier wave reworking in a high-energy beach or shoal environment. The fact that F5 is in close contact with multiple facies (F2, F3, F4) suggests possible allochthonous transportation of sediment (e.g., tempestites). As a result, sedimentation of these skeletal packstones-wackestones may have been due to either storm activity or minor sea level transgressions that affected the restricted intertidal to subtidal regions of the lagoonal environment.

6.6.1.6 Facies 6 (F6): Peloidal Grainstone-Packstone

Facies 6 is a peloidal grainstone-packstone, and allochems include oncoids, ooids, and pisoids. Micritic envelopes (Fig. 6.7E) are identifiable on pisoids and shell fragments. The peloids range in shape from ovoid (Fig. 6.7F) to non-rounded. Comprised of a poor to moderately diverse assemblage of skeletal fragments, bioclasts include ostracodes, crinoids, brachiopods, and bryozoans. The majority of the intervals in Facies 6 are massive bedded (Fig. 6.7G), although low-angle cross-bedding is locally present. Bioturbation is generally preserved locally as indistinct mottling. Gradational with F4 and F5, F6 has a thickness of 30 cm to 1 m.

The presence of irregularly shaped peloids suggests micritization of allochems, such as skeletal fragments or ooids (Bathurst, 1966). Peloids that are either elongated or ovoid in shape suggests a fecal origin (Land and Moore, 1980). Preservation of the peloids indicates deposition within a shallow, low-energy, restricted marine environment (Enos, 1983). Due to the presence of low-angle cross bedding and fragmented fossils, F6 is interpreted to have accumulated in either shallow peloidal shoals or low-relief banks in restricted lagoonal environments (Qing and Nimegeers, 2008).

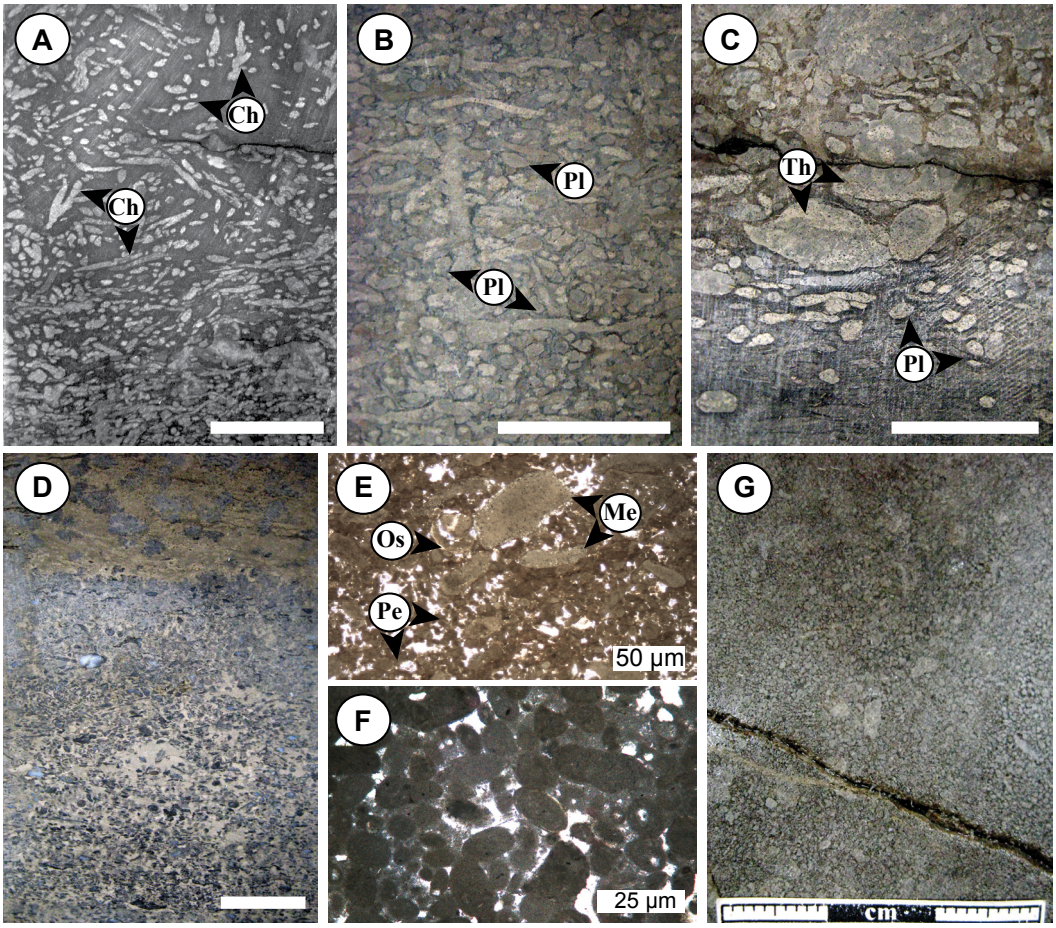

Figure 6.7: Core photographs of subtidal Debolt Formation facies in the Dunvegan gas field. All scale bars are 3 cm unless otherwise noted. **(A)** Highly bioturbated, monospecific assemblage of *Chondrites* (Ch). Well 8-13-81-5W6M, depth 1452.31m. **(B)** Highly bioturbated dolomudstone dominated by a monospecific assemblage of *Planolites* (Pl). The interval forms the principal reservoir in the observed well, with permeabilities ranging above 40 mD. Well 9-18-81-4W6M, depth 1412.15m. **(C)** Bioturbated assemblage of *Planolites* (Pl) and *Thalassinoides* (Th). Well 8-20-80-3W6M, depth 1497.25 m. **(D)** Fossiliferous packstone overlain by laminated mudstone with metasomatic anhydrite. Fossils include crinoids, brachiopods, bryozoans, and ostracodes. Well 7-15-80-3W6M, depth 1439.64m. **(E)** Thin section photomicrograph of peloidal grainstone facies (Pe), where the irregular shape suggest they may have been originally skeletal grainstones. Subordinate amounts of ostracode (Os) and crinoids fragments exist and some of the larger grains display simple micrite envelopes (Me). Calcite cement occludes primary porosity. Well 8-13-81-5W6M, depth 1455.02m. **(F)** Thin section photomicrograph of peloidal grainstone facies, where the rounded character of the grains suggests fecal pellets. Calcite cement occludes primary porosity. Well 5-16-80-3W6M, depth 1457.20m. **(G)** Massive bedded deposit of peloidal grainstone. Well 7-3-81-4W6M, depth 1492.25m.

6.6.2 Petrographic Analysis

Petrographic analysis of the bioturbated fabrics (Facies 4) is shown in Figure 6.8A-D. The dolomite-filled burrows, 0.5 to 2 cm in diameter, commonly contain dolomite crystal sizes ranging from 1 to 35 microns, with an average size of 10 to 15 microns. The dolomite forms microsucrosic (planar-E) fabrics (after Sibley and Gregg, 1987) and is generally euhedral. Dolomitization within the burrows is generally thorough and a sharp contact commonly exists between the burrow-associated dolomite and calcite matrix. Furthermore, it appears that the microcrystalline dolomite within the burrows has been largely preserved and not altered by burial diagenesis. Similarities in textural composition with dolomites from the Holocene Abu Dhabi sabkhas (McKenzie, 1981) help support this observation.

The majority of calcite within the burrows is consistent with cement precipitated in a marine environment (e.g., blocky calcite spar). The lime mudstone-wackestone surrounding the burrows is dominantly fine-matrix sediment that contains minor amounts of disarticulated and fragmented allochems. Dolomite crystals within the matrix are similar to those observed within the burrows, suggesting residual burrow pathways that were dolomitized.

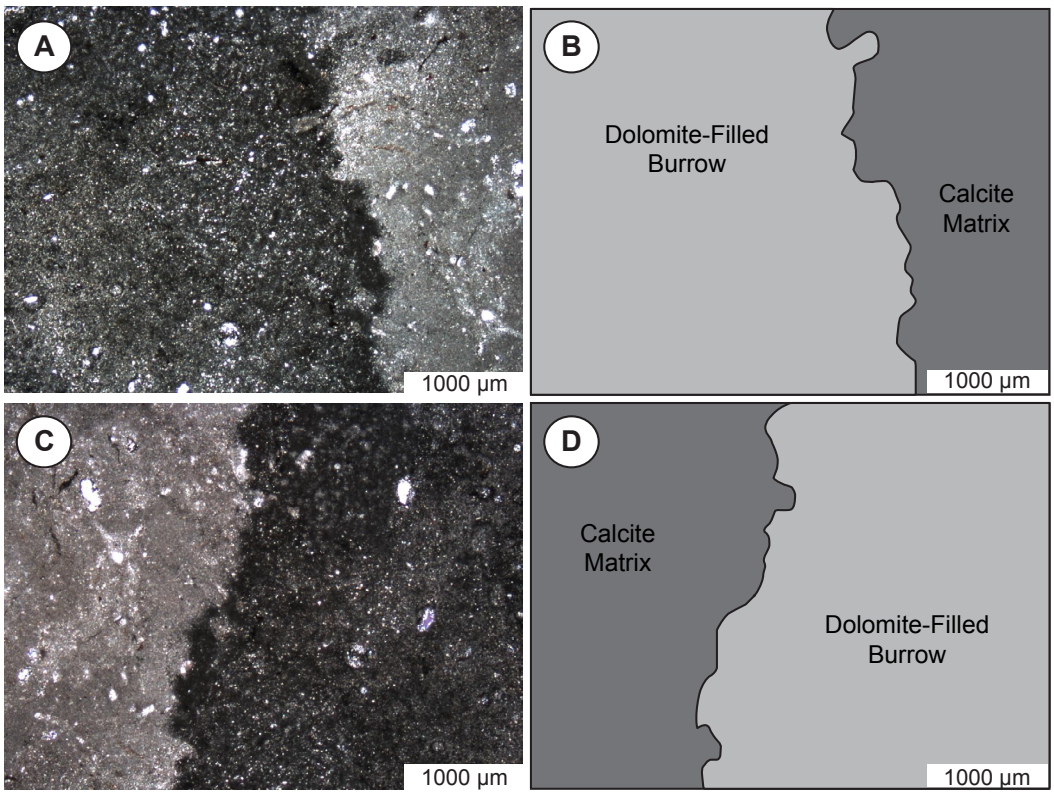

Figure 6.8: Thin section photomicrographs **(A, C)** and corresponding schematic diagrams **(B, D)** of dolomite-filled burrows and surrounding calcite matrices. Both thin section photomicrographs are from Well 9-18-81-4W6M, depth 1412.15m.

6.6.3 Geochemistry

Isotopic analyses of calcites and dolomites are shown in Figure 6.9. To represent the relationship between the calcite and dolomite isotopes within the burrows and matrix, a straight line ($y = mx + b$) was employed. From this equation, the coefficient of determination, R^2, can be deduced. In short, the closer the R^2 is to + 1 or -1, the better the correlation between the isotopes being analyzed. Using R^2, the calcite and dolomite plotted as linear trends with good correlations (i.e., $R^2 > 0.62$), thereby indicating a strong linear relationship for the calcite and dolomite isotopes regardless of sample location (i.e., burrow or matrix).

6.6.3.1 Calcite Isotopic Ratios

Matrix calcite (n = 22) has measured $\delta^{13}C$ values ranging from 1.6 to 5.1‰ (mean = 3.2‰) and $\delta^{18}O$ values of -3.1 to 5.0‰ (mean = 1.4‰). A similar range of values is observed for burrow-hosted calcite (n = 13), where $\delta^{13}C$ range from 1.7 to 4.0‰ (mean = 3.1‰) and $\delta^{18}O$ range from -2.7 to 2.9‰ (mean = 1.1‰). The slope for matrix-hosted calcite (Fig. 6.9A) differs only slightly from that of burrow-hosted calcite (Fig. 6.9B), with values of 0.32 and 0.33 calculated for matrix- and burrow-hosted, respectively.

6.6.3.2 Dolomite Isotopic Ratios

The $\delta^{13}C$ for dolomite ranges from 3.1 to 4.6‰ (mean = 3.4‰) and 3.2 to 4.3‰ (mean = 3.5‰) for samples obtained from the matrix (n = 12) and burrows (n = 25), respectively. In comparison to calcite, dolomite tends to be more enriched in $\delta^{18}O$, with a narrower range of isotopic ratios is observed. For matrix dolomite, $\delta^{18}O$ ranges from 0.7 to 2.9‰ (mean = 2.1‰), and $\delta^{18}O$ for burrow-hosted dolomite between 2.1 and 2.4‰ (mean = 2.4‰). An even smaller difference in calculated slopes is present for the dolomite phases, with values of 0.82 and 0.84 for matrix-hosted (Fig. 6.9C) and burrow-hosted (Fig. 6.9D), respectively.

6.7 DISCUSSION AND INTERPRETATION

6.7.1 Paleoenvironmental Reconstruction

The carbonate facies within the Dunvegan Field are comparable to the modern intertidal flats and sabkhas of the Persian Gulf (Evans, 1966; Butler, 1969; Behairy et al., 1991; Al-Youssef et al., 2006) and the Upper Cretaceous intertidal facies of Hvar Island, Croatia (Diedrich et al., 2011). The six facies described correspond to the shallow inner and middle portions of the carbonate ramp (Fig. 6.10). They extend

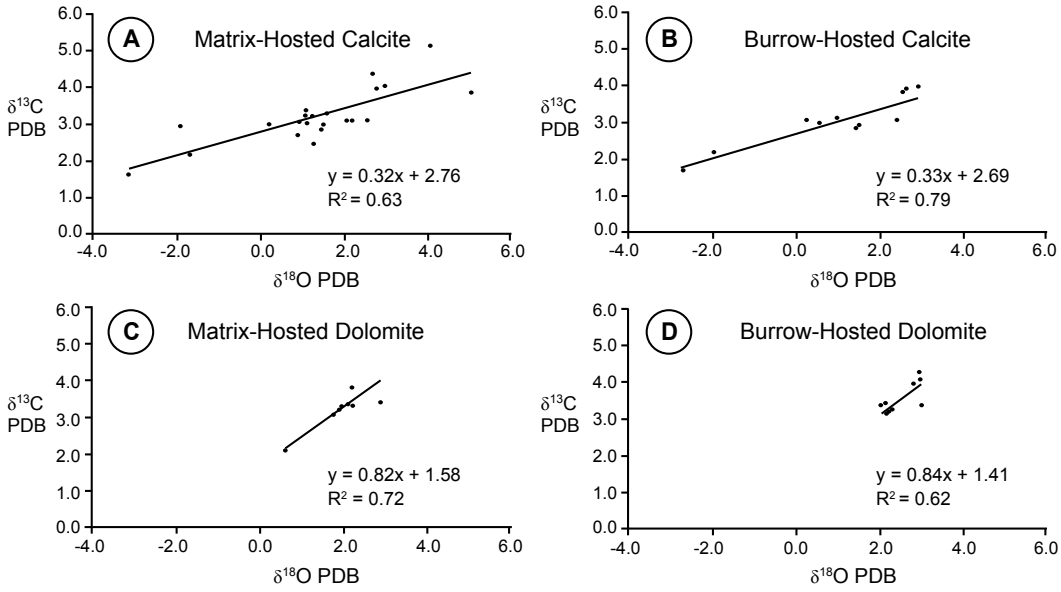

Figure 6.9: Isotopic values for calcite and dolomite from the burrows and adjacent matrix. **(A)** Matrix-hosted calcite (n = 22) has a $\delta^{13}C$ mean of 3.2‰ and $\delta^{18}O$ mean of 1.4‰. **(B)** Burrow-hosted calcite (n = 13) has a $\delta^{13}C$ mean 3.1‰ and $\delta^{18}O$ mean of 1.1‰. **(C)** Matrix-hosted dolomite (n = 12) has a $\delta^{13}C$ mean of 3.4‰ and $\delta^{18}O$ mean of 2.1‰. **(D)** Burrow-hosted dolomite (n = 13) has a $\delta^{13}C$ mean 3.5‰ and $\delta^{18}O$ mean of 2.4‰.

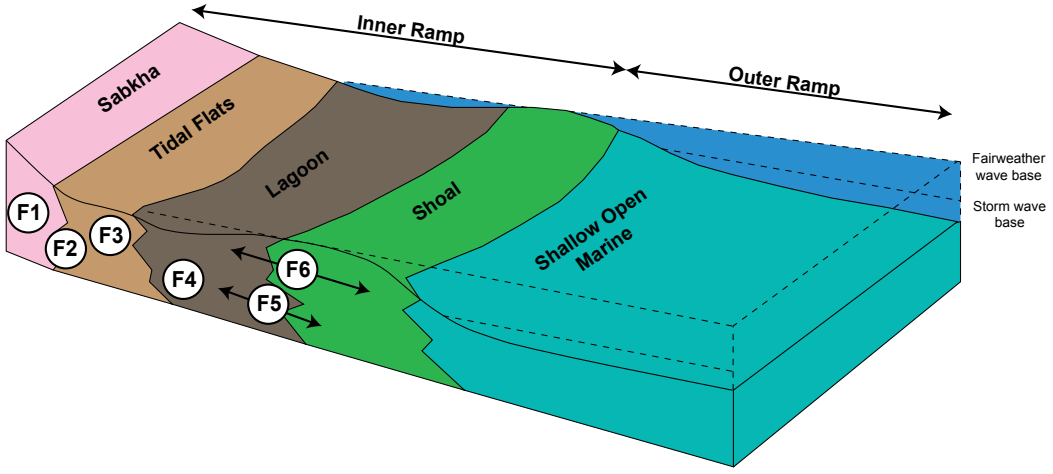

Figure 6.10: A schematic drawing of a low-angle carbonate ramp reflective of sedimentation during the Visean. Superimposed on the carbonate ramp is the location of the six facies identified during core logging. Facies 4 (bioturbated mudstone-wackestone) occurs primarily within the lagoonal portions of the inner ramp and represents the primary reservoir targets in the Dunvegan gas field.

from the peritidal setting to the shallow subtidal zone through a low to moderate energy carbonate shoal facies. Core analysis shows mainly gradational boundaries between the facies, suggesting that they are genetically related and demonstrate a low depositional gradient. For Facies 5 demonstrating an allochthonous origin, tempestites are envisioned as a possible mechanism for sediment transportation.

The lithofacies cycles in the Dunvegan gas field, commonly capped by nodular to nodular mosaic anhydrite, are interpreted as 4th and 5th order transgressive-regressive parasequences that represent the initial flooding and subsequent progradation of a sabkha system (Al-Aasm and Packard, 2000; Packard et al., 2004). The presence of laminated, vertically elongated, and massive nodular anhydrite, as described in F1, suggests numerous other evaporitic sub-environments existed in the backshore adjacent to the sabkha shoreline, such as hypersaline lagoons. The lagoonal facies are characterized by massive, highly bioturbated packstone, wackestone, and mudstone lithofacies. The thin packstone/wackestone beds that were occasionally present between more massive wackestones and mudstones may represent possible storm deposits

Monospecific assemblages of ichnofossils, formation of patterned carbonate, and lack of tidal structures, among other features, supports the interpretation that the lagoon was restricted. Isolating the lagoon from the open marine water was peloidal shoals/low-relief banks composed of fecal material and skeletal fragments. As the geochemical results shows, an abundance of organic carbon (burrows, biolaminated mudstones, EPS), coupled with periods of anoxia within the restricted lagoon, provided favorable conditions for the development of dolomitization.

6.7.2 Dolomitization Models

The $\delta^{13}C$ (3.4‰ matrix, 3.5‰ burrows) and $\delta^{18}O$ (2.1‰ matrix, 2.4‰ burrows) values for the early matrix dolomite in this study are consistent with precipitation from hypersaline marine fluids, as observed elsewhere by Al-Aasm (2000), Al-Aasm and Packard (2000) and Cioppa et al. (2003) within the Dunvegan gas field. The Mg-rich brines, likely derived from Mississippian seawater (Bruckschen et al., 1999; Cioppa et al., 2003), resulted in the replacement of carbonate mud by the early matrix dolomite and precipitation of primary evaporites. Correlation of isotopic values in this study with Holocene dolomites from the Abu Dhabi sabkhas (McKenzie, 1981) support this assertion (Fig. 6.11). Because of the evidence supporting sabkha dolomitization, it is likely that other models of dolomitization have been overlooked within the Dunvegan gas field.

In this context, it must also be noted that recrystallization, due to burial diagenesis, does not appear to have had any significant impact on the texture or geochemical values of the microcrystalline dolomites preserved within the burrow fabrics. This is unique, given that the Debolt Formation within the Dunvegan gas field has undergone over 300 million years of burial history to depths of roughly four km and temperatures in excess of 100°C (Al-Aasm, 2000; Al-Aasm and Packard, 2000). It has been postulated by Al-Aasm (2000), Al-Aasm and Packard, (2000), and Packard et al. (2004) that hydrodynamic isolation, geochemically closed diagenetic systems, and hydrocarbon charging each played a significant role in helping preserve the microcrystalline dolomite. The exact mechanism, however, remains up for debate.

Given this data, burrow-mediated dolomitization is being asserted in this study as an *additional* dolomite-promoting mechanism. This is because the compositional differences observed in the isotopic distributions are interpreted to reflect the different biogeochemical processes occurring within and adjacent to the burrows (Gingras et al., 2004; Konhauser and Gingras, 2007; Rameil, 2008; Lalonde et al., 2010; Konhauser and Gingras, 2011; Petrash et al., 2011; Corlett and Jones, 2012).

6.7.3 Parameters Influencing Dolomitization

When the isotopic values for calcite and dolomite are plotted together (Fig. 6.11), the linear trend observed for calcite is maintained and the dolomite values fall into two general groups either above or below the calcite linear trend. These two fields likely represent dolomite that has precipitated in different spatial environments within the carbonate ramp. The scale of these spatial differences is, at present, unclear.

The zone of relative enrichment of $\delta^{13}C$ in dolomite (i.e., values occurring above the calcite linear trend) is consistent with a biogenically mediated phase. $\delta^{13}C$ enrichment has been interpreted as being associated with methanogenesis (Roberts et al., 2004) and with conditions of anaerobic fermentation (Reitsema, 1980; Dimitrakopoulos and Muehlenbachs, 1987).

An overall enrichment of $\delta^{18}O$ in dolomite relative to calcite suggests that the pore-water associated with dolomitization may have been enriched in $\delta^{18}O$ due to evaporitic and sabkha conditions or due to the dolomite undergoing a greater fractionation factor relative to calcite. Low-temperature experiments of modern dolomite precipitating in equilibrium with calcite under conditions of MSR indicate that dolomite should be enriched in $\delta^{18}O$ by approximately 2.6‰ (Vasconcelos et

al., 2005). Mean $\delta^{18}O$ values for dolomite in this study are enriched by 0.8‰ relative to mean calcite values (1.2‰). This fractionation is closer to values measured in a lab than values extrapolated to low-temperature conditions from high-temperature experiments (e.g., Epstein et al., 1964; Northrop and Clayton, 1966; O'Neill and Epstein, 1966). The similarity in approximated fractionation values calculated between calcite and dolomite in this study with those calculated by Vasconcelos et al. (2005) for dolomite and calcite precipitating from the same parent solution suggests that protodolomite precipitated in equilibrium with calcite rather than by replacement of pre-existing calcite.

There are examples of dolomitized burrows in the rock record, however, wherein $\delta^{18}O$ dolomite is depleted relative to calcite (e.g., Corlett and Jones, 2012). Within their study of burrow dolomites in the Middle Devonian Lonely Bay Formation in Northwest Territories, Canada, Corlett and Jones (2012) showed that a requisite for dolomitization, among others, was a high concentration of marine-dissolved organic matter. On the other hand, the burrows within the Debolt Formation lack marine-derived organic matter due to a sabkha based depositional setting. As

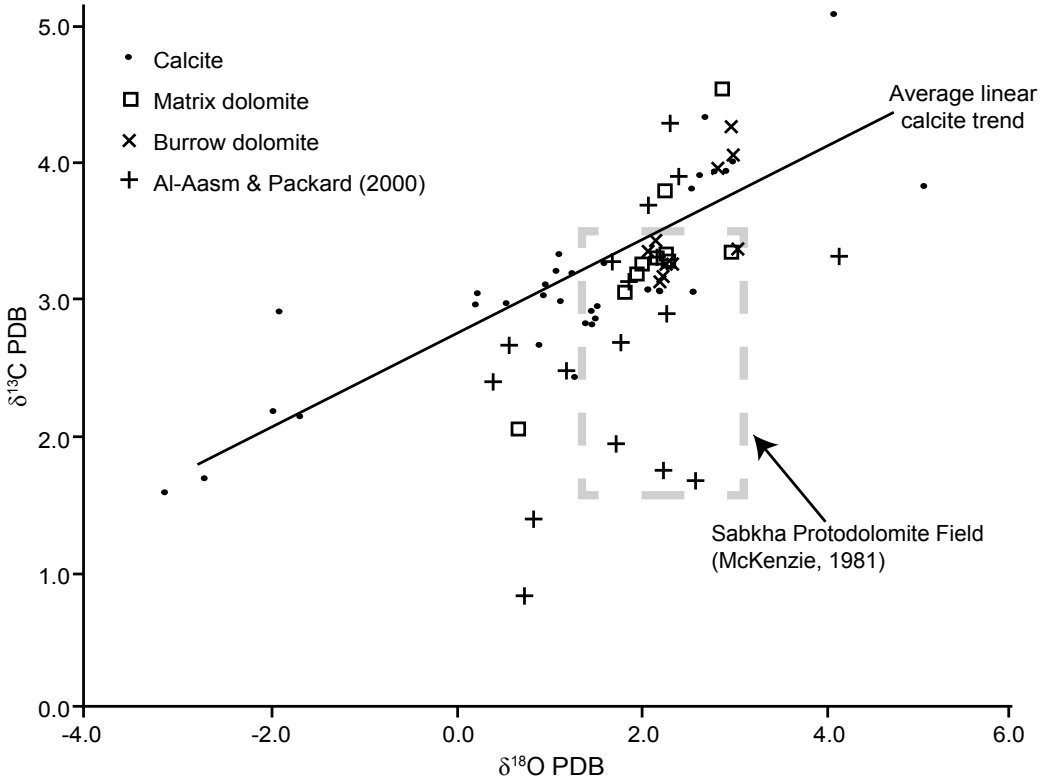

Figure 6.11: Composite plot showing the average linear trend for calcite and the two distinct zones of dolomite occurring either above or below the calcite linear trend line. Observed $\delta^{18}O$ and $\delta^{13}C$ values from the burrow and matrix dolomites in this study are comparable to protodolomities values measured by McKenzie (1981) in the modern Abu Dhabi sabkhas and microdolomite values measured by Al-Aasm and Packard (2000) from the Dunvegan gas field.

a result, a significant portion of the organic content within the Debolt Formation is most likely derived in part from the organisms and their by-products (i.e., fecal material, burrow wall linings) occurring within a lagoonal setting. Consequently, the distribution of $\delta^{18}O$ in dolomite relative to calcite within burrows, at present, appears to be influenced the source of organic matter and depositional setting. Clearly, further work needs to be completed to better define these boundaries throughout the geological rock record.

Less depleted values are thought to result from dolomite formed either: (i) in association with early sulfate reduction (i.e., before pores become saturated with $\delta^{13}C$); or (ii) in sediments with little organic matter, where much of the CO_3^{2-} is derived from seawater (Compton, 1988; Mazzullo, 2000). It has been noted that $\delta^{13}C$ for dolomite precipitated in association with sulfate reduction in modern settings is initially very similar to $\delta^{13}C$ of calcite, but becomes progressively more depleted as sulfate-reducing conditions persist (Vasconcelos et al., 1995; Mazzullo, 2000). Studies of dolomite found associated with MSR in a modern lagoonal environment (e.g., Lagoa Vermelha, Brazil) suggest that dolomite is initially slightly $\delta^{13}C$ enriched relative to organic carbon, and becomes progressively depleted by as much as 5‰ upon shallow recrystallization (Vasconcelos and McKenzie, 1997). For this study, the majority of $\delta^{13}C$ values fall within 1‰ of seawater, although a few samples are as much as 2‰ less than the value of seawater. The similarity of $\delta^{13}C$ values measured in the present study with those measured in modern field and laboratory dolomite associated with MSR suggest that the zone of isotopically light dolomite (i.e., values occurring below the linear calcite trend) most likely formed under early sulfate reducing conditions.

The high degree of similarity of burrow and matrix dolomite $\delta^{13}C$ to seawater values suggests that dolomite formed near the sediment-water interface, under conditions of early sulfate reduction. This is envisaged as occurring potentially within a burrow environment, where sulfate reduction can occur adjacent to or within a burrow (Waslenchuk et al., 1983). It is therefore plausible that heterogeneities within the substrate, such as those made by bioturbation, helped promote dolomitization within the burrows in the Dunvegan gas field.

The presence of anoxia within the lagoonal portions of the carbonate ramp is supported the presence of monospecific assemblages of burrows such as *Chondrites* and *Zoophycos* (Facies 4) (Bromley and Ekdale, 1984; Ekdale and Mason, 1988; Miller, 1991). High concentrations of pyrite (Facies 3) and organic matter preserved within the microbial mats (Facies 2) also confirm anoxic conditions. It can therefore

be suggested that bottom seawater and uppermost sediment pore waters (i.e., burrowed zone) fluctuated from oxic to anoxic. The margins of the burrows walls, due to high organic carbon content, are also believed to have formed a localized reducing zone that allowed for MSR and localized dolomite precipitation.

From a reservoir viewpoint, early dolomitization was critical in preserving the micro-intercrystalline porosity within the burrow fabrics (Al-Aasm and Packard, 2000). Moreover, these dolomitized burrow fabrics commonly provided localized enhancement of permeabilities relative to the impermeable lime mud matrix (see Chapter 2). Becuase dolomitized burows develop anisotropic permeability networks (Gingras et al., 2007b; Gingras et al., 2012; Chapters 2 and 5), natural gas from the matrix most likely migrates into the higher permeability burrows through diffusion. Given the lateral extensiveness of Facies 4 across the Dunvegan Field (Fig. 6.5), proper identification during core logging and subsurface mapping is crucial to drilling success and optimal natural gas recovery.

6.8 CONCLUSIONS

In the Dunvegan gas field of northwestern Alberta, the Mississippian (Visean) Debolt Formation contains numerous indicators of sedimentation within a carbonate ramp setting. Among others, these include reoccurring intervals of patterned carbonate, monospecific assemblages of ichnofossils (e.g., *Chondrites*, *Planolites*), nodular anhydrite, biolaminated mudstones, and peloidal grainstones. The reduction of both fossils and burrows within the lagoonal settings indicates that physico-chemical stresses, such as reduced oxygen and fluctuating salinities, were prevalent during the Visean.

Evidence for burrow-mediated dolomitization, in addition to sabkha, is established when comparing calcite and dolomite isotope data from the burrows and adjacent matrix. The isotopic values for calcite follow a linear trend on a $\delta^{13}C$ versus $\delta^{18}O$ plot, while dolomite plots into two distinct zones either above or below the calcite linear trend. Dolomite that is $\delta^{13}C$ enriched relative to calcite is interpreted to be dolomite that formed in a zone of methanogenesis. The majority of dolomite measured, however, was depleted in $\delta^{13}C$ relative to average calcite values. This amount of isotopic depletion is similar to samples that are measured in laboratory and field-based studies where dolomite has been found in association with bacterial sulfate reduction coupled to the oxidation of organic carbon. High organic content, an essential component for MSR and subsequent near-surface dolomitization, is believed to have been derived in part from the organisms and their by-products.

6.9 REFERENCES CITED

Abed, A.M., and Schneider, W., 1980, A general aspect in the genesis of nodular limestones documented by the Upper Cretaceous limestones of Jordan: Sedimentary Geology, v. 26, p. 329-335.

Al-Aasm, I.S., 2000, Chemical and isotopic constraints for recrystallization of sedimentary dolomites from the Western Canada sedimentary basin: Aquatic Geochemistry, v. 6, p. 227-248.

Al-Aasm, I.S., and Packard, J.J., 2000, Stabilization of early-formed dolomite: A tale of divergence from two Mississippian dolomites: Sedimentary Geology, v. 131, p. 97-108.

Al-Youssef, M., Stow, D.A.V., and West, I.M., 2006, Salt Lake Area, northeastern part of Dukhan Sabkha, Qatar: *in* Khan, M.A., Böer, B., Kust, G.S., and Barth, H.-J., eds., Sabkha Ecosystems: Tasks for Vegetation Science (West and Central Asia). Springer, Netherlands, v. 42, p. 163-181.

Aller, R.C., 1982, The effects of macrobenthos on chemical properties of marine sediment and overlying water: *in* McCall, P.L., and Tevesz, M.J.S., eds., Animal-Sediment Relations: The Biogenic Alteration of Sediments. Plenum Press, New York, p. 53-102.

Aller R.C., 1994, Bioturbation and remineralization of sedimentary organic matter: Effects of redox oscillation: Chemical Geology, v. 114, p. 331-345.

Arvidson, R.S., and Mackenzie, F.T., 1999, The dolomite problem: Control of precipitation kinetics by temperature and saturation state: American Journal of Science, v. 299, p. 257-288.

Bathurst, R.G.C., 1966, Boring algae, micrite envelopes and lithification of molluscan biosparites: Geological Journal, v. 5, p. 15-32.

Beales, F.W., 1953, Dolomitic mottling in Palliser (Devonian) limestone, Banff and Jasper National Parks, Alberta: American Association of Petroleum Geologists Bulletin, v. 37, p. 2281-2293.

Behairy, A.K.A., Durgaprasada Rao, N.V.N., and El-Shater, A., 1991, A siliciclastic coastal sabkha, Red Sea Coast, Saudi Arabia: Journal of King Abdulaziz University (JKAU) Marine Science, v. 2, p. 65-77.

Bromley, R.G., 1996, Trace Fossils: Biology, Taphonomy and Applications, Second Edition. Chapman and Hall, London, United Kingdom, 361 p.

Bromley, R.G., and Ekdale, A.A., 1984, *Chondrites*: A trace fossil indicator of anoxia in sediments: Science, v. 224, p. 872-874.

Bruckschen, P., Oesmann, S., and Veizer, J., 1999, Isotope stratigraphy of the European Carboniferous: Proxy signatures for ocean chemistry, climate, and tectonics: Chemical Geology, v. 161, p. 127-163.

Budd, D.A., 1997, Cenozoic dolomites of carbonate islands: Their attributes and origin: Earth-Science Reviews, v. 42, p. 1-47.

Butler, G.P., 1969, Modern evaporite deposition and geochemistry of coexisting brines, the sabkha, Trucial Coast, Arabian Gulf: Journal of Sedimentary Petrology, v. 39, p. 70-89.

Canfield, D.E., Thamdrup, B., and Hansen, J.W., 1993, The anaerobic degradation of organic matter in Danish coastal sediments: Iron reduction, manganese reduction, and sulfate reduction: Geochimica et Cosmochimica Acta, v. 57, p. 3867-3883.

Cant, D.J., 1988, Regional structure and development of the Peace River Arch, Alberta: A Paleozoic failed-rift system?: Bulletin of Canadian Petroleum Geology, v. 36, p. 284-295.

Chapelle, F.H., Vroblesky, D.A., McMahon, P.B., Dubrovsky, N.M., Fujii, R.F., and Oaksford, E.T., 1995, Deducing the distribution of terminal electron-accepting processes in hydrologically diverse groundwater systems: Water Resources Research, v. 31, p. 359-371.

Choquette, P.W., and Pray, L.C., 1970, Geologic nomenclature and classification of porosity in sedimentary carbonates: American Association of Petroleum Geologists Bulletin, v. 54, p. 207-250.

Chow, N., and Longstaffe, F.J., 1995, Dolomites of the Middle Devonian Elm Point Formation, southern Manitoba: Intrinsic controls on early dolomitization: Bulletin of Canadian Petroleum Geology, v. 43, p. 214-225.

Cioppa, M.T., Al-Aasm, I.S., Symons, T.A., and Gillen, K.P., 2003, Dating penecontemporaneous dolomitization in carbonate reservoirs: Paleomagnetic, petrographic, and geochemical constraints: American Association of Petroleum Geologists Bulletin, v. 87, p. 71-88.

Compton, J.S., 1988, Degree of supersaturation and precipitation of organogenic dolomite: Geology, v. 16, p. 318-321.

Confer D.R., and Logan, B.E., 1998, Location of protein and polysaccharide hydrolytic activity in suspended and biofilm wastewater cultures: Water Research, v. 32, p. 31-38.

Craig, H., 1957, Isotopic standards for carbon and oxygen and correction factors for mass-spectrometric analysis of carbon dioxide: Geochimica et Cosmochimica Acta, v. 12, p. 133-149.

Corlett, H.J., and Jones, B., 2012, Petrographic and geochemical contrasts between calcite- and dolomite-filled burrows in the Middle Devonian Lonely Bay Formation, Northwest Territories, Canada: Implications for dolomite formation in Paleozoic burrows: Journal of Sedimentary Research, v. 82, p. 648-663.

Davies, G.R., 1970, Algal-laminated sediments, Gladstone Embayment, Shark Bay, Western Australia: *in* Logan, B.W., Davies, G.R., Read, J.F., and Cebulski, D.E., eds., Carbonate Sedimentation and Environments, Shark Bay, Western Australia. American Association of Petroleum Geologists, Memoir no. 13, p. 169-205.

Decho, A.W., 1990, Microbial exopolymer secretions in ocean environments: Their role(s) in food webs and marine processes: Oceanography and Marine Biology Annual Review, v. 28, p. 73-154.

Diedrich, C., Caldwell, M.W., and Gingras, M., 2011, High-resolution stratigraphy and palaeoenvironments of the intertidal flats to lagoons of the Cenomanian (Upper Cretaceous) of Hvar Island, Croatia, on the Adriatic Carbonate Platform: Carbonates and Evaporites, v. 26, p. 381-399.

Dimitrakopoulos, R., and Muehlenbachs, K., 1987, Biodegradation of petroleum as a source of ^{13}C-enriched carbon dioxide in the formation of carbonate cement: Chemical Geology, v. 65, p. 283-291.

Dixon, J., 1976, Patterned carbonate- a diagenetic feature: Bulletin of Canadian Petroleum Geology, v. 24, p. 450-456.

Douglas, R.J.W., Gabrielse, H., Wheeler, J.O., Stott, D.F., and Belyea, H.R., 1970, Geology of western Canada: *in* Douglas, R.J.W., ed., Geology and Economic Minerals of Canada. Geological Survey of Canada Economic Geology Report, no. 1, p. 366-488.

Durocher, S., and Al-Aasm, I.S., 1997, Dolomitization and neomorphism of Mississippian (Visean) upper Debolt Formation, Blueberry field, northeastern British Columbia: Geologic, petrologic, and chemical evidence: American Association of Petroleum Geologists Bulletin, v. 81, p. 954-977.

Ekdale, A.A., 1988, Pitfalls of paleobathymetric interpretations based on trace fossil assemblages: Palaios, v. 3, p. 464-472.

Ekdale, A.A., and Mason, T.R., 1988, Characteristic trace-fossil associations in oxygen-poor sedimentary environments: Geology, v. 16, p. 720-723.

Ekdale, A.A., and Lewis, D.W., 1991, The New Zealand *Zoophycos* revisited: Morphology, ethology, and paleoecology: Ichnos, v. 1, p. 183-194.

Enos, P., 1983, Shelf environment: *in* Scholle, P.A., Bebout, D.G., and Moore, C.H., eds., Carbonate Depositional Environments. American Association of Petroleum Geologists, Memoir no. 33, p. 267-295.

Epstein, S., Graf, D.L., and Degans, D.T., 1964, Oxygen isotope studies on the origin of dolomite: *in* Craig, H., Miller, S.L., and Wasserburg, J.G., eds., Isotopic and Cosmic Chemistry. North-Holland Publishing Co., Amsterdam, Netherlands, p. 169-180.

Evans, G., 1966, The recent sedimentary facies of the Persian Gulf region: Philosophical Transactions of the Royal Society A, v. 259, p. 291-298.

Franks, J., and Stolz, J.F., 2009, Flat laminated microbial mat communities: Earth Science Reviews, v. 96, p. 163-172.

Froelich, P.N., Klinkhammer, G.P., Bender, M.L., Luedtke, N., Heath, G.R., Cullen, D., Dauphin, P., Hammond, D., Hartman, B., and Maynard, V., 1979, Early oxidation of organic matter in pelagic sediments of the eastern equatorial Atlantic; suboxic diagenesis: Geochimica et Cosmochimica Acta, v. 43, p. 1075-1090.

Garrison, R.E., and Luternauer, J.L., 1971, Textures of calcitic cements formed during early diagenesis, Fraser Delta, British Columbia: *in* Bricker, O.P., ed., Carbonate Cements. Johns Hopkins Press, Baltimore, Maryland, p. 151-154.

Gerdes, G., Klenke, T., and Noffke, N., 2000, Microbial signatures in peritidal siliciclastic sediments: A catalogue: Sedimentology, v. 47, p. 279-308.

Gingras, M.K., Pemberton, S.G., Muelenbachs, K., and Machel, H., 2004, Conceptual models for burrow-related, selective dolomitization with textural and isotopic evidence from the Tyndall Stone, Canada: Geobiology, v. 2, p. 21-30.

Gingras, M.K., Bann, K.L., MacEachern, J.A., Waldron, J., and Pemberton, S.G., 2007a, A conceptual framework for the application of trace fossils: *in* MacEachern, J.A., Bann, K.L., Gingras, M.K., and Pemberton, S.G., eds., Applied Ichnology. Society of Economic Paleontologists and Mineralogists (SEPM), Short Course Notes, no. 52, p. 1-26.

Gingras, M.K., Pemberton, S.G., Henk, F., MacEachern, J.A., Mendoza, C.A., Rostron, B., O'Hare, R., and Spila, M.V., 2007b, Applications of ichnology to fluid and gas production in hydrocarbon reservoirs: *in* MacEachern, J.A., Bann, K.L., Gingras, M.K., and Pemberton, S.G., eds., Applied Ichnology. Society of Economic Paleontologists and Mineralogists (SEPM), Short Course Notes, no. 52, p. 129-143.

Gingras, M.K., Baniak, G., Konhauser, K.O., La Croix, A., Lemiski, R., Mendoza, C., Pemberton, S.G., Polo, C., and Zonneveld, J.-P., 2012, Porosity and permeability in bioturbated sediments: *in* Knaust, D., and Bromley, R.G., eds., Trace Fossils as Indicators of Sedimentary Environments. Developments in Sedimentology 64, Elsevier, Amsterdam, p. 837-868.

Gunatilaka, A., 1987, The dolomite problem in the light of the recent studies: Modern Geology, v. 11, p. 311-324.

Gunatilaka, A., Al-Zamel, A., Shearman, D.J., and Reda, A., 1987, A spherulitic fabric in selectively dolomitized siliciclastic crustacean burrows, northern Kuwait: Journal of Sedimentary Petrology, v. 57, p. 922-927.

Gunnarsson, J.S., Granberg, M.E., Nilsson, H.C., Rosenberg, R., and Hellman, B., 1999a, Influence of sediment organic matter quality on growth and polychlorobiphenyl bioavailability in *Echinodermata* (*Amphiura filiformis*): Environmental Toxicology and Chemistry, v. 18, p. 1534-1543.

Gunnarsson, J.S., Hollertz, K., and Rosenberg, R., 1999b, Effects of organic enrichment and burrowing activity of the polychaete Neries diversicolor on the fate of tetrachlorobiphenyl in marine sediments: Environmental Toxicology and Chemistry, 18: 1149-1156.

Hardie, L.A., 2003, Anhydrite and gypsum: *in* Middleton, G.V., ed., Encyclopedia of Sediments and Sedimentary Rocks. Kluwer Academic Publishers, Dordrecht, p. 16-19.

Hauck, T.E., Dashtgard, S.E., and Gingras, M.K., 2008, Relationships between organic carbon and Pascichnia morphology in intertidal deposits: Bay of Fundy, New Brunswick, Canada: Palaios, v. 23, p. 336-343.

Hein, F.J., 1999, Mixed ("multi") fractal analysis of Granite Wash fields/pools and structural lineaments, Peace River Arch area, northwestern Alberta, Canada: A potential approach for use in hydrocarbon exploration: Bulletin of Canadian Petroleum Geology, v. 47, p. 556-572.

Hsü, K.J., and Siegenthaler, C., 1969, Preliminary experiments on hydrodynamic movement induced by evaporation and their bearing on the dolomite problem: Sedimentology, v. 12, p. 11-25.

James, N.P., and Kendall, A.C., 1992, Introduction to carbonate and evaporite facies models: *in* Walker, R.G., and James, N.P., eds., Facies Models: Response to Sea Level Change. Geological Association of Canada, St. John's, Newfoundland, p. 265-276.

Jin, J., Harper, D.A.T., Rasmussen, J.A., Rasmussen, C.M.Ø., and Stouge, S., 2008, Occurrence of the Late Ordovician Red River lithofacies and biofacies in North Greenland: Canadian Paleontology Conference Proceedings, v. 6, p 18-21.

Jin, J., Harper, D.A.T., Rasmussen, J.A., and Sheehan, P.M., 2012, Late Ordovician massive-bedded Thalassinoides ichnofacies along the palaeoequator of Laurentia: Palaeogeography, Palaeoclimatology, Palaeoecology, v. 367-368, p. 73-88.

Kendall, A.C., 1977a, Origin of dolomite mottling in Ordovician limestones from Saskatchewan and Manitoba: Bulletin of Canadian Petroleum Geology, v. 25, p. 450-504.

Kendall, A.C., 1977b, Patterned carbonate- a diagenetic feature by James Dixon. Discussion: Bulletin of Canadian Petroleum Geology, v. 25, p. 695-697.

Kendall, A.C., 2010, Marine evaporites: *in* James, N.P., and Dalrymple, R.W., eds., Facies Models 4. Geological Association of Canada, St. John's, Newfoundland, p. 505-539.

Keswani, A.D., 1999, An integrated ichnological perspective for carbonate diagenesis: University of Alberta M.Sc. Thesis, Unpublished, 124 p.

Kirkham, A., 2004, Patterned dolomites: Microbial origins and clues to vanished evaporites in the Arab Formation, Upper Jurassic, Arabian Gulf: *in* Braithwaite, C.J.R., Rizzi, G., and Darke, G., eds., The Geometry and Petrogenesis of Dolomite Hydrocarbon Reservoirs. Geological Society, London, Special Publication, v. 235, p. 301-308.

Holland, S.M., and Patzkowsky, M.E., 2009, The stratigraphic distribution of fossils in a tropical carbonate succession: Ordovician Bighorn Dolomite, Wyoming, USA: Palaios, v. 24, p. 303-317.

Konhauser, K.O., 2007, Introduction to Geomicrobiology. Blackwell Sciences, Oxford, 440 p.

Konhauser, K.O., and Gingras, M.K., 2007, Linking geomicrobiology with ichnology in marine sediments: Palaios, v. 22, p. 339-342.

Konhauser, K.O., and Gingras, M.K., 2011, Are animal burrows a major sedimentary sink for metals?: Ichnos, v. 18, p. 144-146.

Krause, S., Liebetrau, V., Gorb, S., Sánchez-Romá, M., McKenzie, J.A., and Treude, T., 2012, Microbial nucleation of Mg-rich dolomite in exopolymeric substances under anoxic modern seawater salinity: New insight into an old enigma: Geology, v. 40, p. 587-590.

Kristensen, E., 2000, Organic matter diagenesis at the oxic/anoxic interface in coastal marine sediments, with emphasis on the role of burrowing animals: Hydrobiologia, v. 426, p. 1-24.

Krumbein, W.C., and Garrels, R.M., 1952, Origin and classification of chemical sediments in terms of pH and oxidation-reduction potentials: Journal of Geology, v. 60, p. 1-33.

Krumbein, W.E., 1994, The year of the slime: *in* Krumbein, W.E., Paterson, D.M., and Stall, L.J., eds., Biostabilization of Sediments. University of Oldenburg, Oldenburg, Germany, p. 1-7.

Krumbein, W.E., and Cohen, Y., 1977, Primary production, mat formation and lithification: Contribution of oxygenic and facultative anoxygenic cyanobacteria: *in* Flügel, E., ed., Fossil Algae: Resent Results and Development. Springer-Verlag, Berlin, p. 37-56.

Lalonde, S.V., Dafoe, L., Pemberton, S.G., Gingras, M.K., and Konhauser, K.O., 2010, Investigating the geochemical impact of burrowing animals: Proton and cadmium adsorption onto the mucus-lining of *Terebellid* polychaete worms: Chemical Geology, v. 271, p. 44-51.

Land, L.S., 1980, The isotopic and trace element geochemistry of dolomite: The state of the art: *in* Zenger, D.H., Dunham, J.B., and Ethington, R.L., eds., Concepts and Models of Dolomitization. Society of Economic Paleontologists and Mineralogists (SEPM), Special Publication, v. 28, p. 87-110.

Land, L.S., 1998, Failure to precipitate dolomite at 25°C from dilute solutions despite 1000-fold oversaturation after 32 years: Aquatic Geochemistry, v. 4, p. 361-368.

Land, L.S., and Moore, C.H., 1980, Lithification, micritization and syndepositional diagenesis of biolithies on the Jamaican Island slope: Journal of Sedimentary Petrology, v. 50, p. 357-370.

Law, J., 1981, Mississippian correlations, northeastern British Columbia, and implications for oil and gas exploration: Bulletin of Canadian Petroleum Geology, v. 29, p. 378-398.

Lindsay, R.F., Cantrell, D.L., Hughes, G.W., Keith, T.H., Mueller III, H.W., and Russell, S.D., 2006, Ghawar Arab-D reservoir: Widespread porosity in shoaling-upward carbonate cycles, Saudi Arabia: *in* Harris, P.M., and Weber, L.J., eds., Giant Hydrocarbon Reservoirs of the World: From Rocks to Reservoir Characterization and Modeling. American Association of Petroleum Geologists, Memoir no. 88/Society of Economic Paleontologists and Mineralogists (SEPM) Special Publication, p. 97-147.

Logan, B.W., 1961, Cryptozoon and associate stromatolites from the recent, Shark Bay, Western Australia: Journal of Geology, v. 69, p. 517-533.

Macauley, G., 1958, Late Paleozoic of Peace River area: *in* Woodman, A.J., ed., Jurassic and Carboniferous of Western Canada. American Association of Petroleum Geologists, John Andrew Allan Memorial Volume, p. 289-308.

MacEachern, J.A., Pemberton, S.G., Bann, K.L., and Gingras, M.K., 2007, Departures from the archetypal ichnofacies: Effective recognition of environmental stress in the rock record: *in* MacEachern, J.A., Bann, K.L., Gingras, M.K., and Pemberton, S.G., eds., Applied Ichnology. Society of Economic Paleontologists and Mineralogists (SEPM), Short Course Notes, no. 52, p. 65-92.

Machel, H.G., 1993, Anhydrite nodules formed during deep burial: Journal of Sedimentary Petrology, v. 63, p. 659-662.

Machel, H.G., 2004, Concepts and models of dolomitization: A critical appraisal: *in* Braithwaite, C.J.R., Rizzi, G., and Darke, G., eds., The Geometry and Petrogenesis of Dolomite Hydrocarbon Reservoirs. Geological Society, London, Special Publication, v. 235, p. 7-63.

Machel, H.G., and Mountjoy, E.W., 1986, Chemistry and environments of dolomitization- a reappraisal: Earth Science Reviews, v. 23, p. 175-222.

Machel, H.G., and Burton, E.A., 1991, Burial-diagenetic sabkha-like gypsum and anhydrite nodules: Journal of Sedimentary Petrology, v. 61, p. 394-405.

Markham, G.D., Glusker, J.P., and Bock, C.W., 2002, The arrangement of first- and second-sphere water molecules in divalent magnesium complexes: Results from molecular orbital and density functional theory and from structural crystallography: The Journal of Physical Chemistry B, v. 106: p. 5118-5134.

Mayer, C., Moritz, R., Kirschner, C., Borchard, W., Maibaum, R., Wingender, J., and Flemming, H.-C., 1999, The role of intermolecular interactions: Studies on model systems for bacterial biofilms: International Journal of Biological Macromolecules, v. 26, p. 3-16.

Mazzullo, S.J., 2000, Organogenic dolomitization in peritidal to deep-sea sediments: Journal of Sedimentary Research, v. 70, p. 10-23.

McCrea, J.M., 1950, On the isotopic chemistry of carbonates and a paleotemperature scale: The Journal of Chemical Physics, v. 18, p. 849-857.

McKenzie, J.A., 1981, Holocene dolomitization of calcium-carbonate sediments from the coastal sabkhas of Abu Dhabi, U.A.E.: A stable isotope study: Journal of Geology, v. 89, p. 185-198.

McKenzie, J.A., 1991, The dolomite problem: An outstanding controversy: *in* Müller, D.W., McKenzie, J.A., and Weissert, H., eds., Controversies in Modern Geology: Evolution of Geological Theories in Sedimentology, Earth history, and Tectonics. Academic Press, London, p. 37-54.

Miller, M.F., 1991, Morphology and paleoenvironmental distribution of Paleozoic *Spirophyton* and *Zoophycos*: Implications for the *Zoophycos* ichnofacies: Palaios, v. 6, v. 410-425.

Morrow, D.W., 1978, Dolomitization of Lower Paleozoic burrow fillings: Journal of Sedimentary Petrology, v. 48, p. 295-306.

Morrow, D.W., 1982, Diagenesis 1: Dolomite-part 1, the chemistry of dolomitization and dolomite precipitation: Geoscience Canada, v. 9, p. 5-13.

Needham, S.J., Worden, R.H., and McIlory, D., 2004, Animal sediment interactions: The effect of ingestion and excretion by worms on mineralogy: Biogeosciences, v. 1, p. 113-121.

Nicholson, J.A.M., Stolz, J.F., and Pierson, B.K., 1987, Structure of a microbial mat in a saltmarsh: Federation of European Microbiological Societies (FEMS) Microbiology Ecology, v. 45, p. 343-364.

Nimegeers, A.R., and Qing, H., 2002, Depositional model of the Mississippian Midale Beds, Steelman Field, southeastern Saskatchewan: Summary of Investigations, Saskatchewan Geological Survey, Industry and Resources, p. 47-67.

Northrop, D.A., and Clayton, R.N., 1966, Oxygen-isotope fractionations in systems containing dolomite: Journal of Geology, v. 74, p. 174-196.

O'Connell, S.C., Dix, G.R., and Barclay, J.E., 1990, The origin, history, and regional structural development of the Peace River Arch, Western Canada: Bulletin of Canadian Petroleum Geology, v. 38A, p. 4-24.

O'Connell, S.C., 1994, Geological history of the Peace River Arch: *in* Mossop, G. D., and Shetsen, I., comps., Geological Atlas of the Western Canada Sedimentary Basin. Canadian Society of Petroleum Geologists and Alberta Research Council, p. 431-438.

O'Neil, J.R., and Epstein, S., 1966, Oxygen isotope fractionation in the system dolomite-calcite-carbon dioxide: Science, v. 152, p. 198-201.

Packard, J.J., Al-Aasm, I.S., and Devon Canada Exploration Team., 2004, Reflux dolomitization of Mississippian-age sabkha and restricted subtidal sediments resulting in a 1.6 Tcf giant gas field: The Upper Debolt Formation of west-central Alberta. Canadian Society of Petroleum Geologists, Core Seminar and Abstracts, Calgary, Alberta, 26 p.

Pak, R., and Pemberton, S.G., 2003, Ichnology of the Yeoman Formation; *in* Summary of Investigation, Saskatchewan Geological Survey: Saskatchewan Industry and Resources, Misc. Rep. 2003-4.1, CD-ROM, v. 1, Paper A-3, 16 p.

Pak, R., Pemberton, S.G., and Stasiuk, L., 2010, Paleoenvironmental and taphonomic implications of trace fossils in Ordovician kukersites: Bulletin of Canadian Petroleum Geology, v. 58, p. 141-158.

Pemberton, S.G., and Gingras, M.K., 2005, Classification and characterizations of biogenically enhanced permeability: American Association of Petroleum Geologists Bulletin, v. 89, p. 1493-1517.

Peterhänsel, A., 2003, Depositional dynamics of a giant carbonate platform- The Fammennian Palliser Formation of western Canada: University of Saskatchewan PhD Thesis, Unpublished, 220 p.

Petrash, D.A., Lalonde, S.V., Gingras, M.K., and Konhauser, K.O., 2011, A surrogate approach to studying the chemical reactivity of burrow mucous linings in marine sediments: Palaios, v. 26, p. 595-602.

Qing, H., and Nimegeers, A.R., 2008, Lithofacies and depositional history of Midale carbonate-evaporite cycles in a Mississippian ramp setting, Steelman-Bienfait area, southeastern Saskatchewan, Canada: Bulletin of Canadian Petroleum Geology, v. 56, p. 209-234.

Rameil, N., 2008, Early diagenetic dolomitization and dedolomitization of Late Jurassic and earliest Cretaceous platform carbonates: A case study from the Jura Mountains (NW Switzerland, E France): Sedimentary Geology, v. 212, p. 70-85.

Reeburgh, W.S., 1980, Anaerobic methane oxidation: Rate depth distributions in Skan Bay sediments: Earth and Planetary Science Letters, v. 47, p. 345-352.

Reitsema, R.H., 1980, Dolomite and nahcolite formation in organic rich sediments: Isotopically heavy carbonates: Geochimica et Cosmochimica Acta, v. 44, p. 2045-2049.

Richards, B.C., 1989, Upper Kaskaskia sequence: Uppermost Devonian and Lower Carboniferous: *in* Ricketts, B.D., ed., Western Canada Sedimentary Basin: A Case History. Canadian Society of Petroleum Geologists, p. 165-201.

Richards, B.C., Bamber, E.W., Higgins, A.C., and Utting, J., 1993, Carboniferous: *in* Stott, D.F., and Aitken, J.D., eds., Sedimentary Cover of the Craton in Canada. Geological Survey of Canada, Geology of Canada, no. 5, p. 202-271.

Richards, B.C., Barclay, J.E., Bryan, D., Hartling, A., Henderson, C.M., and Hinds, R.C., 1994, Carboniferous strata of the western Canada sedimentary basin: *in* Mossop, G.D., and Shetsen, I., comps., Geological Atlas of the Western Canada Sedimentary Basin. Canadian Society of Petroleum Geologists and Alberta Research Council, p. 221-249.

Roberts, J.A., Bennett, P.C., Gonzales, L.A., Macpherson, G.L., and Milliken, K.L., 2004, Microbial precipitation of dolomite in methanogenic groundwater: Geology, v. 32, p. 277-280.

Sibley, D.F., and Gregg, J.M., 1987, Classification of dolomite rock textures: Journal of Sedimentary Petrology, v. 57, p. 967-975.

Steward C.C., Nold, S.C., Ringelberg, D.B., White, D.C., and Lovell, C.R., 1996, Microbial biomass and community structures in the burrows of bromophenol producing and non-producing marine worms and surrounding sediments: Marine Ecology Progress Series, v. 133, p. 149-165.

Stolz, J.F., 1990, Distribution of phototrophic microbes in the flat laminated microbial mat at Laguna Figueroa, Baja California, Mexico: Biosystems, v. 23, p. 345-357.

Swart, P.K., Cantrell, D.L., Westphal, H., Handford, C.R., and Kendall, C.G., 2005, Origin of Dolomite in the Arab-D Reservoir from the Ghawar Field, Saudi Arabia: Evidence from petrographic and geochemical constraints: Journal of Sedimentary Research, v. 75, p. 476-491.

Taylor, M.E., and Halley, R.B., 1974, Systematics, environments, and biogeography of some Late Cambrian and Early Ordovician trilobites from eastern New York State: United States Geological Survey Professional Paper 834, 38 p.

Thompson, L.C., and Pritchard, A.C., 1969, Osmoregulatory capacities of *Callianassa* and *Upogebia* (Crustacea: Thalassinidea): Biological Bulletin, v. 136, p. 114-129.

van Lith, Y., Warthmann, R., Vasconcelos, C., and McKenzie, J.A., 2003, Sulfate-reducing bacteria induce low-temperature Ca-dolomite and high Mg-calcite formation: Geobiology, v. 1, p. 71-79.

Vasconcelos, C., and McKenzie, J.A., 1997, Microbial mediation of modern dolomite precipitation and diagenesis under anoxic conditions (Lagoa Vermelha, Rio de Janeiro, Brazil): Journal of Sedimentary Research, v. 67, p. 378-390.

Vasconcelos, C., McKenzie, J.A., Bernasconi, S., Grujic, D., and Tien, A.J., 1995, Microbial mediation as a possible mechanism for natural dolomite formation at low temperatures: Nature, v. 377, p. 220-222.

Vasconcelos, C., McKenzie, J.A., Warthmann, R., and Bernasconi, S.M., 2005, Calibration of the $\delta^{18}O$ paleothermometer for dolomite precipitated in microbial cultures and natural environments: Geology, v. 33, p. 317-320.

Wacey, D., Wright, D.T., and Boyce, A.J., 2007, A stable isotope study of microbial dolomite formation in the Coorong Region, South Australia: Chemical Geology, v. 244, p. 155-174.

Warren, J.K., 2000, Dolomite: Occurrence, evolution and economically important associations: Earth-Science Reviews, v. 52, p. 1-81.

Warren, J.K., and Kendall, C.G.S., 1985, Comparison of sequences formed in marine sabkha (subaerial) and salina (subaqueous) settings- modern and ancient: American Association of Petroleum Geologists Bulletin, v. 89, p. 1013-1023.

Warthmann, R., Lith, Y.V., Vasconcelos, C., McKenzie, J.A., and Karpoff, A.M., 2000, Bacterially induced dolomite precipitation in anoxic culture experiments: Geology, v. 28, p. 1091-1094.

Warthmann, R., Vasconcelos, C., Sass, H., and McKenzie, J.A., 2005, *Desulfovibrio brasiliensis* sp. nov., a moderate halophilic sulfate-reducing bacterium from Lagoa Vermelha (Brazil) mediating dolomite formation: Extremephiles, v. 9, p. 255-261.

Waslenchuk, D.G., Matson, E.A., Zajac, R.N., Dobbs, F.C., and Tramontano, J.M., 1983, Geochemistry of burrow waters vented by a bioturbating shrimp in Bermudian sediments: Marine Biology, v. 72, p. 219-225.

Wright, D.T., and Wacey, D., 2005, Precipitation of dolomite using sulfate-reducing bacteria from the Coorong Region, South Australia: Significance and implication: Sedimentology, v. 52, p. 987-1008.

Zenger, D.H., 1992, Burrowing and dolomitization patterns in the Steamboat Point Member, Bighorn Dolomite (Upper Ordovician), northwest Wyoming: Contributions to Geology, v. 29, p. 133-142.

Zenger, D.H., 1996, Dolomitization patterns in widespread 'Bighorn Facies' (Upper Ordovician), Western Craton, USA: Carbonates and Evaporites, v. 11, p. 219-225.

CHAPTER 7: SUMMARY AND CONCLUSIONS

This thesis has approached the characterization of subsurface hydrocarbon reservoirs using a unique blend of ichnology, sedimentology, and geochemistry. Instead of focusing solely on depositional environment characterization and trace fossil identification, this thesis has instead explored the utility of using trace fossils to evaluate reservoir quality and better understand burrow-associated diagenesis. Using the biogenic permeability classification scheme outlined by Pemberton and Gingras (2005) as a foundation, subsurface examples from offshore Norway (Upper Jurassic Ula Formation) and western Alberta, Canada (Upper Devonian Wabamun Group/Palliser Formation and Mississippian Debolt Formation) were used as a database to explore the influence trace fossils have on reservoir quality and burrow diagenesis.

Three major concepts were presented in this thesis. Firstly, the value of using two- and three-dimensional (2D and 3D) imaging techniques to visualize trace fossils and permeability contrasts within core samples was shown using X-ray microtomography (micro-CT) and helical computed tomography (helical-CT). Secondly, detailed characterization of fluid flow within carbonate (Wabamun Group) and siliclastic (Ula Formation) reservoirs was presented using numerical models and conceptual ideas. Thirdly, the characterization of burrow diagenesis (Debolt Formation) was examined. To a large degree, most of these applications outlined above are not independent from one another and therefore cannot be separated. As a result, most of the chapters presented in this thesis demonstrate a mixture of these applications.

7.1 IMAGINING OF BURROW FABRICS

Chapter 2 explored the value of using micro-CT to examine burrow fabrics and their associated permeabilities in 2D and 3D. Among the key findings was that X-ray attenuation (transmissivity or absorptivity of a sample to the incident X-rays) of the burrows and matrix is commonly different due to factors such as grain size and sorting (i.e., porosity). This was found to be particularly true for samples with moderate to extreme contrasts in lithology and permeability. As such, the micro-CT images were able to help show the complexity in burrow connectivity and burrow orientation within a sample. Perhaps more importantly, by using the 2D and 3D micro-CT volumes of the burrow fabrics, clearer quantification of the permeability distribution within a core sample was made.

For the these reasons outlined above, this thesis proposes that reservoir

geologists and engineers further consider the ichnological data presented in Chapter 2 when evaluating reservoirs. For example, when the micro-CT was used in conjunction with helical-CT in Chapter 5, detailed images of the vertical and horizontal orientations of burrow fabrics in core samples from the Wabamun Group were obtained. In short, both the micro-CT and helical-CT images show that the dimensions and orientations of the burrows are highly variable at the millimeter to centimeter scale, with horizontal connectivity being most common. Consequently, fluid flow within the Wabamun Group is believed to be anisotropic with a preferred bedding parallel flow direction. As such, the permeable dolomitized burrows are spatially heterogeneous and therefore difficult to assess based solely on thin sections and core samples. Consequently, it is believed that utilization of micro-CT and helical-CT on bioturbated samples will help enhance reservoir models and hence make them more accurate.

7.2 FLUID FLOW IN BIOTURBATED FABRICS

Chapter 4 explores the relationship between bioturbation and fluid flow within the Upper Jurassic Ula Formation of the Norwegian Central Graben. Using the depositional fabrics outlined in Chapter 3 as a foundation, it was observed using thin sections and spot-permeametry that that burrow fabrics within the Ula Formation represent examples of weakly defined and cryptic textural heterogeneities (after Pemberton and Gingras, 2005). Both of these biogenic heterogeneities represent dual-porosity flow networks and their influence on fluid flow was categorized using analytical arithmetic, harmonic, and geometric modeling techniques. It was observed that harmonic mean best characterized samples with low bioturbation intensities or vertical burrows and would therefore conceptually represent examples of the archetypal *Skolithos* ichnofacies (e.g., MacEachern et al., 2007). The arithmetic mean was observed to best characterize intervals dominated by high bioturbation intensities or horizontal to sub-vertical burrows and would therefore conceptually include examples of the distal *Skolithos* to proximal *Cruziana* ichnofacies (e.g., MacEachern et al., 2007). The geometric mean was found to best characterize cryptically bioturbated samples, as both the vertical and horizontal permeabilities are roughly equivalent.

To quantify the influence of bioturbation on fluid flow, SBED numerical modeling was performed on examples of *Ophiomorpha* populated within two different sedimentary fabrics (laminated sandstones and massive appearing sandstones). In short, horizontal mud layers and low bioturbation intensities were

found to promote bedding-parallel fluid flow in the laminated sandstone model. Conversely, fluid flow was found to exhibit increasingly isotropic behaviors at higher bioturbation intensities due to higher levels of burrow interpenetrations across the mud layers. Within the massive appearing sandstone model, fluid flow was found to be controlled dominantly by bioturbation intensity as no flow barriers existed. As such, low levels of bioturbation resulted in only minor influences on fluid flow. At higher bioturbation intensities, greater burrow interconnectivity occurred and an enhancement of both vertical and horizontal burrow permeabilities resulted. Because of the dual-porosity nature of the Ula Formation, the greatest fluid flow will therefore occur within the burrows and interaction with the surrounding matrix will be moderate to extensive.

Using concepts similar to those presented in Chapter 4, categorization of fluid flow within carbonates was examined in Chapter 5 using the Upper Devonian Wabamun Group as an example. Representing an example of a diagenetic textural heterogeneity (after Pemberton and Gingras, 2005), the burrows are dolomitized and contain enhanced permeabilities relative to the surrounding lime mud matrix. Because the permeabilities within the matrix are commonly below 1 mD, while burrows comprise permeabilities ranging from 1 to 350 mD, the Wabamun Group represents a mixture of dual-porosity and dual-permeability flow fabrics. The dolomitized burrows signify the primary flow conduits that deliver natural gas from the matrix, with greater fluid flux occurring within the dual-permeability fabrics. Ichnofossil Hosted Tight Gas (IHG) is a new term introduced in Chapter 5 to demarcate such occurrences within the geological rock record.

Using this data, along with examples from subsurface wells in the Pine Creek gas field in west-central Alberta, Canada, conceptual models assessing fluid flow within an IHG reservoir were presented. In brief, it is believed that the majority of the natural gas will remain stored within the matrix regardless of burrow permeability in scenarios where burrow-associated dolomite is minimal. On the other hand, in scenarios where burrow-associated dolomite is abundant, the burrows will act as the primary flow conduits as they help increase the overall amount of flow media. Although this interpretation is limited to the Wabamun Group, it is thought that this data will have significant application to other subsurface reservoirs with comparable IHG properties. Consequently, the potential for work in other bioturbated tight gas reservoirs is massive.

7.3 BURROW-ASSOCIATED DIAGENESIS

Chapter 6 explores the influence trace fossils have in mediating dolomitization within the Debolt Formation. As a whole, dolomitization occurs primarily within the oxidized muds and highly bioturbated sediments in the Debolt Formation, with the primary mode being sabkha-associated precipitation (Al-Aasm, 2000; Al-Aasm and Packard, 2000; Cioppa et al., 2003).

In this context, dolomitization within the burrows also appears to be mediated by sulfate-reducing bacteria. Measured $\delta^{13}C$ and $\delta^{18}O$ values for dolomite within burrows are enriched slightly compared to relative measured calcite values within the burrows. The trends revealed by the oxygen isotopes suggest that dolomite and calcite precipitated from the same solution. Likewise, the carbon isotopic trends are similar to modern dolomite that has precipitated in equilibrium with seawater. Within these modern settings (e.g., Lagoa Vermelha, Brazil), concomitant sulfate reduction and organic carbon-oxidation is inferred to occur near the surface and therefore help mediate dolomitization.

From an ichnological and sedimentological viewpoint, dolomitization commonly occurs within intervals of patterned carbonate and monospecific assemblages of trace fossils. These two intervals are interpreted to represent a restricted lagoon setting (e.g., Butler, 1969; Dixon, 1976; Bromley and Ekdale, 1984; Ekdale and Mason, 1988) and physico-chemical stresses such as anoxia and elevated pH levels were likely prominent. As the geochemical results indicated, an abundance of organic carbon associated with the burrows, coupled with periods of anoxia and elevated pH, probably provided favorable conditions for the development of localized dolomitization within the burrows.

Although research into burrow-mediated dolomitization is still in its infancy (examples of the most recent work includes Gingras et al., 2004; Rameil, 2008; and Corlett and Jones, 2012), Chapter 6 helps underscore the benefit of using ichnology to interpret dolomitized successions. In the case of the Debolt Formation, an additional mechanism other than sabkha was introduced to help explain dolomitization.

7.4 APPLICABILITY

As outlined in the Introduction, the ever-increasing demand for hydrocarbons has resulted in a significant shift in paradigm within the petroleum industry. Focus has now been shifted towards hydrocarbon deposits once considered non-producible or uneconomical (e.g., Fort McMurray oil sands, deep-sea drilling in the arctic, shale oil and gas). Many of these new reservoir deposits, both conventional

and unconventional, contain intervals that are moderately to highly bioturbated. Accordingly, the incorporation of biogenic permeability into the realm of reservoir modeling is essential if we are to prolong the lifespan of current oil and gas fields and maximize recovery from future reservoir intervals.

Through integrating ichnological, sedimentological, and geochemical data into different datasets in this thesis, innovative theories and ideas have blossomed into practical solutions for understanding bioturbated intervals (e.g., IHG reservoirs). The data presented in this thesis is unique in that it combines paleoenvironmental interpretation, sample imaging, numerical fluid flow modeling, isotopic analysis, and conceptual models to categorize bioturbated reservoirs. In short, many of the methods and ideas presented in this thesis should find applicability in both academic and industry settings.

For example, analytical and numerical models in Chapters 4 and 5 showed the complexity in fluid flow in both carbonates and siliciclastics by using data obtained from core analysis, sample imaging, thin sections, and spot-permeametry measurements. For reservoir engineers and geologists, this type of data is of critical importance and should be undoubtedly incorporated into their models if a better understanding of flow barriers and fluid recovery is desired. Diagenetic models presented in Chapter 6, though generally academic, have helped shift the focus from regional scale processes (e.g., sabkha) to small-scale processes occurring within the burrows (e.g., microbial sulfate reduction). Although most likely to find limited application within the petroleum industry in the near future, it does represent a significant shift in paradigm for geologists wishing to understand the diagenetic history of a bioturbated deposit and will likely continue to be debated and studied for many years to come.

7.5 REFERENCES CITED

Al-Aasm, I.S., 2000, Chemical and isotopic constraints for recrystallization of sedimentary dolomites from the Western Canada sedimentary basin: Aquatic Geochemistry, v. 6, p. 227-248.

Al-Aasm, I.S., and Packard, J.J., 2000, Stabilization of early-formed dolomite: A tale of divergence from two Mississippian dolomites: Sedimentary Geology, v. 131, p. 97-108.

Bromley, R.G., and Ekdale, A.A., 1984, *Chondrites*: A trace fossil indicator of anoxia in sediments: Science, v. 224, p. 872-874.

Butler, G.P., 1969, Modern evaporite deposition and geochemistry of coexisting brines, the sabkha, Trucial Coast, Arabian Gulf: Journal of Sedimentary Petrology, v. 39, p. 70-89.

Cioppa, M.T., Al-Aasm, I.S., Symons, T.A., and Gillen, K.P., 2003, Dating penecontemporaneous dolomitization in carbonate reservoirs: Paleomagnetic, petrographic, and geochemical constraints: American Association of Petroleum Geologists Bulletin, v. 87, p. 71-88.

Corlett, H.J., and Jones, B., 2012, Petrographic and geochemical contrasts between calcite- and dolomite-filled burrows in the Middle Devonian Lonely Bay Formation, Northwest Territories, Canada: Implications for dolomite formation in Paleozoic burrows: Journal of Sedimentary Research, v. 82, p. 648-663.

Dixon, J., 1976, Patterned carbonate- a diagenetic feature: Bulletin of Canadian Petroleum Geology, v. 24, p. 450-456.

Ekdale, A.A., and Mason, T.R., 1988, Characteristic trace-fossil associations in oxygen-poor sedimentary environments: Geology, v. 16, p. 720-723.

Gingras, M.K., Pemberton, S.G., Muelenbachs, K., and Machel, H., 2004, Conceptual models for burrow-related, selective dolomitization with textural and isotopic evidence from the Tyndall Stone, Canada: Geobiology, v. 2, p. 21-30.

MacEachern, J.A., Bann, K.L., and Gingras, M.K., and Pemberton, S.G., 2007a, The ichnofacies paradigm: High-resolution paleoenvironmental interpretation of the rock record: in MacEachern, J.A., Bann, K.L., Gingras, M.K., and Pemberton, S.G., eds., Applied Ichnology. Society of Economic Paleontologists and Mineralogists (SEPM), Short Course Notes, no. 52, p. 27-64.

Pemberton, S.G., and Gingras, M.K., 2005, Classification and characterizations of biogenically enhanced permeability: American Association of Petroleum Geologists Bulletin, v. 89, p. 1493-1517.

Rameil, N., 2008, Early diagenetic dolomitization and dedolomitization of Late Jurassic and earliest Cretaceous platform carbonates: A case study from the Jura Mountains (NW Switzerland, E France): Sedimentary Geology, v. 212, p. 70-85.